UNIVERSITY OF SOUTHAMPTON

FACULTY OF ENGINEERING, SCIENCE AND MATHEMATICS

School of Ocean and Earth Science

Nutrient fluxes into the seasonal thermocline of the Celtic Sea

by

Jacqueline Fiona Tweddle

Thesis for the degree of Doctor of Philosophy

April 2007

UNIVERSITY OF SOUTHAMPTON

ABSTRACT

FACULTY OF ENGINEERING, SCIENCE AND MATHEMATICS
SCHOOL OF OCEAN AND EARTH SCIENCES

Doctor of Philosophy

NUTRIENT FLUXES INTO THE SEASONAL THERMOCLINE OF THE CELTIC SEA

by Jacqueline Fiona Tweddle

Estimates of vertical fluxes of nitrate (J_N) into the subsurface chlorophyll maximum from the bottom mixed layer were made in a variety of hydrological regimes over the Celtic Sea in 2003 and 2005. Over a topographically flat shelf J_N varied with the spring-neap tidal cycle (1.1 (neap) – 2.8 (spring) mmol m^{-2} day^{-1}), driven by changes in barotropic shear generated vertical diffusivities (K_z) at the base of the thermocline. Further increases in nitrate fluxes were possible through small shear perturbations. J_N is further enhanced over topographic features, such as banks on the shelf or the shelf break, by the generation and dissipation of lee waves. The strength of mixing driven by the lee waves also varies with the spring-neap cycle, with higher K_z at the base of the thermocline occurring around spring tide, compared to neap tide, associated with the greater occurrence of short period internal waves. Over banks vertical nitrate fluxes varied between 2.9 (neap) – 15.7 (spring) mmol N m^{-2} day^{-1} and over the shelf break estimated vertical nitrate fluxes were 4 (neap) –15 (spring) mmol m^{-2} day^{-1}.

These fluxes are capable of supporting new production of 207 mg C m^{-2} day^{-1} over the Celtic Sea shelf, which over the summer stratified period is potentially greater than the new production taking place in the spring bloom. Enhanced production of 1200 mg C m^{-2} day^{-1} is supportable over regions of the shelf affected by the generation of lee waves over banks. This equated to a 4% increase in new production within the SCM over the Celtic Sea shelf. 31% of new production in the Celtic Sea was associated with the shelf break, where 660 mg C m^{-2} day^{-1} could be supported in the shelf break region.

CONTENTS

LIST OF FIGURES

Chapter 1

Chapter 2

Chapter 3

Chapter 4

Chapter 5

Chapter 6

Chapter 7

LIST OF TABLES

Chapter 2

Chapter 3

Chapter 4

Chapter 5

Chapter 6

LIST OF EQUATIONS

Chapter 1

Chapter 2

DECLARATION OF AUTHORSHIP

I, JACQUELINE FIONA TWEDDLE, declare that the thesis entitled

NUTRIENT FLUXES INTO THE SEASONAL THERMOCLINE OF THE CELTIC SEA

and the work presented in it are both my own, and have been generated by me as the result of my own original research. I confirm that:

- this work was done wholly or mainly while in candidature for a research degree at this University;
- where any part of this thesis has previously been submitted for a degree or any other qualification at this University or any other institution, this has been clearly stated;
- where I have consulted the published work of others, this is always clearly attributed;
- where I have quoted from the work of others, the source is always given. With the exception of such quotations, this thesis is entirely my own work;
- I have acknowledged all main sources of help;
- Where the thesis is based on work done jointly with others, I have made clear exactly what was done by others and what I have contributed myself;
- Parts of this work have been published as:

Moore, CM, Suggett, DJ, Hickman, AE, Kim, YN, Tweddle, JF, Sharples, J, Geider, RJ & Holligan, PM (2006). Phytoplankton photoacclimation and photoadaptation in response to environmental gradients in a shelf sea. *Limnology and Oceanography* **51** 2: 936-949

Rippeth, TP, Palmer, MR, Tweddle, JF, Sharples, J, Inall, M, Fisher, N, Hickman, AE, Holligan, P, Kim, YN, Moore, CM & Simpson, JH (In Press). Diapycnal nutrient fluxes in seasonally stratified shelf seas. *Limnology & Oceanography*

Sharples, J, Tweddle, JF, Green, JAM, Palmer, MR, Kim, YN, Hickman, AE, Holligan, PM, Moore, CM, Rippeth, TP, Simpson, JH & Krivtsov, V (In Press). Spring-neap modulation of internal tide mixing and vertical nitrate fluxes at a shelf edge in summer. *Limnology & Oceanography*

Signed:.....

Date: 11/04/07 .....

Graduate School of the National Oceanography Centre, Southampton

ADVISORY PANEL

Panel Chair: Prof. Ian S. Robinson (National Oceanography Centre, Southampton)

Supervisors: Dr. J. Sharples (Proudman Oceanographic Laboratory)

Prof. P. M. Holligan (National Oceanography Centre, Southampton)

ACKNOWLEDGEMENTS

I would like to thank NERC for funding this work [NER/S/J/2002/11128].

Many thank yous to my two supervisors, Patrick and Jonathan, for their advice, encouragement and support over the past few years, and for reading over chapters so quickly! Special thanks to Mark Moore for his help, the first year or so in particular. It was very much appreciated and gave me a great start. Thank you also to Ian Robinson for his work as my advisory panel chair, and his encouragements.

The work presented in this thesis relied heavily on FLY data collected by the University of Wales, Bangor Turbulence Group, so thank you, particularly to Matthew Palmer, for supplying the data, answering my many questions and making me very welcome whenever in Bangor. All who were involved in this multi-disciplinary, multi-institute project were a pleasure to work with, and I enjoyed our time at sea together. It really was a team effort.

Many friends contributed to the sanity of this author by being, well, generally fabulous. My housemates through the years have been saints, and I am constantly amazed at how long Kate managed to live with me. A testament to her niceness! Thanks to The Guys for introducing me to surfing and Sam and Jo for keeping up the good work. My partner in metaphorical crime Steph provided coffee and cake in times of need (well... every weekend... ok, most days). My head was (mostly) kept intact by Chris, who supplied chat and Mighty Boosh hilarity, and forced me to run exceedingly long distances.

The Ranelagh Gardens Posse got the pleasure of living with me towards the end and were great at calming me down through a combination of endless Lost episodes and by being willing yoga victims.

The last, but not the least, of my housemates, Auntie Jacqui, wee coz Cata and Maisie, have been amazingly brilliantly awesome, letting me stay way past my original invite to let me get this thesis finished. They even let me watch NCIS.

Of course I could never have done this without all my family's support, and the frequent telephone calls (especially to Grandma who let me haver for hours)! Thank you, thank you, thank you!

Abbreviations used

JR98	2003 cruise
CD173	2005 cruise
SCM	Subsurface chlorophyll maximum
[Chl *a*]	Chlorophyll *a* concentrations
[Nitrate]	Nitrate concentrations
z	Depth
ε	Turbulent dissipation rate
K_z	vertical diffusivities
$\Delta N/\Delta z$	vertical nitrate concentration gradient
$\Delta[Chl\ a]/\Delta z$	vertical chlorophyll *a* concentration gradient
$\Delta[Chl\ a]/\Delta T$	chlorophyll *a* concentration gradient against temperature
J_N	vertical nitrate flux
Ri	Richardson number
N^2	Brunt-Väiäslä (Buoyancy) frequency
h/u^3	Simpson-Hunter stratification parameter
M_2	Semi-diurnal lunar tidal constituent
S_2	Semi-diurnal solar tidal constituent
PAR	Photosynthetically available radiation
SUV6	Valeport SUV6 nitrate sensor
CI	Confidence intervals
F	F-value in ANOVA analysis (see Eq 2.9)
F_{crit}	Critical value of F in ANOVA analysis
p	probability (p = 0.05 = 95% probability)
$\chi 2$	measure of fit of least squares analysis
SST	Sea surface temperature
$SST_{\%}$	Normalised sea surface temperature (Eq 2.23)
$[Chl\ a]_{\%}$	Normalised chlorophyll a concentrations (Eq 2.24)
$nLw_{555(551)}$	Single band 555 nm (551 nm) normalized water leaving radiance

Chapter 1: Introduction

Shelf seas are shallow seas covering the continental shelf margins, extending from the coastline to the shelf break where the shelf slopes steeply down to the ocean basins. Around the UK the shelf break is usually considered to be coincident with the 200 m depth contour.

A range of influences affect the movement and structure of the water column over the shelf, ranging from tides to inertial motions, wind waves to internal waves. By controlling the physical structure, these processes also influence the phytoplankton living within the water column. Some of these processes and their biological consequences will be looked at in more depth in the following sections.

1.1. Tides, mixing and stratification

As the moon orbits the earth, and the earth orbits the sun, the effect of gravity creates a 'bulge' in the oceans' waters which travels round the ocean basins in the form of a wave (Godin 1988, Pond & Pickard 1995). This is known as the barotropic tide. The position of the sun and moon relative to each other, and to the earth, results in modulation of the tide, giving rise to cycles in tidal height and amplitude, for example a 14.8 day spring-neap cycle. As a wave, the

tide can be broken down into harmonic constituents, with phase, period and amplitude relating to, for example, a semidiurnal lunar constituent (M_2), a semidiurnal solar constituent (S_2), a diurnal lunar (O_1), a luni-solar diurnal (K_1), and a semidiurnal lunar elliptic (N_2). Tidal elevation can be described as:

$$\eta(t) = \sum_{i=1,N_c} A_i \cos(\omega_i t + \psi_i) \qquad \textbf{Eq. 1.1}$$

where η is tidal elevation, t is time, A_i the amplitude, and ψ_i the phase and ω_i the frequency associated with constituent i, and the sum is over N_c constituents.

Individual constituents change in amplitude and phase according to position on the earth's surface, giving rise to changes in tidal height, tidal current strength, and timings. Sea level can also be modified through other, non-tidal, hydrodynamics, such as storm surges and current rectification.

1.1.1. Seasonal stratification

Radiation from the sun is constantly heating the surface of the sea. The heat acts as a stabiliser to the water column, the warmer surface waters being less dense than the cooler waters below. This stratifying effect is stronger when more heat reaches the sea surface, i.e. when the net heat flux is greater. The net heat flux at mid-latitudes, such as the Celtic Sea, varies with season. The greatest net heat fluxes into the sea, and so the strongest stabilising effect, occur in spring and summer.

Concurrent to heating, water currents interact with the sea bed through friction, creating a region of maximum vertical shear generation which moves up

through the water column (Simpson et al. 1996, Sharples et al. 2001b). The level of bed generated shear is controlled by the local barotropic current amplitude plus any local residual current from other sources (Simpson et al. 1996). In shallower areas, or where higher current velocities lead to intensified shear generation, it is possible for turbulent dissipation to reach closer to the surface of the water column.

The structure of the water column in a particular place is a function of the competition between mixing from the bed and heating of the surface. In regions where tidal mixing is strongest barotropic, bed-generated turbulence can overcome the stratification generated by heating and the water column will remain mixed. Alternatively, where the heating effect is stronger, stratification develops. Between the two areas a transitional region develops, called a "shelf sea" or "tidal mixing" front. Mixing generated by the interaction of the wind with the sea surface can also cause the weakening of stratification. Although not a major contributing factor in the Celtic Sea, regions of freshwater influence (ROFIs) can affect stratification, through the input of fresh (different density) water (Sharples & Simpson 1995).

Over short temporal scales in summer, and on small spatial scales, for example over the Celtic Sea, heating (Q, W m^{-2}) can be regarded as approximately constant. Using simple energy arguments Simpson & Hunter 1974) derived a parameter useful as a descriptor of stratification:

$$h/u^3 = \frac{8c\rho C_D \mathrm{E}}{3\pi\alpha g Q} \qquad \textbf{Eq. 1.2}$$

with h being water column depth (m), u tidal stream velocity (m s^{-1}), c the specific heat capacity of seawater (J kg^{-1} K^{-1}), ρ density (kg m^{-3}), C_D a constant

in the assumed quadratic friction law (=0.0025), E the fraction of turbulent energy available for mixing the water column (=0.003), α the thermal expansion coefficient of water, and g acceleration due to gravity (m s^{-2}). The parameter h/u^3 (m^{-2} s^3) is a guide to where stratification will and will not occur, and where fronts will be positioned. Pingree (1978) extended the concept to come up with a stratification parameter, S:

$$S = \log_{10}\left[\frac{h}{C_D|u|^3}\right] \qquad \textbf{Eq. 1.3}$$

Values of S>2 predict stratified waters, S<1 mixed waters, and S=1.5 are transitional, and thus indicate the expected position of fronts. This assumes no wind driven mixing.

Areas of stratified water start to develop in the spring in seasonally stratified shelf seas, and spread and strengthen into the summer as solar radiation becomes stronger. In autumn solar radiation decreases and the stratification weakens through convective mixing, with wind and barotropic shear generated turbulence assisting in breaking down stratification completely, returning the shelf sea to its winter mixed state.

1.1.2. The importance of the pycnocline

In a seasonally stratified water column the pycnocline is the region of strong vertical density gradient, separating the surface (wind-mixed) layer from the bottom (tidally mixed) layer, and acting as a barrier to mixing.

Light levels within the water column are affected by the attenuation of light with depth (Kirk 1994). E_o, the level of irradiance just below the sea surface, is absorbed exponentially with depth following the rule:

$$E(z) = E_o e^{-k_d z} \qquad \textbf{Eq. 1.4}$$

where E is the irradiance at depth z, and k_d is the attenuation coefficient. Thus, for the biochemistry of the shelf sea, the pycnocline is a critically important region, situated between the light rich, (in summer) nutrient poor surface mixed layer and the nutrient rich, light poor bottom mixed layer.

1.1.3. Mixing at the pycnocline

The pycnocline is not a perfect barrier, and mixing can occur within and between the pycnocline and the surface and bottom layers. The gradient Richardson number (R_i) is a dimensionless parameter which describes the ratio of strength of stratification to strength of mixing:

$$R_i = \frac{N^2}{(\partial u/\partial z)^2} \qquad \textbf{Eq. 1.5}$$

where N^2 is the Brunt-Väiäslä, or buoyancy, frequency, u is the current velocity, z is depth, and $\partial u/\partial z$ is vertical current shear. When R_i is small (<0.25) velocity shear is considered sufficient to overcome the tendency of the water column to remain stratified and some mixing may occur. When R_i is large turbulent mixing within the pycnocline is suppressed.

Sources of shear can reduce the Richardson number, leading to instabilities and mixing (MacKinnon & Gregg 2003, Rippeth et al. 2005). This mixing will act to redistribute water column properties, for example supplying nutrients from the bottom layer into the pycnocline and possibly the surface layer, or mixing phytoplankton from the surface and pycnocline into the bottom waters. The energy for mixing in the pycnocline can be supplied through shear generated by a variety of sources, including the barotropic tide (Simpson et al. 1996, Sharples et al. 2001b), the baroclinic tide and other internal waves (Inall et al. 2000, Nash & Moum 2001, MacKinnon & Gregg 2003), and inertial oscillations (Rippeth et al. 2005).

Barotropic tide driven mixing

The balance between bed generated shear and stratifying influences is not universal across a shelf sea. In areas of stronger mixing, and/or shallower water, the bed generated turbulence "pushes" the pycnocline nearer to the surface, and sharpens it, compared to regions of lower turbulence generation, and/or deeper water (Fig 1.1 a and b). This process not only modifies the position and sharpness of the pycnocline but also mixes properties and particles out of, and into, the pycnocline, for example entraining phytoplankton into the bottom mixed layer, or supplying nutrients into the pycnocline.

Barotropic tidally driven mixing varies not only on a spatial scale but also temporally, for instance over the spring-neap cycle. Increasing current velocities approaching spring tides drive turbulence progressively higher into the water column, entraining water situated at the base of the thermocline and SCM into the bottom water layer (Holligan 1978, Sharples 1999, Sharples et al. 2001b).

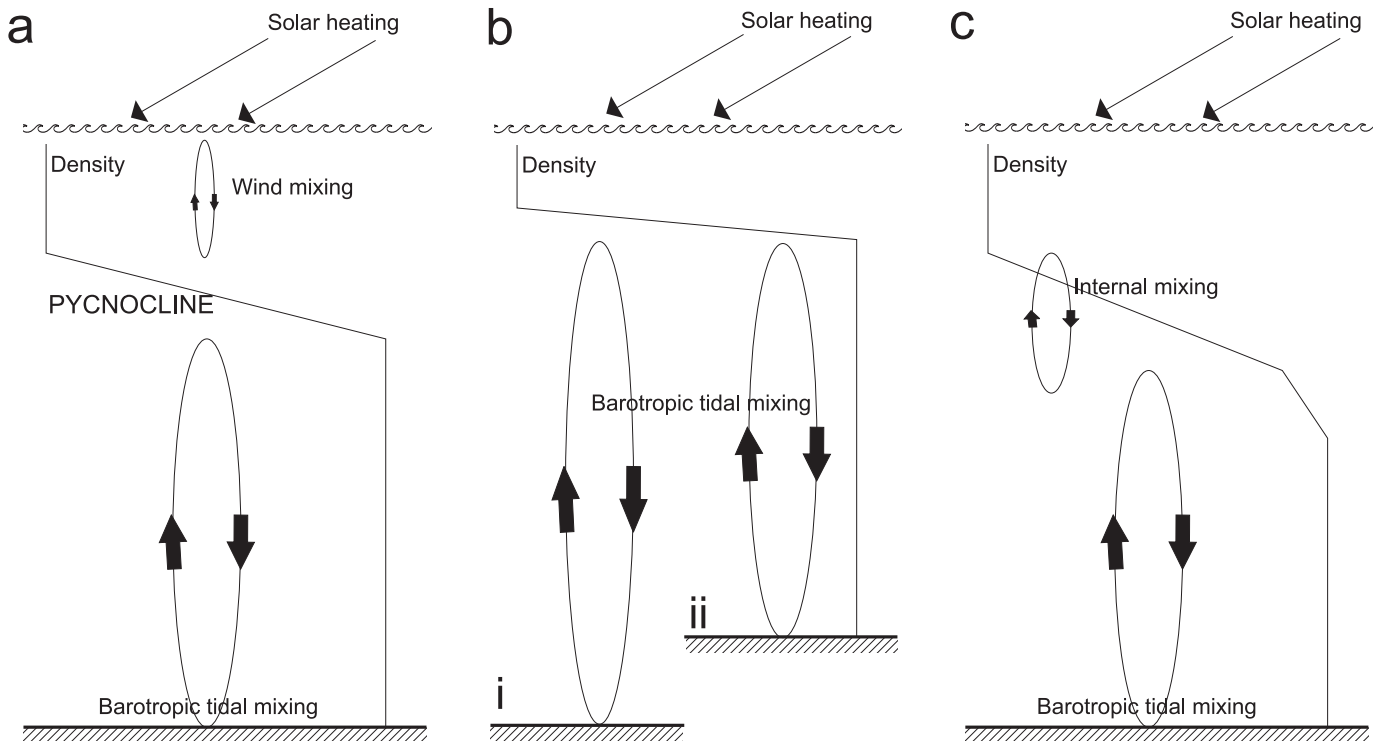

Figure 1.1

A schematic of the influence of mixing on stratification. a) The wind mixed warmer surface layer is separated from the cooler barotropic tidally mixed bottom layer by the pycnocline. b) The pycnocline rises and sharpens when i) barotropic tidally driven mixing increases or ii) water depth decreases. c) Mixing internal to the pycnocline (e.g. driven by internal waves or inertial oscillations) leads to a more diffuse thermocline.

This process acts to sharpen the temperature gradient at the base of the thermocline. The opposite occurs approaching neap tides. Decreasing current velocities allow surface generated turbulence to deepen the thermocline as barotropic turbulence decreases at the base of the thermocline (Sharples 1999).

Tidal mixing events attributable to the spring-neap cycle, particularly approaching spring tide, can provide a periodic supply of nutrients to phytoplankton in the pycnocline. It has also been suggested the redevelopment of the neap tide pycnocline depth after springs will also involve further entrainment of nutrients to within the pycnocline (Holligan & Harbour 1977, Holligan 1978, Sharples et al. 2001b).

Inertial oscillation driven mixing

Inertial oscillations are energetic motions within the water column which can be induced by periodic winds (Rippeth et al. 2002) or sudden changes in wind direction (van Haren et al. 1999). Wind stress induces water movements (Pollard 1980) of up to 70 cm s^{-1} (Salat et al. 1992), energy propagates downward into the water column, with an increasing phase delay with depth (Millott & Crépon 1981, Maas & van Haren 1987, Rippeth et al. 2002). These motions can cause shear instabilities in the flow, which induces mixing within the pycnocline by lowering the Richardson number (Baines 1986, Rippeth et al. 2005).

Internal wave driven mixing

Internal waves propagate along a density interface within the water

column, such as the seasonal pycnocline in shelf seas, and have been observed throughout the world's oceans, as early as Helland-Hansen & Nansen (1909), at varying frequencies. They occur when currents in a stratified water column interact with topography, as first suggested by Zeilon (1912). Two types of internal wave are particularly important in the context of this thesis: internal tides, generated at the shelf break, and smaller lee waves, generated over topographic features on the shelf. As with the barotropic tide, internal waves can provide energy to contribute to mixing of the water column (Fig 1.1 c).

Baroclinic, or internal, tides are internal waves with tidal periodicity and have been observed in many regions associated with shelf breaks, such as the Australian North West shelf (Holloway 1994), Scotian shelf (Sandstrom & Elliott 1984, Sandstrom et al. 1989, Sandstrom & Oakey 1995), Portuguese shelf (Jeans & Sherwin 2001), Malin shelf (Sherwin 1988, Inall et al. 2000) and the Celtic Sea and Bay of Biscay (Heathershaw 1985, Holligan et al. 1985, Pingree & Mardell 1985, Pingree et al. 1986, New & Pingree 1990, New & Pingree 2000, da Silva et al. 2002).

As with all internal waves, the baroclinic tide is generated when currents interact with a topographic feature, in this case the continental shelf slope (Sandstrom & Elliott 1984, Heathershaw 1985, Holloway 1996). Barotropic tidal currents flowing off-shelf (Pingree et al. 1986) cause a depression to form in the isopycnals above the shelf slope (Fig 1.2). As the off-shelf ebb flow relaxes the depression is "released" and propagates both on- and off-shelf (Baines 1982, Sandstrom & Elliott 1984, Pingree & Mardell 1985, Huthnance 1995, Guizien et al. 1999), following three ray paths (Baines 1974, New & Pingree 1990, New & Da Silva 2002b). Both the degree of stratification (Holloway 1996) and the

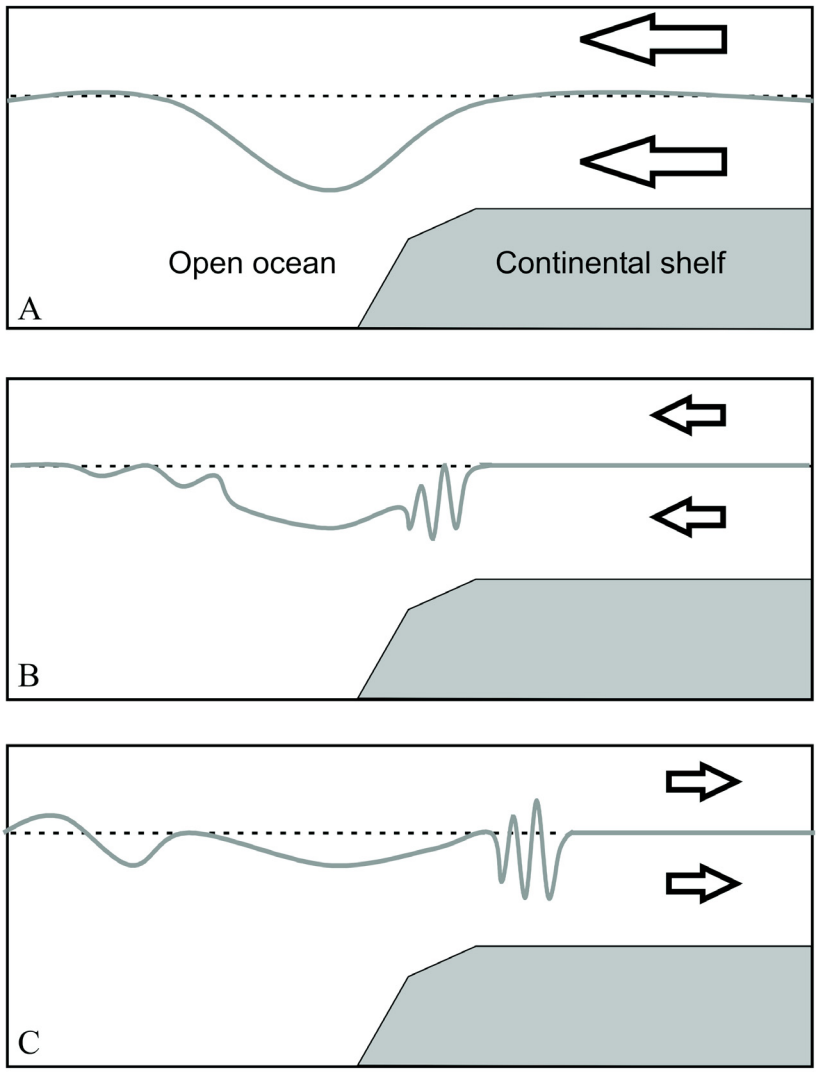

Figure 1.2

A schematic of the generation and dissipation of the internal tidal wave. As tidal currents flow off shelf isothermals are depressed (a), forming the main internal tidal wave. As the current velocity begins to weaken the internal tidal wave begins to propagate on and off shelf (b), as the waves propagate onto the shallower shelf they may steepen and amplitude may increase. The reversal of the tidal currents (c) may additionally steepen the internal wave train over the shelf, resulting in solitons and potentially solibores. Figure based on Figure 1 Sharples et al. (In Press) and the results of Gerkema (1996) relevant to the spring tide at the Celtic Sea shelf break.

gradient of the continental slope (Baines 1982, Holloway 1996) appear to affect internal tide generation, as does the intensity of the tidal current, with spring-neap cycles in baroclinic tide generation apparent (Sherwin 1988, New & Pingree 1990, Gerkema 1996, Inall et al. 2000).

The internal tide, once generated, propagates away from the shelf break generation zone as a wave with tidal period (Holloway 1994, Holloway 1996, Inall et al. 2000, New & Pingree 2000, Baumert et al. 2005). Two ray paths are predicted to radiate into the open ocean (New & Pingree 1990), one which travels outwards and upwards, and causes maximum mixing around 20 km from the generation site, and another that reflects off the ocean floor before travelling surface-ward and creating local generation of internal waves and mixing hundreds of km from the shelf break (Holligan et al. 1985, New & Pingree 1990, New & da Silva 2002).

A third wave moves onto the shelf. As the wave propagates nonlinear effects become important (Mazé 1987). As the internal tidal wave propagates into shallower water it steepens, eventually breaking down into a cnoidal wave train or a series of solitary waves, known as solitons, or in extreme cases to internal hydraulic jumps or solibores (Sandstrom & Elliott 1984, Holloway 1987, Holloway 1991). These propagating solitons have been observed in many regions, and have been shown to cause mixing within the pycnocline (Pingree 1988, New & Pingree 1990, New & Pingree 2000, Jeans & Sherwin 2001, Rippeth & Inall 2002, Moum et al. 2003). The waves have increased shear and vertical eddy diffusivity associated with them (Sandstrom & Elliott 1984, Sharples et al. 2001a), particularly at spring tides (Inall et al. 2000). Inall et al. (2000) found up to 30% of dissipation in the water column occurred within the

pycnocline, with Sandstrom & Oakey (1995) and Sandstrom et al. (1989) estimating 20-25% of energy in the tides is lost due to turbulent dissipation in the pycnocline. Although most tidal energy is dissipated through barotropic bed generated shear, the efficiency with which the baroclinic shear is converted to turbulence, and by its being concentrated in the pycnocline, means the baroclinic tide can be of major impact in mixing the water column (Hearn 1985, Sandstrom & Oakey 1995, Baumert et al. 2005, Rippeth et al. 2005).

The shelf edge is an example of an extreme topographic feature in the ocean. But, internal waves are also frequently seen associated with smaller topographic features. Studies over small banks (Moum & Nash 2000, Nash & Moum 2001), fjord-like sills (Farmer & Armi 1999a, Farmer & Armi 1999b, Farmer & Armi 2001, Klymak & Gregg 2001, Armi & Farmer 2002, Cummins et al. 2003, Klymak & Gregg 2003, Inall et al. 2004, Klymak & Gregg 2004, Inall et al. 2005) and other topographic features (Lueck & Mudge 1997, Edwards et al. 2004) have investigated moving stratified water, for example by tidal currents, and the mechanisms which generate an observed increase in turbulence. Lee waves and internal hydraulic jumps form downstream of the crest, intensifying turbulence within the area of the pycnocline. The formation of a bifurcation has been seen to give rise to internal solitary waves travelling upstream from the bank crest (Farmer & Armi 1999a), and the relaxation of the lee wave/internal hydraulic jump also generates internal waves (Cummins et al. 2003, Klymak & Gregg 2004). In the majority of investigations into topographically controlled mixing a two dimensional flow was envisaged, hence the three dimensional hydraulics remain unknown, with the exception of one fjord sill case, where 3D effects were shown to be important (Klymak & Gregg 2001).

Stonewall Bank, a small topographic feature on the Oregon shelf, has been used to investigate the effect of banks on hydraulic flow (Moum & Nash 2000, Nash & Moum 2001). Turbulence was found to be increased, in comparison to flat topography, in 3 distinct regions over the bank: in the benthic boundary layer (skin friction), within the pycnocline where isopycnals were depressed, and downstream of the bank crest, associated with the lee wave or internal hydraulic jump (the last two being due to form drag). Overall turbulent diffusivity was increased over 100 times.

The influence of small banks in the topography of shelf seas on tidally generated turbulent mixing has previously been considered of interest principally for its influence on the dissipation of tidal energy (Munk 1997) and not with respect to primary production. The increased mixing rates may result in increased supply of nutrients to phytoplankton living within the pycnocline.

Impacts of internal mixing

The effects of internal waves can be viewed using satellite imagery. Bands of increased surface chlorophyll relating to wave crests elevating the subsurface chlorophyll maximum layer situated within the pycnocline can be occasionally seen (da Silva et al. 2002), and SAR images (Jeans & Sherwin 2001, da Silva et al. 2002, New & Da Silva 2002) make use of the rough/smooth pattern induced on the ocean surface by internal wave crests and troughs respectively (Ewing 1950). This can also be utilised by ship-borne radar to track internal wave propagation (Inall et al. 2000).

Cool bands of water over continental shelf breaks have been observed for many years, both in situ (Pingree et al. 1986, New & Pingree 1990) and by

satellite (Dickson et al. 1980, Pingree & Mardell 1981, Holligan & Groom 1986), and have been attributed to the action of internal tide driven mixing. The internal tides have been further hypothesised to be responsible for the increased chlorophyll bands also observed by pumping nutrients into the pycnocline and photic zone (Pingree & Mardell 1981, Pingree et al. 1982, Sandstrom & Elliott 1984, Pingree et al. 1986). Temporal variations in nutrient fluxes driven by internal tide and related internal waves have not been fully investigated previously.

1.2. Primary production and the shelf sea subsurface chlorophyll maximum.

Primary production is the manufacture, usually photosynthetically, of new organic matter from carbon contained in CO_2 (Hale et al. 1995) and is the main means of energy entering an aquatic ecosystem.

The distribution of phytoplankton and the relative rates of primary production throughout the world's oceans are of interest for a variety of reasons, particularly with respect to the global carbon budget (Anderson & Williams 1998, DuRand et al. 2001, Huisman & Sommeijer 2002, Behrenfeld et al. 2006) and CO_2 flux into the ocean, which is controlled to an extent by phytoplankton concentration (Longhurst & Harrison 1989, Joint & Groom 2000). Shelf seas have been estimated to account for 15–30% of total oceanic production (Wollast 1998, Muller-Karger et al. 2005) and are therefore an important contributor to the

ocean sink for atmospheric CO_2 (Tsunogai et al. 1999, Frankignoulle & Borges 2001, Yool & Fasham 2001, Thomas et al. 2004, Borges et al. 2005, Cai et al. 2006).

As well as being of importance to the global biogeochemical cycles, phytoplankton form the base of the food chain, providing a source of food for pelagic herbivores, including larval fish (Nielsen et al. 1993, Napp et al. 1996, Richardson et al. 2000) and supporting commercial fisheries (Young et al. 2001).

1.2.1. Photosynthesis

Photosynthesis consists of two stages, the 'light', or 'light-dependent', and 'dark', or 'light-independent', reactions (Bell 1992, Kirk 1994, Campbell 1996, Falkowski & Raven 1997). In eukaryotic cells the reactions take place in specialised organelles within the cytoplasm called chloroplasts. Two membranes enclose the chloroplast's stroma, a dense solution of proteins the majority of which are involved in carbon dioxide fixation. Thylakoid sacs, composed of chlorophyll containing thylakoid membranes separating the stroma from the thylakoid lumen, can be densely layered into stacks called grana. In prokaryotic cells such as cyanobacteria the chloroplasts are absent and the thylakoid membranes are arranged in sheets placed within the cytoplasm of the cell. Regardless of the cell morphology the light reaction occurs within the thylakoid membrane, and the dark reaction within the stroma, or cytoplasm of cyanobacteria.

The light reactions occur in reaction centres associated with light

harvesting chlorophyll pigment-protein complexes and electron transfer agents. These reaction centre complexes are called photosystems I and II. Both reaction centres absorb light energy of a particular wavelength (700 nm and 680 nm respectively) and utilise the energy to excite an electron to a higher energy state. Pigments with other maximum absorbance wavelengths may be present and will pass their absorbed energy along to the reaction centres. The two photosystems work together to transfer electrons into a system of oxidation and reduction reactions called the "Z-scheme" for photosynthetic electron transport (Falkowski & Raven 1997).

Overall this electron transport results in the pumping of H^+ across the thylakoid membrane, establishing a chemical (pH) and electrical gradient between the stroma and the thylakoid lumen. ATP-synthase works to disperse the proton gradient and creates ATP in the process (Geider & MacIntyre 2002):

$$2H_2O + 2NADP^+ + 3ADP + 8\,photons \overset{Chl}{\rightarrow} O_2 + 2NADPH + 2H^+ + 3ATP$$

Eq. 1.6

The products of the light reaction (ATP and NADPH) drive the dark reaction in the stroma (Adapted from Geider & MacIntyre 2002):

$$CO_2 + 2NADPH + 3ATP \overset{enzymes}{\rightarrow} (CH_2O) + H_2O + 2NADP^+ 3ADP + 3Pi$$

Eq. 1.7

Combining Eq. 1.6 and 1.7 gives the sum equation of both the light and dark reactions:

$$CO_2 + 2H_2O \underset{nutrients}{\overset{light}{\rightarrow}} (CH_2O) + H_2O + O_2 \qquad \textbf{Eq. 1.8}$$

1.2.2. Biology of the shelf sea subsurface chlorophyll maximum

Development of the subsurface chlorophyll maximum

In temperate shelf seas a phytoplankton 'spring bloom' coincides with stratification development in the spring (Pingree et al. 1976, Fasham et al. 1983, van Haren et al. 1998). As the irradiance levels intensify and phytoplankton are mixed only throughout the surface layer due to the developing stratification, the depth-averaged light intensity the phytoplankton are exposed to is increased and, combined with non-limiting nutrient levels, results in increased population growth in the surface mixed layer. Nutrients are depleted in the upper mixed layer during the spring bloom through growth and subsequent sinking and grazing (Tett 1987).

The spring bloom is followed by development of a subsurface chlorophyll maximum (SCM) at the pycnocline (Holligan & Harbour 1977, Richardson et al. 2000). After the spring bloom, phytoplankton in the euphotic zone are limited to regenerated nutrients or to nutrients mixed across the pycnocline. Provided the pycnocline is shallow enough to receive sufficient irradiance, phytoplankton can photosynthesis and grow within the pycnocline, where diffusion and mixing of nutrients into the surface mixed layer is taking place. A subsurface chlorophyll maximum will result within the pycnocline (Pingree et al. 1977, Holligan et al. 1984a, Holligan et al. 1984b, Nielsen et al. 1993, Lizon et al. 1995). Shelf sea SCM can also be biomass maximums (Holligan et al. 1984a, Figueiras & Pazos 1991, Richardson et al. 1998, Nincevic et al. 2002), although differences in chlorophyll per cell through the vertical water column can account for much of the chlorophyll increase (Moore et al. 2006).

A sharp nutricline can develop at the base of the SCM, which creates a

greater diffusive flux of nutrients into the SCM and makes it the primary site of new production in the water column (Probyn et al. 1995).

The SCM throughout the summer

The pycnocline provides relative security for phytoplankton from being mixed into either the light limited bottom layers, or the nutrient limited upper layer, whilst providing sufficient nutrients and light for in situ growth. As the irradiance level experienced by phytoplankton depends on depth, one of the foremost sources of variation in light intensity incident on phytoplankton is due to vertical motion in the upper ocean (Denman & Gargett 1983, van Haren et al. 1998), either through the motile abilities of the cell, or from turbulence and water movements. The phytoplankton living in the SCM are exposed to lower irradiance levels than those living higher in the euphotic zone. As such the SCM comprises mostly of species with adaptations to allow them to live and photosynthesis in low light environments, such as coccolithophores (Sharples et al. 2001b) and dinoflagellates (Richardson et al. 2000).

In shelf sea SCM there is some risk of physical removal from the euphotic zone, as barotropic tidal turbulence periodically removes large amounts of phytoplankton to the bottom mixed layer (Sharples et al. 2001b). Intensified turbulence associated with spring tides, whilst increasing supply of nutrients to the SCM, also results in greater erosion of the bottom of the thermocline and subsurface chlorophyll maximum (Holligan 1978, Sharples et al. 2001b). The effect of this mixing on primary production within the pycnocline is a balance between nutrient supply fuelling production, and removal of phytoplankton through the same turbulent mechanism.

Due to the lower irradiance levels the SCM phytoplankton are exposed to, the rate of production is slower than that of the surface spring bloom and the affect of shading brought on by the high levels of chlorophyll will also serve to reduce growth rates already lowered by the low irradiance. However the period over which the SCM grows is longer, as it persists throughout the stratified period, and hence total primary production occurring over the summer in the SCM can be greater than during the spring bloom (Richardson & Chistoffersen 1991, Gowan & Bloomfield 1996, Richardson et al. 2000, Weston et al. 2005).

1.3. Celtic Sea

The Celtic Sea is situated south of Eire and west/southwest of England, extending out to the continental shelf break, which marks the start of the Bay of Biscay (Fig 2.1). It is a seasonally stratifying temperate shelf sea with a generally gently sloping topography with a deep channel, St. Georges Channel and Celtic Deep, linking it to the Irish Sea, but with a large region peppered with topographic banks (Fig 2.1). As stratification develops a series of distinct fronts also develop, marking the boundaries between the Celtic Sea and the well mixed Irish Sea (Celtic Sea front) and the English Channel (Ushant front).

1.4. Thesis Aims

A preliminary SeaSoar transect taken across the Celtic Sea in 2003 (see section 2.1.2 for methods), from the shelf break across the shelf, through the Celtic Sea Front, into the mixed waters of the Southern Irish Sea, revealed distinct patchiness in chlorophyll contained within the thermocline (Fig 3.1). Chlorophyll concentrations are a function of the balance between production of chlorophyll and removal of chlorophyll. In terms of production of chlorophyll, i.e. primary production, this is controlled by light and nutrient supply. If light is assumed to be supplied reasonably equally over the Celtic Sea, any differences in chlorophyll concentrations could be due to differences in nutrient supply. Thus, the main questions being investigated by this work are-

1) What are the rates of supply of nitrate to the thermocline, and hence the subsurface chlorophyll maximum, across the Celtic Sea?
2) How do these rates of supply change temporally and spatially?
3) What levels of production are supported by the estimated nitrate fluxes across the shelf?

The thesis is split into 4 chapters, two of which focus on work undertaken over the shelf, with results from cruises which took place in 2003 and 2005, and two of which focus over the shelf break, one using in situ and the other remotely sensed data. A final discussion chapter brings together the sections into a more complete picture of nitrate supply in the Celtic Sea.

Chapter 2: Methods

The work presented in this thesis was part of an interdisciplinary project studying physical, chemical and biological processes affecting the thermocline and subsurface chlorophyll maximum of the Celtic Sea. Scientists and engineers from several institutes, including the National Oceanography Centre (part of the University of Southampton), Proudman Oceanographic Laboratory, and the Turbulence and Mixing Group at the University of Wales in Bangor, took part in two cruise programs in the summers of 2003 and 2005. Due to the nature of the cruises not all data presented were collected, nor initially processed, by the author; data obtained in this manner are acknowledged in square brackets where appropriate, and in Appendix 1. The empirical data collected during these cruises is supplemented in this thesis by further data obtained through both remote sensing and modelling work by the author. An overview of the data collection sites, of both cruise and satellite data, is presented in Fig 2.1.

This chapter provides descriptions of the collection and initial processing and analysis of data utilized in this thesis.

2.1 Shipboard Observations

The empirical data presented in this thesis were collected over two two-ship cruises in the Celtic Sea, the first from the 25th July to the 15th August 2003 onboard the RRS *James Clark Ross* and RV *Prince Madog* (JR98), the second from the 14th July to the 6th August 2005 onboard the RRS *Charles Darwin* and RV *Prince Madog* (CD173). The cruise reports for all ships are archived at BODC.

During both cruises, a number of positions (stations) were occupied for approximately 25 hours (Fig 2.1 and Table 2.1). During these stations hourly CTD casts were taken from the RRS *James Clark Ross* or RRS *Charles Darwin* and FLY profiles approximately every 10 minutes from the RV *Prince Madog* throughout each station's duration. There were two exceptions to this. Throughout both visits to CS2 during CD173 all instrumentation was deployed from the RRS *Charles Darwin*. In order to maintain continuity in FLY turbulence measurements during these stations CTD casts were carried out less often, generally at two to four hour intervals. Times of casts are marked throughout on all appropriate figures. Water samples were collected using Niskin bottles attached to the CTD rosette frame during all stations. SeaSoar runs of varying length were also undertaken (Fig 2.1).

In this chapter the key instrumentation and analysis methods are described. The individual details on individual experimental setups are given where appropriate in the results chapters.

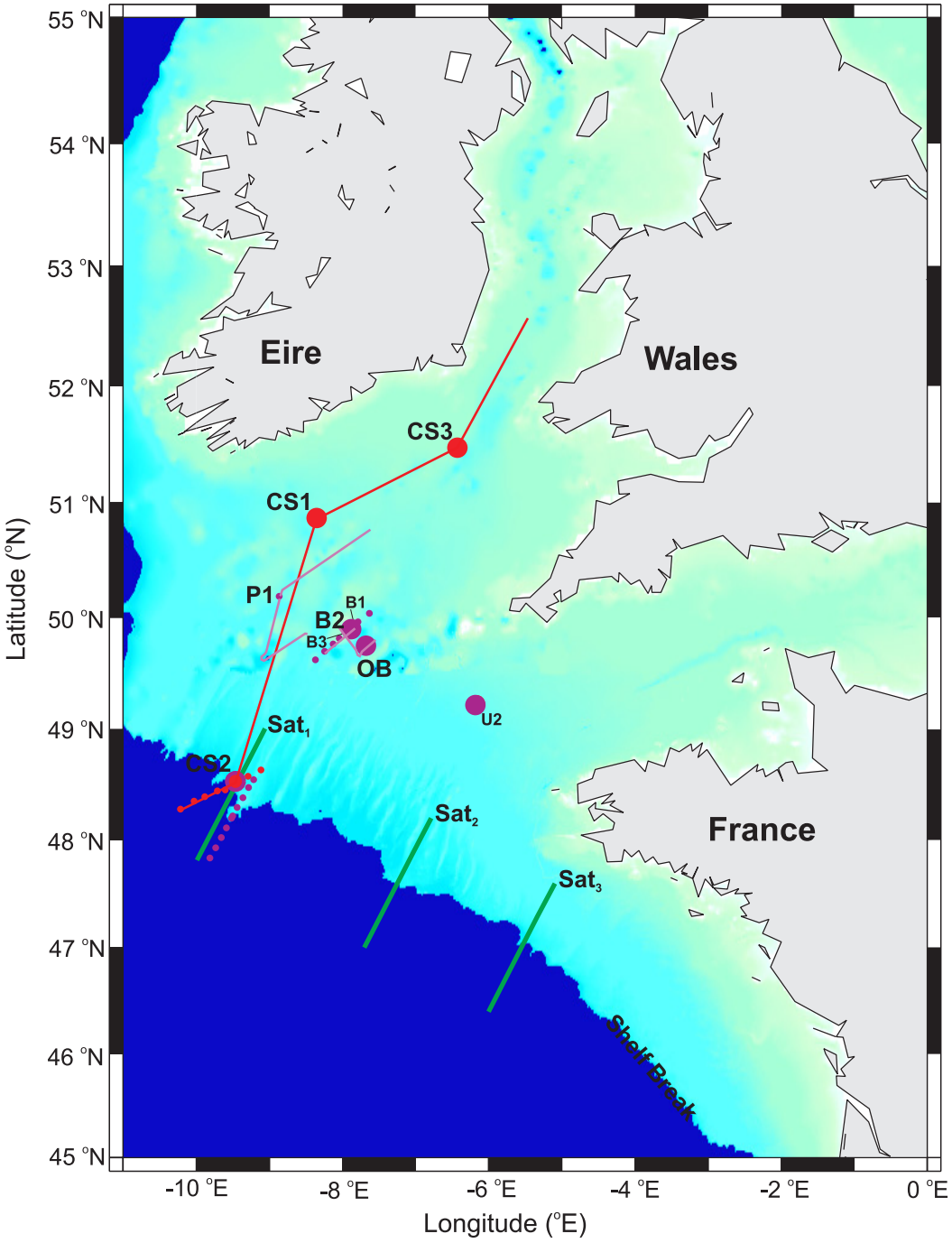

Figure 2.1

CTD and FLY station positions and SeaSoar transects of cruise JR98 (red), which took place July 25th to August 15th 2003 (Yearday 206 to 227), and cruise

CD173 (purple) which took place July 14th to August 6th 2005 (Yearday 194 to 217), within the Celtic Sea. Large filled circles represent mooring and station positions, smaller dots represent CTD positions, and lines represent SeaSoar tracks. The green solid lines show the positions of the data transects taken from satellite images. The bathymetry colour scale runs from 0 – 200 m (white – blue), below 200 m masked dark blue. Bathymetry data is from IOC et al. (2003).

Table 2.1.

Names, dates and positions of the CTD and FLY joint stations carried out during both JR98 in 2003 and CD173 in 2005.

Cruise	Station Name	Start and end dates and times (GMT)	Position	Topographic Type	Position in spring-neap tidal cycle	Comments
JR98	CS2a	29/07/03 02:55 -30/07/03 05:10	48.532°N -9.463°E	Shelf break	Spring	
JR98	CS1	31/07/03 03:00 -01/08/03 04:25	50.867°N -8.350°E	Bank	Spring	Data gaps due to problems with CTD winch and FLY termination failed and was replaced
JR98	CS3a	05/08/03 03:00 -06/08/03 04:20	51.473°N -6.430°E	Flat	Approaching neaps	
JR98	CS3b	10/08/03 02:55 -11/08/03 04:25	51.473°N -6.430°E	Flat	Approaching springs	
CD173	CS2b	17/07/05 18:55 -18/07/05 20:20	48.532°N -9.463°E	Shelf break	Neap	CTD large data gap due to problems with CTD wire
CD173	CS2c	22/07/05 21:30 -24/07/05 04:05	48.532°N -9.463°E	Shelf break	Spring	Gap in FLY data at start as FLY cable replaced
CD173	B2a	26/07/05 13:40 -27/07/05 15:00	49.896°N -7.883°E	Bank	½ way between spring & neap	1st CTD data gap due to optical rig cable tangled in rudder and 2nd due to problems with CTD wire
CD173	B2b	31/07/05 03:15 -01/08/05 04:55	49.896°N -7.883°E	Bank	Neap	CTD data gap due to problems with CTD wire
CD173	OB	01/08/05 13:00 -02/08/05 14:10	49.75°N -7.675°E	Flat	Neap	CTD data gap due to problems with CTD wire

2.1.1 CTD sampling and calibration

[*J. Sharples, J. Tweddle & S. Bates*]

The CTD was the main means of profiling the water column for hydrographic parameters over the two cruises. A Seabird 911 CTD (conductivity, temperature, depth) system was deployed from both RRS *James Clark Ross* and RRS *Charles Darwin*. The CTD was deployed using standard protocol, and carried sensors for pressure (depth), temperature, salinity, fluorescence, dissolved oxygen, transmittance and PAR, a fast repetition rate fluorometer (FRRF), and, for the majority of stations, an SUV6 nitrate sensor (Finch et al. 1998). The pressure sensor was corrected for atmospheric pressure for each cast using the on-deck pressure measurement. The CTD was vital in estimation of nitrate gradients in order to calculate nitrate fluxes, both through carrying the SUV6 nitrate sensor and providing temperature profiles, which could be regressed against water samples analysed for nitrate concentrations (sections 2.1.6 and 2.3).

Temperature and salinity

Throughout both cruises profiles of temperature and conductivity (subsequently converted to salinity (PSS78)) against depth were collected. Temperature was calibrated against SIS reversing thermometers and discrete water samples analysed on a Guildline Autosal salinometer were used to calibrate salinity. Temperature errors of the CTDs were of the order ± 10^{-3} ^{o}C, based on laboratory calibrations carried out by UKORS. Salinity uncertainties

were ± 0.004 and ± 0.003 for JR98 and CD173 respectively, taken as the standard deviation of the mean difference between the CTD and water sample salinities, both referenced to standard seawater.

Small oscillations in temperature and salinity (Fig 2.2) were identified as the result of an oscillating winch veer speed, coupled with water trapping within the bulk of the CTD. As the CTD slowed water trapped within the CTD, warmer than the surrounding water, would bulge downwards and cause an abnormally high temperature data reading. Then when the CTD sped up again the water would be pushed up into the frame and the temperature reading would reflect the surrounding water once more.

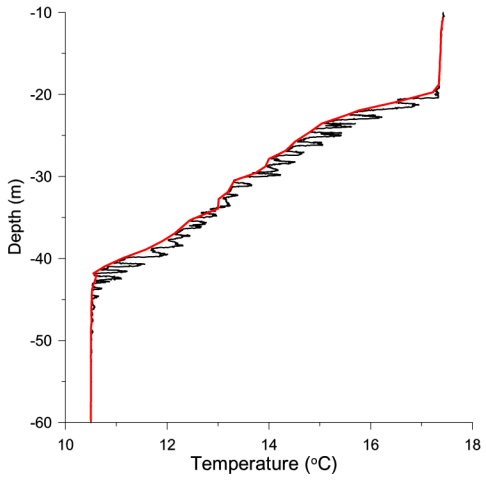

Figure 2.2.

Example of a CTD temperature profile through the thermocline from station OB, CD173. The black line is the raw temperature signal, the red line the analysis based on the average of the lowest 10 samples within each 0.5m depth bin.

CTD data on the downwards direction was corrected by a method of processing which averaged the lowest 10 data values from each 0.5m bin (Fig 2.2), which assumed that these lower temperatures were a true reflection of temperature at that depth.

The consequence of this was not critical in terms of the mean profiles, and the temperature and chlorophyll *a* gradients, so had little effect on nitrate gradient estimations and hence vertical nitrate fluxes. However, the processing method removed small scale detail, which could have been useful in the thermocline, in particular for looking at fine scale overturnings.

Chlorophyll a

The CTD frame carried a Chelsea Instruments Aquatracka MKIII chlorophyll fluorometer, which was calibrated (mg Chl *a* m^{-3}) against High Performance Liquid Chromatography (HPLC) analysed water samples (section 2.1.8). Station CS2 and casts near the shelf edge were calibrated separately to stations over the shelf due to a difference in the Chl *a* concentration to fluorescence ratio at the shelf edge. The calibrations produced an error of ± 0.2 mg Chl *a* m^{-3} at the shelf edge for both cruises, and errors of ± 0.2 and ± 0.1 mg Chl *a* m^{-3} on the shelf for JR98 and CD173 respectively. Throughout this thesis square brackets will be used to denote concentrations, e.g. [Chl *a*] for chlorophyll *a* concentrations.

2.1.2 SeaSoar sampling and calibration

[*J. Sharples*]

SeaSoar is an undulating towed body, marketed by Chelsea Technologies Group, controlled and powered by the PENGUIN (Practical Environmental Network for Grouping Underwater Instrumentation Nodes– developed at the Ocean Engineering Division of the National Oceanography Centre, Southampton) underwater data-handling unit. PENGUIN managed the collection of temperature, salinity, and fluorescence data using a Chelsea Instruments Minipack package and also controlled a Chelsea Instruments FRRF housed in the SeaSoar body. Packets of data were sent by PENGUIN up the tow cable to be copied to a shipboard PC.

Calibration of the minipack data was accomplished by taking a vertical profile with SeaSoar at CS3b during cruise JR98 and at P1 during cruise CD173, and comparing it to adjacent calibrated CTD casts. The pressure sensor was calibrated by comparing on-deck pressure of the SeaSoar to on-deck pressure of the CTD. This provided an offset which allowed correction to be applied to the SeaSoar pressure so it was compatible with the CTD. The average of before tow and after tow on-deck pressure was used to provide an atmospheric offset. The two offsets were applied to pressure data every SeaSoar tow.

Both salinity and temperature were calibrated only against bottom layer, non-pycnocline data during JR98, and bottom and surface layer, non-pycnocline data during CD173, due to vertical movement of the pycnocline in the time between the SeaSoar and CTD profiles. Resulting uncertainties in salinity

calibrations were of the order ± 0.01 and ± 0.02, and temperature ± 0.03 ^{o}C and ± 0.01 ^{o}C for JR98 and CD173 respectively.

The SeaSoar standard fluorometer was calibrated to Chl *a* concentration using water sample [Chl *a*] from the pycnocline of an adjacent CTD cast. The uncertainties in the data resulted from both uncertainties in the calibration regression and from the water sample [Chl *a*] values. The uncertainties were ± 0.22 mg m^{-3} for JR98 and ± 0.1 mg m^{-3} for CD173.

The SeaSoar data was merged with ship's GPS Latitude and Longitude to give position. Ship's ADCP (JR98) or echosounder (CD173) data was merged with the SeaSoar data to give the depth of the seabed associated with each data point.

2.1.3 Microstructure sampling

[*M. Palmer, M. Green*]

FLY was used to obtain profiles of turbulence measurements during both JR98 and CD173. FLY provided profiles of the vertical diffusivity, K_z, which were used in the estimation of vertical nitrate fluxes.

A Fast Light Yo-yo (FLY) shear profiler was deployed from the RV *Prince Madog* during the 2003 cruise campaign and the RRS *Charles Darwin* (at CS2) and RV *Prince Madog* (all other stations) in 2005. The RV *Prince Madog* was never sampling more than ~2 km from the ship profiling with the CTD.

FLY free-falls though the water column at a rate of around 0.80 m s^{-1} and resolves horizontal velocity shear with scale of around 0.01 m using an airfoil shear probe (Dewey et al. 1987). FLY also has a fast temperature sensor and a separate conductivity cell to obtain profiles of temperature and salinity.

Dissipation rate, ε, can be estimated directly from FLY (Osborn 1974), assuming the turbulent regime is isotropic, using:

$$\varepsilon = 7.5\mu\overline{\left(\frac{\partial u}{\partial z}\right)^2} \qquad \textbf{Eq. 2.1}$$

where μ is the dynamic viscosity of seawater ($\mu = 1.0 \times 10^{-6}$ $m^2 s^{-1}$). $\overline{\left(\frac{\partial u}{\partial z}\right)^2}$, the mean square shear estimate, is calculated from vertical FLY profiles for each 1.5 m section of the profile using the power spectrum of the vertical velocity gradient microstructure (Simpson et al. 1996).

Calculation of the buoyancy frequency, N^2,

$$N^2 = \frac{-g}{\rho}\frac{\partial \rho}{\partial z} \qquad \textbf{Eq. 2.2}$$

(g is acceleration due to gravity, z is depth and ρ is density) then further allows calculation of the eddy diffusivity of density (Osborn 1980):

$$K_\rho = \frac{R_f}{\left(1 - R_f\right)}\frac{\varepsilon}{N^2} \qquad \textbf{Eq. 2.3}$$

where R_f is the flux Richardson number (= 0.17, Moum 1996). Below a critical value of N^2, related to error in density measurements ($N^2_{\min} \sim \frac{g}{\rho}.\frac{\sigma_t\, error}{\Delta z_{FLY}}$), K_ρ

calculations will give spuriously high vertical diffusivities.

The eddy diffusivity was assumed to be consistent between properties, i.e. K_ρ (eddy diffusivity of density) = K_z (vertical diffusivity). This allowed calculation of the vertical nutrient fluxes using (Lewis et al. 1986, Horne et al. 1996, Sharples et al. 2001b, Moore 2002):

$$J_A = -K_z \left(\frac{\Delta A}{\Delta z} \right) \qquad \textbf{Eq. 2.4}$$

where J_A is the flux of nutrient A and $\Delta A/\Delta z$ is the vertical nutrient concentration gradient, for example that of nitrate.

When in use the FLY was deployed for 5–7 full profiles to the sea bed before being brought onboard to recharge the battery for ~20mins. This was repeated throughout the duration of the station.

The errors associated with ε and K_z vary, but are at a maximum of ~50% at low values ($\varepsilon \sim 10^{-6}$ W m^{-3}, Dewey et al. 1987).

2.1.4 Moorings

[*M. Palmer, UKORS*]

Moorings deployed during both cruises provided temporally longer data sets than those collected from CTD and FLY stations. Several moorings and landers were deployed over the two cruise campaigns, including both ADCP moorings and benthic landers, to collect current velocity information, and

temperature logger moorings, providing information on the structure of the water column (Table 2.2). Details of all moorings used are contained within the cruise reports held at the British Oceanographic Data Centre (BODC, www.bocd.ac.uk).

VEMCO temperature loggers were moored during both cruises. These loggers were arrayed at 5 to 10 m intervals between ~3m above the sea floor and ~4m below the sea surface. They were calibrated relative to one another pre-deployment, and had a resolution of 0.015 ˚C, with an accuracy of ± 0.1 ˚C.

Both on shelf and at the shelf edge 300 kHz RDI Workhorse Acoustic Doppler Current Profilers (ADCP) were deployed both in the middle of the water column and on the seabed. A 150 kHz SC NB-ADCP was also deployed on the seabed at the shelf break during both cruises.

A SUBS buoy was deployed, which consisted of a 600 kHz RDI Workhorse Sentinel ADCP and a VEMCO Minilog temperature logger at a set sub-surface depth, in order to provide high resolution measurements in the thermocline.

Due to a variety of reasons, such as acoustic release failure or trawler activity, several moorings were not recovered, and so the data was unavailable (marked in Table 2.2 as lost). The temperature logger mooring deployed at CS2 during JR98 was recovered damaged, and data was only available until the 31st July.

Table 2.2.

Positions, names, and dates of the mooring types deployed during either JR98 in 2003 or CD173 in 2005.

Cruise	Station	Position	Type	ADCP velocity standard deviation of recorded data/ ping rate	Duration
JR98	CS2	48.571 °N -9.510 °E	Temperature Logger	–	28/07/03 – 12/08/03
			SUBS Buoy (inc. ADCP)	2 cm s^{-1} 0.5 Hz	28/07/03 – 12/08/03
			150 kHz ADCP Lander	1 cm s^{-1} 1 Hz	28/07/03 – 12/08/03
			300 kHz ADCP Lander	5 cm s^{-1}1 Hz	28/07/03 – 12/08/03
	CS3	51.47 °N -6.43 °E	Temperature Logger	–	1/08/03 – 11/08/03
			300 kHz ADCP Lander	5 cm s^{-1} 1 Hz	1/08/03 – 11/08/03
CD173	CS2	48.571 °N -9.510 °E	Temperature Logger	–	17/08/05 – 24/08/05
			Subsurface 300 kHz ADCP	3 cm s^{-1} 0.5 Hz	17/08/05 – 24/08/05
			300 kHz ADCP Lander	3 cm s^{-1} 0.5 Hz	17/08/05 – 24/08/05
			150 kHz ADCP Lander	1 cm s^{-1} 2 Hz	18/08/05 – 24/08/05
	B1	49.940 °N -7.792 °E	Temperature Logger	–	26/08/05 – lost
			300 kHz ADCP Lander	3 cm s^{-1} 4 Hz	27/08/05 – 29/08/05
	B2	49.896 °N -7.872 °E	Temperature Logger	–	20/08/05 – 4/09/05
			SUBS Buoy (inc. ADCP)	7 cm s^{-1} 1 Hz	26/08/05 – 4/09/05
			300 kHz ADCP Lander	3 cm s^{-1} 1 Hz	26/08/05 – 4/09/05
	B3	49.854 °N -7.948 °E	Temperature Logger	–	26/08/05 – 3/09/05
			300 kHz ADCP Lander	2 cm s^{-1} 4 Hz	26/08/05 – lost
	U2	49.233 °N -6.167 °E	Temperature Logger	–	19/08/05 – lost
			300 kHz ADCP Lander	3 cm s^{-1} 0.5 Hz	15/08/05 – lost

2.1.5 Acoustic Doppler Current Profilers (Vessel Mounted)

[*J. Sharples (RRS James Clark Ross & RRS Charles Darwin) & M. Palmer (RV Prince Madog)*]

An RDI narrow band 153.6 kHz Acoustic Doppler Current Profiler (ADCP) was mounted in the hull of the RRS *James Clark Ross* during the 2003 cruise and the RRS *Charles Darwin* during the 2005 cruise. The RV *Prince Madog* carried a hull mounted 300 kHz broadband RDI Workhorse Mariner ADCP system on both cruises. These provided vertical profiles of current velocities and total seabed depth. RV *Prince Madog* ADCP velocity standard deviation was 2 cm s^{-1} with a ping rate of 2 Hz. The data was 4 m binned and averaged over 5 minutes. The ensemble averaging of the ADCPs on the RRS *James Clark Ross* and RRS *Charles Darwin* (2 minute averages over 4 m depth bin) led to velocity errors of less than 1 cm s^{-1}. The currents in this thesis are quoted as north/south velocities, unless otherwise stated. This was due to the direction of current being relevant at many of the stations. The major axis of the tidal current was ~042^{o}.

At CS2 the ships' ADCP data were lost through recording problems.

2.1.6 Nutrient sampling and the SUV6 nitrate sensor

Water samples

[*D. Hydes (JR98), Y.N. Kim & M. Qurban (CD173)*]

Water samples were collected for nutrient analysis during both JR98 and CD173, and analysed onboard ship for nitrate (plus nitrite), silicate, and phosphate on a Skalar autoanalyser using standard AA_II methods (Grasshoff et al. 1983). The working range was 0-10 mmol m^{-3} for nitrate and silicate, and 0–2 mmol m^{-3} for phosphate, with detection limits of 1% of the range for all, and a precision of ± 0.1 mmol m^{-3} for nitrate and silicate and ± 0.02 mmol m^{-3} for phosphate. The measurement error, based on replicate analysis was around ± 0.6%.

SUV6 nitrate sensor

[*J. Tweddle*]

For the majority of JR98 CTD work (with the exception of station CS2) a Valeport SUV6 was deployed with the CTD, measuring light absorbance at 220, 235 and 250 nm (Finch et al. 1998). The relationship between absorbance of light at 220 nm and 235 nm using

$$SUV6_{out} = \log_{10}\left({Abs_{220} - Abs_{235}}/{1} \right) \qquad \textbf{Eq. 2.5}$$

can be calibrated linearly against analysed water sample nitrate concentrations, [$Nitrate_{sample}$], to give

$$\left[Nitrate_{sample} \right] = M \times SUV6_{out} + C \qquad \textbf{Eq. 2.6}$$

where *M* and C are constants, calculated for each CTD cast, and then averaged over all casts per station (Table 2.3).

The errors associated with C were so large that a reliable absolute calibration of $SUV6_{out}$ to give [$Nitrate_{SUV6}$] could not be achieved. However the smaller errors (~33%) associated with the regression slope, *M*, show $SUV6_{out}$ did measure a reliable rate of change of [Nitrate], allowing calculation of $\Delta N/\Delta z$ for each CTD cast.

As

$$\Delta N/\Delta z = \left(\Delta SUV6_{out}/\Delta z\right) \times \left(\Delta SUV6_{out}/\Delta N\right)^{-1} \qquad \textbf{Eq. 2.7}$$

then

$$\Delta N/\Delta z = \left(\Delta SUV6_{out}/\Delta z\right) \times M^{-1} \qquad (\pm \text{ M error}) \qquad \textbf{Eq. 2.8}$$

where ΔN is change in [Nitrate], Δz change in depth, $\Delta SUV6_{out}$ change in $SUV6_{out}$ signal, and *M* is taken from Eq. 2.6.

As the SUV6 was being used to calculate nitrate fluxes into the thermocline the lack of absolute values was not a disadvantage, as this calculation requires the nitrate gradient, $\Delta N/\Delta z$ (Eq. 2.4).

The SUV6 was deployed during CD173, but the instrument failed to work.

Table 2.3.

Calibration constants, and associated errors, of Eq. 2.6 for each station where the SUV6 was used. The SUV6 did not work during CD173.

Station	*N*	*P*	*M*	*M* error (±%)	*C*	*C* error (±%)	J_N error (±%)
CS1	95	<0.05	0.003	33	0.04	25	60
CS3a	153	<0.05	0.003	13	0.01	1000	52
CS3b	142	<0.05	0.003	33	0.01	100	60

2.1.7 Chlorophyll and primary production rates

Chlorophyll and other pigments

[*P. Holligan*]

Chlorophyll *a* concentrations were measured by filtering water samples through Whatman GF/F filters, from which the chlorophyll was extracted using 90% acetone, and the solute analysed onboard ship on a calibrated Turner Designs A-10 Fluorometer (Welschmeyer 1994).

Water samples were also filtered and stored frozen at -80˚C for HPLC analysis of pigment composition upon return to the shore laboratory, using a ThermoFinigan HPLC system (Barlow et al. 1993).

Primary production rates

[*A. Hickman*]

^{14}C production experiments were carried out onboard both cruises following the standard method (Steemann-Nielsen 1952) and the carbon fixation rate calculated (Joint & Pomroy 1986). Production (*P*) versus irradiance (*E*) curves (PE curves) were obtained from incubation experiments on water samples taken at various depths during dawn CTD casts at all stations. These were adjusted to *in situ* light fields using measured phytoplankton absorption spectra (Tilstone et al. 2003, Moore et al. 2006).

PE parameters (chlorophyll normalised α^* and P^*_m) were linearly interpolated through the water column and assumptions were made both that these would be constant throughout the day, and that photoinhibition was negligible.

Mean air- water interface transmittance, average in-water surface spectra, and attenuation versus chlorophyll *a* concentration relationships at six wavelengths, using data from a SATLANTIC profiler [*G. Tilstone (JR98), V. Krivtsov (CD173)*] were used to recreate the *in situ* light field. The reconstructed light fields were combined with the dawn production casts to provide an estimate of total daily production through the water column at each station for a variety of light conditions (Morel et al. 1996, Tilstone et al. 2003, Lorenzo et al. 2004, Hickman In prep).

2.1.8 Other data

Photosynthetically available radiation

[*J. Tweddle*]

Photosynthetically available radiation (PAR) through the water column was measured using a Chelsea Instruments 2π PAR Irradiance Sensor, attached to the top of the CTD frame. A range of 2000-0.002 μE m^{-2} s^{-1} was covered. Errors associated with the instruments were small in comparison to variations due to shading by the CTD package and the ship, or the ship's motion.

Phytoplankton

Water samples were fixed using Lugol's iodine and formalin for microscope identification and counts of phytoplankton using a Leica DMIRB light microscope. [*Y.N. Kim*]

Analytical flow cytometry was carried out on stored water samples following Zubkov et al. (1998) on a Beckton Dickinson FACSort flow cytometer. [*Y.N. Kim (JR98), C.M. Moore (CD173)*]

In situ Fast Repetition Rate Fluorometry

[*J. Tweddle, C.M. Moore*]

Two Chelsea Instruments Fast^{tracka} FRRF instruments were deployed attached to the CTD frame during JR98 and one instrument during CD173, in order to obtain vertical profiles of phytoplankton physiological parameters through the water column. SeaSoar also carried an FRRF instrument during both cruises. Another instrument was kept permanently attached to the ships non-toxic supply in order to provide a continuous record of changes in near surface phytoplankton physiology and to provide a comparison and means of data quality verification with the other instruments deployed *in situ*. During processing, saturation curves measured by the FRRF were fitted to a physiological model (Kolber et al. 1998) using software provided by Sam Laney (Laney 2000). For the FRRF on the CTD and SeaSoar results from the dark chamber only were used in order to limit contamination of the results by ambient irradiance. Further

deployment information can be found in the cruise reports held at BODC (www.bodc.ac.uk).

SURFMET underway system

[*UKORS*]

The SURFMET system on both JR98 and CD173 recorded sea surface data every 30 seconds, including temperature, salinity, fluorescence, transmittance, PAR, total irradiance, air pressure, temperature and humidity, and absolute wind speed and direction. This was merged with GPS data, and depth from the ships ADCP (JR98) or echosounder (CD173). The data has not been calibrated, with the exception of [Chl *a*] for which underway and CTD surface water sample [Chl *a*] was used as a calibration. All data, with the exception of [Chl *a*] was therefore considered in a relative, not absolute, sense.

2.2 Data analysis and statistics

This section will deal with both with general data analysis and statistical techniques, and analysis specific to an instrument or methodology used in this thesis.

2.2.1 Confidence in the data

Confidence intervals

Confidence intervals are a way by which to express the range of measurements expected by a series of random samples. The confidence intervals quoted throughout this thesis were calculated at 95% confidence, meaning there was a 95% chance any measurement would be within those limits. This can be calculated as ± 1.960 × the standard deviation of normally distributed data (Moore & McCabe 1998), or by using a bootstrapping technique.

The confidence interval of a data value is distinct from its error. The error is the precision range for the instrument or methodology. The confidence interval indicates how accurate the methodology or instrument is at catching the true population mean.

Bootstrapping

Bootstrapping is a statistical method used to calculate confidence

intervals on small data populations (Efron & Gong 1983). It is a useful method of calculating confidence intervals when there is insufficient data to calculate them accurately using standard deviation and is acceptable if you are sampling a population with a mean and any distribution around it. The distribution is not required to be normal, which allows it to be used on FLY turbulence data. The population is re-sampled many times, and a mean value taken for each set of re-samples. A distribution of those means is then calculated, and from this a confidence interval can be derived.

2.2.2 Population differences

Analysis of variance (ANOVA) between data populations was used to compare population means for significant differences. Microsoft® Excel XP was used to run the calculations, with the confidence level set to 95% ($\alpha = 0.05$). Results were stated as an *F* value and *p* value, which work in concert to allow interpretation of the results.

The *F* value is a comparison of the variance of the means between the populations and of the variance within the populations (Moore & McCabe 1998):

$$F \approx \frac{variance\,amongst\,the\,population\,means}{variance\,within\,populations} \qquad \textbf{Eq. 2.9}$$

ANOVA tests the null hypothesis that all the populations are similar. The *F* value increases as the ratio of variance amongst the means' of the populations

to variance within the populations increases. A low F value indicates there is less variance between population means than there is within the populations and so would occur when the populations vary more internally than between populations.

The p value gives the probability of obtaining the calculated F value (or larger) if the populations are similar. The higher the p value, the more likely that F value could occur with the populations being similar. If the p value is lower than the significant level of 0.05 (95%) then the calculated F value is not probable if the populations are equal, and the populations are significantly different. Excel also calculates a critical value of F, F_{crit}, for which p= 0.05. Therefore, F values less than the F_{crit} (p values greater than 0.05) indicate the populations being significantly similar, and F values greater than the F_{crit} (p values less than 0.05) indicate the populations being significantly different.

2.2.3 Modelling data trends

Least-squares analysis

Analysis of many of the results uses a regression onto some function, e.g. to find a relationship between nitrate and temperature. All of the regressions are based on least squares analysis.

Model 1 least-squares analysis fits the data by minimising total squared differences between the observations and the predictions of the regression:

$$\sum (error)^2 = \chi^2 = \sum \left(y_i - f(x_i)\right)^2 \qquad \textbf{Eq. 2.10}$$

for observations y_i and x_i and modelled line $f(x_i)$.

Least-squares analysis can be used to fit a variety of models to data, such as a basic linear regression, or more complicated functions such as Gaussian curves, or a spring-neap tidal cycle time series.

Linear Regression

The most common regression is linear regression, used in many of the calibration procedures, and is particularly important in determination of nitrate gradients.

The linear regression models employed fit a line to the data points using least-squares analysis (Eq. 2.10). The square of the correlation, r^2, between x_i and y_i, gives the fraction of the variation in y_i that is explained by the least-squares regression of y_i on x_i.

Both Golden Software's Grapher program and the statistical package R were used to perform linear regressions.

Gaussian curve fitting

Quantifying the results of the satellite image analysis required fitting the data to a more complicated regression than a simple linear type. The data was fitted to a Gaussian curve, superimposed on a straight line, which can be described by:

$$Y = A1 \times \exp^{-\left[(x - A2)^2 / A3^2\right]} + (A4 \times x) + A5 \qquad \textbf{Eq. 2.11}$$

where-

x = predictor value of Y

$A1$ = height/depth of curve

$A2$ = x co-ordinate of curve's peak/trough

$A3$ = ½ width of curve, taken at ½ height of curve

$A4$ = slope of line curve superimposed upon

$A5$ = vertical offset curve sits upon

The maximum/minimum value of Y occurs when x is equal to $A2$, and can be derived from Eq.2.11:

$$Y_{\max/\min} = A1 + A5 + (A4 \times A2) \qquad \textbf{Eq. 2.12}$$

This was not a standard curve fitting found in most software and so a MATLAB program was written [*J. Tweddle*] to perform the regression and fit data to a Gaussian curve using least squares analysis (Bevington & Robinson 1991). Unfortunately, due to coding errors, this did not work, so an acquired FORTRAN code (personal communication, J Sharples) was used. Initial estimates of $A1$, $A2$, $A3$, $A4$ and $A5$ were supplied to the fitting program, and each of the 5 variables altered in turn to search for a minimum χ^2 value (Eq. 2.10) between the predictor of Eq. 2.11 and the observations. Several iterations of this process were carried out, until χ^2 did not change appreciably between iterations.

2.3 Calculation of Nitrate fluxes

[*J. Tweddle*]

Equation 2.4 was used to calculate vertical nitrate fluxes, J_N, into the subsurface chlorophyll maximum at all sampled stations. In order to do so assessments both of the nitrate concentration gradient, $\Delta N/\Delta z$, and the vertical diffusivity, K_z, were required. K_z was acquired from FLY.

The vertical nitrate flux was from high nitrate concentrations below the thermocline to low nitrate concentrations within and above the thermocline. A point flux measured at the base of the thermocline would be a valid estimate of the new nitrate supplied per unit time from the bottom mixed layer to phytoplankton in the SCM and surface mixed layer. In other words, nitrate supply supporting new production.

However, neither the nitrate gradient nor K_z were known at very fine depth resolution, but instead each required a finite depth over which to be measured or calculated. J_N was therefore taken to be the average of calculated J_N, $\overline{-K_z\left(\frac{\Delta N}{\Delta z}\right)}$, within a ± 0.25 ^{o}C temperature range situated at the base of the thermocline. This range was chosen as a realistic vertical scale over which $\Delta N/\Delta z$ and K_z were physically and biologically resolvable and relevant. Temperature was used rather than depth due to vertical movements of the thermocline and SCM over time at many stations. Alternatively, σ_t could be used, however in the Celtic Sea density is primarily controlled by temperature.

The position within the nitrate profile of the isotherm at the centre of the temperature range had to be chosen carefully at each station. Allowing the temperature range to extend below the base of the nitracline (Fig 2.3 a, range 1) will give a high J_N value due to high K_z, if $\Delta N/\Delta z$ is non-zero. However uptake of upwards moving nitrate would not be high as not all of the nitrate flux would reach the SCM. Much of the nitrate would be stirred downwards again by the high vertical diffusivity below the thermocline.

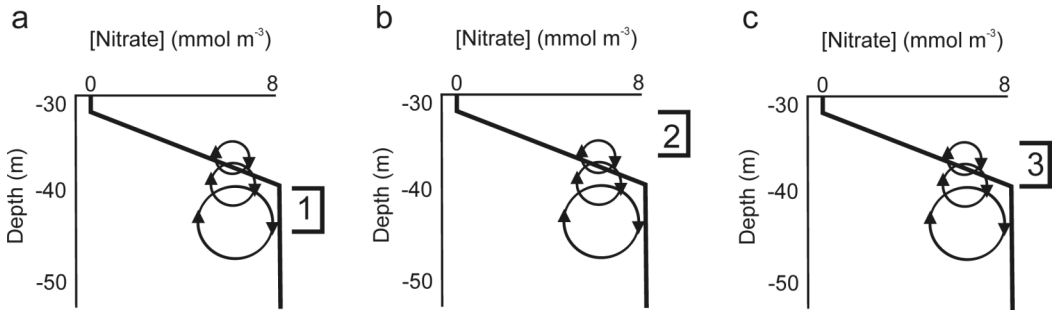

Figure 2.3

Schematic of a typical Celtic Sea nitracline. The thick black line represents nitrate concentrations. The arrowed circles represent the vertical diffusivity, K_z. The size of the circles is proportional to the strength of K_z. The bracketed numbers symbolise the averaging interval for J_N in each profile.

Placing the temperature range too high in the nitracline (Fig 2.3 b, range 2), would provide a real vertical flux of nitrate, but it will be of both nitrate from the bottom mixed layer which has not been subject to uptake lower in the SCM and regenerated nitrite produced within the SCM. J_N would not be a measure of all of the flux of new nitrogen into the SCM, as much would have been taken up by phytoplankton deeper in the SCM before reaching the temperature range over which J_N was calculated.

A temperature range placed at the base of the nitracline (Fig 2.3 c, range 3) will incorporate the upwards flux of new nitrogen from below the nitracline into the SCM where it will be subject to uptake and so not retuned downwards. Only in this position is J_N a measure of the nitrate supplied which will support new, and not regenerated, production. The temperature ranges for each station are given in Table 2.4. The errors associated with each J_N value were the combination of the errors in $\Delta N/\Delta z$ and K_z.

Although the analysed water samples gave accurate [Nitrate] (section 2.1.7), $\Delta N/\Delta z$ calculated from the samples was often of low vertical resolution ($\Delta z > 10$ m), and well sampled vertical profiles ($\Delta z \sim 2 – 5$ m) through the nitracline were taken only one to three times at each station. Therefore a suite of methods for assessing $\Delta N/\Delta z$ was developed, to allow evaluation of J_N through time at all sampled stations. All methods required the nitrate concentrations from water samples for calibration purposes.

Table 2.4

Temperature ranges over which J_N was calculated for each station.

Station	Temperature Range (^oC)
CS2a	13.25 – 13.75
CS1	10.4 – 10.9
CS3a*	11.6 – 12.1 (i)
	11.3 – 11.8 (ii)
CS3b*	12.25 – 12.75 (i)
	11.6 – 12.1 (ii)
CS2b	12.5 – 13
CS2c	13.25 – 13.75
B2a	10.5 – 11
B2b*	NA
OB	10.6 – 11.1

* During CS3a and CS3b advected patchiness caused J_N into the SCM to occur over two different temperature ranges. During B2b $\Delta N/\Delta z$ was estimated from the bottom and surface layer depths (see below for method details). This gave only one $\Delta N/\Delta z$ value for each profile, so no temperature range was needed.

ΔN/Δz measured by the SUV6

$\Delta N/\Delta z$ calculated from the SUV6 (see section 2.1.7) gave the best measurement of [Nitrate] gradient, with a high vertical resolution (equivalent to CTD bin size), reasonable errors (± 13–33 %) and a measurement of $\Delta N/\Delta z$ independent of other CTD or FLY parameters. To calculate J_N, K_z from all FLY casts carried out within 30 minutes, before and after, of each CTD cast were binned over 3m in the vertical, with the bins centred on the CTD/SUV6 data. A bin size of 3 m was used as it was felt to be a valid reflection of the vertical extend of the effect of K_z (personal communication, M. Palmer). The mean K_z in each depth bin over the hour was multiplied by the corresponding $\Delta N/\Delta z$ (Eq. 2.4) to calculate J_N. The range of errors was ± 52–60%, thus the 50% error from FLY dominated over the 13–33% error in $\Delta N/\Delta z$.

There were inaccuracies associated with the CTD and FLY measurements being spatially and temporally separated. The dynamic nature of the water column at some of the stations meant the water column temperature structure and the vertical positioning of properties, such as the nitracline, may have changed over the hour time period. It is difficult to assess how important the spatial difference was. The spatial extent of many of the physical phenomena looked at were of the scale 1-10 km, such as the wave length of internal waves, or horizontal patchiness in the thermocline. The ships were positioned as close as weather and sea conditions allowed, which equated to distances of less than 1 km at minimum, to a maximum of 2 km.

This method was used at CS1, CS3a and CS3b. The SUV6 was not deployed at CS2a, CS2b or CS2c, and malfunctioned during CD173.

ΔN/Δz derived from a Temperature to [Nitrate] relationship

At certain stations temperature and nitrate concentrations had a linear relationship through the thermocline. Temperature could be calibrated against water sample nitrate concentrations, [$Nitrate_{sample}$]:

$$\left[Nitrate_{sample} \right] = m \times T + c \qquad \textbf{Eq. 2.13}$$

where T is temperature, and *m* and *c* are constants. The regression was fitted to all data from each station to obtain *m* and *c*, and the regression also calculated for each cast, then averaged to give mean values of *m* and *c*, and their associated uncertainties for each station (Table 2.5).

From the regression constants in Eq. 2.13:

$$\Delta N/\Delta z = \left(\Delta T/\Delta z\right) \times M^{-1} \text{ (± } m \text{ error)} \qquad \textbf{Eq. 2.14}$$

Obtaining Δ*N*/Δ*z* directly from temperature gave high vertical resolution of the nitrate gradient (Δ*z* equivalent to the CTD or FLY vertical bin size). The assumption was made that the temperature to nitrate relationship would be similar between CTD and FLY temperature data. The relationships were applied preferentially to FLY to estimate Δ*N*/Δ*z* profiles, as FLY profiled the water column at each station more frequently than the CTD. Using the temperature to nitrate relationship with FLY eliminated inaccuracies due to the differing sampling times and positions of CTD and FLY casts, as with FLY K_z was available co-located in time and space for every temperature (Δ*N*/Δ*z*) data point.

Table 2.5

Calibration constants between temperature and nitrate, and associated errors, of Eq. 2.13 for stations without an SUV6.

Station	*n*	*p*	r^2	*m*	*m* error (±%)	*c*	*c* error (±%)	J_N error (±%)
CS2a	81	<0.001	0.87	-2.38	30.8	38.11	25.0	58.8
CS2b	44	<0.001	0.98	-2.44	6.6	37.97	4.9	50.4
CS2c	38	<0.001	0.96	-2.41	10.6	37.93	8.5	51.1

The method allowed estimates of J_N to be attempted where no SUV6 data was available and a strong relationship could be found between temperature and [Nitrate] gradients, i.e. at the shelf break.

$\Delta N/\Delta z$ derived from a Temperature and [Chl a] to [Nitrate] relationship

At CS3a and OB a simple temperature to [$Nitrate_{sample}$] relationship did not exist, however including [Chl *a*] in the regression allowed reasonable estimates of [Nitrate] (± rms of regression, mmol m^{-3}) to be calculated. It was not possible to get a TChl:N relationship for B2a, B2b or CS3b. Although SUV6 data was available for CS3a obtaining a temperature and [Chl *a*] to [Nitrate] relationship allowed comparison of the different methods. Hence all possible methods were used to calculate $\Delta N/\Delta z$ and vertical nitrate fluxes at CS3a.

CS3a: $$[Nitrate] = 55.9 - 6.6(T) + 0.2(T^2) - 2.1([Chl\,a]) \quad \textbf{Eq. 2.15}$$

n = 148, $p < 2.2 \times 10^{-16}$, $r^2 = 0.96$, rms = 0.6 mmol m^{-3}

$\Delta N/\Delta z$ error = ± 0.9 mmol m^{-4} (± 129%)

J_N error = ± 138%

OB: $$[Nitrate] = 307.1 - 61.4(T) + 4.1(T^2) - 0.1(T^3) - 2.4([Chl\,a]) + 1.2([Chl\,a]^2) \quad \textbf{Eq. 2.16}$$

n = 69, $p < 2.2 \times 10^{-16}$, $r^2 = 0.99$, rms = 0.4 mmol m^{-3}

$\Delta N/\Delta z$ error = ± 0.6 mmol m^{-4} (± 75%)

J_N error = ± 90%

FLY did not carry a fluorometer and so this relationship could only be applied to CTD data. K_z was extracted as before (section *ΔN/Δz measured by the SUV6*). This again involved uncertainties associated with differing times and positions of the CTD and FLY casts.

Although neither the T:N or TChl:N method gave robust relationships at B2a, further investigation into the vertical structure of the water column revealed two distinct SCM forms which occurred at different times. One displayed a diffuse SCM when plotted against temperature ($B2a_d$), the other an asymmetrical profile ($B2a_{as}$). It was possible to obtain a T:N relationship for $B2a_d$ and a TChl:N for $B2a_{as}$, and apply each to CTD profiles as appropriate to the SCM form of that cast.

$B2a_d$: $[Nitrate] = 254.0 - 50.0(T) + 3.3(T^2) - 0.1(T^3)$ **Eq. 2.17**

$n = 44$, $p < 2.2 \times 10^{-16}$, $r^2 = 0.97$, rms = 0.6 mmol m^{-3}

$\Delta N/\Delta z$ error = ± 0.9 mmol m^{-4} (± 162 %)

J_N error = ± 170%

$B2a_{as}$: $[Nitrate] = 70.2 - 8.9(T) + 0.3(T^2) - 4.1([Chl\,a])$ **Eq. 2.18**

$n = 52$, $p < 2.2 \times 10^{-16}$, $r^2 = 0.98$, rms = 0.5 mol m^{-3}

$\Delta N/\Delta z$ error = ± 0.6 mmol m^{-4} (± 123%)

J_N error = ± 133%

ΔN/Δz estimated from bottom and surface mixed layers.

To enable an estimation of J_N where no SUV6 data was available, and neither a temperature to [Nitrate] nor temperature and [Chl *a*] to [Nitrate] relationship was found to be suitable a final method was developed.

$$J_N = -K_z \times \left(\frac{\left[N_{bottom\,mixed\,layer} \right] - \left[N_{surface\,mixed\,layer} \right]}{z_{bottom\,mixed\,layer} - z_{surface\,mixed\,layer}} \right)$$

Eq. 2.19

Each station's [$Nitrate_{sample}$] were plotted against temperature, and used to evaluate bottom and surface mixed layer [Nitrate] ([$N_{bottom\ mixed\ layer}$] and [$N_{surface\ mixed\ layer}$] respectively). The temperatures above and below which these layers occurred marked the boundaries of the bottom and surface mixed layers with the nitracline. The depths of the two isothermals at each CTD cast were then extracted and used to ascertain the thickness of the thermocline, from $Z_{bottom\ mixed\ layer}$ to $Z_{surface\ mixed\ layer}$. The error in $\Delta N/\Delta z$ was around ± 0.14 mmol m^{-4}. The error in J_N was taken as a combination of the FLY and $\Delta N/\Delta z$ errors.

This method could be applied to both CTD and FLY data, assuming [Nitrate] had the same relationship with temperature for FLY as for the CTD. K_z was taken to be the mean K_z of each profile within the 10 m above the base of the nitracline. The mean K_z between the two isothermals used to estimate $\Delta N/\Delta z$ was not used as this would include the low values of K_z well within the thermocline and provide a value of K_z which was below that which was applicable for calculating J_N.

Comparison of J_N estimation methods

At CS3a SUV6 derived $\Delta N/\Delta z$ was available, along with $\Delta N/\Delta z$ derived from a temperature to [Nitrate] relationship and from the mixed layer estimation. Table 2.6 gives the daily average values and errors of $\Delta N/\Delta z$, K_z and J_N, calculated as means of the 25hr data sets for each. In brackets are the bootstrapped 95% confidence intervals.

Comparison of the 25 hour time series using ANOVA revealed no significant differences in J_N between the methods (F=0.05, F_{crit}=2.6, p=1). Further investigation ensured the similar values in J_N were due to similarities in $\Delta N/\Delta z$ and K_z between methods. However it must be recalled that J_N is $\overline{\left(-K_z\left(\frac{\Delta N}{\Delta z}\right)\right)}$ and not $\overline{(-K_z)}\times\overline{\left(\frac{\Delta N}{\Delta z}\right)}$ for each profile.

K_z demonstrated no significant difference between the various methods (F=0.25, F_{crit}=2.6, p=0.86). $\Delta N/\Delta z$ calculated using the mixed layer method on both CTD and FLY temperature were lower than $\Delta N/\Delta z$ from the SUV6. However, this change of ~50% is masked in the J_N calculations by the large variations in K_z. $\Delta N/\Delta z$ values appear to only have little significant affect on J_N, only providing a way to estimate the base of the nitracline, over which J_N represents a flux of new nitrate into the SCM.

In conclusion, although there are variations between $\Delta N/\Delta z$, they are small in comparison to K_z. K_z and J_N are statistically similar between all methods, therefore the methods are all inter-comparable.

Although the methods are all valid and comparable, an order of preference was established as to their use. Small variations in $\Delta N/\Delta z$ were not of

great importance in affecting the value of the nutrient flux, however good vertical resolution is preferred to enable accurate location of the position of the nitracline, and estimation of the most relevant flux value for new nitrate supply to the SCM. As such, the SUV6 method was the preferred method, followed by the temperature, or temperature and [Chl *a*], to [Nitrate] method. Finally, if none of the other methods could be reasonably applied, J_N was calculated from the mixed layer method. If the mixed layer method was used, applying it to FLY temperature was preferable, as it gave a more synoptic temporal view.

Table 2.6

Comparison of methods of estimating J_N at CS3a

Method	$\Delta N/\Delta z$ (mmol m^{-4})	K_z (m^2 s^{-1})	J_N (mmol m^{-2} day^{-1})
SUV6	-0.6 ± 0.1 (-0.8 – -0.5)	$13.3x10^{-5} \pm 6.6x10^{-5}$ ($1.8–37\ x10^{-5}$)	3.8 ± 1.9 (0.8 – 10.5)
T:N	-0.7 ± 0.9 (-0.8 – -0.5)	$2.7x10^{-5} \pm 1.4x10^{-5}$ ($1.3–4.8\ x10^{-5}$)	1.7 ± 2.3 (0.6 – 3.1)
Mixed layer CTD	-0.3 ± 0.14 (-0.3 – -0.3)	$6.8x10^{-5} \pm 3.4x10^{-5}$ ($2.4–17.1\ x10^{-5}$)	1.5 ± 1.0 (0.6 – 3.6)
FLY	-0.3 ± 0.14 (-0.3 – -0.3)	$8.1x10^{-5} \pm 4.0x10^{-5}$ ($2.9–18.8\ x10^{-5}$)	1.8 ± 1.2 (0.7 – 4.3)

2.4 Remote Sensing

Satellite imagery is used in Chapter 6 to investigate temporal and spatial changes in sea surface temperature and [Chl *a*] over a variety of scales. Pre-processed images were obtained from the Remote Sensing Data Analysis Service (RSDAS) at Plymouth Marine Laboratory. The data was originally acquired directly from the satellites by the Dundee Receiving Station. Permission was obtained from both GES DAAC (Goddard Earth Sciences Distributed Active Archive Center) and RSDAS for use of SeaWiFS data. Images covered the Celtic Sea and part of the upper Bay of Biscay (45–55 ^{o}N, 0 – -11 ^{o}E), through the pre- and fully stratified period of March to August, for years 2000–2005.

2.4.1 Data extraction

Sea Surface Temperature

Sea surface temperature (SST, ^{o}C) data were taken from the Advanced Very High Resolution Radiometer (AVHRR) flown on the NOAA polar orbiting series of satellites. RSDAS provided images of sea surface temperature with land, sun-glint, and the majority of clouds masked. Sea surface temperature was extracted from the image by (RSDAS 2006):

$$SST\left({}^{0}C\right) = \left(pixel\,value * 0.1\right) + 0.5 \quad \pm 0.3\text{-}0.5\ {}^{o}\text{C} \qquad \textbf{Eq. 2.20}$$

using only the earliest pass of each day, minimising bias due to diurnal heating.

Chlorophyll a concentration

The NASA Sea-viewing Wide Field-of-view Sensor (SeaWiFS), flown on the SeaStar spacecraft, provided raw data for years 2000–2004. RSDAS processed the data using the current SeaWiFS instrument calibration file, with gain settings adjusted using the NASA vicarious calibration, and RSDAS land and cloud masks (personal communication, P. Miller, RSDAS). The OC4 algorithm (O'Reilly et al. 2000) was used calculate the surface in-water chlorophyll *a* concentration ([Chl *a*], mg m^{-3}). From the image (RSDAS 2006):

$$[Chl\,a]\left(mg\,m^{-3}\right) = 10^{[(pixel\,value*0.015)+\log_{10}(0.01)]} \quad \pm 30\%$$

Eq. 2.21

SeaWiFS single band 555nm normalised water leaving radiance (nLw_{555}, mW cm^{-2} um^{-1} sr^{-1}) was used as a proxy for suspended sediment and coccolithophore concentrations.

$$nLw_{555}\left(mW\,cm^{-2}\,um^{-1}\,sr^{-1}\right) = pixel\,value * 0.02$$

Eq. 2.22

2005 [Chl *a*] and nLw_{551} RSDAS processed data were taken from the NASA Moderate Resolution Imaging Spectroradiometer (MODIS) instruments, flown on the Terra and Aqua satellites. [Chl *a*] and nLw_{551} were extracted from the images as with SeaWiFS [Chl *a*] and nLw_{555} (Eq 2.23 & 2.24 respectively).

nLw_{555} and nLw_{551} are not incorporated in the [Chl *a*] algorithm, and so do not directly affect [Chl *a*] values. However the presence of a coccolithophore bloom, partially defined by nLw_{555} values above 0.9 mW cm^{-2} um^{-1} sr^{-1} (Cokacar et al. 2004), will affect the determination of [Chl *a*], giving potentially extraneous Chl *a* concentrations. $nLw_{555/551}$ data were used to assist in analysis and possible removal of spurious [Chl *a*] values.

Data selection

Three transects were selected which crossed the Celtic Sea shelf break (Fig 2.1 & Table 2.7) in order to compare regions of different h/u^3 values over the shelf margin of the shelf break. Shelf break position was determined by the position of the 200 m isobath.

A MATLAB script was written to extract data at 1 km intervals along each transect, from SST, [Chl *a*] and nLw images. At each km the pixel centred closest to that transect point was selected as the centre pixel of a 10 km, 11 pixel wide "swath" perpendicular to the transect. Pixels masked due to cloud and sun glint were removed before the 11 data point swath was averaged to give a single value for that point on the transect. Spurious values caused by sub-pixel clouds, cloud edge effects, airplane vapour trails, or coccolithophore blooms were removed by eye before further analysis took place.

It was determined from SST images that stratification had fully developed, and from [Chl *a*] images that the spring bloom was over, by Yearday 150, in all years and under all transects. Thus further analysis was only carried

out on data acquired after Yearday 150.

Under Sat_1 data points with latitudes less than 47.9 were considered oceanic, and latitudes greater than 49 ^{o}N as shelf. Mean values of all transect pixels with oceanic or shelf latitudes were extracted from each image in order to evaluate the oceanic SST and [Chl *a*] (SST_{ocean} and $[Chl\ a]_{ocean}$) and shelf SST and [Chl *a*] (SST_{shelf} and $[Chl\ a]_{shelf}$).

Table 2.7

Satellite data transect positions.

Transect	Start Position	End position	Shelf break position
Sat_1	47.795^{o}N -10.363 ^{o}E	49.269^{o}N -8.563 ^{o}E	48.532^{o}N -9.463^{o}E
Sat_2	46.863^{o}N -8.200 ^{o}E	48.337^{o}N -6.400 ^{o}E	47.600^{o}N -7.300 ^{o}E
Sat_3	46.263^{o}N -6.400 ^{o}E	47.737^{o}N -4.600 ^{o}E	47.000^{o}N -5.500 ^{o}E

2.4.2 Image analysis

Normalisation of data

Both oceanic and shelf surface waters continue to warm throughout the summer stratified period, and surface chlorophyll *a* concentrations changed also. SST and [Chl *a*] at each transect data point were normalised against the transect mean:

$$SST_{\%} = \frac{SST_{pixel} - mean_{transect\ SST}}{mean_{transect\ SST}} * 100 \qquad \textbf{Eq. 2.23}$$

or

$$[Chl\,a]_{\%} = \frac{[Chl\,a]_{pixel} - mean_{transect[Chl\,a]}}{mean_{transect[Chl\,a]}} * 100 \qquad \textbf{Eq. 2.24}$$

where SST_{pixel} and $[Chl\ a]_{pixel}$ represents each original transect data point, and $mean_{transect}$ represents the mean of the transect for the image from which the data point came. Thus positive values represent a percentage increase in signal relative to the mean and, conversely, negative values a percentage decrease relative to the mean. $SST_{\%}$ and $[Chl\ a]_{\%}$ are therefore directly comparable throughout the stratified season in terms of relative increases and decreases in SST and [Chl *a*] over the shelf break. As a consequence of this, a single, yearly mean $SST_{\%}$ or $[Chl\ a]_{\%}$ value was calculated for each point on the transects, for each year. The normalisation of data also allowed direct comparison between SeaWiFS and MODIS originated data as it is a relative, not absolute, value.

Description of transects by Gaussian curve fitting

Gaussian curves were fitted to both non-normalised SST and [Chl *a*] and normalised $SST_{\%}$ and $[Chl\ a]_{\%}$ in order to describe the position (latitude), shape (½ width) and intensity (height) of the cool, high chlorophyll *a* band situated over the shelf break. This allowed easy comparison of the shape and situation of the SST and [Chl *a*] bands through time and between transects.

Spring-neap tidal cycle time series analysis

Analysis was carried out into variations in satellite transect data and Gaussian variables over spring-neap tidal cycles, by fitting data to a function with frequency ($^{2\pi}/_{14.8}$) using least squares analysis.

The time series was assumed to have form:

$$Y = \bar{y} + C\cos\left(\omega t - \phi\right) \qquad \textbf{Eq. 2.25}$$

expanded to:

$$Y = \bar{y} + \left(A\cos\omega t + B\sin\omega t\right) \qquad \textbf{Eq. 2.26}$$

where $\bar{y}$ is the mean value of the record, C is the amplitude, ω is the frequency ($^{2\pi}/_{14.8}$ for spring-neap cycles), ϕ is the phase lag, A and B are constants, and:

$$C = \left(A + B\right)^{1/2} \qquad \textbf{Eq. 2.27}$$

$$\phi = \tan^{-1}\left(\frac{B}{A}\right) \qquad \textbf{Eq. 2.28}$$

Least squares analysis was used to minimise the variance, χ^2, in Eq. 2.26 giving the best fit of the data to a function of spring-neap periodicity. A and B could then be substituted into Eq. 2.27 and Eq. 2.28, giving C and ϕ respectively. χ^2 was an indication of the strength of the fit of the data, a small χ^2 indicating a good fit, and a strong spring-neap periodicity in the data, and a large χ^2 indicating a poor fit, and a weak spring-neap periodicity.

2.5 Modelling

Phyto_1D (Sharples 1999), a one-dimensional (vertical) coupled physical-biological model, was used as the basis for all modelling work. It allows investigation into the effect of vertical turbulence throughout the year on water column primary production, for example the effect of the spring-neap tidal cycle on production in the SCM. Vertical mixing is driven by tides and daily mean meteorological data. The vertical mixing generated is only barotropic or surface wind in origin, so the model cannot simulate internally generated turbulence. It is thus applicable to problems on the shelf, but not at the shelf edge where baroclinic generated turbulence dominates.

Phyto_1D can be used in two modes, normal and cross-front. Normal simulates a year's worth of data for 1 position, with the tidal equations and the depth remaining constant throughout the year. This method was used to simulate data for the 25h station positions. Tidal components were taken from the Proudman Oceanographic Laboratory's Continental Shelf Sea Model (CS3, personal communication, POL).

The other mode, cross-front, runs as the normal mode, but will extract data for a single day out of the yearly data. Then a parameter such as depth, or tidal amplitude or phase can be changed to mimic a change in position, the model run again, and the new extracted data added to the previous runs' data. In this way a 'transect' can be built up, for example used in this thesis to simulate transects over banks. The assumption here is that vertical mixing will dominate

over horizontal processes.

Where appropriate in the thesis the mode of model run will be given, along with further details of experimental set-up. Bin size was always 1 m.

Chapter 3: Results from JR98 over the shelf; the subsurface chlorophyll maximum and vertical fluxes of nitrate.

3.1. Introduction

Historically it was thought the subsurface chlorophyll maximum (SCM) in shelf seas was supported by nutrients regenerated within the SCM itself (Pingree & Pennycuick 1975), by episodic supply from the bottom, nitrogen rich layer through wind driven mixing or upwelling (Pingree et al. 1978), or by adjustment of thermocline depth by the spring-neap tidal cycle incorporating nutrient rich water into the base of the thermocline (Holligan & Harbour 1977, Holligan 1978). Holligan et al. (1984b) calculated a daily background turbulent flux into the thermocline from the bottom mixed layer, but did not report on temporal variations.

Recent work has found barotropic generated shear can provide a source of turbulence to mix nitrate into the SCM from below (Sharples et al. 2001b). Also in recent years, work focusing on the physics of the shelf sea thermocline has highlighted mechanisms which can increase mixing within the thermocline, and between the thermocline and bottom mixed layer. Several sources of generation of internal mixing have been found, such as internal tides and waves generated at the shelf break (Rippeth & Inall 2002) which can provide a source

of mixing for vertical nitrate fluxes (Sharples et al. 2001a), internal mixing generated over banks on the shelf (Moum & Nash 2000, Nash & Moum 2001) and inertial oscillations (Rippeth et al. 2002, Rippeth et al. 2005) which also would supply turbulence to drive vertical nutrient fluxes (van Haren et al. 1999). These mechanisms have not previously been investigated fully in terms of their influence on nutrient fluxes and hence on biological production.

The purpose of cruise JR98 to the Celtic Sea in 2003 was to investigate physical influences on the subsurface chlorophyll maximum. A SeaSoar transect was carried out and several CTD and FLY stations were occupied over the shelf (CS3 and CS1, Fig 2.1). This chapter will present the results of cruise JR98 from over the shelf, describing the broad hydrographic characteristics, calculating the nutrient fluxes, and discussing these in terms of possible driving mechanisms, and of biological consequences.

3.2. Basic observations from a cross shelf transect.

The seafloor of the Celtic Sea continental shelf can be split into two topographic types; the mostly flat regions as found around CS3 and OB, and regions containing topographic features (banks), for example in the vicinity of CS1 and B2 (Fig 2.1). In 2003 a SeaSoar transect (see section 2.1.2 for methods) was carried out which ran from the shelf break, over the shelf, and into the mixed waters of the Irish Sea (Fig 3.1).

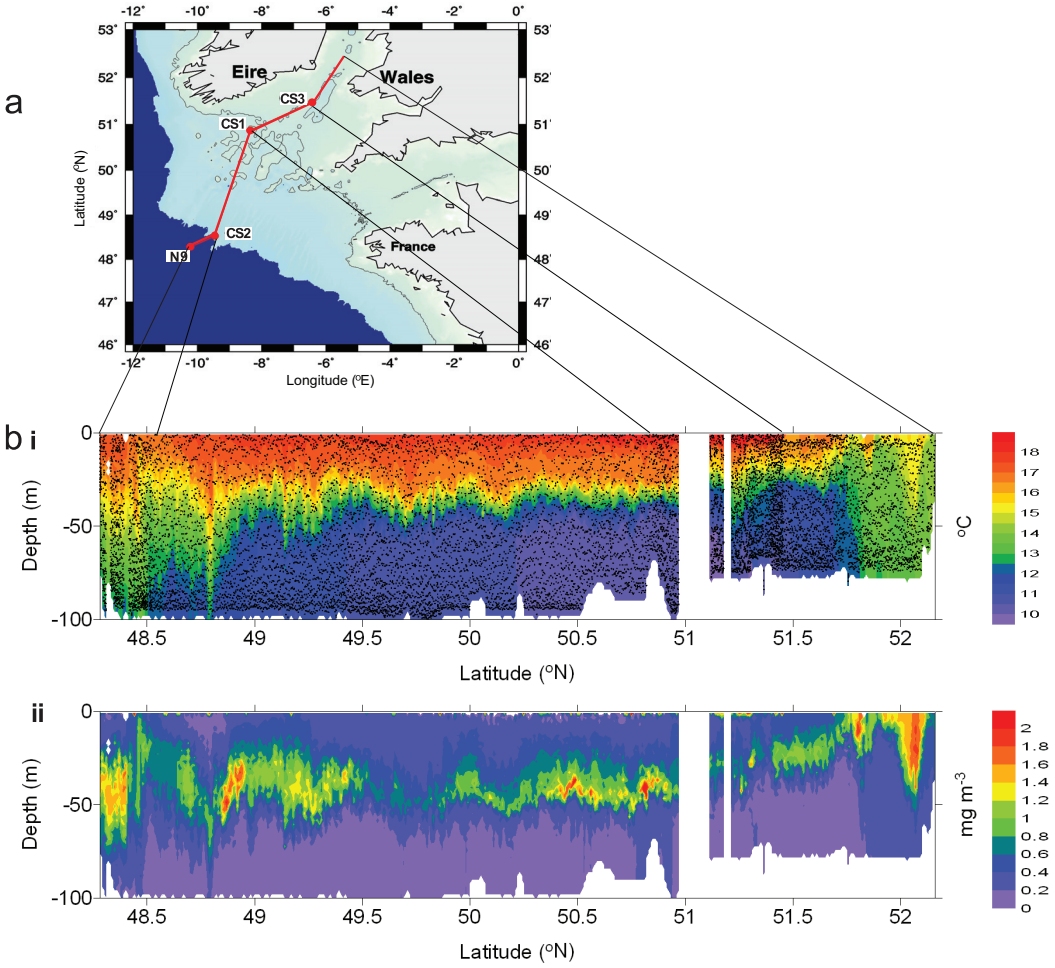

Figure 3.1

SeaSoar transect during cruise JR98 (14:30 August 8th to 01:30 August 10th 2003, Yearday 219 to 221), within the Celtic Sea. a) Transect indicated by solid red line, large red circles represent station positions. The bathymetry colour scale runs from 0 – 200 m (white – blue), with depths below 200 m masked dark blue. 100m seafloor contour marked in black. Bathymetry data is from IOC et al. (2003). b) SeaSoar i) temperature (every 10th data point indicated) and ii) chlorophyll *a* concentrations sections.

A tightly stratified water column dominated over the shelf (Fig 3.1 b i), with a more diffusely stratified region positioned over the continental shelf slope (approximately latitudes 48.3–48.5 ^{o}N). This region will be looked at in more detail in Chapters 5 and 6. Patchiness of chlorophyll *a* concentrations within the SCM was a feature across the entire shelf (Fig 3.1 b ii).

Focusing on the section of transect collected over the banks (Fig 3.1 a, red transect Latitudes 49.100 ^{o}N – 50.968 ^{o}N) it was noticeable that bottom layer density was often slightly reduced over the banks (Fig 3.2 ii). The lower densities extending to the seabed over banks either could imply mixing between the thermocline and bottom mixed layer, or could have been due to local warming of a shallower water column. Chlorophyll *a* concentrations ([Chl *a*]) also appeared to show a change in signature over some of the banks, compared to over flat topography, with an increase in [Chl *a*] both in the subsurface chlorophyll maximum (SCM) and bottom mixed layer (Fig 3.2 iii and iv). The changes in [Chl *a*] distribution in the bottom boundary layer suggested evidence of mixing between the thermocline and bottom mixed layer. If mixing was increased over banks, either by the barotropic tide or internally generated turbulence, it could increase the vertical supply of nutrients to the SCM, potentially increasing the amount of primary production which could be supported. The increased SCM [Chl *a*] suggests the possibility of greater primary production being supported in the SCM over the banks. However, increased mixing also suggests increased flux of organic carbon out of the SCM into the bottom boundary layer. Away from the banks patchiness in the SCM chlorophyll *a* concentration was also apparent (Fig 3.1 b ii), though not to the extent seen over the banks.

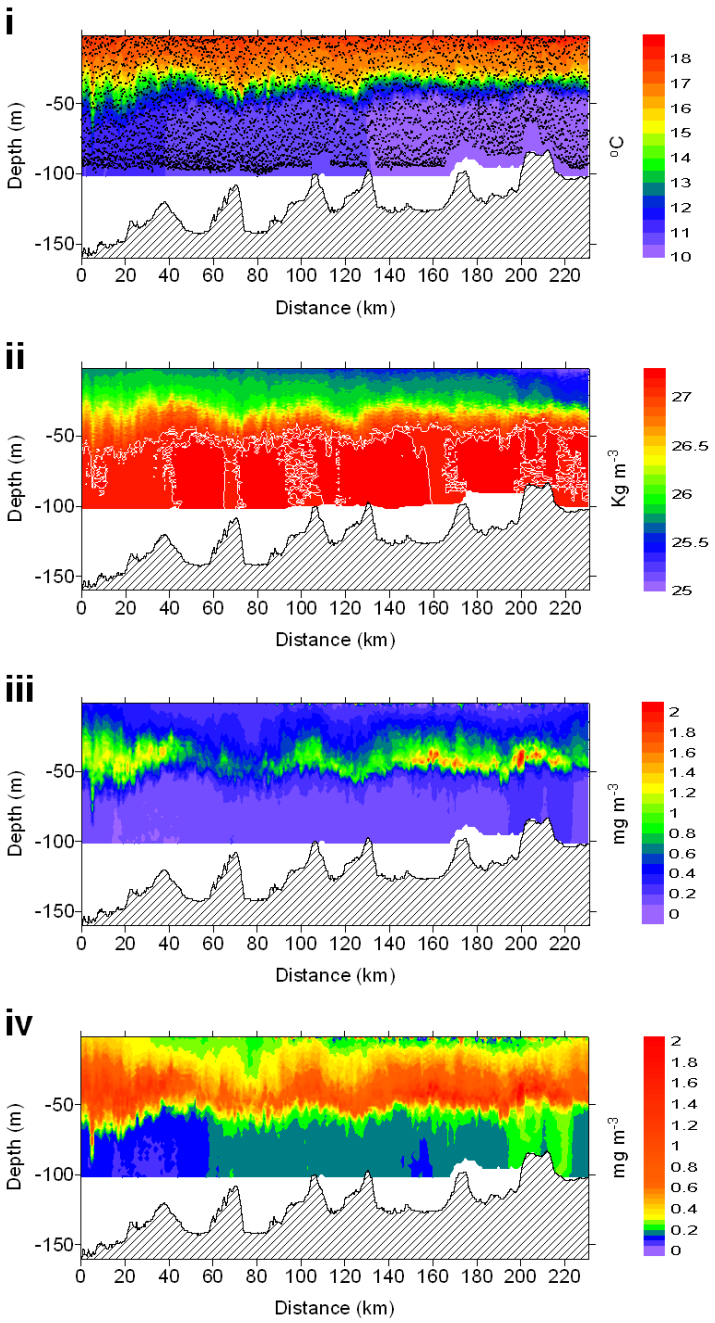

Figure 3.2

SeaSoar data over banks (Latitudes 49.100–50.968 ^{o}N, 00:30–17:10 August 9th 2003) during the cross shelf transect in 2003. SeaSoar i) temperature (every 10th data point indicated), ii) density (σ_t, white lines indicate 27.1 & 27.2 σ_t isopycnals), iii) chlorophyll *a* concentrations and iv) chlorophyll *a* concentrations (scale skewed to lower chlorophyll *a* concentrations).

3.3. CS3: Results from over a flat shelf site.

CS3 was situated in water of a depth of around 97 m over a topographically flat shelf seabed (Fig 2.1), in a region with a moderate stratification parameter (calculated from h/u^3, Simpson & Hunter 1974). Because of this the thermocline at CS3 should be subject to spring-neap tidal modification. CS3 was visited twice, approaching both neap (CS3a, 5^{th}–6^{th} August) and spring (CS3b, 10^{th}–11^{th} August) tides, in order to investigate differences in nutrient fluxes into, and organic carbon fluxes out of, the SCM during changing tidal conditions (see Chapter 2 for methods). It was hypothesised mixing at the base of the thermocline would be greater approaching spring, rather than neap, tides, thus increasing vertical fluxes towards spring tides.

3.3.1. Hydrographic characteristics of the thermocline, chlorophyll *a* concentrations and the nitracline.

Both CS3 station occupations exhibited a defined thermocline of the order 5–10 meters thick, with, at minimum, a 4.5 ^{o}C difference in temperature between the bottom and surface layers (Fig 3.3 a and b). Both CS3a and CS3b demonstrated gradual but weak stratification from the seabed to the base of the thermocline. Density was controlled primarily by temperature ($r^2 > 0.997$ for both stations, $p<0.05$).

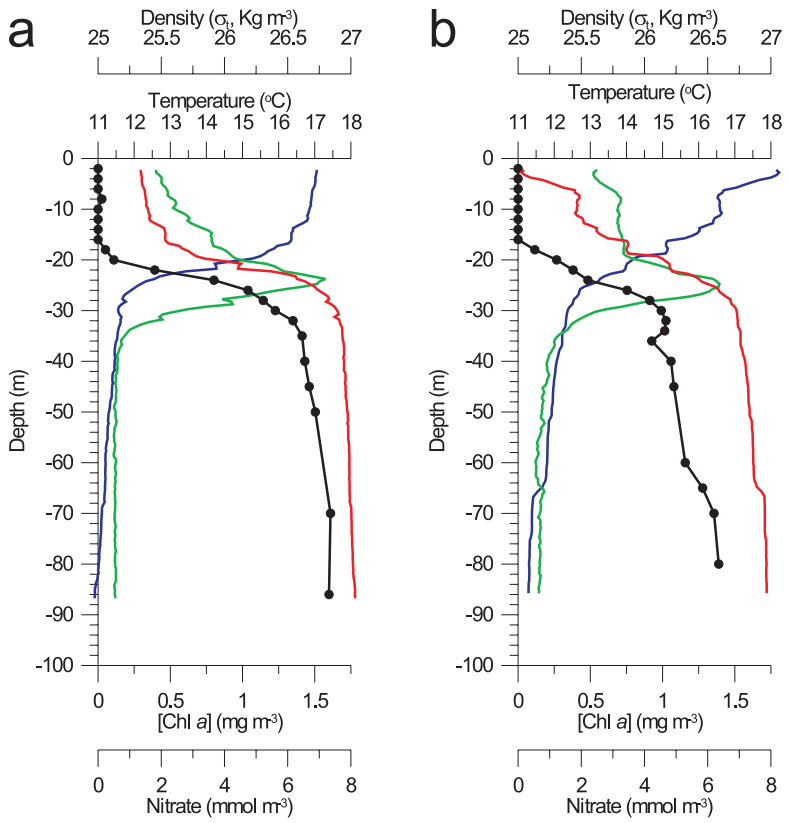

Figure 3.3

Examples of CTD and water sample nutrient profiles for a) CS3a (12:00, 5th August 2003, approaching neap tide) and b) CS3b (14:00, 10th August 2003, approaching spring tide). Blue represents CTD temperature, red CTD density, green CTD chlorophyll *a* concentrations, and black water sample nitrate concentrations.

During both station occupations the subsurface chlorophyll maximum was located within the thermocline (Fig 3.4). Previous literature (Holligan 1978, Holligan et al. 1984a, Nielsen et al. 1993) suggest shelf sea subsurface chlorophyll maxima are biomass maxima. At CS3 the ratio of fluorescence to cell volume for individual phytoplankton cells increased 3 fold between the

surface and the SCM accounting for some of the increase in fluorescence (Moore et al. 2006), however around 50% of the increase in [Chl *a*] was due to a total biomass increase (personal communication C.M. Moore). [Chl *a*] increases seen in the SCM and bottom layer during individual stations were most probably due to biomass increases rather than further changes in the cell fluorescence to cell volume ratio (personal communication C.M. Moore).

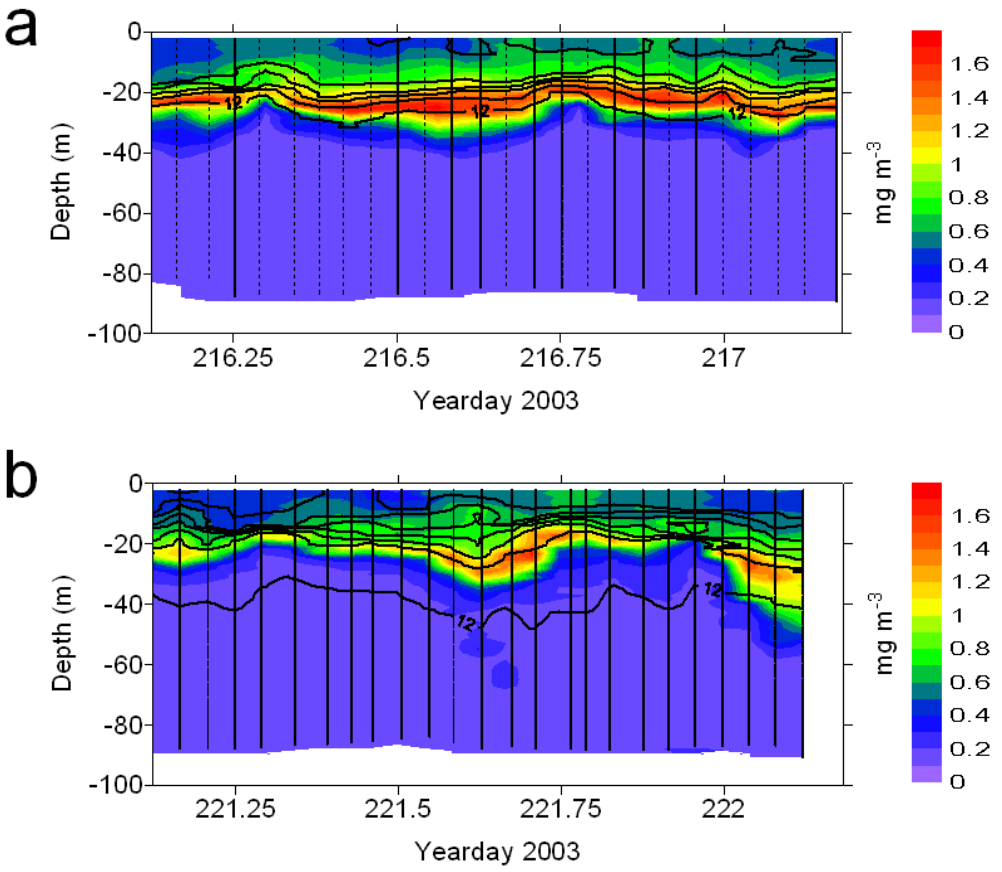

Figure 3.4

Time series of CTD chlorophyll *a* concentrations (coloured contours) and temperature (black lines, every 1 °C) against depth during a) CS3a (approaching neap tide) and b) CS3b (approaching spring tide). CTD cast times indicated.

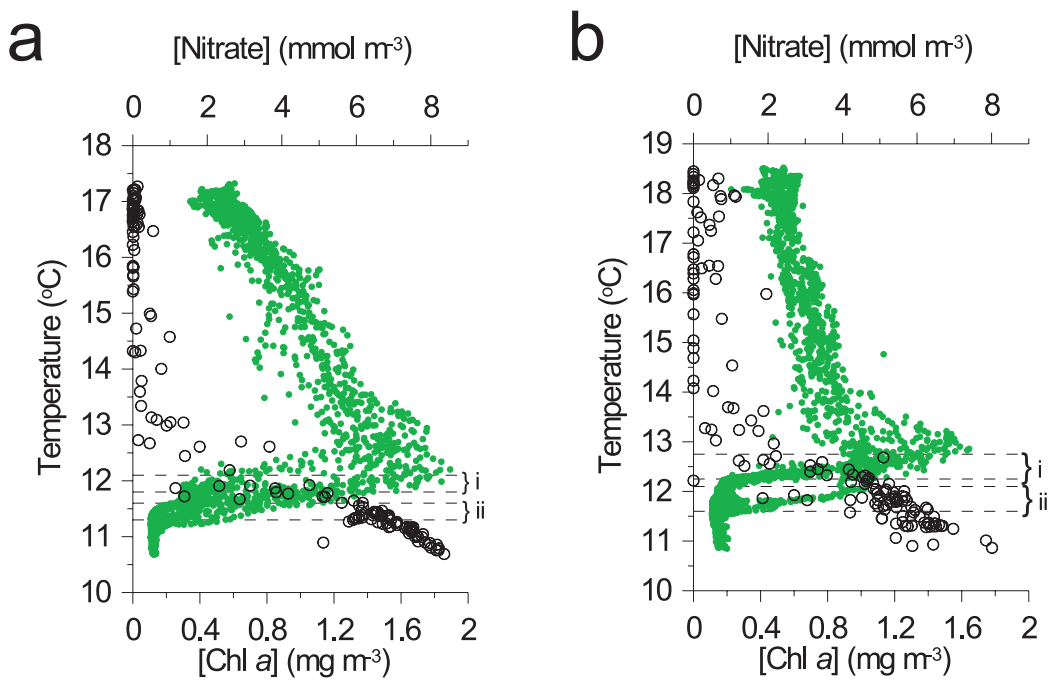

Figure 3.5

Stations a) CS3a (approaching neap tide) and b) CS3b (approaching spring tide) CTD chlorophyll *a* concentrations (green dots) and water sample nitrate concentrations (black circles) against temperature. Note differing scales. The black dashed lines mark the boundaries of the temperature range over which the vertical nitrate flux into the SCM was calculated for each profile. CS3a i) 11.6–12.1 °C, ii) 11.3–11.8 °C, CS3b i) 12.25–12.75 °C, ii) 11.6–12.1 °C.

When plotted against temperature (Fig 3.5) chlorophyll *a* concentrations exhibited an asymmetrical distribution within the thermocline, skewed to lower temperatures, i.e. increased [Chl *a*] at the base of the thermocline.

The thickness of the thermocline and SCM changed over time with a semi-diurnal signature (Fig 3.4) at CS3. Changes in thermocline thickness at a fixed point in space can be caused by a variety of processes, for example

turbulent mixing at the base of the thermocline, the action of mode 2 internal tides, or advection of different thermocline thicknesses past the stationary position.

Turbulent mixing is an irreversible process, resulting in warming of the bottom mixed layer, and would result in permanent thickening of the thermocline over the short timescales sampled at these stations. As the sampled CS3 thermocline narrowed again shortly after widening (Fig 3.4) this mechanism was unlikely to be the cause of periodic changes in the thermocline and SCM thickness at each station.

Advection could cause changes in thermocline thickness with time, by advecting horizontal patches of different thermocline vertical thickness past a station, thus changing thermocline thickness at that fixed point over time. The SeaSoar section carried out over the shelf in 2003 passed over CS3. The section surrounding CS3 (Fig 3.6) showed horizontal patchiness in both thermocline and SCM thickness, and SCM [Chl *a*]. The variability of the horizontal patches in the thickness of the SCM and thermocline, and SCM [Chl *a*], are similar in magnitude to the variability seen at CS3 over time. The horizontal patches appeared to be ~1–2.5 km in scale.

Horizontal patchiness at the time of station CS3a was estimated by assuming a comparatively stable velocity field in the region of CS3, and using the north-south and east-west velocities to calculate a cumulative displacement, i.e. the position of each water sample at the beginning of the CS3a time series (Fig 3.7). The passage of possible horizontal patches of diffuse thermocline and SCM and patches of high SCM [Chl *a*] (red ellipses marked on Fig 3.7 i, ii and iii respectively), which are of similar spatial scale to the horizontal patches seen

in the SeaSoar data, through CS3 would explain the variation in thermocline and SCM thickness and [Chl *a*] seen in the time series. CS3b showed similar evidence of advection.

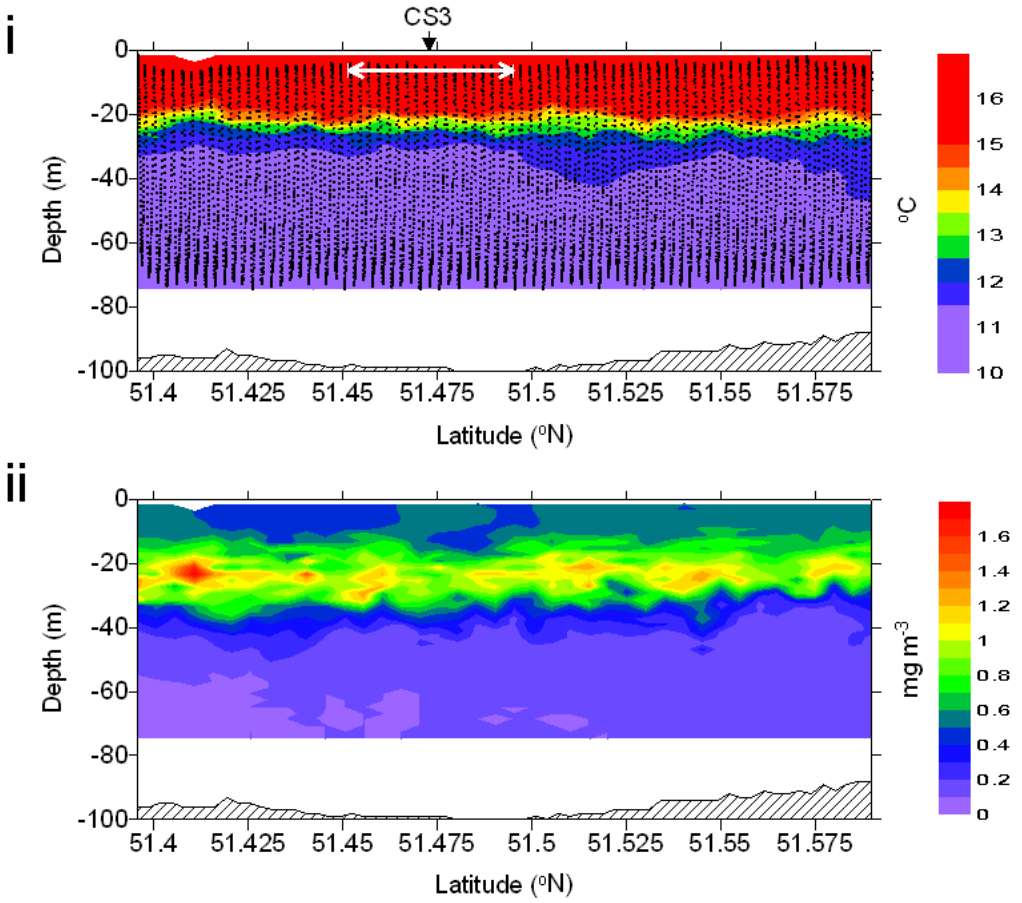

Figure 3.6

SeaSoar data around CS3 (Latitudes 51.396–51.590 °N, 23:10 9th August to 01:25 10th August 2003) during the cross shelf transect in 2003. SeaSoar i) temperature (SeaSoar data points indicated) and ii) chlorophyll *a* concentrations. The white arrow denotes approximately one tidal excursion.

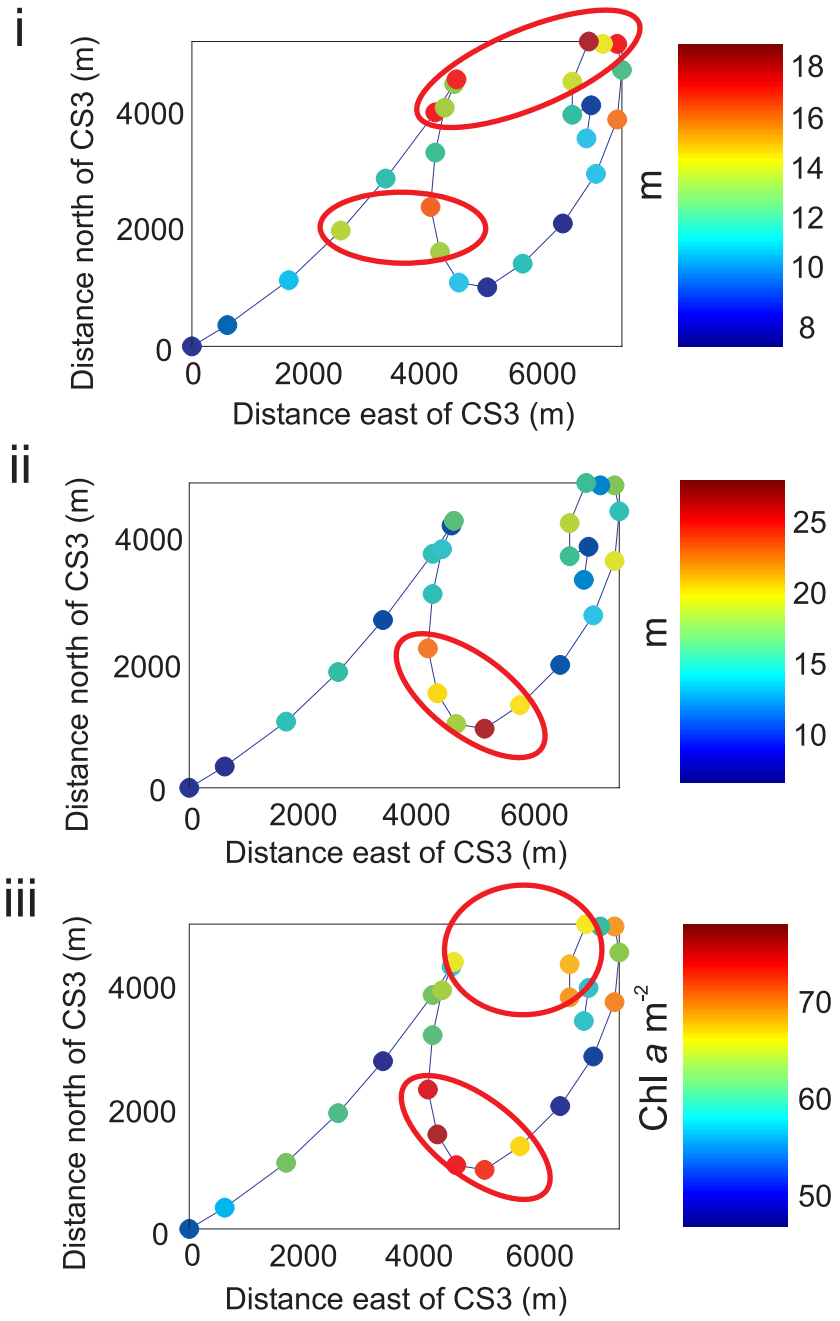

Figure 3.7

CS3a i) thermocline thickness, ii) SCM thickness and iii) total water column integrated Chl *a* concentrations, plotted against distance from CS3 as an indication of the original origin of the water parcels. Red ellipses suggest possible horizontal patches of i) a more diffuse thermocline, ii) a more diffuse SCM and iii) a higher [Chl *a*].

At both stations water samples were collected for nutrient analysis (section 2.1.7). Profiles of nitrate concentrations (Fig 3.3) from the samples showed a well defined nitracline, which corresponded in position to the location of the SCM (Fig 3.5). $\Delta N/\Delta z$ was estimated for the two occupations of CS3 using the methods described in section 2.3, *$\Delta N/\Delta z$ measured by the SUV6*. $\Delta N/\Delta z$ was closely correlated with the SCM (Fig 3.8), maximum $\Delta N/\Delta z$ occurring between the base of the SCM and peak [Chl *a*] values during both stations.

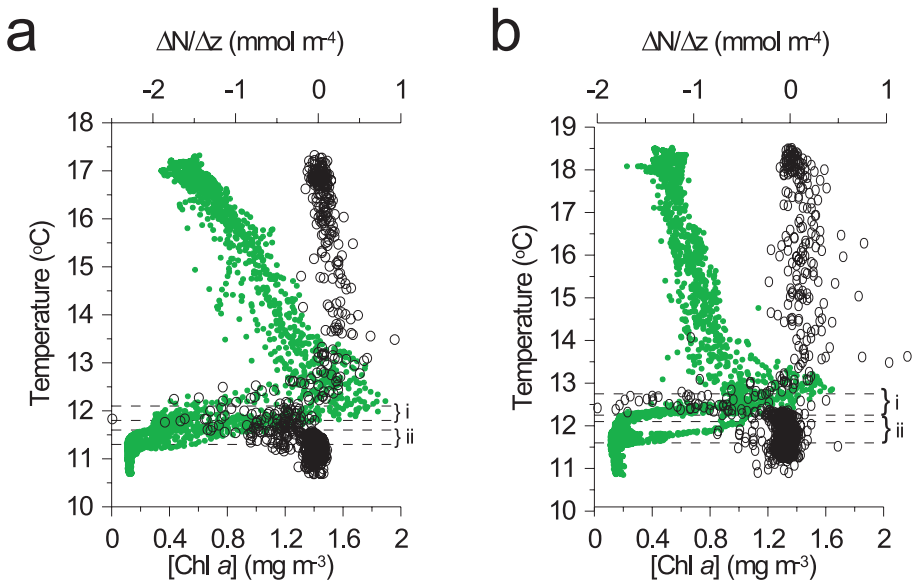

Figure 3.8

Stations a) CS3a (approaching neap tide) and b) CS3b (approaching spring tide) CTD chlorophyll *a* concentrations (green dots) and SUV6 derived nitrate gradients (black dots) against temperature. Note differing scales. The black dashed lines mark the boundaries of the temperature range over which the vertical nitrate flux into the SCM was calculated for each profile. CS3a i) 11.6–12.1 °C, ii) 11.3–11.8 °C, CS3b i) 12.25–12.75 °C, ii) 11.6–12.1 °C.

The mean $\Delta N/\Delta z$ at the base of the thermocline (Fig 3.9) was calculated for each profile during the stations. For both station visits two different temperature ranges were used to estimate mean $\Delta N/\Delta z$, reflecting the advection of patches with different temperature and [Chl *a*] profiles through CS3.

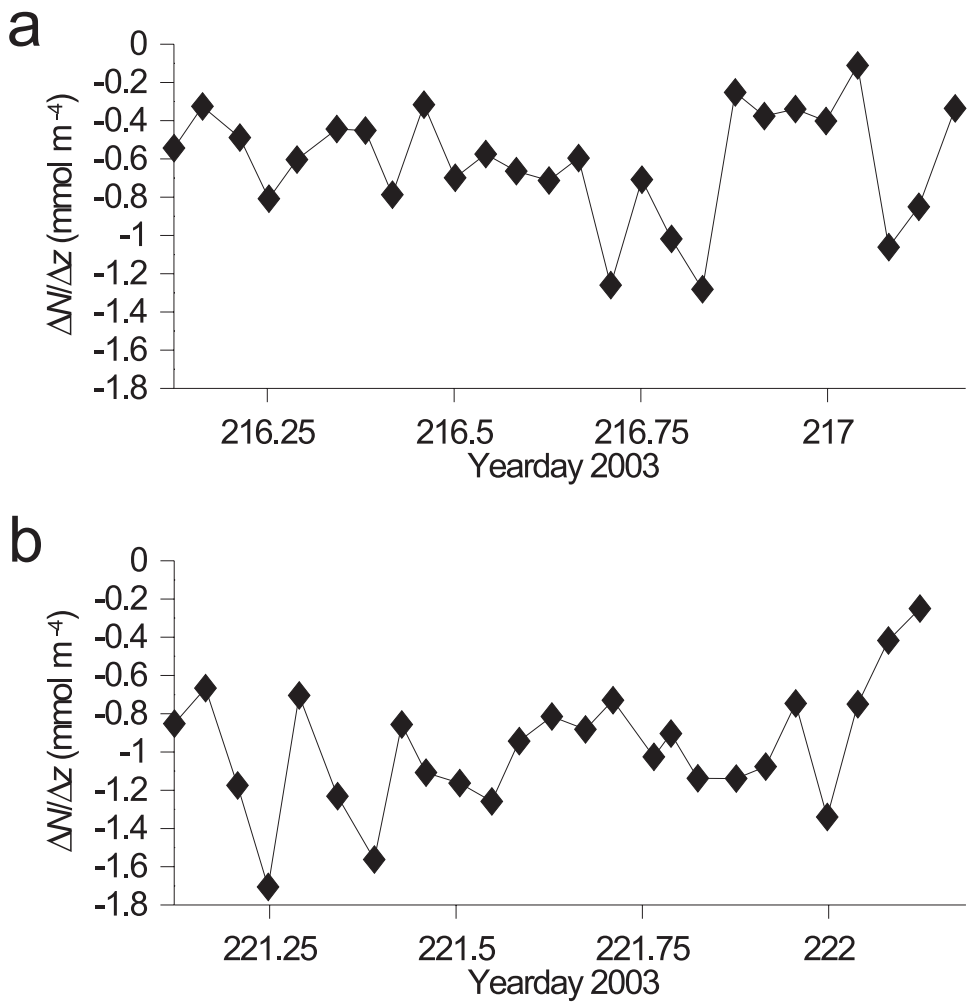

Figure 3.9

Mean nitrate gradient, over the temperature ranges used to calculate the vertical nitrate flux, for each SUV6 profile during a) CS3a (approaching neap tide) and b) CS3b (approaching neap tide).

There were significant changes in $\Delta N/\Delta z$ during each station (Fig 3.9). Δ[Chl *a*]/Δz, used as a proxy for nitrate uptake, explained ~18% of variability in $\Delta N/\Delta z$ during CS3a and 29% during CS3b (r^2=0.18 and r^2=0.29 respectively, p<0.05). Larger Δ[Chl *a*]/Δz values lead to increased $\Delta N/\Delta z$. CS3b, with higher Δ[Chl *a*]/Δz, showed significantly increased nitrate gradients at the base of the thermocline, compared to CS3a.

The nitrate gradient changed significantly between CS3a and CS3b (F=16.9, F_{crit}=4.0, p<0.05). CS3b, sampled approaching spring tide, had generally higher values of $\Delta N/\Delta z$ than CS3a, sampled approaching neap tide. Daily mean $\Delta N/\Delta z$ (Table 3.1), taken as the average of the time series, reflected this, with the nitrate gradient greatest at CS3b, and lowest at CS3a.

3.3.2. Currents, turbulence and mixing

ADCP data for CS3a (Fig 3.10 i) and CS3b (Fig 3.11 i) exhibited a strong semi-diurnal barotropic tidal signal. Near bed velocities during individual profiles reached maximums of ~-0.33 m s^{-1} at CS3a and ~-0.4 m s^{-1} at CS3b. The difference between velocities during the two CS3 visits was attributable to the spring-neap cycle, as CS3a was sampled approaching neap and CS3b approaching spring tides. The ADCP mooring positioned at CS3 also demonstrated spring-neap periodicity in maximum current velocities.

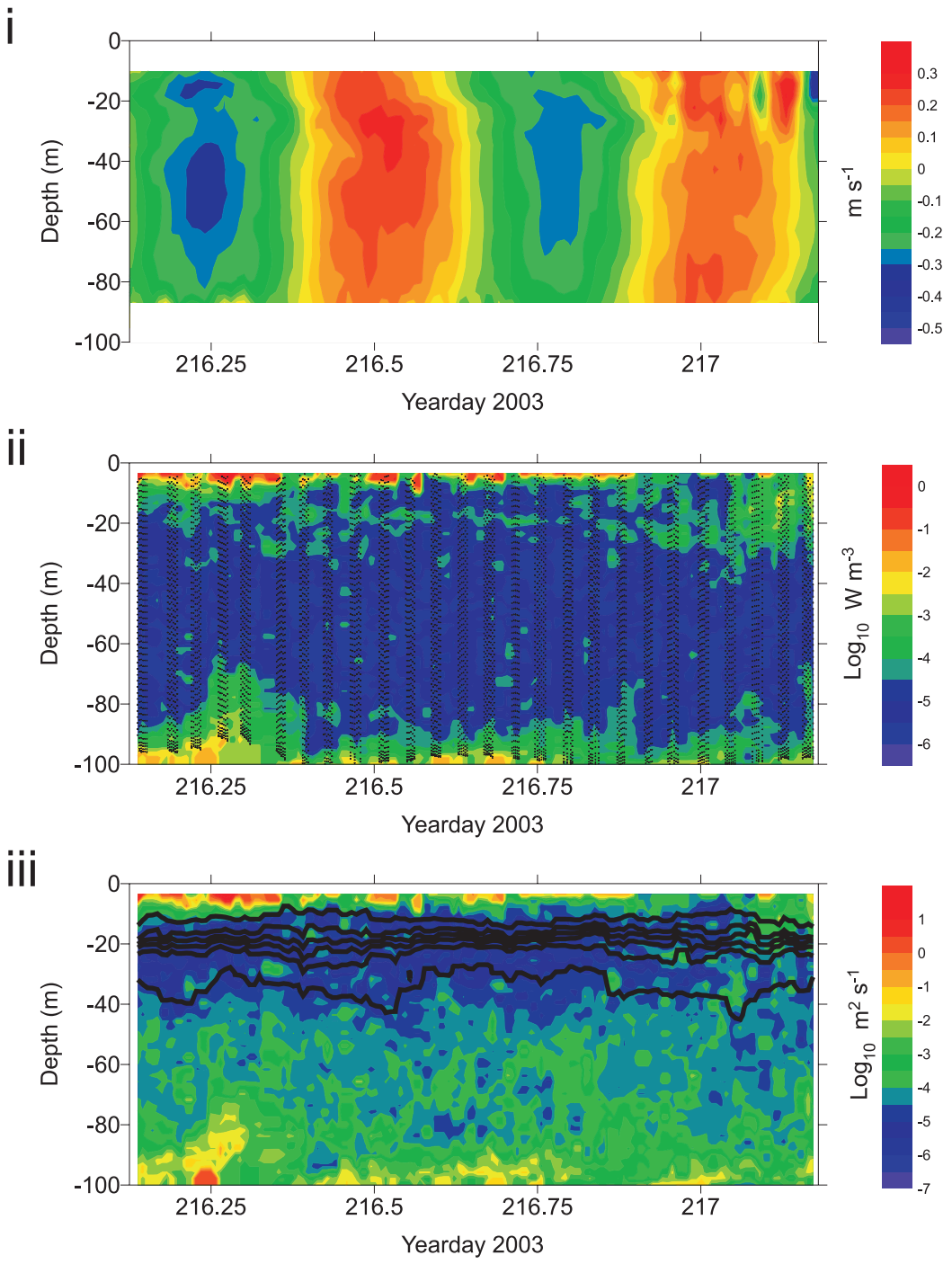

Figure 3.10

CS3a i) Ships ADCP northwards current velocity, ii) FLY turbulent dissipation rate (every 2nd FLY data point marked) and iii) FLY vertical diffusivity (coloured contours) and FLY temperature (black lines, 1 °C intervals, lowest isothermal =11.5 °C)

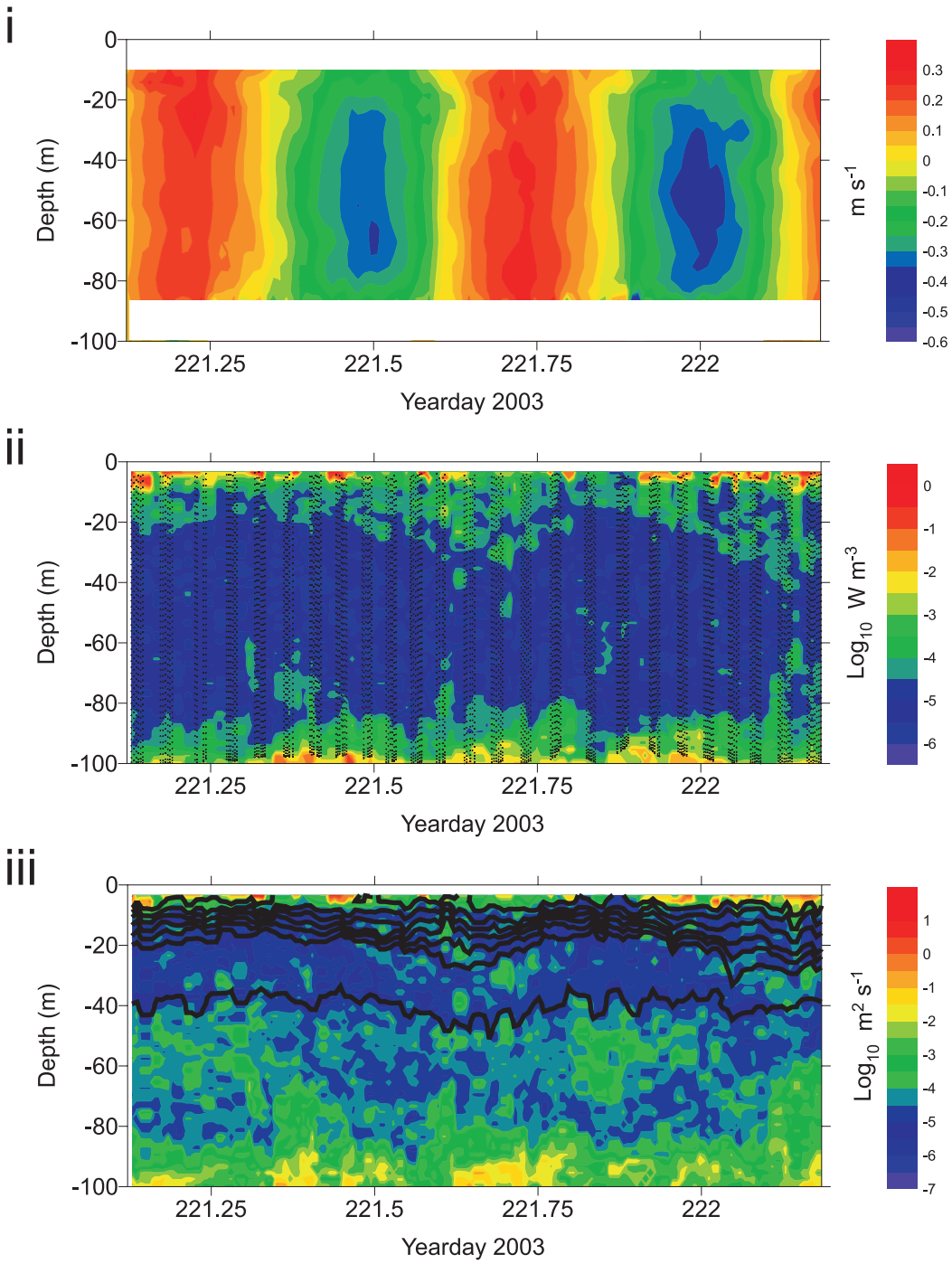

Figure 3.11

CS3b. As Fig 3.10 (lowest isothermal =12 ^{o}C).

A quarter-diurnal signal was present in the near bed turbulent dissipation rates (ε) (Figs 3.10 ii and 3.11 ii). ε reached a maximum of ~1.3 W m^{-3} towards the bed at CS3a and CS3b. Periods of maximum near bed ε correlated with times of maximum near bed current velocities. Analysis of individual profiles showed these quarter-diurnal increases in turbulent dissipation reached ~20–30 m above the sea bed at maximum extent. The lag between maximum near bed turbulent dissipation and maximum dissipation further up the water column was attributed to the vertical change in position of the region of maximum shear during the tidal cycle (Simpson et al. 2000). Towards the sea surface, above the thermocline, values of ε also increased, due to wind or wave action at the air-sea interface and possibly some contamination from the ships wake.

During both CS3 occupations ε was at a minimum in the interior of the water column, with a notable vertical diffusivity minimum within the thermocline (Figs 3.10 ii & iii and 3.11 ii & iii). Periodic increases in ε and K_z within the thermocline at CS3a and CS3b were not associated with the semidiurnal tidal signal. Spectral analysis of the ADCP mooring data from CS3 revealed baroclinic energy and shear in the upper water column and thermocline was dominated by inertial oscillations, which may have caused an increase in ε and K_z (Rippeth et al. 2005).

The mean K_z at the base of the thermocline for each cast (Fig 3.12) varied throughout both stations. Increases of up to two orders of magnitude were seen at CS3a (around Yearday 217.0), and around one order of magnitude at CS3b (around Yearday 221.69). K_z at the base of the thermocline was not significantly different between the two CS3 stations (F=1.5, F_{crit}=4.0, p>0.05). However, the daily average of K_z (Table 3.1), calculated as the mean of the SUV6 cast time

series, was larger at CS3a, the two very large K_z values around Yearday 217.0 biasing the mean.

During CS3b K_z values at the base of the thermocline were highest in association with, and just after, maximum tidal currents, particularly strongly during northwards flow (Fig 3.12 b). A similar signal was not seen at CS3a (Fig 3.12 a).

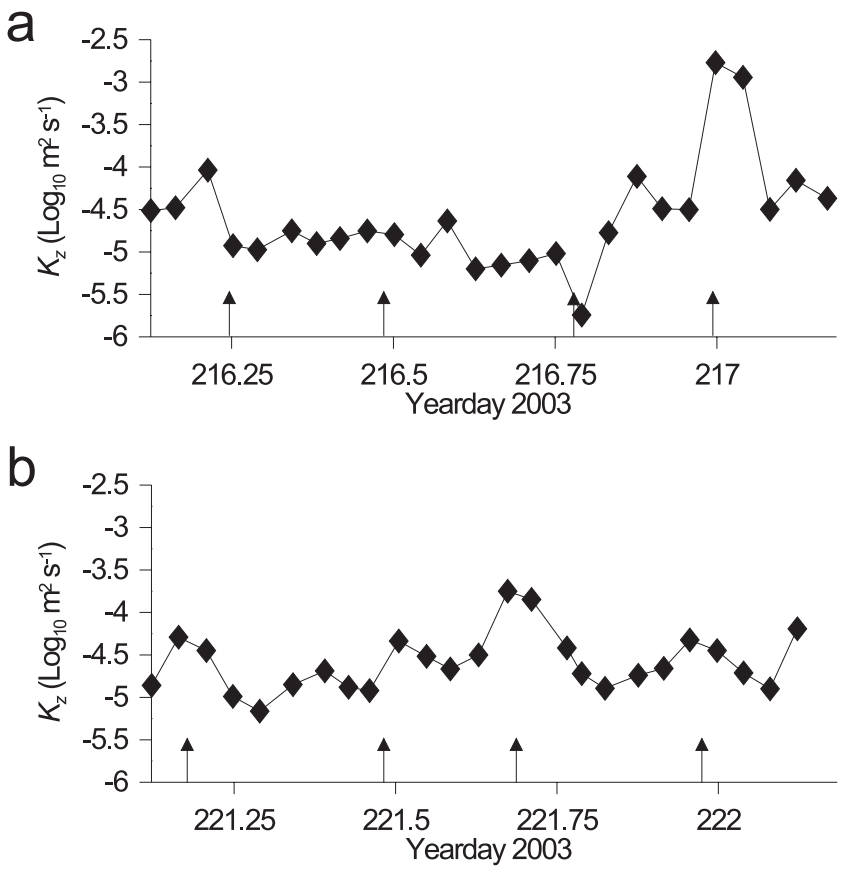

Figure 3.12

Mean vertical diffusivity, over the temperature ranges used to calculate the vertical nitrate flux, for each SUV6 profile during a) CS3a and b) CS3b. Arrows indicate approximate times of peak near bed currents.

3.3.3. Nitrate fluxes

Estimates of J_N for each SUV6 profile (see section 2.3 for methods) demonstrated how vertical fluxes of new nitrate into the SCM varied throughout the sampling periods at each station (Fig 3.13). During both stations J_N varied by at least one order of magnitude, and was controlled to a large extent by K_z (linear relationship, $r^2>0.82$, $p<0.05$), rather than $\Delta N/\Delta z$ (linear relationship, $r^2<0.04$, $p>0.05$), during both stations. Although $\Delta N/\Delta z$ varied with time it was by less than an order of magnitude, unlike K_z which varied by up to two orders of magnitude. Thus potential changes in J_N caused by $\Delta N/\Delta z$ would be masked by K_z.

There was no significant difference between the vertical nitrate fluxes at CS3a and CS3b ($F=0.2$, $F_{crit}=4.0$, $p>0.05$), however exclusion of the large event during CS3a, around Yearday 217.0, demonstrated CS3b had significantly higher nitrate fluxes the majority of the time ($F=6.3$, $F_{crit}=4.0$, $p<0.05$). The daily mean J_N at each station was calculated from the time series (Table 3.1), and did not vary between the stations. Again, exclusion of the large nitrate flux event during CS3a resulted in a lower daily flux (1.3 ± 0.7 mmol m^{-2} day^{-1}, 0.7–1.9 mmol m^{-2} day^{-1} 95% confidence interval) at CS3a, and consequently an appreciably higher daily vertical nitrate flux into the SCM during CS3b.

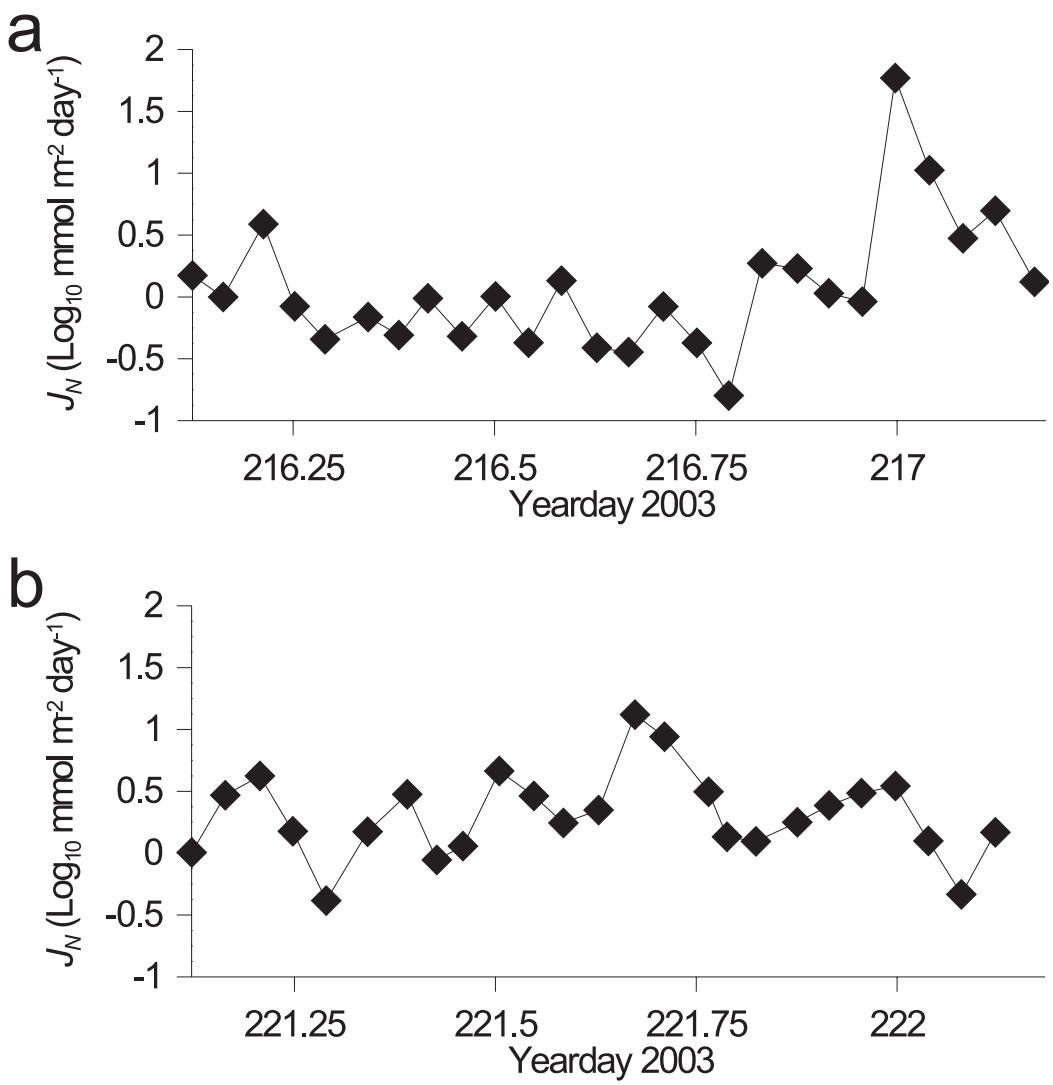

Figure 3.13

Vertical nitrate fluxes, J_N, into the subsurface chlorophyll maximum from below the thermocline for each SUV6 profile during a) CS3a and b) CS3b.

Table 3.1

Daily mean vertical nitrate flux into the SCM from the bottom layer (J_N) and associated mean nitrate gradient ($\Delta N/\Delta z$), turbulent dissipation (ε) and vertical diffusivity (K_z) for stations CS3a (approaching neap tide) and CS3b (approaching spring tide), positioned over a topographically flat seabed.

Station	$\Delta N/\Delta z$ (mmol m^{-4})	ε (W m^{-3})	K_z (m^2 s^{-1})	J_N (mmol m^{-2} day^{-1})
CS3a	-0.6 ± 0.1 (-0.8 – -0.5)	6.5 ± 3.2 x10^{-5} (1.3–19 x10^{-5})	13.3 ± 6.6 x10^{-5} (1.8–37 x10^{-5})	3.8 ± 1.9 (0.8 – 10.5)
CS3b	-1.0 ± 0.3 (-1.2 – -0.8)	3.9 ± 2.0 x10^{-5} (1.8–7.1 x10^{-5})	3.7 ± 1.8 x10^{-5} (2.0–6.2 x10^{-5})	2.8 ± 1.5 (1.6 – 4.5)

3.4. CS1: Results from a shelf bank slope site

The region around CS1 (Fig 2.1) was originally selected as one with a higher h/u^3 than CS3, and therefore should be very strongly stratified. The ADCP used at this station had depth limitations, so the station was repositioned on a bank slope (96 m depth) to allow full water column profiling by the ADCP.

3.4.1. Hydrographic characteristics of the thermocline, chlorophyll *a* concentrations and the nitracline

CS1 was sampled on the 31st July – 1st August 2005 at spring tide (see Chapter 2 for methods). The station displayed well mixed bottom and surface layers, separated by a distinct thermocline (Fig 3.14) with a temperature difference of ~6.5 ^{o}C across a thermocline thickness of around 15 m. Density was primarily controlled by temperature (r^2>0.999, p<0.05).

An SCM occurred within the thermocline (Fig 3.15), of which around 50% of the [Chl *a*] increase was due to an increase in biomass (personal communication C.M. Moore). The bottom mixed layer contained chlorophyll *a*, indicating possible mixing between the SCM within the thermocline and the bottom mixed layer.

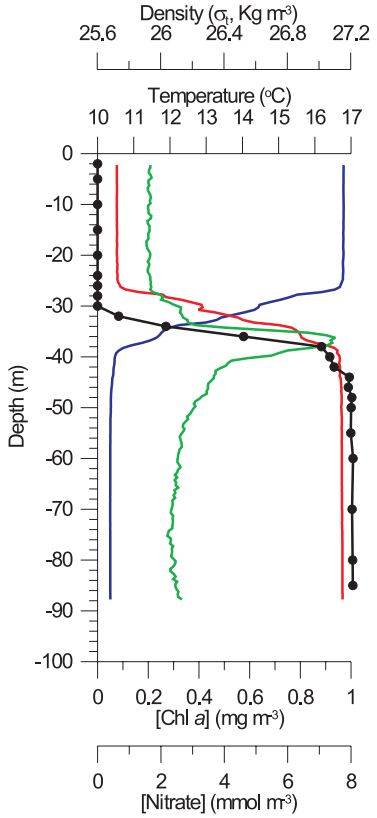

Figure 3.14

Example of a CTD and water sample nutrient profile for CS1 (05:05, 31st July 2003). Blue represents CTD temperature, red CTD density, green CTD chlorophyll *a* concentrations and black water sample nitrate concentrations.

The SCM had an asymmetrical distribution when plotted against temperature (Fig 3.16) with increased chlorophyll *a* towards the base of the thermocline. However, compared to CS3 (Fig 3.5) SCM chlorophyll *a* at CS1 was not as concentrated within the base of the thermocline, but instead exhibited a more diffuse peak.

Thermocline and SCM thickness varied temporally (Fig 3.15). The top of the thermocline and SCM appeared to be moderately stable with depth. The

times of thickest thermocline corresponded to the end of each southward flowing ebb tide, e.g. around Yeardays 211.5 and 212.05. During CS1 the thickness of the SCM was closely correlated with the thickness of the thermocline ($r^2 = 0.813$, $p<0.05$). This was unlike the flat shelf sites where the thickness of the thermocline and SCM were unrelated (Fig 3.4), due to advection of horizontal patches (section 3.3). The correlation between thermocline and SCM thickness at CS1 suggested the same control mechanism was acting on both, i.e. a physical mechanism, not a biological one.

Total SCM Chl *a* and total water column Chl *a* were related to the width of the SCM ($r^2 = 0.94$ & 0.59 respectively, $p<0.05$), i.e. the thickest SCM contained the most [Chl *a*], it was not just the same total amount stretched over a greater depth.

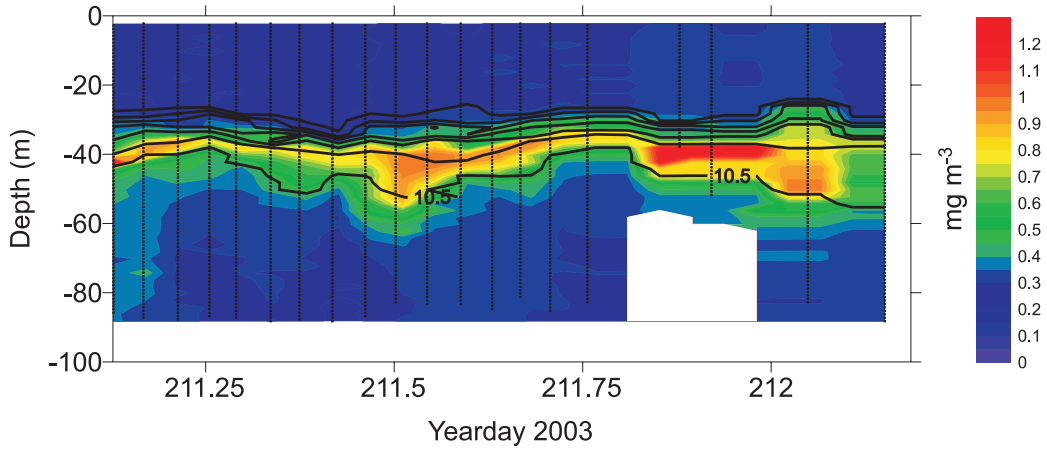

Figure 3.15

Time series of CTD chlorophyll *a* concentrations (coloured contours) and temperature (black lines, 1 °C intervals) for CS1. CTD cast times indicated. The data gaps were caused by CTD winch problems.

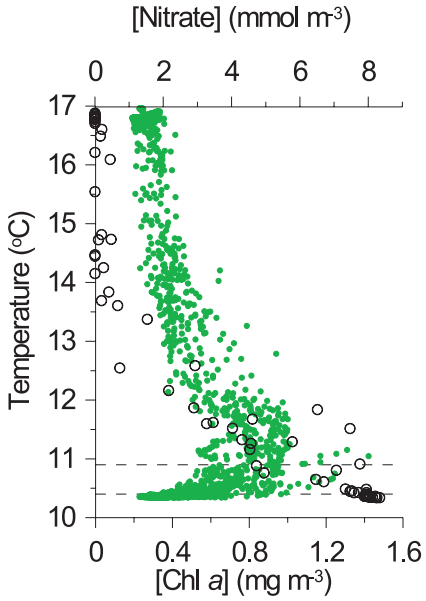

Figure 3.16

Station CS1 CTD chlorophyll *a* concentrations (green dots) and water sample nitrate concentrations (black circles) against temperature. The black dashed lines mark the boundaries of the temperature range over which the vertical nitrate flux into the SCM was calculated for each profile. 10.4–10.9 °C.

From water samples nitrate concentrations were found to be around 8 mmol m^{-3} in the bottom mixed layer and below detection limits in the surface mixed layer (Fig 3.14), with the nitracline corresponding to the position of the SCM (Fig 3.16).

$\Delta N/\Delta z$ was obtained at CS1 using the methods described in section 2.3, *$\Delta N/\Delta z$ measured by the SUV6*. Maximum $\Delta N/\Delta z$ was situated between the base of the SCM and peak [Chl *a*] (Fig 3.17).

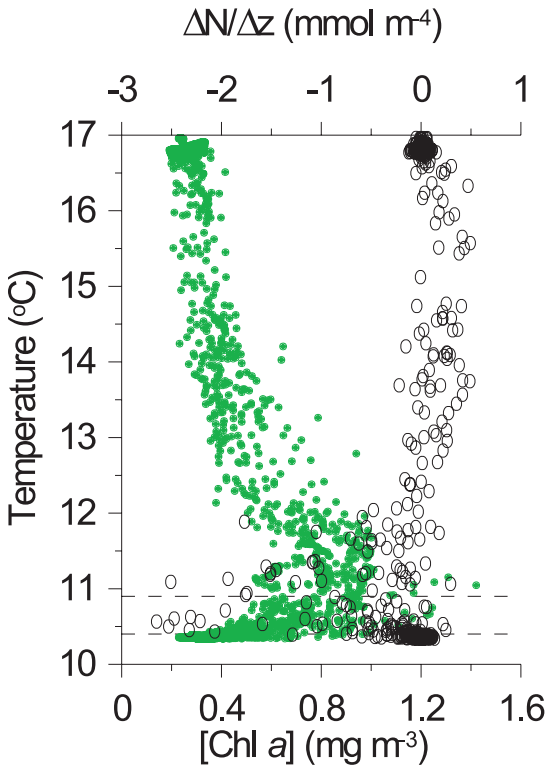

Figure 3.17

Station CS1 CTD chlorophyll *a* concentrations (green dots) and SUV6 derived nitrate gradients (black dots) against temperature. The black dashed lines mark the boundaries of the temperature range over which the vertical nitrate flux into the SCM was calculated for each profile. 10.4–10.9 °C.

Mean $\Delta N/\Delta z$ at the base of the SCM value varied throughout the duration of the station (Fig 3.18). Unfortunately, due to CTD technical problems, sampling resolution between Yeardays 211.75 and 212.05 was poor, with only one profile taken which passed through the thermocline in a 7 hour period. This made it more difficult to establish what caused variations in mean $\Delta N/\Delta z$. However, around 48% of variation in $\Delta N/\Delta z$ at the base of the thermocline was linked to the chlorophyll *a* gradient at the base of the SCM (r^2=0.48, p<0.05).

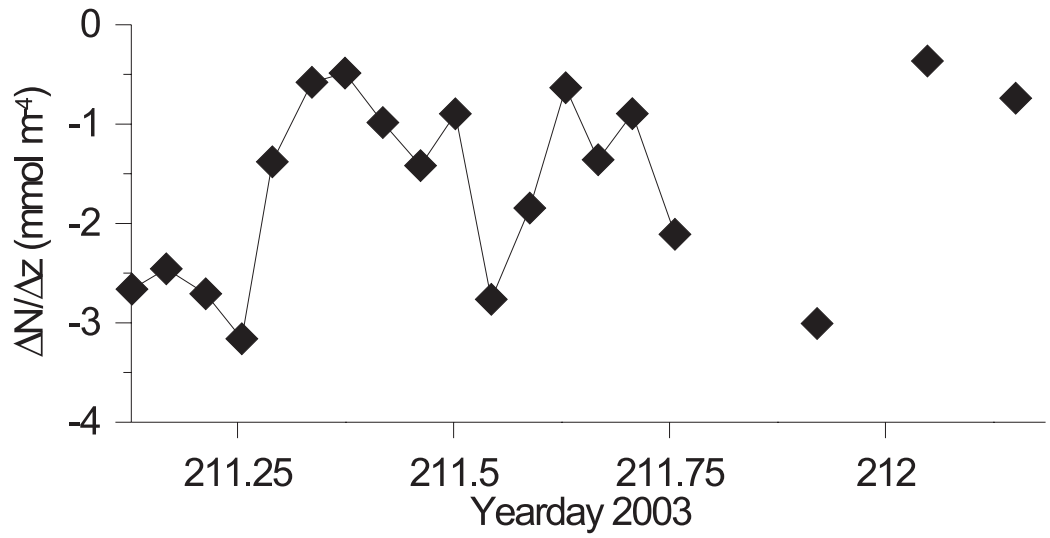

Figure 3.18

Mean nitrate gradient, over the temperature ranges used to calculate the vertical nitrate flux, for each SUV6 profile during CS1.

3.4.2. Currents, turbulence and mixing

CS1 exhibited a strong semi-diurnal signal in barotropic tidal current velocity (Fig 3.19 i). Analysis of individual velocity profiles from the ship's ADCP showed near bed currents reached a maximum velocity of ~ -0.4 m s^{-1} during CS1. There was a lag in current velocities between the thermocline and the surface and bottom layers.

Due to failure of the FLY instrument termination between Yearday 211.45 – Yearday 211.71, the time series of the rate of turbulent dissipation, ε, and the vertical diffusivity, K_z, were interrupted for around 6.25 hours. Nevertheless, it was possible to distinguish maxima in ε at the seafloor and

surface (Fig 3.19 ii), due to barotropic tidal currents generating shear, and wind and wave action and ship's wake, respectively. A quarter-diurnal signal of increased ε would be expected at the seabed, generated by each ebb and flood of the barotropic tide, however due to the time gap in the FLY data no clear signal was easily recognisable.

ε was generally at a minimum within the water column (Fig 3.19 ii), particularly within the thermocline, as was K_z (Fig 3.19 iii). However, between 211.72 – 211.965 very high values of K_z (up to 1×10^{-2} m^2 s^{-1} in individual profiles) occurred within the thermocline as the tide was flowing off the bank towards CS1, after maximum flow. This equated to an increase in K_z of ~4 orders of magnitude. Values of ε within the thermocline during this period were of the same order of magnitude as those near the bed. Values of K_z this high have rarely been measured within shelf sea thermoclines.

K_z away from the thermocline at CS1 must be treated with caution, due to the lack of stratification in the surface and bottom mixed layers causing very low N^2 (section 2.1.3).

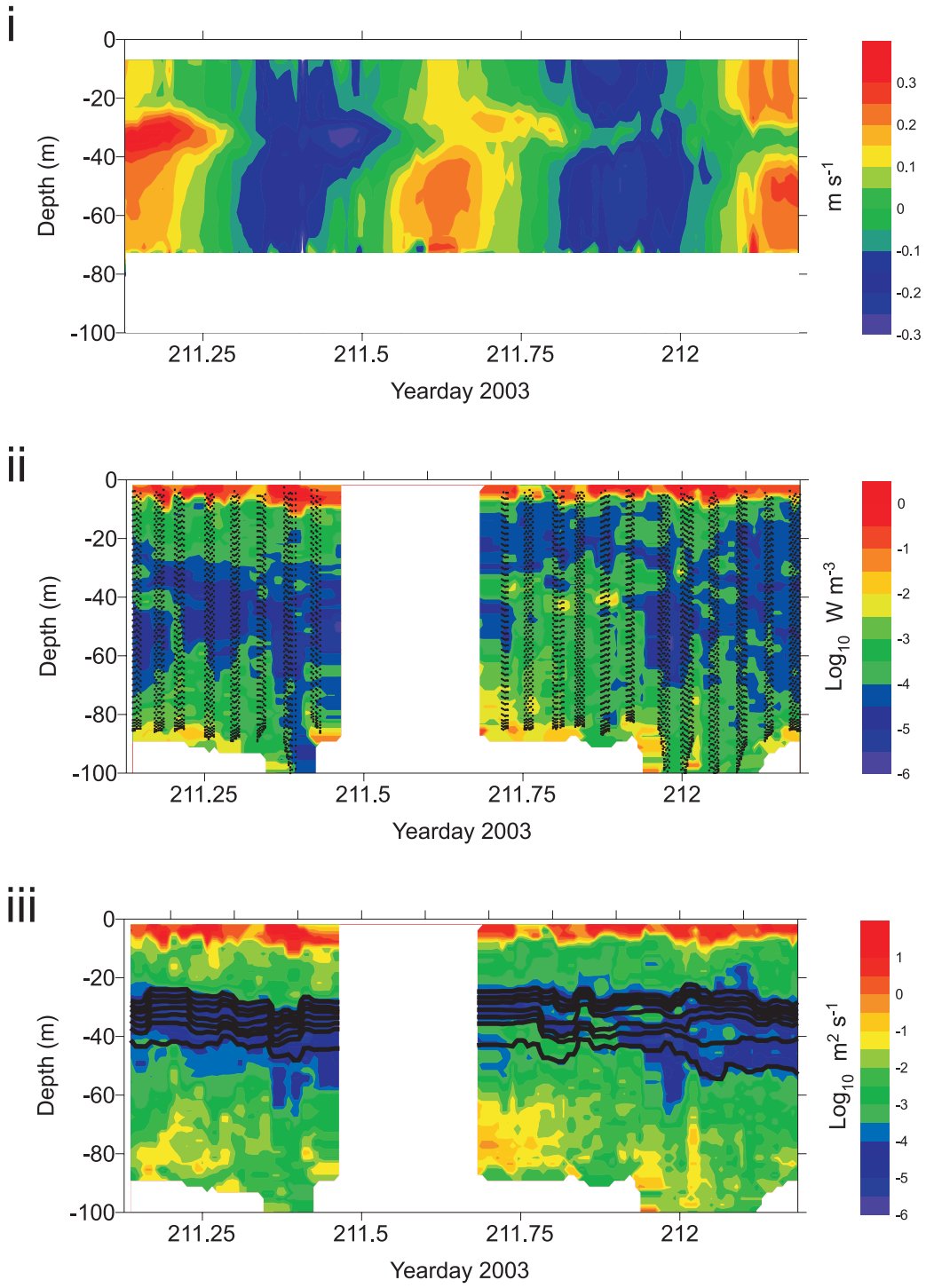

Figure 3.19

CS1 i) Ships ADCP northwards current velocity, ii) FLY turbulent dissipation rate (every 2nd FLY data point marked) and iii) FLY vertical diffusivity (coloured contours) and FLY temperature (black lines, 1 °C intervals, lowest isothermal =10.5 °C)

Mean K_z at the base of the SCM for each CTD cast varied by 3 orders of magnitude over the observed 25 hours (Fig 3.20). Unfortunately the thermocline was poorly sampled by the SUV6 during the high turbulence event, with only two CTD profiles passing through the nitracline in that period. A gap in the FLY data also meant a K_z value was not available for all CTD casts.

Increases in K_z occurring just after the times of maximum currents (~Yearday 211.17, 211.35 and 212.15) appear to be due to barotropic generated turbulence reaching the base of the thermocline. The gap in the FLY data meant no K_z data was available for the maximum northward currents occurring around Yearday 211.62 and the SUV6 gap missed a period of maximum southward currents (~Yearday 211.83).

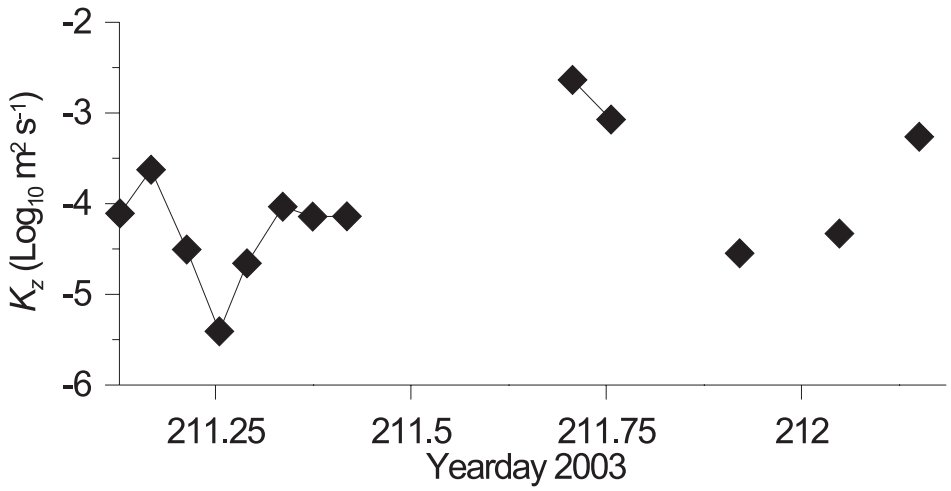

Figure 3.20

Mean vertical diffusivity, over the temperature range used to calculate the vertical nitrate flux, for each SUV6 profile during CS1.

3.4.3. Nitrate fluxes

The range of estimates of vertical nitrate flux into the SCM for all CTD profiles which passed through the thermocline at CS1 are shown in Fig 3.21. Despite the gaps in both the CTD and FLY data, which were not coincident, it can be seen that J_N fluctuated by up to three orders of magnitude at least.

Around 83% of variance in J_N was explained by variance in K_z (r^2=0.83, p<0.05), variance in $\Delta N/\Delta z$ did not have a significant effect on J_N (r^2=0.003, p>0.05). As such, very large J_N values were associated with the turbulent event, which occurred around Yearday 211.75 (Fig 3.21), and strongly biased the mean daily vertical nitrate flux (Table 3.2). Because of the large gaps in the time series the mean daily value must be treated with caution. J_N was also intensified to a lesser degree (~1 order of magnitude) during maximum flow, when K_z was also increased, seen at Yearday 211.17, 211.35 and 212.15.

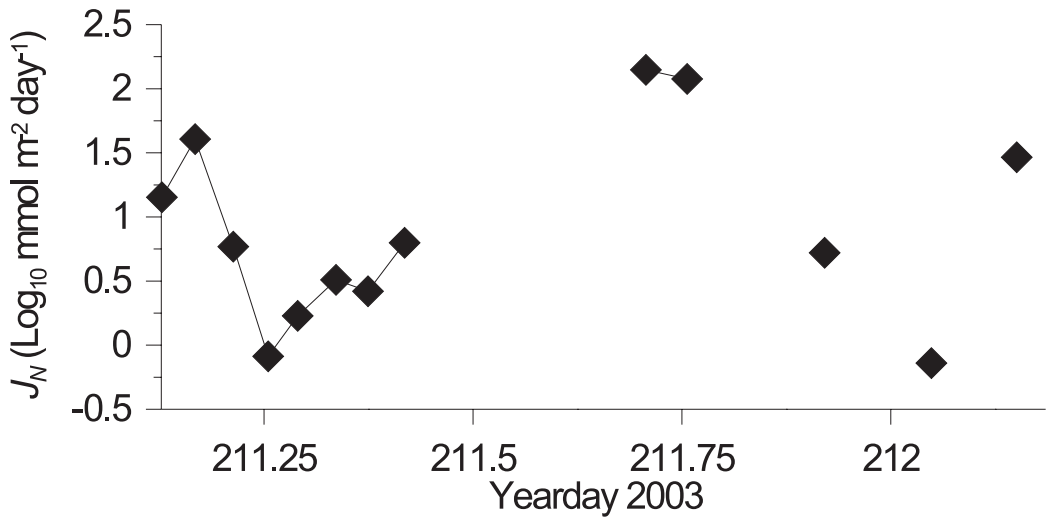

Figure 3.21

Vertical nitrate fluxes, J_N, into the subsurface chlorophyll maximum from below the thermocline for each SUV6 profile during CS1.

Table 3.2

Daily mean vertical nitrate flux into the SCM from the bottom layer (J_N) and associated mean nitrate gradient ($\Delta N/\Delta z$), turbulent dissipation (ε) and vertical diffusivity (K_z) for station CS1, positioned over a bank slope.

Station	$\Delta N/\Delta z$ (mmol m^{-4})	ε (W m^{-3})	K_z (m^2 s^{-1})	J_N (mmol m^{-2} day^{-1})
CS1	-1.6 ± 0.5 (-2.2 – -1.0)	3.2 ± 1.6 x10^{-4} (0.3–9.7 x10^{-4})	3.4 ± 1.7 x10^{-4} (0.9–9.4 x10^{-5})	28.4 ± 17.0 (3.3 – 70.1)

3.5. Modelling the effect of barotropic mixing over banks

A 1-dimensional model was used to investigate the extent to which barotropic generated turbulence affected the SCM over banks. It was hypothesised that the banks, through decreasing the depth of the seabed, would increase turbulence at the base of the thermocline and both increase flux of nitrate into the SCM, increasing [Chl *a*], and increase the flux of chlorophyll *a* out of the SCM into the bottom mixed layer.

The model, PHYTO_1D, was run using cross-front mode (see section 2.5 for methods) to simulate conditions in early August both over a 100 m deep flat seabed and over three simple banks which rose to heights of 10, 20 and 30 metres above a flat seabed of 100m depth. The simulations were run with tidal constituents for the region of Jones Bank, using M_2 tidal constituents only, and M_2 and S_2 tidal constituents together.

The model reproduced the two layer stratified water column seen in the Celtic Sea in August, with a subsurface chlorophyll maximum within the thermocline (Fig 3.22). It was clear in both M_2, and M_2 plus S_2 simulations that reducing the water depth, i.e. over banks, caused the thermocline to be positioned closer to the surface. This was more pronounced when currents had a spring-neap cycle (when both M_2 and S_2 tidal constituents were used, Fig 3.22). Over the banks higher levels of barotropic generated shear and turbulence came in contact with the base of the thermocline, simply because of the shallower bottom mixed layer. This mixing consequently changed the position of the stratification depth by eroding the base of the thermocline. The effect was greater when a spring-neap tidal cycle was used, due to the higher currents at spring tides.

Mixing between the thermocline (and SCM) and the bottom mixed layer was clearly evident, with concentrations of chlorophyll *a* in the bottom mixed layer proportional to the height of the bank (Fig 3.22), as mixing at the base of the thermocline increased with increasing height. Levels of [Chl *a*] in the bottom mixed layer were higher when currents had a spring-neap cycle than using M_2 alone. This effect was caused by the depth of the thermocline, and SCM, relaxing downwards during neap tides, only to be eroded again at the next spring tide (Sharples 1999, Allen et al. 2004).

Although bottom mixed layer water [Chl *a*] was affected, neither mean nor integrated [Chl *a*] within the SCM was increased by the presence of banks, either in M_2 or M_2 and S_2 simulations. Conversely, increased mixing at the base of the thermocline caused the removal of chlorophyll *a* from the base thermocline, and reduced [Chl *a*] within the SCM.

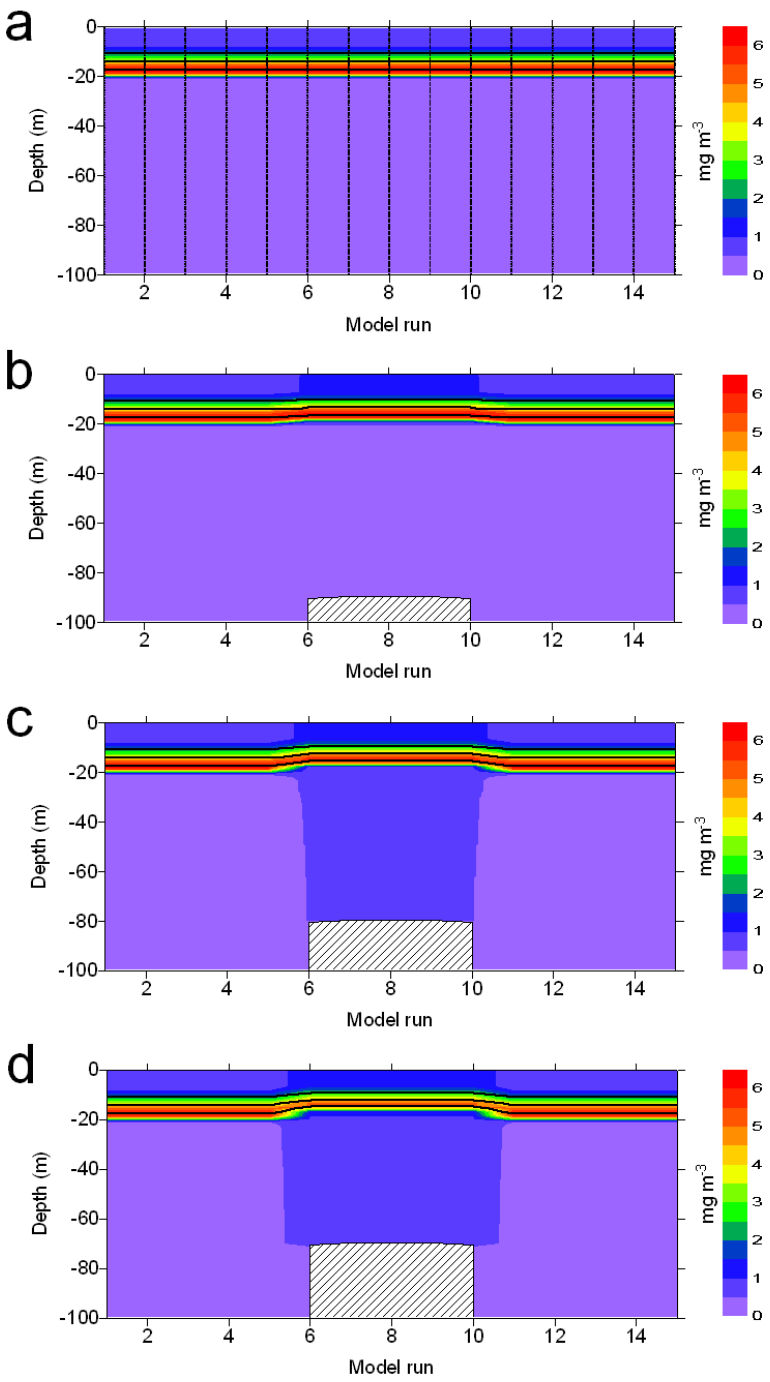

Figure 3.22

Chlorophyll *a* concentrations (coloured contours) and temperature (black lines, every 2 ^{o}C) over a) a flat seafloor (data points marked), and modelled banks of heights b) 10 m, c) 20 m and d) 30 m, simulated using M_2 and S_2 tidal constituents.

3.6. Discussion

The aim of cruise JR98 was to evaluate physical influences on the thermocline and subsurface chlorophyll maximum in the Celtic Sea and, specifically, to investigate the linkage between physical and biological processes through turbulence driven vertical nutrient fluxes (J_N) into the SCM. The mechanisms affecting vertical nutrient fluxes into the Celtic Sea shelf sea subsurface chlorophyll maximum were of interest, and, in particular, possible variations in J_N due to spring-neap tidal cycles.

This discussion will be split principally according to topographic type (flat–CS3 and bank–CS1). Further discussion, including placing the information into a larger setting, will be undertaken in Chapter 7.

3.6.1. Vertical nitrate fluxes into the SCM over a flat shelf (CS3)

Variations in vertical nitrate fluxes at CS3

In shallow stratified shelf seas, modification of the depth of the base of the thermocline occurs over the spring-neap tidal cycle (see section 1.1.3, *Barotropic tide driven mixing*). CS3 was deliberately sampled between, rather than at, spring and neap tides. Although the current velocity and vertical diffusivity profiles were not particularly different between the two CS3 stations (section 3.3.2) profiles of velocity and K_z previous to the stations' sampling periods would have been, with higher current velocities and vertical diffusivities at spring tide raising and sharpening the base of the thermocline previous to

CS3a, and lower current velocities and vertical diffusivities at neap tide allowing the base of the thermocline to widen and deepen previous to CS3b.

The preceding conditions therefore changed the position of the thermocline and SCM base within the K_z profile. As such, although the K_z profiles were similar at CS3a and CS3b, CS3b, sampled after neap tide where the base of the SCM was lower, had generally higher K_z values at the base of the thermocline compared to CS3a, and quarter-diurnal variations in K_z associated with to the maximum tidal current velocities could be seen at the base of the SCM (Fig 3.12 b and section 3.3.2).

CS3a showed no quarter-diurnal signal in K_z. Approaching neaps barotropic generated turbulence would reach progressively less far into the water column with each tidal cycle, causing lower K_z to be measured at the base of the raised thermocline. CS3a showed one period of exception to the mainly lower K_z values, occurring at ~Yearday 217.0. An event occurred which increased K_z by ~2 orders of magnitude at the base of the thermocline (Fig 3.12) which was not directly related to the barotropic tide or inertial oscillations. K_z was strongly correlated to shear during both CS3 occupations and the thermocline was only marginally stable with Richardson number of ~1 the majority of the time (personal communication M. Palmer). Thus even seemingly small shear events could cause instability for a short time, by providing enough energy to overcome the marginal stability of the thermocline and therefore causing mixing.

The distribution of chlorophyll *a* against temperature (Fig 3.5) demonstrated how the varying barotropic tidally generated mixing also had an effect on SCM distribution within the thermocline. The asymmetric distribution of [Chl *a*] against temperature during both CS3 visits implied little internal

mixing taking place within the thermocline, allowing [Chl *a*] to build up at the base of the thermocline. Approaching springs (CS3b), turbulence sharpening the base of the thermocline also caused the base of the SCM to sharpen both against temperature (Δ[Chl *a*]/ΔT, Fig 3.5 b) and depth (Δ[Chl *a*]/Δz). Approaching neaps (CS3a), the deepening, widening thermocline allowed the SCM to also broaden at the base, reducing Δ[Chl *a*]/ΔT (Fig 3.5 a), causing a reduction in Δ[Chl *a*]/Δz also. These changes in Δ[Chl *a*]/Δz in turn influenced $\Delta N/\Delta z$.

As the nitrate gradient is caused by nitrate uptake by phytoplankton the position and shape of the SCM will determine where nitrate uptake is taking place. Approaching spring tide Δ[Chl *a*]/Δz was increased, and had significantly larger nitrate gradients at the base of the thermocline, compared to approaching neap tide (section 3.3.1). Approaching spring tides $\Delta N/\Delta z$ would also be directly affected by increasing turbulence sharpening the nitracline, as well as indirectly through sharpening the [Chl *a*] (i.e. uptake) gradient.

Exclusion of nitrate fluxes driven by the large K_z event during CS3a allowed comparison of barotropic tidally driven vertical nutrient fluxes at CS3 approaching neap and spring tides. As J_N was primarily controlled by K_z rather than $\Delta N/\Delta z$ at both stations (section 3.3.3), similar influences apply to J_N as to K_z. Approaching neaps vertical nutrient fluxes were significantly lower (1.3 mmol m^{-2} day^{-1}) than approaching springs (2.8 mmol m^{-2} day^{-1}), reflecting the differences in K_z at the base of the SCM. J_N also showed quarter-diurnal variations approaching spring tides (CS3b) due to variations in K_z driven by flooding and ebbing tidal currents (Fig 3.13 b). This was not seen in J_N when approaching neaps (CS3a, Fig 3.13 a).

Approaching neaps (CS3a) both ε and K_z, and hence J_N, were increased

throughout the time series by the presence of inertial oscillations driven by higher winds immediately prior to CS3a (personal communication M. Palmer, Rippeth et al. 2005). In addition to vertical turbulent flux of nitrate into the SCM, the downwards migration of the thermocline would allow incorporation of bottom water with higher [Nitrate] into the base of the thermocline, and make it available to phytoplankton within the SCM (Holligan 1978).

Inclusion of the single large K_z event at CS3a in J_N calculations increased the mean daily flux of nitrate into the SCM, and J_N became not significantly different between CS3a and CS3b. There was no unique temperature signal associated with the event so the temperature logging mooring could not be used to assess the frequency of such events. The frequency can only be estimated by how often such events were observed. Only once (two adjacent FLY profiles) were spuriously high K_z values observed at the base of the SCM throughout CS3a.

FLY profiles were carried out over 8.75 hours at CS3, ~36 % of the time. Assuming the events occur randomly through out the tidal cycle and FLY sampling was also random relative to the tide, ~36 % of high K_z events were sampled. As the events were a major influence on vertical nitrate flux having sampled all potential events would have raised the measured flux at CS3a to ~15 mmol m^{-2} day^{-1}. No such events were seen during CS3b suggesting there was less reliance on sporadic shear events to drive vertical nitrate flux into the SCM.

Vertical nitrate fluxes and new primary production at CS3

The primary production supported by the flux of new nitrate into the SCM from below the thermocline (Table 3.3), i.e. new production, was

calculated from the vertical nitrate fluxes J_N (Table 3.1) using the Redfield ratio (106C:16N). The daily vertical nitrate fluxes, 3.8 and 2.8 mmol m^{-2} day^{-1} during CS3a and CS3b respectively, were capable of supporting primary production of 352 and 259 mg C m^{-2} day^{-1}. Without the increased flux event at CS3a 1.3 mmol m^{-2} day^{-1} nitrate would be supplied and 120 mg C m^{-2} day^{-1} new production supported.

Vertically integrated primary production estimates above the base of the thermocline were calculated for both the cloudiest and sunniest days experienced on the cruise (Table 3.3, personal communication A Hickman, see section 2.1.7 for methods). Primary production was not found to be significantly different approaching spring or neap tides.

The large errors associated with both the primary production estimates and the nutrient fluxes make comparison problematical. However, it appears that approaching neap tide sufficient nitrate was supplied to support primary production rates in both cloudy and sunny conditions. However exclusion of nitrate supplied by the single, large turbulent event gave a daily mean supply of new nitrate which was less than that required to support the primary production, suggesting an *f*-ratio of around 0.3–0.6, dependent on the weather.
Approaching spring tide the supply of new nitrate appeared sufficient to support production during cloudy days. Sunny days were not fully supported and suggested an *f*-ratio of up to 0.7. However the irradiance levels on the sunny day were the highest measured on the cruise and not representative of an average day.

This suggests the *f*-ratio will vary between spring and neaps as supply of new nitrate into the SCM varies. The large errors meant calculation of those *f*-ratios with any accuracy or precision was extremely difficult.

Table 3.3

Calculated primary production rates (personal communication A Hickman) and new production supported by calculated vertical nitrate fluxes into the SCM from the bottom layer.

Station	Integrated Primary Production (mg C m^{-2} day^{-1})		New primary production supported (mg C m^{-2} day^{-1})
	Cloudy	Sunny	
CS3a	185 (± 56)	363 (± 109)	352 (± 183)
CS3b	198 (± 59)	397 (± 119)	259 (± 155)

3.6.2. Vertical nitrate fluxes into the SCM over a bank slope (CS1)

Variations in vertical nitrate fluxes at CS1

As hypothesised from the h/u^3 value, CS1 was more strongly stratified than CS3 (Figs 3.14 and 3.3), although CS1 was sampled at spring tide which would also act to sharpen the thermocline. Although CS1 was positioned over the slope of a bank, spring-neap tidal adjustments to the thermocline and SCM would still be expected (section 1.1.3 *Barotropic tide driven mixing*).

K_z increased at the base of the thermocline with a quarter-diurnal signal, associated with maximum near bed current velocities. Variability in J_N was influenced greatly by K_z (r^2=0.83, p<0.05), therefore J_N also displayed quarter-diurnal increases.

In addition to barotropic related turbulence at CS1 there was also a large internal mixing event around Yearday 211.72–211.965. The very large vertical

dissipation rates measured were on a par with those measured close to the seabed. Vertical diffusivities such as this within a shelf sea thermocline have only previously been reported associated with the generation and dissipation of lee waves over topographic features (e.g. Moum & Nash 2000, Nash & Moum 2001, section 1.1.3 *Internal wave driven mixing*). This level of vertical diffusivity has been previously unknown in the Celtic Sea shelf thermocline away from the shelf break.

The model bank simulations reproduced variations in thermocline and SCM depth and in K_z at the base of the thermocline, such as seen at CS3 and CS1 due to spring-neap tidal cycles. However the model did not produce any periods of greatly enhanced turbulence. The model reproduces only one-dimensional (vertical) generated turbulence. Thus if the high K_z were due to horizontal lee wave generation, as described over Stonewall Bank on the Oregon shelf by Nash & Moum (2001), and suggested over the CS1 bank slope by the large K_z values, the event would not be simulated.

CS1 chlorophyll *a* was asymmetrically distributed towards lower temperatures within the thermocline (Fig 3.16), though not to the same extent as over the flat shelf at CS3 (Fig 3.5). Within the SCM peak, Chl *a* was relatively evenly distributed, suggesting internal mixing (such as the large K_z event) was causing redistribution of phytoplankton away from the base of the thermocline. The shape of the SCM base would have an effect on the nitrate gradient, via nitrate uptake by phytoplankton. At CS1, although the chlorophyll *a* distribution within the SCM was relatively diffuse, the turbulence associated with the spring tide currents sharpened the SCM base ($\Delta[Chl\ a]/\Delta z$) and hence tightened $\Delta N/\Delta z$,

causing CS1 to have $\Delta N/\Delta z$ values significantly higher than at CS3 (F>9.5, F_{crit}=4.1, p<0.05).

As only one CTD cast passed through the thermocline during the internal mixing event, the immediate effect on phytoplankton distribution within the SCM and on $\Delta N/\Delta z$ is unknown. FLY temperature data gave an indication of the effect of the enhanced turbulence on the temperature structure of the thermocline (Fig 3.23), and by inference how the structure of the SCM was affected by the increased mixing. Temperature gradients did not appear to be particularly affected at the top of the thermocline. The base of the thermocline was more diffuse at the beginning of the measured event. Thereafter the internal mixing appeared to broaden the central thermocline section into a more diffuse structure.

It is unclear why the base of the thermocline sharpens again, possibly thorough advection of different water masses, or the effect of the increasing barotropic tidal currents approaching maximum southward tidal flow. Assuming the temperature gradients at the base of the thermocline are an indicator of $\Delta[Chl\ a]/\Delta z$ (related to $\Delta N/\Delta z$), this could explain why the only SUV6 measurement of $\Delta N/\Delta z$ during the event (Fig 3.18, Yearday 211.921) did not indicate a diffuse nitrate gradient.

A gap in the FLY data led to the start time of the event being unknown. However, if caused by lee wave formation, e.g. as in Nash & Moum (2001), the high turbulence would have been initiated after the tidal currents started flowing over the bank crest towards CS1 (southwards), i.e. about when FLY measurements started. One tidal cycle earlier no high K_z event was measured, though temperature profiles displayed some indication of increased diffuseness in the central thermocline (Fig 3.23 i between dashed lines), suggesting a similar

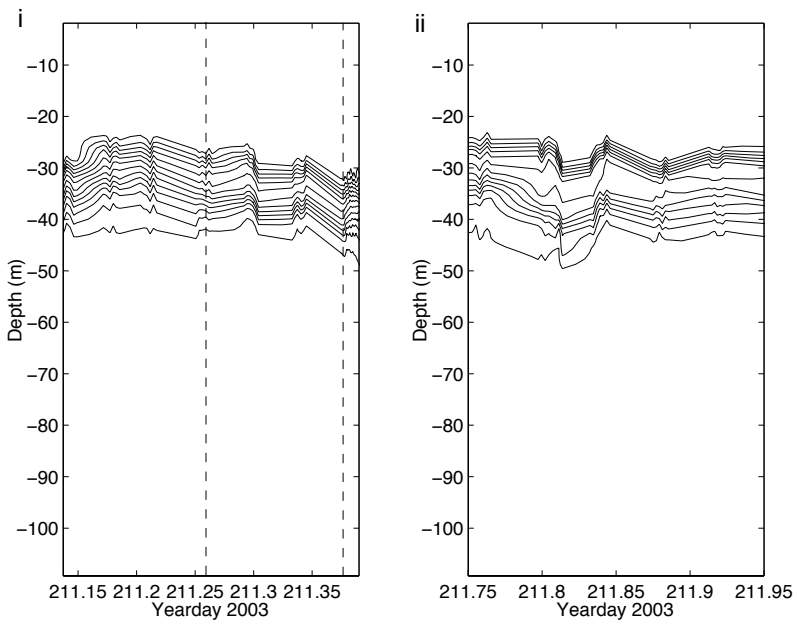

Figure 3.23

Time series of CS1 FLY temperature. Black lines mark 0.5 ^{o}C isotherms (lowest 10 ^{o}C) i) before and ii) during and immediately after the high turbulence event. Between the dashed lines indicated one tidal cycle before the high K_z event.

event had possibly occurred away from the ships position and then the affected water patch advected past the ship.

Interpretation of data at site CS1 is complicated by movement of the water column by advection. Horizontal patches, as seen in the SeaSoar section, when advected through a station cause changes in, for example, the thermocline or SCM thickness, as seen at CS3. However, at CS1 the advection signal will be complicated by modifications occurring related to the state of the tide, for example thickening of the thermocline by internal mixing, possibly driven by lee wave formation and dispersion as the tidal currents flow off a bank.

Vertical nitrate fluxes and new primary production at CS1

A daily mean vertical nitrate flux into the SCM was difficult to estimate, due to the large data gaps. The daily mean value of 28.4 mmol m^{-2} day^{-1} (Table 3.2) was vastly biased by very large fluxes during the increased mixing event. However, the length of the event was unknown and therefore its full contribution to the daily flux unknown. The daily average vertical nitrate flux due to barotropic tidally driven mixing was 10 mmol m^{-2} day^{-1}, calculated by excluding the large mixing event. This was higher than either CS3a or CS3b, driven by increased K_z at the base of the SCM caused partly by the shallower water column and partly by the spring tide.

The relationship between J_N and K_z made it possible to apply a regression equation to mean K_z at the base of the SCM to obtain J_N for all fly profiles. The calculated daily average using this method was ~26 mmol N m^{-2} day^{-1} which is not significantly different from the 28.4 mmol N m^{-2} day^{-1} estimated using SUV6 cast data, however, there is still a large temporal gap where there were no FLY measurements.

The daily flux of 28.4 mmol N m^{-2} day^{-1} is capable of supporting 2635 mg C m^{-2} day^{-1} (assuming the Redfield ratio). The estimated production values at CS1 were 148 mg C m^{-2} day^{-1} on a cloudy day and 303 mg C m^{-2} day^{-1} on a sunny day. These are significantly below what could have potentially been supported. Nitrate samples were always below detection limits in the surface mixed layer. This implies either the nitrate was taken up, even if not utilised, almost immediately or nutrient sampling missed times of measurable surface [Nitrate] at CS1.

There are several possible explanations why the primary production rates were not higher. Firstly the phytoplankton may have been light limited, even during the sunniest of days. In the SCM, the PE curve derived E_k, the light intensity at which the phytoplankton reach maximum primary production rates, was higher than the in situ light levels, thus the available light fueled a rate of photosynthesis lower than the phytoplankton were capable of (Moore et al. 2006). Lizon et al. (1998) found phytoplankton were less productive when subjected to increased vertical mixing, as they were unable to photoacclimate quickly enough vertical changes in the light field as they were mixed.

Tidal currents in the region of CS1 results in a net north-eastern advection. The production values were based on samples taken from the dawn CTD cast, corresponding to tidal currents reaching the end of northwards flow. The phytoplankton had therefore been newly advected to CS1 and the bank from over a flat seabed of deeper depth than CS1, where mixing at the base of the thermocline would have been lower and there was unlikely to be increased mixing due to topographic effects. Thus the water measured at the dawn cast, when there was no turbulent event, was not, and had not been, subject to high nutrient fluxes and would give production values associated with phytoplankton with access to lower [Nitrate].

Chapter 4 : Results from CD173 over the shelf; the subsurface chlorophyll maximum and vertical fluxes of nitrate.

4.1 Introduction

During cruise JR98 in 2003 a station was occupied which happened to be situated over the slope of a small bank. The unexpected high K_z event at this station (CS1, section 3.4), in conjunction with the JR98 cross shelf SeaSoar data (section 3.2), prompted a more focused investigation around banks in 2005 during cruise CD173. The 2005 cruise was planned knowing that, based on the 1_D model experiments, the mixing signals over the banks were not only the result of increased barotropic mixing on a shallow water column.

Four SeaSoar sections were carried out over three banks during cruise CD173, and these data were used in the selection of suitable sites for mooring arrays and the exact positions of CTD and FLY stations. The stations visited in 2005 were designed to assess the importance of the edges of the banks in both affecting the hydrology, and primary production through influencing vertical nutrient fluxes.

4.2 Basic observations from transects across banks

Although the SeaSoar survey undertaken in 2003 (section 3.2) suggested topography had some influence on mixing between the thermocline and the bottom mixed layer, and therefore possibly had an effect on primary production within the SCM, the data was opportune and had insufficient detail to fully elucidate where, or how, any effects took place. Station CS1 further supported a hypothesis of topographic influence on hydrography over banks (section 3.4).

Further SeaSoar sections in 2005 were designed to focus over three banks (Fig 4.1), Labadie Bank (July 30th), Jones Bank (July 20th and August 1st), and a small bank located around 35 km west of Jones Bank (July 29–30th, referred to as Small Bank), to investigate the phenomena in more detail. The data was also used to assist in situating moorings and 25 hour stations (section 4.3). All banks were traversed in the direction of the major axis of the tidal current ellipse, with an additional transect perpendicular to the tidal current ellipse major axis over Jones Bank.

Over Labadie Bank (Fig 4.2) and Jones Bank (Fig 4.3) the SCM demonstrated increased peak [Chl *a*], in particular in patches over the bank edge slopes in the Jones Bank example. The second Jones Banks transect, perpendicular to the tidal ellipse major axis, crossed Jones Bank between the two [Chl *a*] patches seen on the along bank transect. The perpendicular transect showed no increase in [Chl *a*] within the SCM either over the bank or slopes. Thus it would appear the mechanism causing the increase in [Chl *a*] arose over bank edge slopes which run perpendicular to the major tidal currents only.

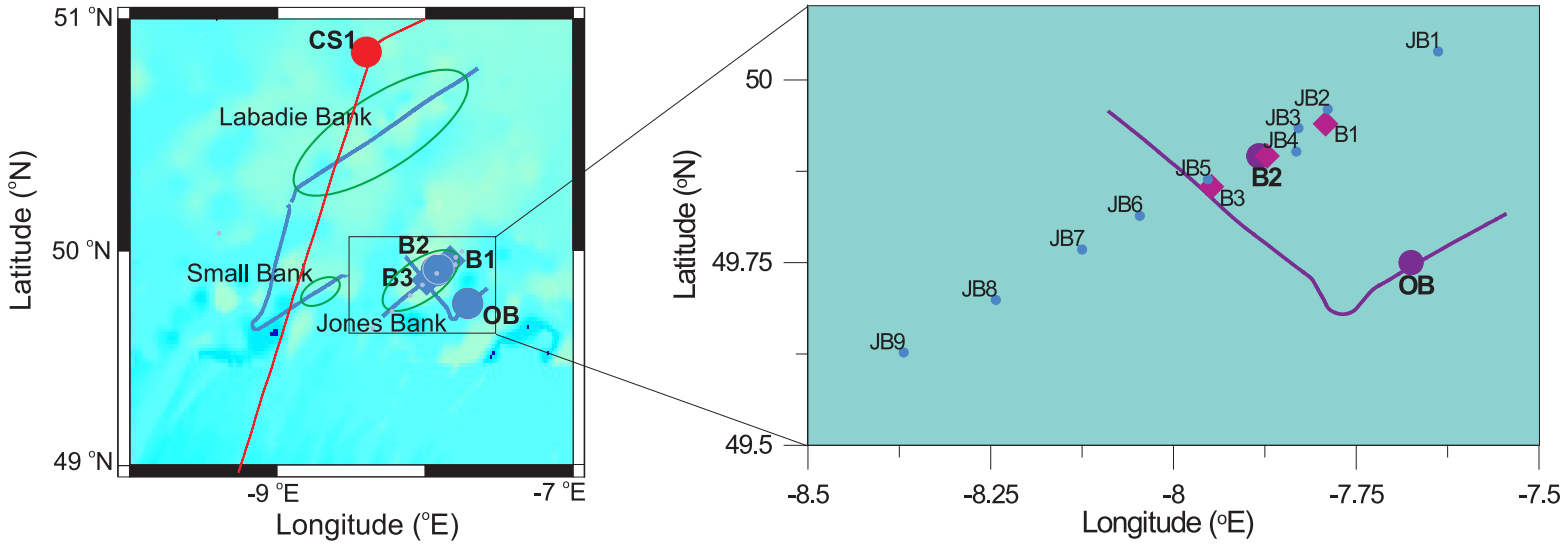

Figure 4.1

Celtic Sea shelf, in the region dominated by topographic banks. The expanded section covers Jones Bank. The large circles show positions used for CTD and FLY stations, smaller dots are CTD casts, diamonds are the mooring positions, and solid lines are the SeaSoar transects, carried out during JR98 (2003, red) and CD173 (2005, purple). See chapter 2 for detailed positions and methods. Green ellipses indicate positions of banks studied. The bathymetry colour scale runs from 0 – 200 m (white – blue), below 200 m masked dark blue. Bathymetry data from IOC et al. (2003)

All four transects showed evidence of increased mixing from the thermocline and SCM into the bottom mixed layer, with higher temperatures and elevated [Chl *a*] in the bottom mixed layer over all three banks compared to away from the banks (Figs 4.2–4.5). Bottom water chlorophyll *a* concentrations seemed to be highest over the slopes of the banks, seen clearest in the Jones Bank transect following the major axis of the tidal ellipse (Fig 4.6). This could be due to the increased [Chl *a*] within the thermocline, i.e. more phytoplankton available to be mixed out. However there appears to be proportionally more chlorophyll *a* mixed out of the SCM over the bank slopes, supporting mixing occurring particularly strongly over the bank slopes.

The thermocline and SCM tended to exhibit changes in depth over the banks. Along Jones Bank and Small Bank the thermocline (taken as the 13 ^{o}C isothermal) seemed to lower ~5 m (Fig 4.3 and 4.5), however over Labadie Bank the thermocline appeared to rise ~5 m over summit of the bank (Fig 4.2). The transect across Jones Bank, at right angles to the major axis of the tidal ellipse, exhibited a change in thermocline depth over the bank of around 12 m (Fig 4.4), but as the thermocline depths away from the bank had similar variations it was difficult to ascertain what was caused by the bank itself.

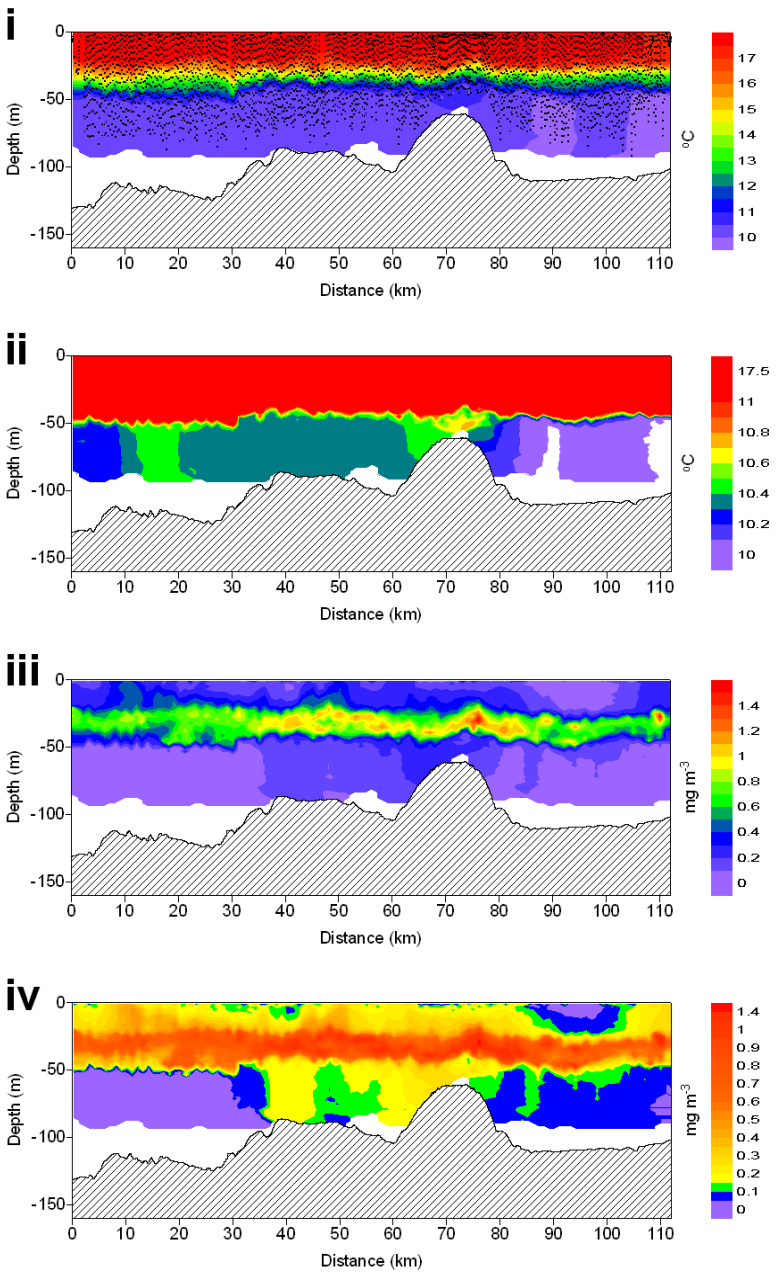

Figure 4.2

Labadie Bank SeaSoar transect along the tidal ellipse major axis, 09:10–18:15 30th July 2005. i) Temperature (°C), every 5th SeaSoar data point shown, ii) Temperature (°C, scale skewed to lower temperatures), iii) chlorophyll *a* concentrations (mg m^{-3}) and iv) chlorophyll *a* concentrations (mg m^{-3}, scale skewed to lower concentrations).

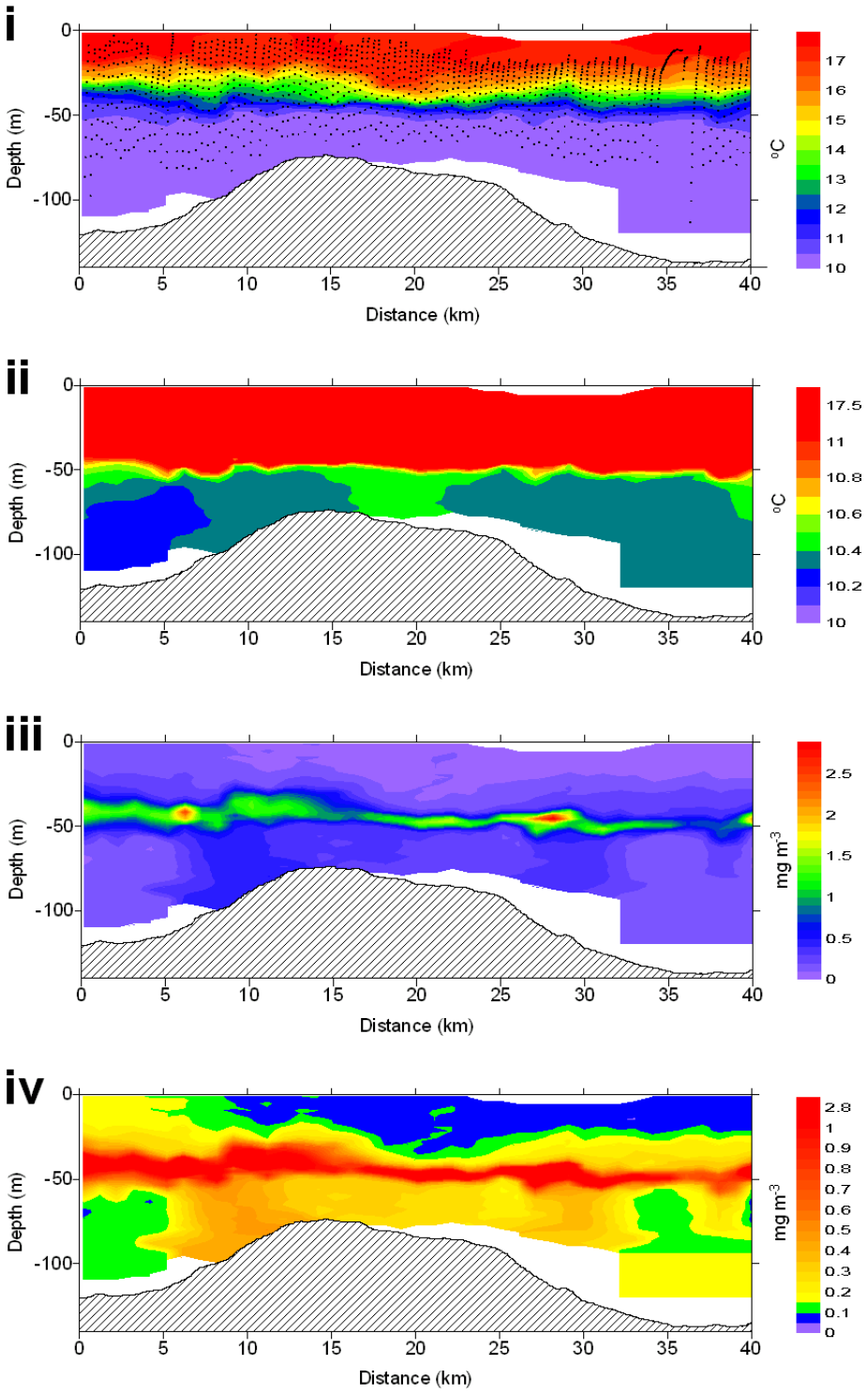

Figure 4.3

Jones Bank SeaSoar transect along the tidal ellipse major axis, 05:30–08:10

20th July 2005. As Figure 4.2

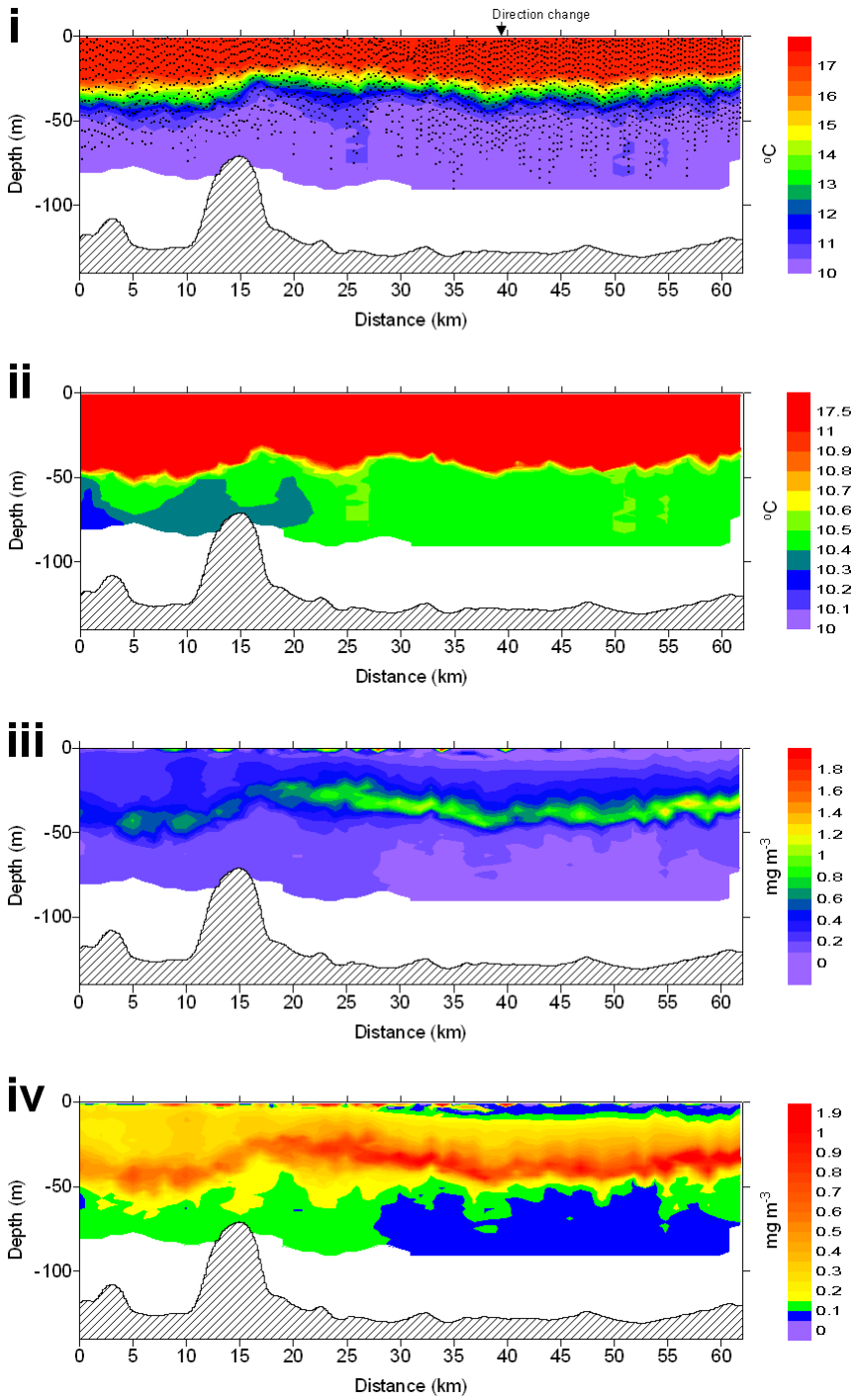

Figure 4.4

Jones Bank SeaSoar transect perpendicular to the tidal ellipse major axis with extension over flat seafloor around OB, 06:20–11:30 1st August 2005.

As Figure 4.2

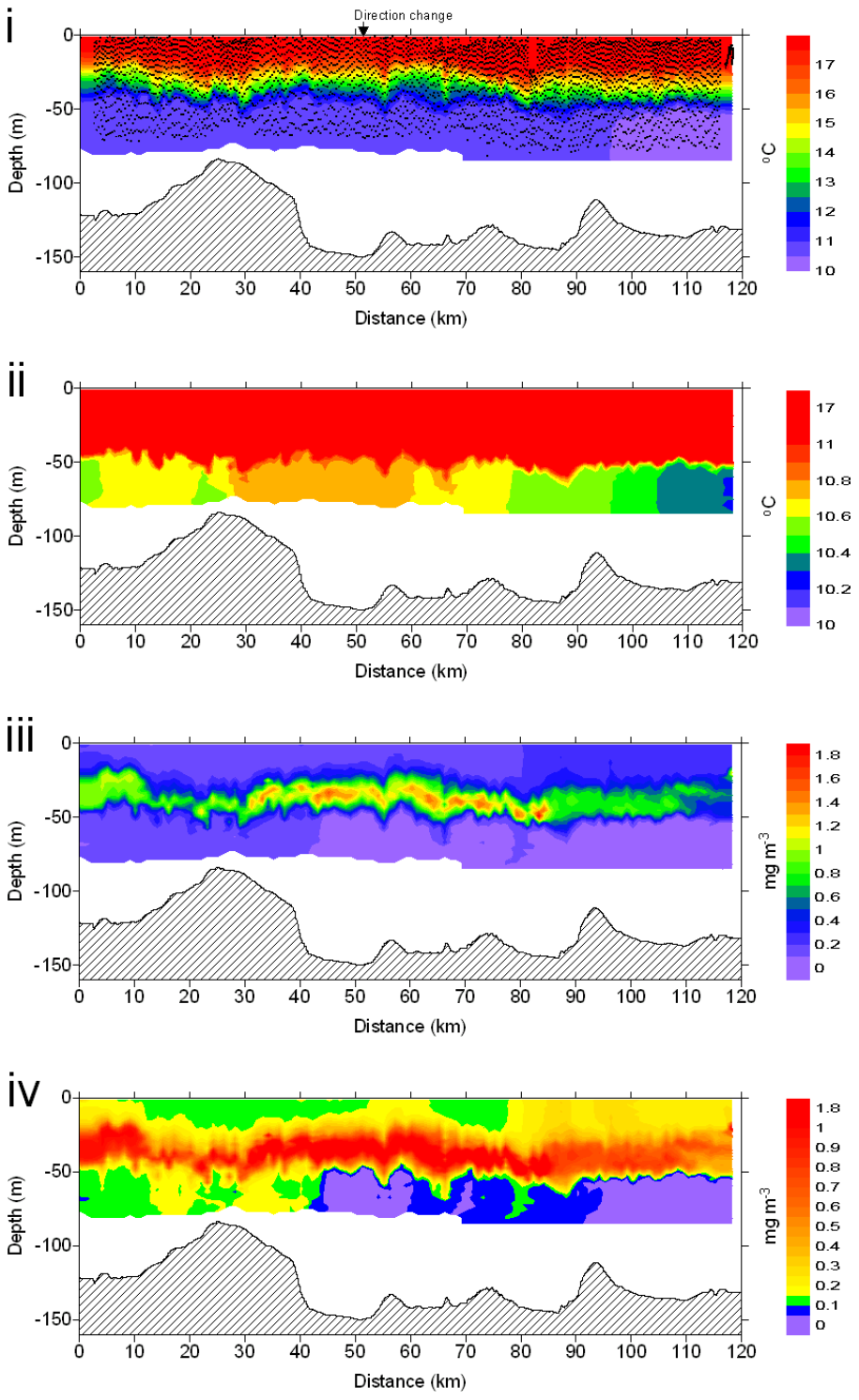

Figure 4.5

Small Bank SeaSoar transect along the tidal ellipse major axis with extension over flat seafloor, 18:00 29th –03:35 30th July 2005. As Figure 4.2

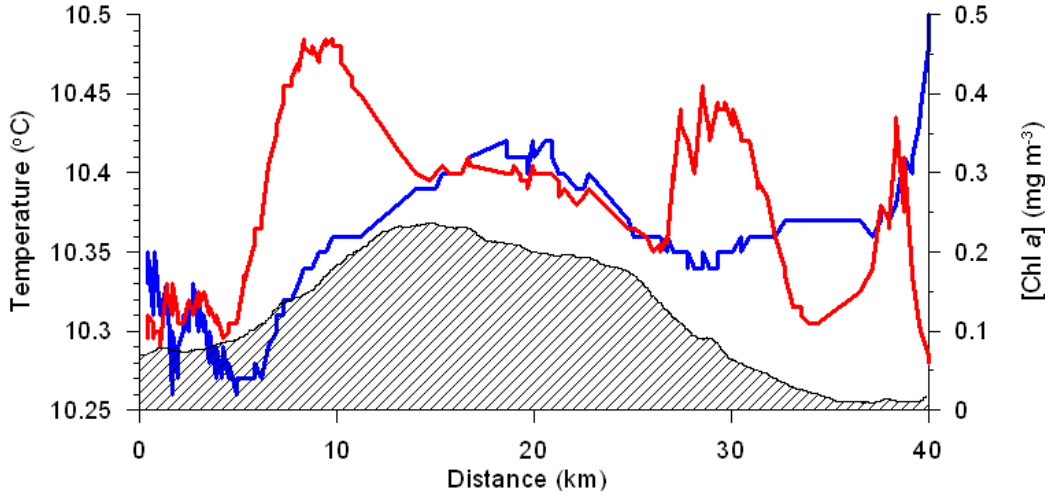

Figure 4.6

Mean SeaSoar temperature (blue) and chlorophyll *a* concentrations (red) between -60 m and -70 m depth from the Jones Bank SeaSoar transect along the major tidal ellipse axis, 2005. Topography of Jones Bank is superimposed, scaled as fig 4.3.

4.3 Jones Bank experiment

Jones Bank was selected as a potential focus of CD173 previous to the cruise by virtue of it being named, implying high fish stocks hopefully supported by high primary production in the region. SeaSoar data collected over Jones Bank displayed distinct high [Chl *a*] patches situated within the SCM and bottom mixed layer over both the north and south slopes of the bank (Fig 4.3). Due to Jones Bank length (~25 km), any signal generated over one slope would not be

advected to the opposite slope over a tidal cycle, as the tidal excursion of ~8 km is less than the length of the bank. The north-northeast slope of the bank was chosen for situating the moorings and CTD and FLY stations as it lay perpendicular to the major axis of the tidal ellipse.

B2 was selected as the position of a 25 hour CTD and FLY station (Table 2.1 and Fig 4.1), as it was situated within the high [Chl *a*] patch over the Jones Bank slope, based on the results of the SeaSoar sections. B2 was sampled twice, B2a on the 26th – 27th July, midway between spring and neap tide, and B2b on the 31st July – 1st August, around neap tide. Moorings were ranged over the same bank slope, placed at the bank crest (B3), halfway down the slope (B2) and at the bottom of the slope (B1, Fig 4.1).

A CTD transect (casts JB 1–9, Fig 4.1) was carried out (29th July 2005). The CTD transect confirmed the findings of the SeaSoar transect of the same orientation (Fig 4.3) which took place 9 days before, with high [Chl *a*] within the SCM over the bank edge slopes, along with increased [Chl *a*] in the bottom mixed layer. The temperature of the bottom mixed layer was increased over the bank also.

A FLY transect took place back and forth between B1 and B3 (2nd–3rd August 2005). Unfortunately, the FLY transect was at the same locations over the bank at the same points in the tidal cycle, and not in position to catch any possible lee wave formation (see Chapters 3 and 4 discussion). The temperature logging mooring deployed at B1 was lost, as was the B3 ADCP mooring. See chapter 2 for more detail on all methods.

As a comparison to the bank stations a site situated over a flat seabed was also visited. OB was occupied once (1st–2nd August 2005, Fig 4.1), at neap tide.

4.3.1 Hydrographic characteristics of the thermocline, chlorophyll *a* concentrations and the nitracline.

B2 was located in ~125 m depth of water and OB in a depth of around 132 m. Both occupations of B2 and the station at OB had well mixed bottom and surface layers, separated by a thermocline with a temperature difference of ~7–8 ^{o}C across a thickness averaging 30 m at B2 and 20 m at OB (Fig 4.7). Density was primarily controlled by temperature at all stations (r^2>0.999, p<0.05).

Chlorophyll *a* concentrations peaked in a subsurface maximum located towards the base of the thermocline during B2a, B2b and OB (Fig 4.8). Around 50% of the [Chl *a*] increase was due to an increase in biomass (personal communication, C.M. Moore). The [Chl *a*] distribution against temperature (Fig 4.9) was asymmetrical at B2b and OB, and B2a the majority of the time, suggesting phytoplankton were able to concentrate towards the base of the thermocline without being redistributed within the thermocline at too great a rate to allow accumulation. The SCM chlorophyll *a* was not as concentrated within the base of the thermocline over the bank slopes at B2 as over the flat shelf at OB, suggesting potentially higher mixing rates over the bank slope. B2b in particular displayed a less sharp peak. At B2a the distribution of [Chl *a*] with temperature (Fig 4.9 a) occasionally changed. Over two periods [Chl *a*] became evenly distributed throughout the thermocline (centred on Yeardays 206.88 and 207.4).

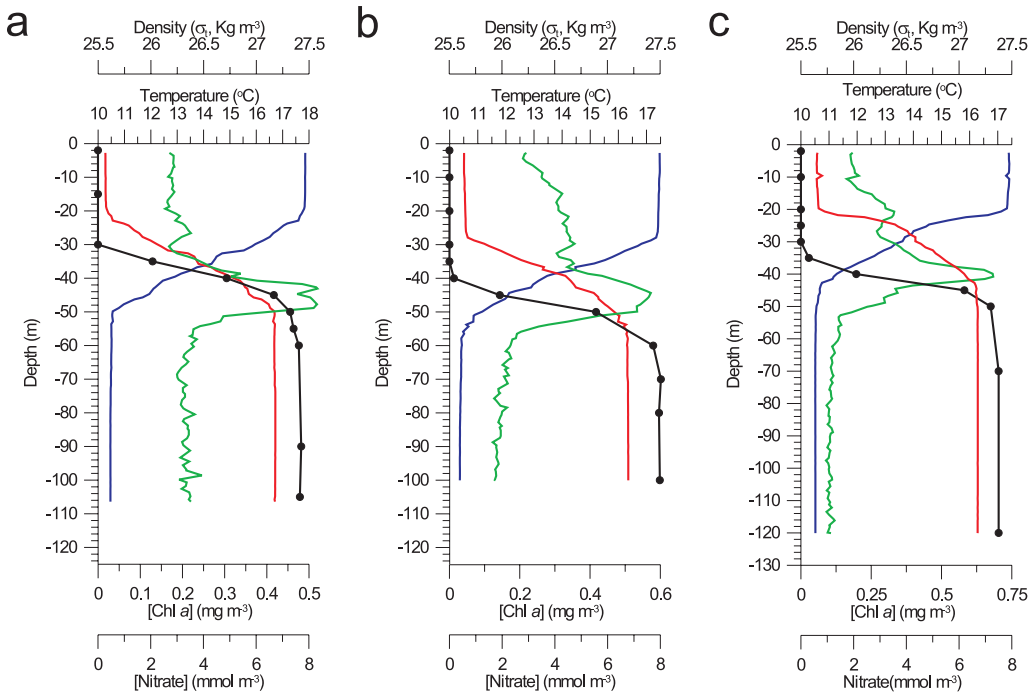

Figure 4.7

Examples of CTD and nutrient sample profiles for a) B2a (20:10, 26th July 2005, b) B2b (16:00, 31st July 2005) and OB (11:10, 2nd August). Blue represents CTD temperature, red CTD density, green CTD chlorophyll *a* concentrations and black water sample nitrate concentrations. Note differing scales.

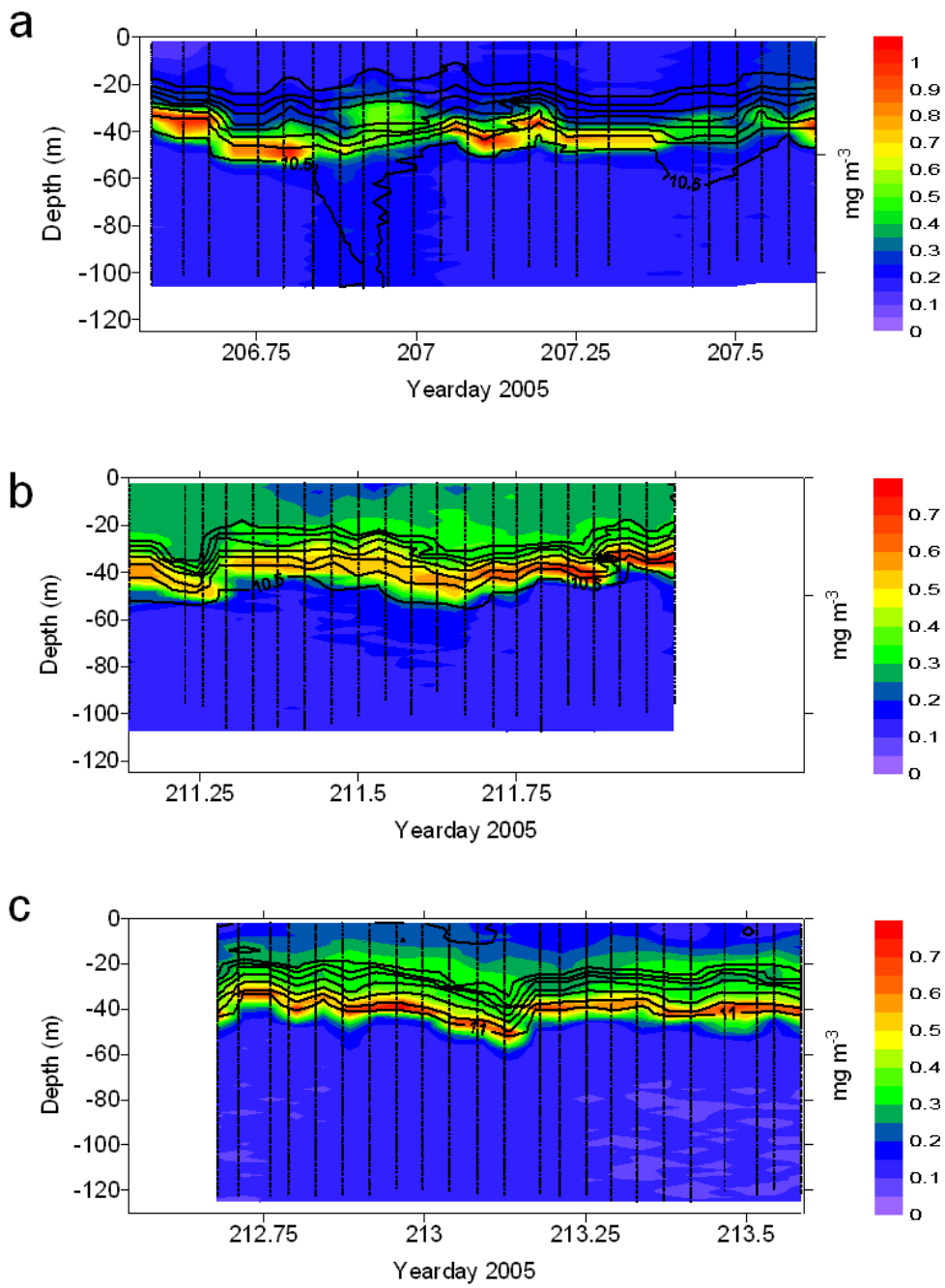

Figure 4.8

Time series of CTD chlorophyll *a* concentrations (coloured contours) and temperature (black lines, every 1 ^{o}C) against depth during a) B2a, b) B2b and c) OB. Data points indicated. The data gaps were caused by problems with the CTD wire. Note differing scales.

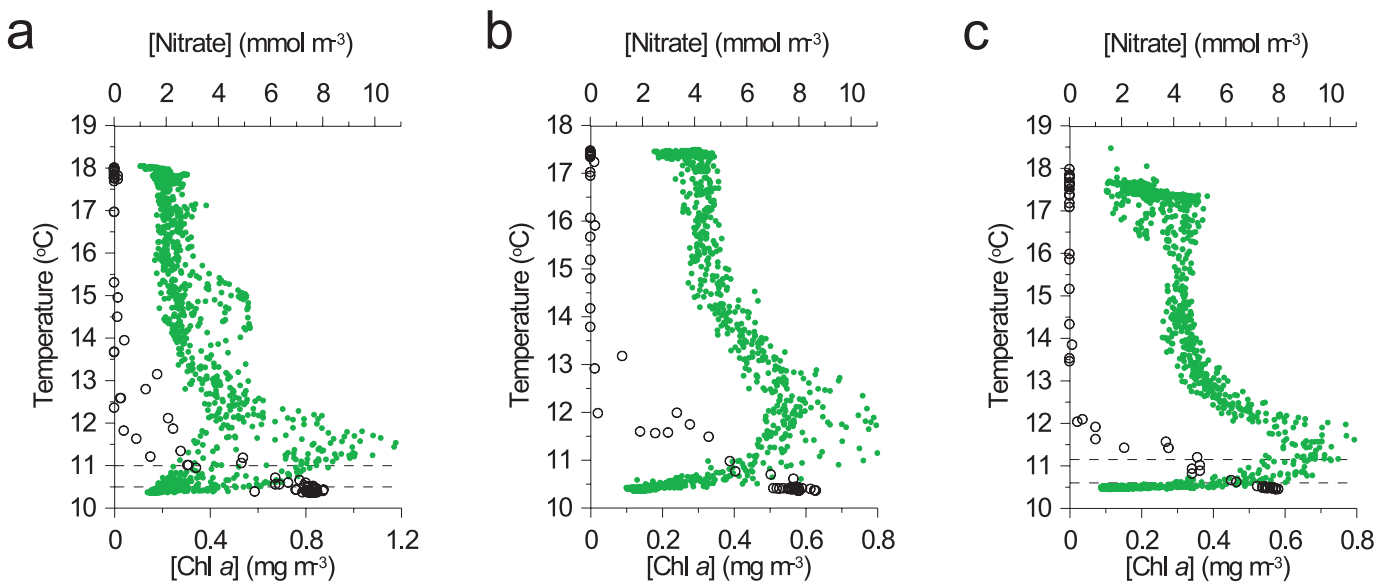

Figure 4.9

Stations a) B2a, b) B2b and c) OB CTD chlorophyll *a* concentrations (green dots) and water sample nitrate concentrations (black circles) against temperature. Note differing scales. The black dashed lines mark the boundaries of the temperature range over which the vertical nitrate flux into the SCM was calculated for each profile. B2a 10.5–11 °C, OB 10.6–11.1 °C. Method of calculating J_N at B2b requires no temperature range (see section 2.3).

The bottom mixed layer of all three stations contained non-zero concentrations of chlorophyll *a*. Both B2a and B2b had proportionally higher [Chl *a*] in the bottom mixed layer, compared to peak SCM values, than OB (Fig 4.7). This suggested mixing between the bottom mixed layer and the SCM was greater at B2 than OB.

Thermocline and SCM thickness fluctuated over time, as did their position within the water column (Fig 4.8). At B2 thermocline and SCM thickness were not related ($r^2<0.18$, $p>0.05$ for both B2a and B2b).

At OB changes in thermocline and SCM properties could be attributed to advection. A section of the SeaSoar transect across Jones Bank passed over the position of OB (Fig 4.10) and demonstrated horizontal patchiness in thermocline and SCM thickness and [Chl *a*] within the SCM with similar range to the variability seen during OB. During OB bottom mixed layer temperature increased periodically by up to 0.1 ^{o}C (data not shown), however there was no corresponding increase in [Chl *a*] in the bottom mixed layer nor change in the nitrate profile to support mixing without advection as the cause.

Water samples were collected for nitrate analysis at all stations. Nitrate concentrations in the bottom mixed layer were around 8 mmol m^{-3}, whereas [Nitrate] in the surface mixed layer (Fig 4.7) were below detection limits during all stations. The layer of minimum [Nitrate] extended into the top of the thermocline. The position of the nitracline corresponded to the position of the SCM (Fig 4.9).

There was no SUV6 sensor on the CTD during B2a, B2b or OB. $\Delta N/\Delta z$ was estimated using the methods detailed in section 2.3. During B2a and OB $\Delta N/\Delta z$ was maximum between the base of the SCM, and peak [Chl *a*] (Fig 4.11).

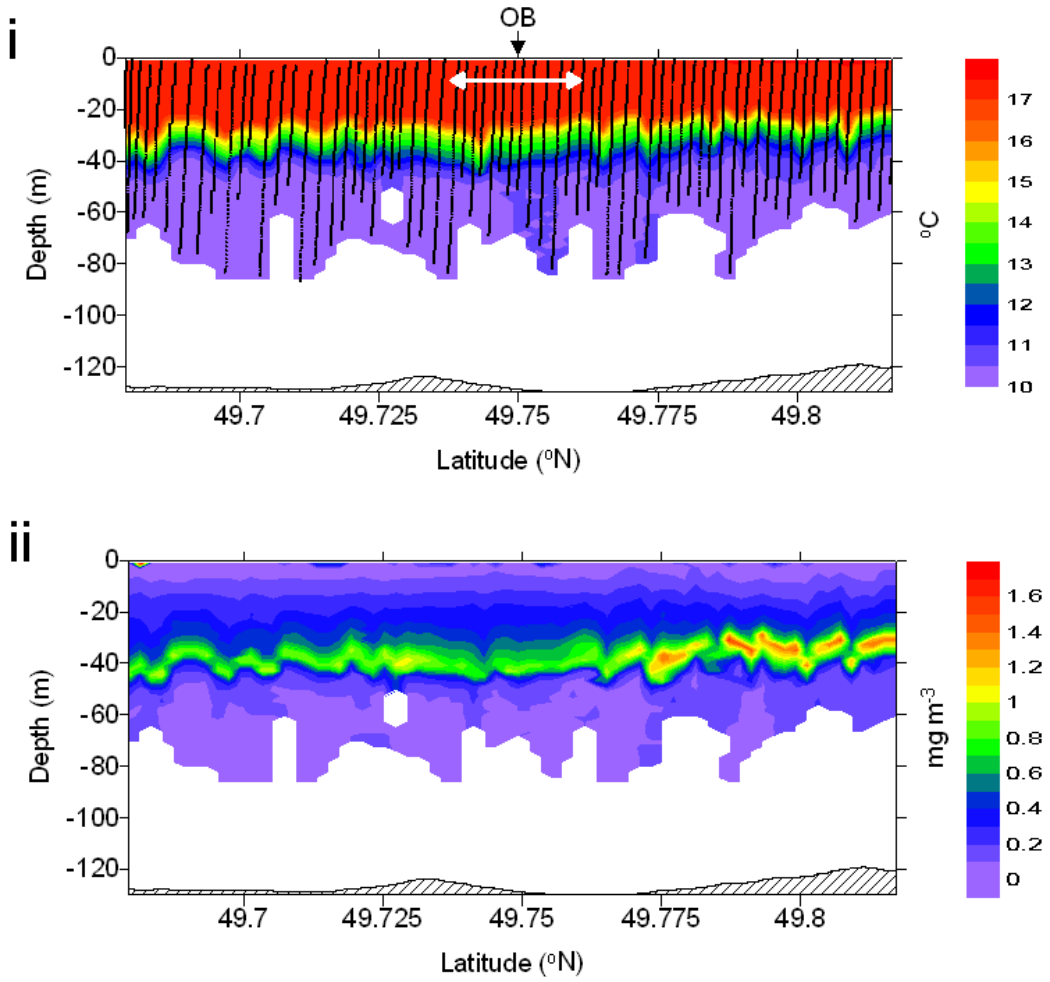

Figure 4.10

SeaSoar data around OB (Latitudes 49.680–49.817 °N, 09:30– 1:30 1st August 2005, taken from the across Jones Bank transect southwest-northeast extension over a flat seabed, Fig 4.4). SeaSoar i) temperature and ii) chlorophyll *a* concentrations. Every 2nd SeaSoar data point indicated in i). The white arrow denotes approximately one tidal excursion.

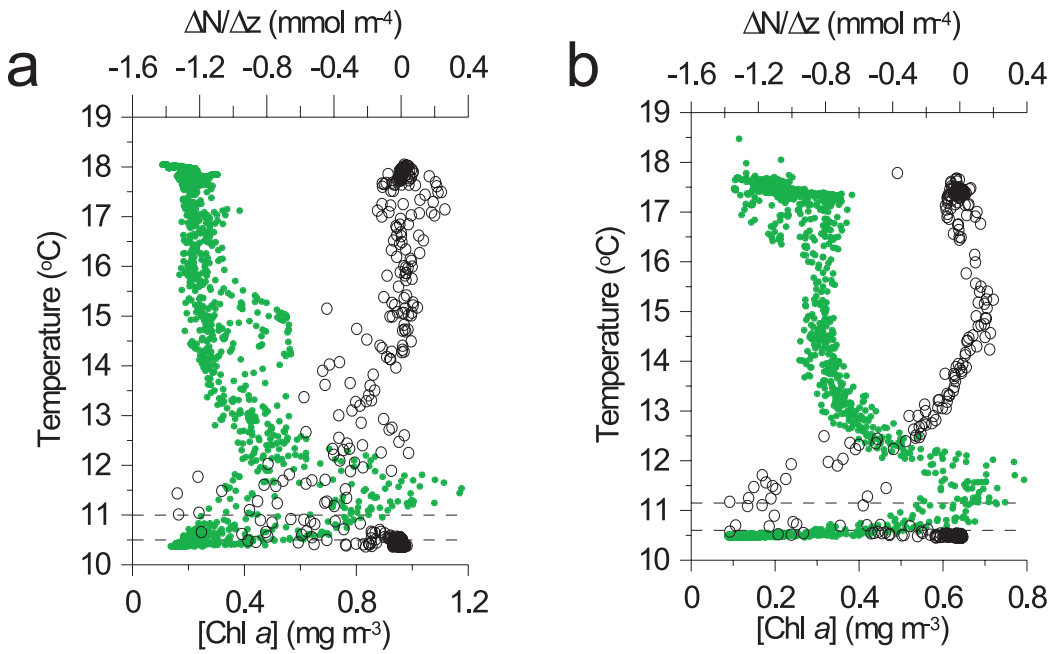

Figure 4.11

Stations a) B2a and b) OB CTD chlorophyll *a* concentrations (green dots) and derived nitrate gradients (black circles) against temperature. Note differing scales. The black dashed lines mark the boundaries of the temperature range over which the vertical nitrate flux into the SCM was calculated for each profile. B2a 10.5–11 °C, OB 10.6–11.1 °C.

At B2b $\Delta N/\Delta z$ was calculated differently (see section 2.3 *$\Delta N/\Delta z$ estimated from bottom and surface mixed layers*). This gave only one $\Delta N/\Delta z$ data point per cast, so the distribution of $\Delta N/\Delta z$ against depth or temperature, compared to that of [Chl *a*], could not be established.

Mean $\Delta N/\Delta z$ at the base of the SCM (section 2.3) at B2a and OB, and estimated $\Delta N/\Delta z$ at B2b, fluctuated over the duration of all stations (Fig 4.12).

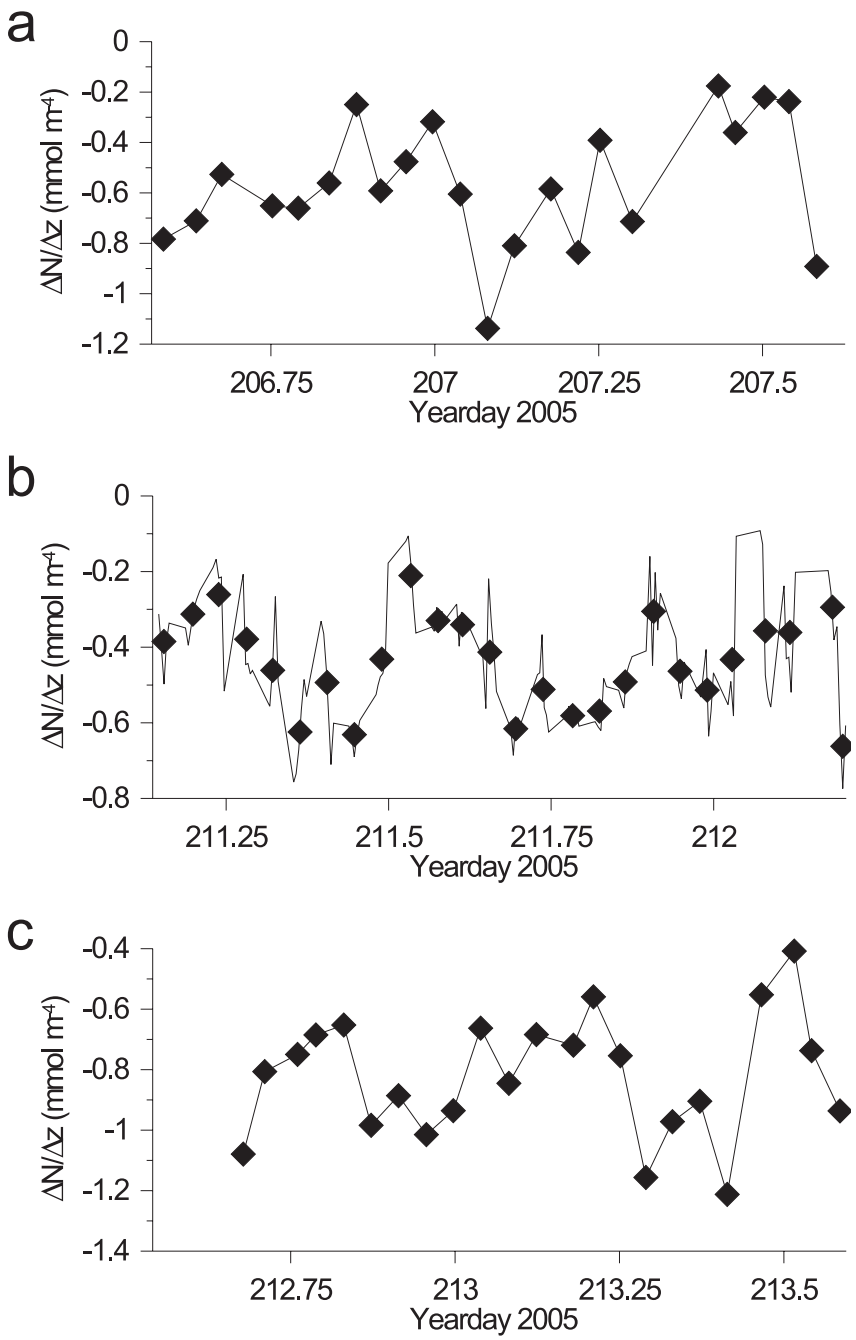

Figure 4.12

Mean nitrate gradient, over the temperature ranges used to calculated vertical nitrate flux, for each CTD or FLY profile during a) B2a (CTD), b) B2b (FLY, the black diamonds mark the average value for each FLY ensemble) and c) OB (CTD). Note differing scales.

During B2 around 70% of variability in $\Delta N/\Delta z$ was explained by variations in the chlorophyll *a* gradient ($\Delta[Chl\ a]/\Delta z$) at the base of the thermocline ($r^2>0.68$, $p<0.05$). During OB only around 20% of variability was explained by changes in $\Delta[Chl\ a]/\Delta z$ ($r^2=0.20$, $p<0.05$).

The nitrate gradient at the base of the thermocline was significantly higher at B2a (Fig 4.12 a) compared to B2b (Fig 4.12 b, $F=11.0$, $F_{crit}=3.9$, $p<0.05$). However, OB (Fig 4.12 c) had significantly higher mean nitrate gradients than either B2a ($F=14.3$, $F_{crit}=4.1$, $p<0.05$) or B2b ($F=111$, $F_{crit}=3.9$, $p<0.05$). The daily mean nitrate flux into the SCM from the bottom mixed layer reflected this (Table 4.1).

4.3.2 Currents, turbulence and mixing

All stations exhibited a clear semi-diurnal signal in tidal current velocity (Figs 4.13 –4.15 i). Near bed currents on individual ADCP profiles reached maximum velocities of ~-0.4 m s^{-1} and ~-0.3 m s^{-1} during B2a and B2b respectively and ~0.2 m s^{-1} at OB. Regrettably, the ADCP moorings at B2 were not in place long enough to cover a full spring-neap cycle, however the data do show the transition between spring and neap tides (Fig 4.16). At neap tide (B2b) surface currents were weaker, and had a phase difference of almost 90^o, compared to the bottom layer tidal currents.

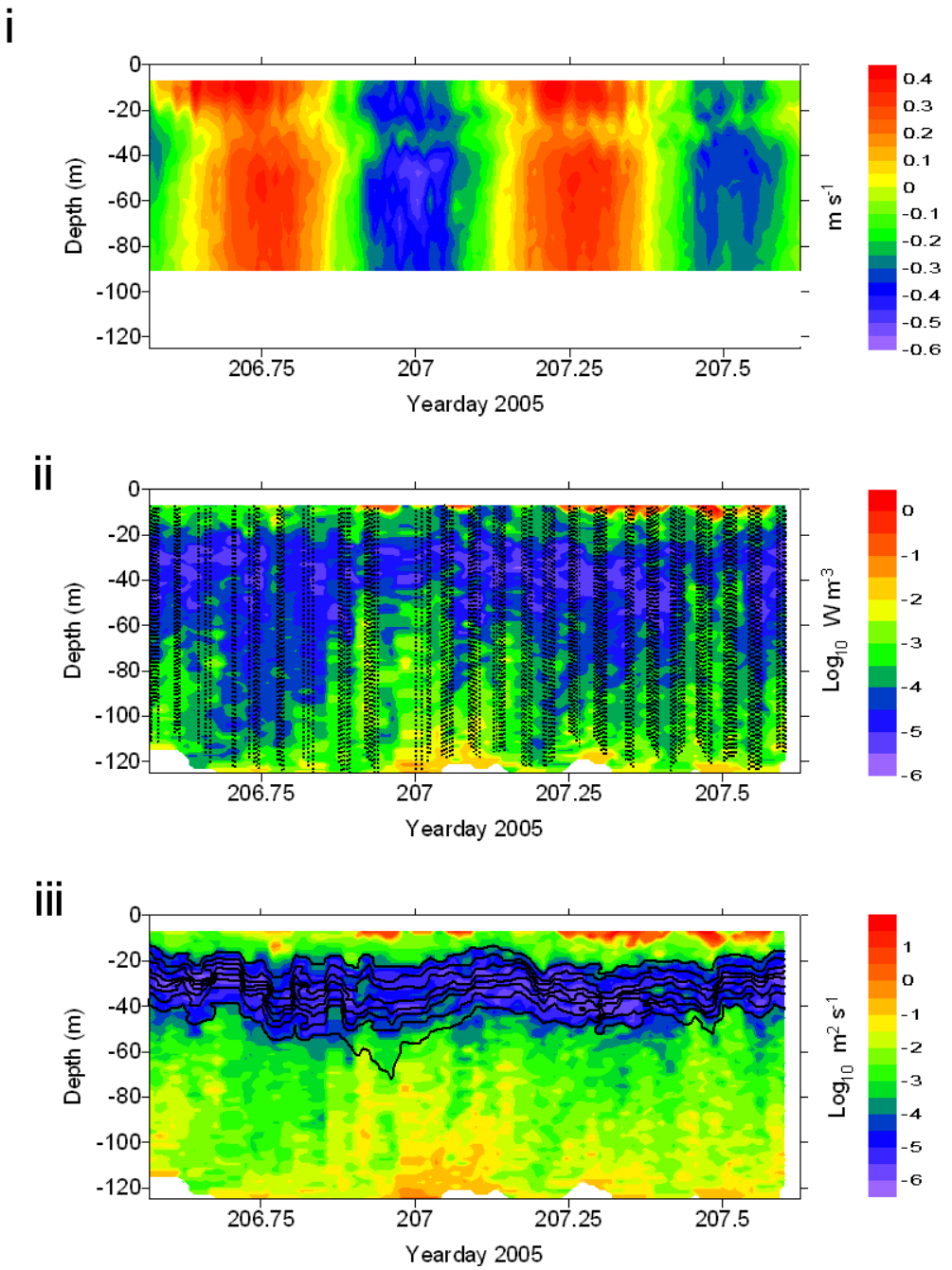

Figure 4.13

B2a i) Ships ADCP northwards current velocity, ii) FLY turbulent dissipation rate (every 2nd FLY data point marked) and iii) FLY vertical diffusivity (coloured contours) and FLY temperature (black lines, 1 °C intervals, lowest isothermal=10.5 °C)

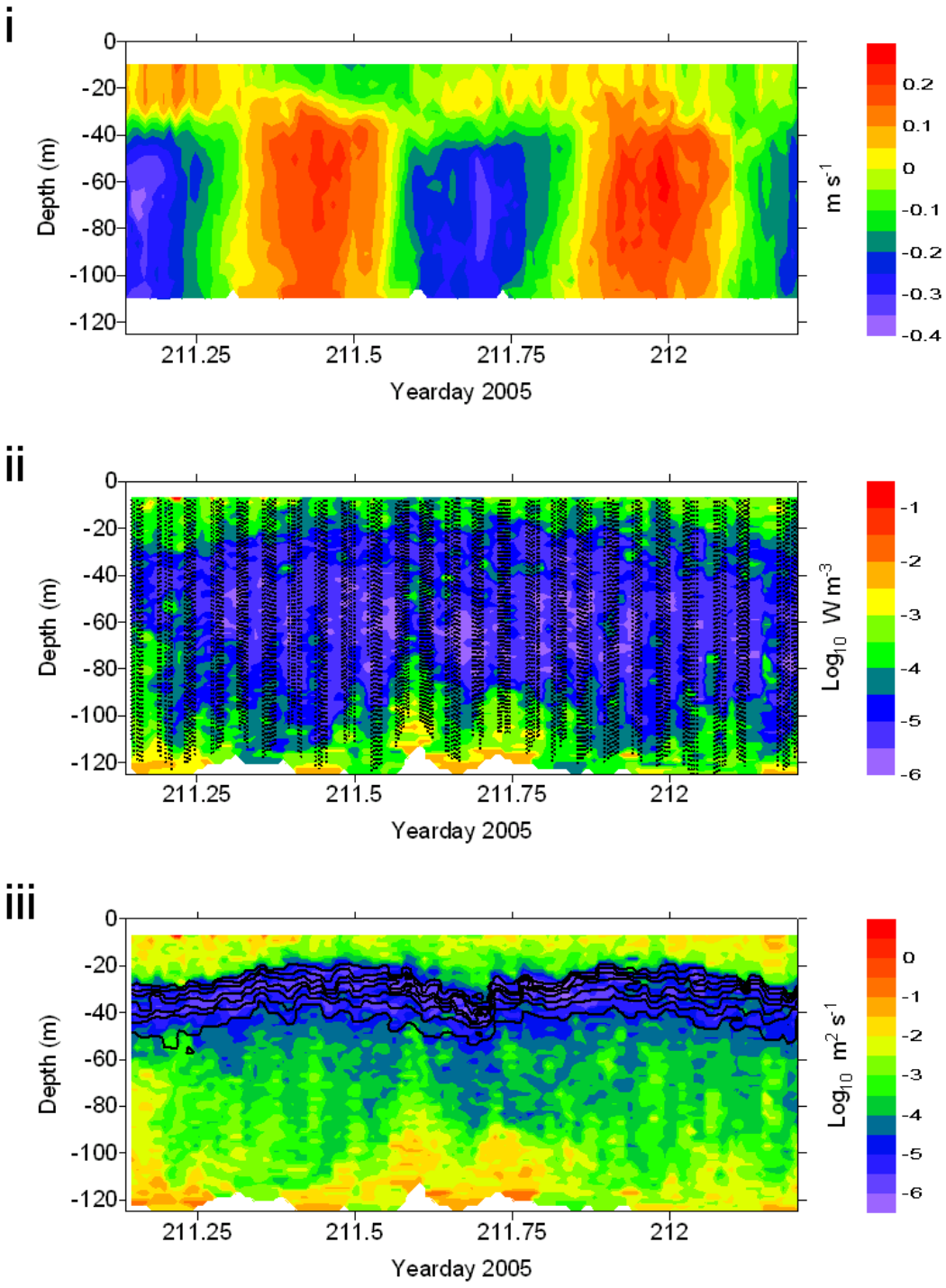

Figure 4.14

B2b. As Fig 4.13.

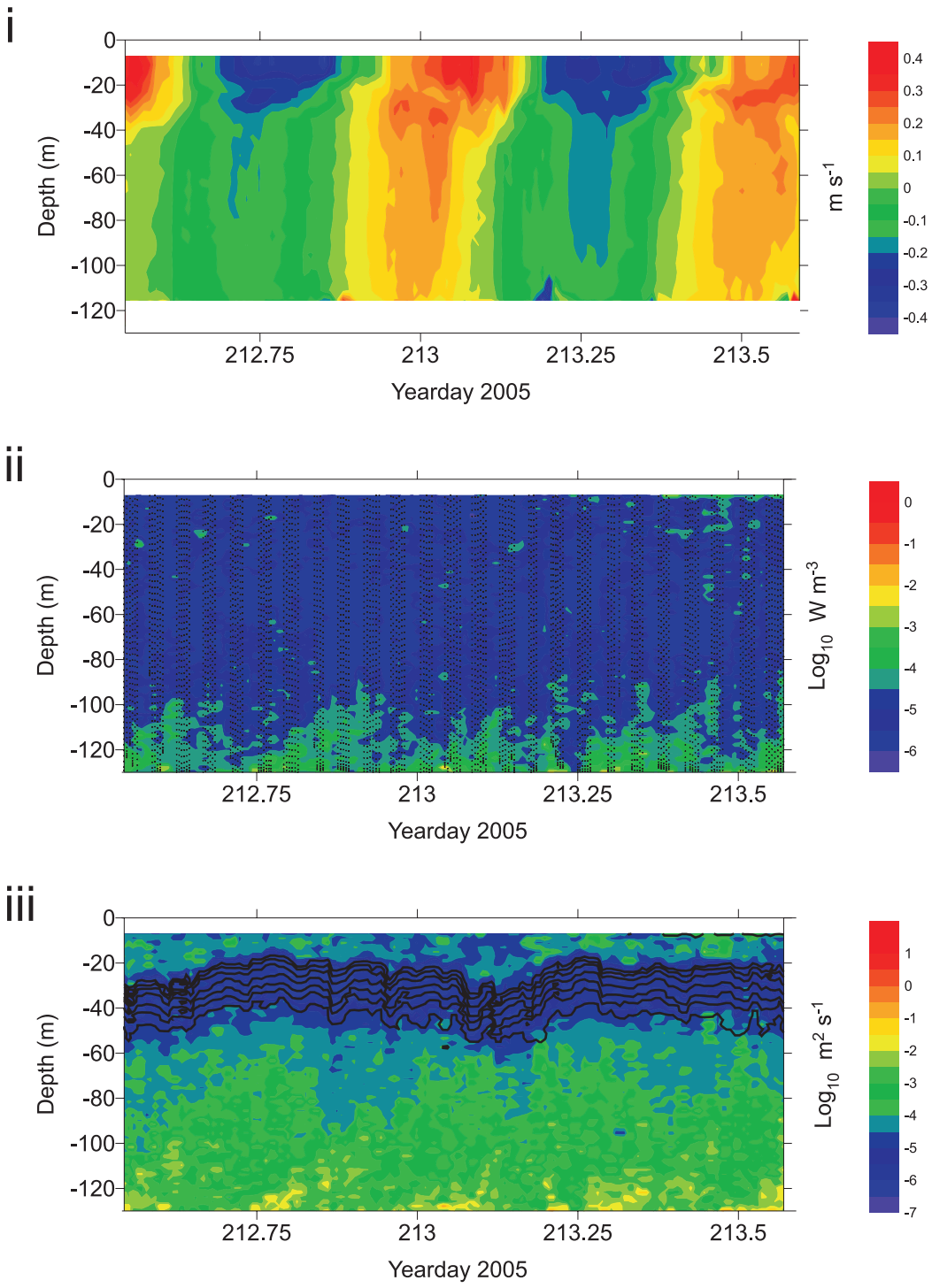

Figure 4.15

OB. As Fig 4.13.

Strongest rates of turbulent dissipation, ε, were seen at the surface and base of the water column during all stations (Figs 4.13 ii, 4.14 ii and 4.15 ii). Surface turbulence, caused by contamination by the ships wake, and wind and wave action, did not penetrate far into the thermocline, and so was of no consequence at the base of the thermocline where it would have affected nitrate flux into the SCM. There was a quarter-diurnal signal in ε close to the bed, with increased values associated with maximum near bed current velocities. Examination of individual FLY profiles revealed the quarter-diurnal intensified turbulent dissipation signal reached maximum heights off the bed of ~60 m during B2a, ~40 m during B2b and ~30m during OB. There was a lag between maximum near bed ε and ε higher in the water column due to vertical change in the region of maximum shear (Simpson et al. 2000).

All three stations displayed minimum turbulent dissipation in the interior of the water column, and minimum vertical diffusivity, K_z, within the thermocline (Figs 4.13 iii, 4.14 iii and 4.15 iii), although care must be taken in interpreting K_z out with the thermocline, where stratification, and hence N^2, was low (section 2.1.3). During B2a there were periods of increased ε and K_z within the thermocline (~Yeardays 206.88–207.06 and 207.46–207.52), which were not associated with high near bed currents. These occurred as the tidal currents were flowing southward, towards the top of the bank from B2.

Mean K_z at the base of the SCM for each $\Delta N/\Delta z$ profile varied through the stations' durations by over three orders of magnitude (Fig 4.17). The range of mean K_z values at B2a were significantly higher than those at B2b (F=4.8, F_{crit}=3.9, p<0.05). Mean K_z throughout OB was significantly lower than at B2a

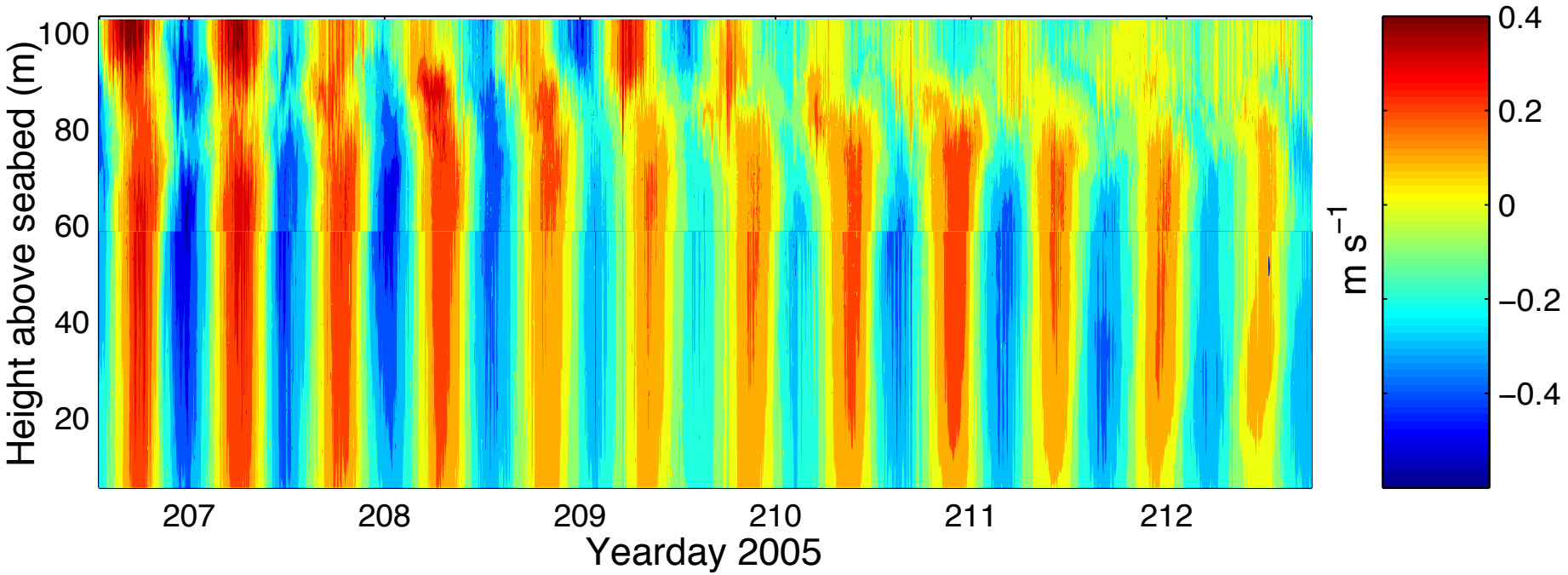

Figure 4.16

ADCP northwards current velocity from the moorings deployed at B2 in 2005. 0–60 m above bed data from 300 kHz ADCP Lander, 60 m–surface data from 600 kHz SUBS buoy ADCP. Spring tide occurred at ~Yearday 203, neap tide ~Yearday 211

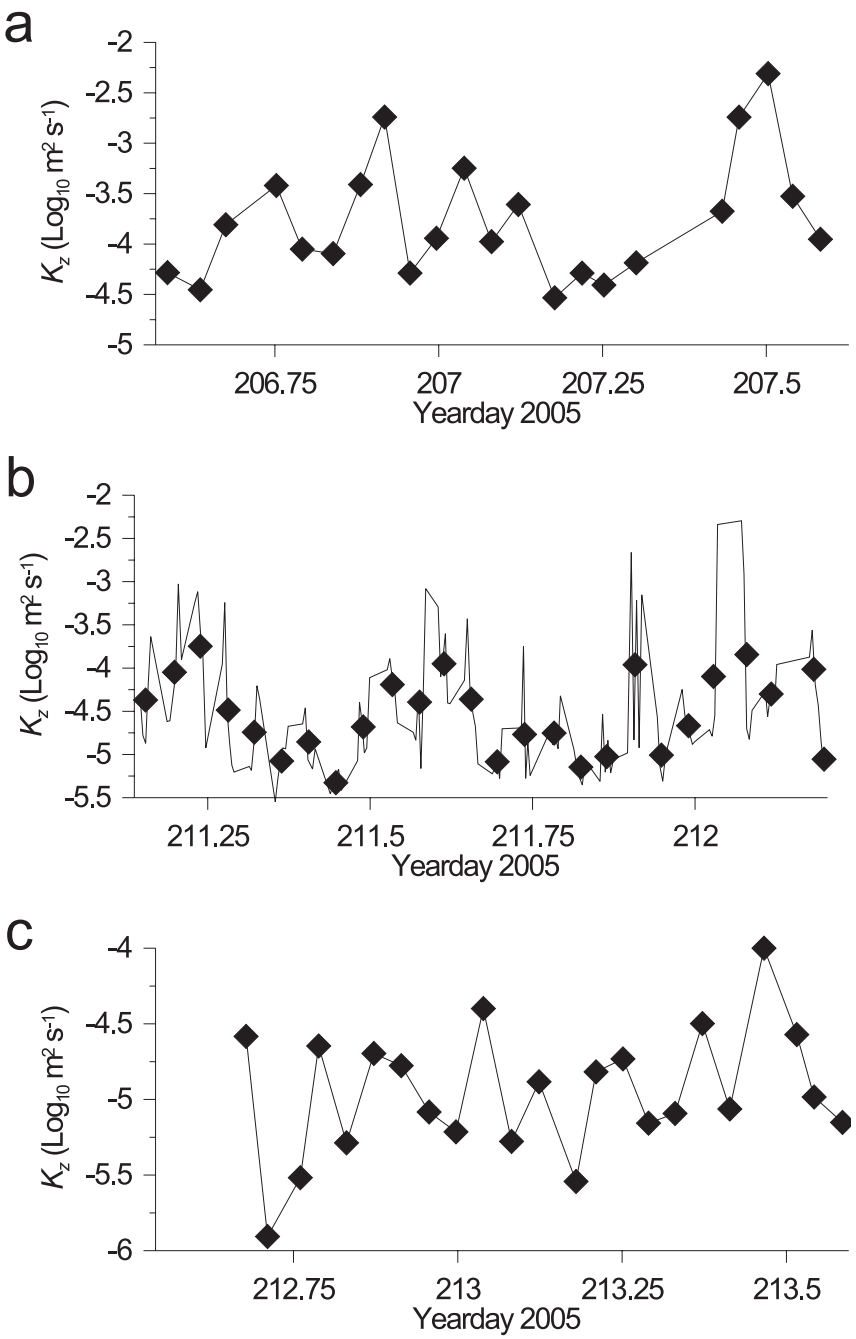

Figure 4.17

Mean vertical diffusivity, over the temperature ranges used to calculate the vertical nitrate flux, for each CTD or FLY profile during a) B2a (CTD), b) B2b (FLY, the black diamonds mark the average value for each FLY ensemble) and c) OB (CTD). Note differing scales.

(F=5.0, F_{crit}=4.1, p<0.05) but was not significantly different from mean K_z at B2b (F=1.4, F_{crit}=3.9, p>0.05). This was reflected in the daily mean K_z for the stations (Table 4.1), which demonstrated higher vertical diffusivities at B2a, compared to both B2b and OB.

4.3.3 Nitrate fluxes

Estimates of the vertical nitrate flux, J_N, from the bottom mixed layer into the SCM for each profile (see section 2.3 for methods) varied by around 1.5 orders of magnitude over the durations of the CD173 stations (Fig 4.18). The time series of J_N at B2a was significantly higher than that of B2b or OB (F=23.4, F_{crit}=3.9, p<0.05 and F=6.8, F_{crit}=4.1, p<0.05), with daily mean J_N greatest at B2a also (Table 4.1).

During all stations 80–90% of variability in J_N was explained by K_z (r^2=0.81 for B2a, r^2=0.84 for B2b and r^2=0.89 for OB, p<0.05 for all). Therefore higher vertical fluxes occurred at times of increased vertical diffusivity. $\Delta N/\Delta z$ explained around 20% of variance in J_N during B2b (r^2=0.22, p<0.05). However $\Delta N/\Delta z$ had no significant effect at B2a or OB.

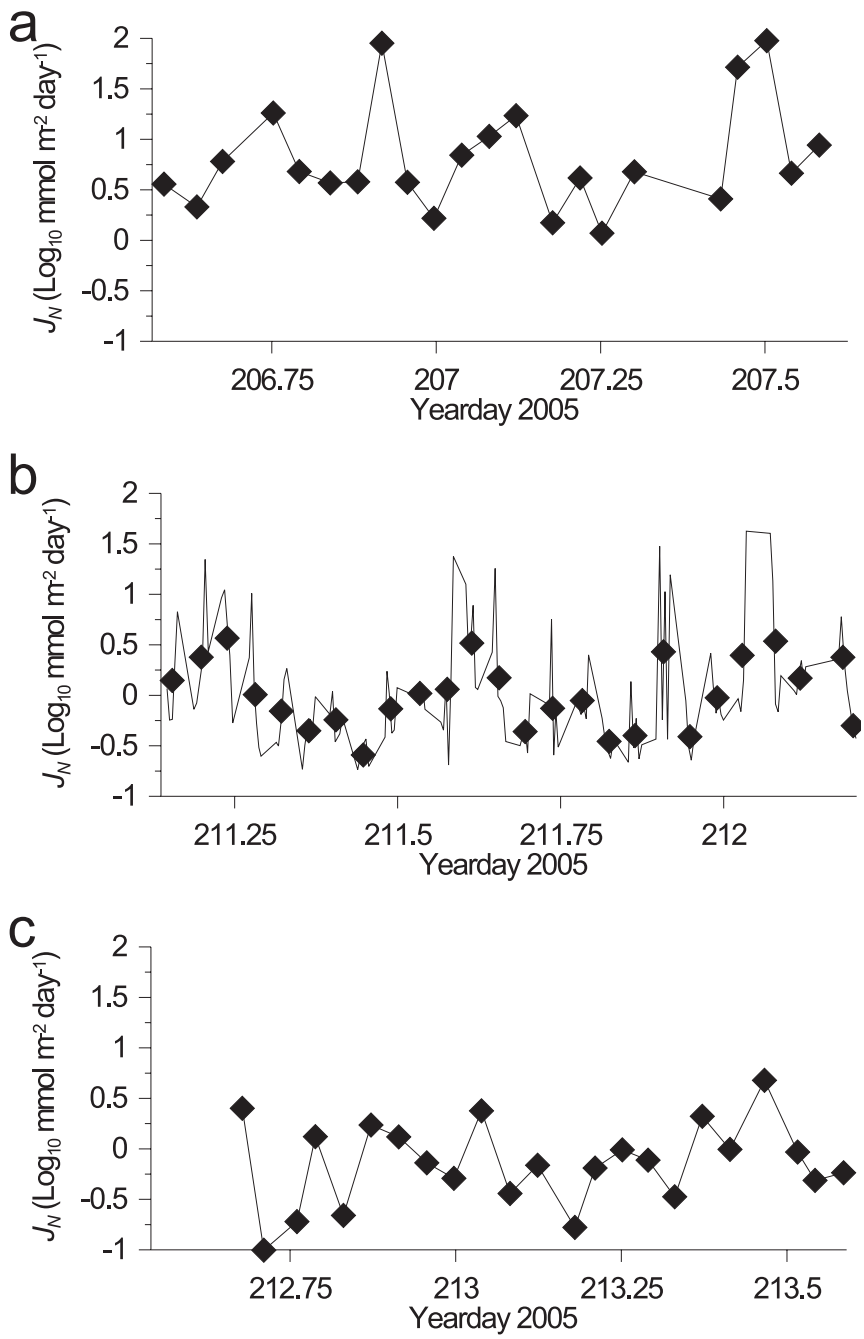

Figure 4.18

Vertical nitrate fluxes, J_N, into the subsurface chlorophyll maximum from below the thermocline for each CTD or FLY profile during a) B2a (CTD), b) B2b (FLY, the black diamonds mark the average value for each FLY ensemble) and c) OB (CTD).

Table 4.1

Daily mean vertical nitrate flux into the SCM from the bottom layer (J_N) and associated mean nitrate gradient ($\Delta N/\Delta z$), turbulent dissipation (ε) and vertical diffusivity (K_z) for stations B2a, B2b and OB, sampled during cruise CD173. Stated as average of all profiles ± error, with bootstrapped 95% confidence intervals in brackets.

Station	$\Delta N/\Delta z$ (mmol m^{-4})	ε (W m^{-3})	K_z (m^2 s^{-1})	J_N (mmol m^{-2} day^{-1})
B2a	-0.6 ± 0.9 (-0.7 – -0.4)	1.4 ± 0.7 x10^{-4} (0.4–2.7 x10^{-4})	5.3 ± 2.6 x10^{-4} (1.1–13.0 x10^{-4})	15.7 ± 26.7 (4.5 – 32.5)
B2b	-0.4 ± 0.14 (-0.5 – -0.4)	3.0 ± 1.5 x10^{-5} (2.0–4.4 x10^{-5})	1.7 ± 0.8 x10^{-4} (0.6–3.4 x10^{-4})	2.9 ± 1.8 (1.5 – 4.5)
OB	-0.8 ± 0.57 (-0.9 – -0.7)	5.4 ± 2.7 x10^{-6} (3.4–8.5 x10^{-6})	1.8 ± 0.9 x10^{-5} (0.9–3.1 x10^{-5})	1.1 ± 1.0 (0.6 – 1.8)

4.4 Discussion

The purpose of cruise CD173 in 2005 was to clarify the effect of topographic banks on the hydrology of overlying water. Of specific interest was if, and how, banks affect primary production, focusing in this thesis on nutrient supply to the subsurface chlorophyll maximum. Data from cruise JR98 in 2003 (Chapter 3), in particular station CS1, suggested banks control hydrology over

bank slopes through hydraulic control of tidal flows, i.e. lee wave formation (Moum & Nash 2000, Nash & Moum 2001). The data collected on CD173 will be used to investigate what physical processes appear to control the mixing environment over a bank, and how the bank's mixing environment affects vertical nitrate fluxes. Through this the consequences for primary production over banks are considered.

4.4.1 Physical processes controlling the mixing environment over banks.

Transect data collected using SeaSoar (section 3.2) was utilized in order to evaluate what influence banks did have on hydrology. All the surveyed banks (Jones bank, Labadie Bank and Small Bank) showed evidence of mixing in their vicinity, with increased [Chl *a*], and temperatures, in the bottom mixed layer (Figs 4.2–4.5 d).

The bottom water temperature increase, seen particularly over the bank crests (Figs 4.2–4.5 b), is most likely attributable to a combination of heating a shallower water column (i.e. more heat energy input per cubic metre than a deeper water column) and greater barotropic tidally forced boundary driven mixing at the base of the thermocline, due to the shallower depth bringing the bed closer to the thermocline. The balance between greater heat input per cubic meter water (acting to lower the isothermals against depth) and barotropic mixing (acting to raise the thermocline) could explain the variations in

thermocline depth over the different banks, with depth depending on previous heat input, i.e. weather, and position in the spring-neap tidal cycle.

Maximum bottom water heating was not necessarily co-located with the positions of increased [Chl *a*] (Fig 4.6). Although chlorophyll *a* concentrations were increased in the bottom water over the banks (Figs 4.2–4.5 d) in a similar manner to temperature, bottom water [Chl *a*] increased particularly strongly over both bank slopes of the along Jones Bank transect (Fig 4.3 d). The SeaSoar transect across Jones Bank (perpendicular to the tidal ellipse major axis, Fig 4.4) passed between the bank slope patches seen in the along Jones Bank transect (parallel to the tidal ellipse major axis, Fig 4.3). It displayed similar temperatures and Chl *a* concentrations in bottom waters over top of the bank to the along bank transect, but no additionally increased [Chl *a*] over the over the bank slopes.

This [Chl *a*] distribution, in combination with model simulations (Chapter 3), suggested two mixing processes will affect bottom water [Chl *a*] over the bank. Barotropic forcing appears to have caused some mixing at the base of the thermocline and SCM over the top of the banks, where the depth was shallower, increasing [Chl *a*] in, and assisting warming of, the bottom mixed layer. Over the bank slopes which run perpendicular to the major axis of the tidal ellipse, i.e. the tide flows across the slope from deep to shallow and shallow to deep, another mechanism further enhances mixing between the SCM and the bottom mixed layer.

Stations B2b and OB were sampled at comparable points in the spring-neap tidal cycle and were not greatly different in depth. In spite of this, B2b, and B2a, had proportionally higher [Chl *a*] in the bottom mixed layer compared to peak SCM values than OB (Fig 4.7). This corroborated enhanced mixing

between the bottom mixed layer and the SCM over bank slopes compared to a topographically flat seafloor. The heating of the shallower water column over the top of the banks possibly would mask any increase in bottom temperature over the bank slopes caused by increased mixing.

As there was an increased flux of phytoplankton out of the SCM it is likely there was an enhanced flux of nitrate in, which may explain the increased [Chl *a*] seen within the SCM over the along Jones Bank transect's bank slopes, and associated with the other banks.

Maxworthy (1979) described the formation of a lee wave downstream of a bank crest by currents flowing over the bank. As currents stopped flowing over the bank crest in that direction the wave propagated back towards the bank crest and a train of solitary waves possibly produced. The data collected at station CS1 in 2003 (see Chapter 3) suggested the possibility of the formation of lee waves over some banks in the Celtic Sea, similar to those seen over a bank on the Oregon Shelf (Moum & Nash 2000, Nash & Moum 2001).

The reversing flow of tidal currents in the Celtic Sea over banks could potentially trigger lee waves to form over opposing sides of the bank on opposing tidal current directions. Tidal excursion along the plane of the SeaSoar transects was ~8 km (calculated using ships ADCP at B2a and so slightly greater at a spring tide). If the length between opposite bank slopes over any bank was less than a tidal excursion this would result in one large affected patch rather than 2 distinct patches associated with each slope. Jones Bank was longer over the top of the bank than a tidal excursion and therefore showed a separate clear signal in both bottom water and peak and total SCM [Chl *a*] over both of the bank slopes.

Considerable increases in vertical diffusivities were seen within the thermocline at B2a which were not generated directly by the barotropic tide (Fig 4.13 c). Analysis of individual profiles demonstrated vertical diffusivities within the thermocline that were enhanced by up to 2.5 orders of magnitude over a layer up to 15 meters thick for almost 1½ hours during the first tidal cycle (Yearday 206.877–206.889) and over 2 hours of the second tidal cycle (Yearday 207.346–207.437). These periods of enhanced vertical diffusivities were associated with periods of warmer bottom water temperatures (up to 0.1 ^{o}C increase) and a more diffuse thermocline and SCM. The periods of increased turbulence occurred almost immediately after the turning of the tide from northwards to southwards velocities, as would be caused by lee wave formation.

At the base of the thermocline, where vertical diffusivities directly drive the vertical nitrate flux, periodic increases of vertical diffusivities occurred at both B2a and B2b. The intensity of the increased vertical diffusivities was correlated with the spring-neap tidal cycle, i.e. approaching neap tide (B2a) had higher K_z values than at neap tide (B2b). The increased K_z values occurred earlier in the tidal cycle during B2b than B2a. The B2 ADCP mooring (Fig 4.19 b) also showed higher shears associated with times of higher tidal current velocities (spring compared to neap) and also showed an increasing lag between maximum shear and position in the tidal cycle as tidal current velocities increased (personal communication J. Sharples).The difference in the timing of the waves reaching B2 was explained by the lower tidal current velocities during neap tide allowing the lee wave signature to reach B2 earlier, as the wave initially travels against the tidal stream (Maxworthy 1979).

The temperature logging mooring at B2 showed thickening and thinning of the thermocline at the same times as the FLY and CTD data during B2a, and no changes in thermocline diffuseness during B2b (Fig 4.19 a).The mooring displayed deepening of the isothermals associated with flow towards the bank. The temperature logging mooring at B3 also displayed semi-diurnal lowering of isothermals, with the isothermals dropping as the tide flowed southwards, onto the bank (Fig 4.19 c). From the data available there appears to have been more high frequency vertical isothermal movements at spring tide than neap tide at both B2 and B3.

There was a lag between B2 and B3, with the wave appearing ~3.5 hours later at B3 during neaps (when the starts of the semi-diurnal waves were easy to identify). The semi-diurnal wave appears to have formed further away from the bank crest than B2 during northwards current flows, possibly over B1. Unfortunately the temperature mooring deployed at B1 was lost, so there is no direct evidence of whether the internal lee wave formed there. The wave then propagated back over the bank, passing first B2 and then B3, as predicted (Maxworthy 1979).

4.4.2 How does the bank mixing environment affect vertical nitrate fluxes?

Chlorophyll *a* was more diffusely distributed through a wider thermocline at B2 than OB (Fig 4.9), as internal mixing was more prevalent over the bank than over flat topography. During B2a the distribution of [Chl *a*] with temperature (Fig 4.9 a) occasionally changed. Over two periods [Chl *a*] became

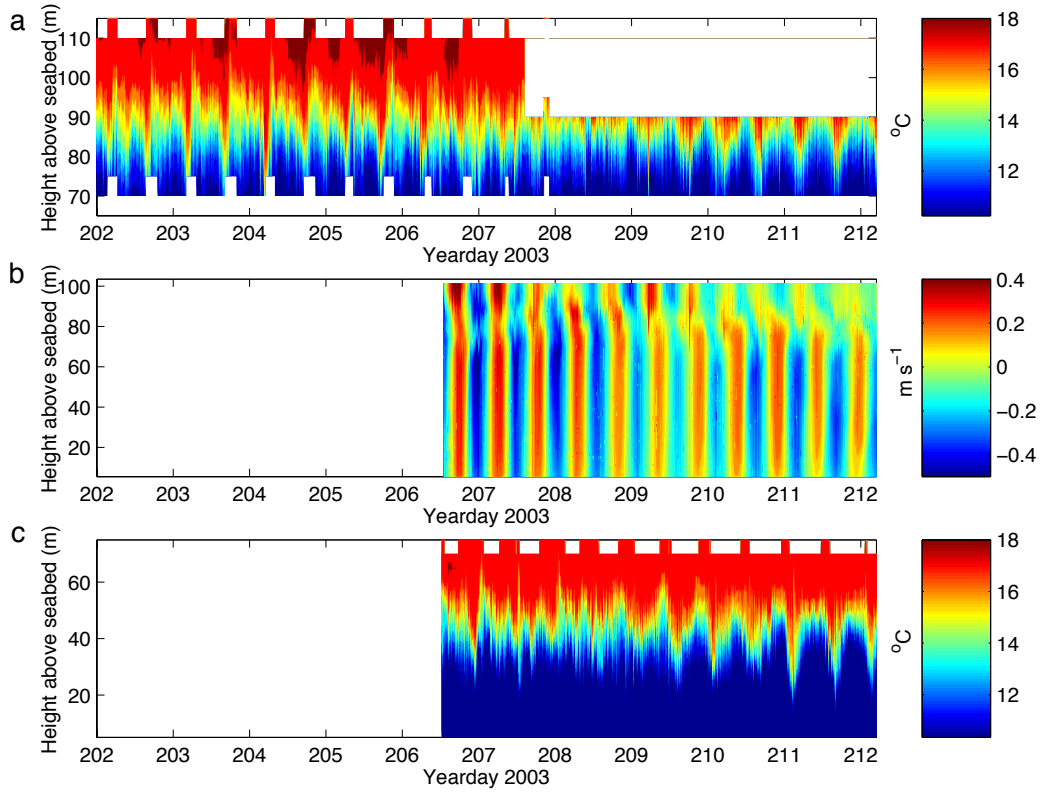

Figure 4.19

Data from a) B2 temperature logging mooring, b) B2 300 kHz ADCP Lander northwards velocity and c) B3 temperature logging mooring. Spring tide occurred at ~Yearday 203, neap tide ~211

evenly distributed throughout the thermocline. Variations in $\Delta N/\Delta z$ during B2a were strongly related (~68%) to changes in $\Delta Chl\ a/\Delta z$ (r^2=0.68, p<0.05). Thus the lowest values of $\Delta N/\Delta z$ were seen during the periods of diffuse thermocline and SCM.

A diffuse SCM is indicative of strong internal mixing having occurred and indeed the diffuse periods during B2a occurred at times of increased vertical

diffusivity within the thermocline. The broader nitrate gradient over the bank slope would affect vertical nitrate fluxes directly through the $\Delta N/\Delta z$ term of Eq. 2.4, and through potential shifting of the base of the SCM in the vertical K_z field. At B2 turbulent mixing would be minimal at the base of the thermocline approaching and during neap tides, i.e. as sampled during B2a and B2b respectively, but at spring tides the vertical diffusivities may substantially increase at the base of the SCM through boundary-driven processes (as seen at CS3 in Chapter 3).

During all stations (B2a, B2b and OB) greater than 80% of variation in vertical nitrate fluxes into the subsurface chlorophyll maximum was explained by variations in K_z at the base of the SCM (r^2=0.81 for B2a, r^2=0.84 for B2b, r^2=0.89 for OB, p<0.05 for all). Thus B2a, with higher K_z at the base of the thermocline, had significantly higher vertical nitrate fluxes than B2b (F=4.8, F_{crit}=3.9, p<0.05) both throughout the sampling period, and in the daily mean.

OB experienced the lowest vertical diffusivities at the base of the SCM, due to being sampled at neap tide and having no topographically generated lee wave associated mixing. However the lower K_z compared to B2 stations was partially offset by greater $\Delta N/\Delta z$, which increased the mean daily flux by a factor of two, compared to if OB had had a similar $\Delta N/\Delta z$ to B2a. This suggests that although changes in $\Delta N/\Delta z$ are small compared to changes in K_z for explaining variations in J_N, factors influencing $\Delta N/\Delta z$, such as the diffuseness of the SCM, do have an impact on the mean daily nitrate flux.

4.4.3 The consequences of the mixing environment over banks for primary production.

The daily mean vertical nitrate flux into the SCM (Table 4.1) was converted to a rate of carbon production using the Redfield ratio for all stations (Table 4.2). Primary production rate estimates were provided by A. Hickman (Table 4.2, see section 2.1.7 for methods) for both cloudy and sunny conditions. Over the flat seafloor (OB) nitrate supply was below demand, with *f*-ratios ranging from ~0.7 to ~0.3 dependent on light conditions (cloudy and sunny respectively). Consequently, regeneration of organic nitrogen is likely to be important at OB during neap tide, as vertical turbulent supply of nitrate is not high enough to sustain the measured production rates.

Over the bank slope at neap tide (B2b) supply of nitrate appeared to be sufficient to support the observed rates of primary production under lower light conditions, but not under high light, where the *f*-ratio was ~0.55. Production was higher at B2b compared to OB, although both were sampled at neap tide. This may be due to the higher nutrient fluxes measured at B2b though other factors would also influence primary production rates, such as previous light history and species composition (personal communication A. Hickman). The *f*-ratios of ~0.5 are similar to those found by Holligan et al. (1984b) in the English Channel.

The estimated primary production rates over the bank slopes at B2 were lower during B2a than B2b, despite dramatically higher vertical nitrate fluxes into the SCM. The PE curves were carried out on water collected from the dawn cast, so all phytoplankton were considered dark adapted. The method would therefore not take into account increased turbulence within the thermocline

lowering the production rate through not allowing short-term photoacclimation to changing light fields as the phytoplankton were mixed within the thermocline (e.g. similar to Lizon et al. 1998).

Table 4.2

Calculated primary production rates (personal communication A Hickman) and new production supported by calculated vertical nitrate fluxes into the SCM from the bottom layer.

Station	Integrated Primary Production (mg C m^{-2} day^{-1})		New primary production supported (mg C m^{-2} day^{-1})
	Cloudy	Sunny	
B2a	147 (± 44)	291 (± 87)	1457 (± 2477)
B2b	246 (± 74)	489 (± 147)	269 (± 164)
OB	149 (± 45)	344 (± 103)	102 (± 89)

The large difference between the vertical flux of nitrate into the SCM during B2a and the production suggested the flux was greater than the uptake capacity of the phytoplankton. If this was the case it would be expected that measurable concentrations of nitrate would be seen in the surface mixed layer, as it would not be used up in the SCM. Patches of surface water with non-zero surface [Nitrate] were not measured, however nitrate measurements in the surface were temporally sporadic and any patches could have been missed.

Chapter 5: The shelf break: Temperature, chlorophyll *a* and nitrate supply to phytoplankton.

5.1 Introduction

The Celtic Sea shelf edge, where the shallow (< 200 m) continental shelf of the Celtic Sea drops off into the deeper oceanic Bay of Biscay, is an acknowledged region of cooler sea surface temperature (SST) and increased sea surface chlorophyll *a* concentrations ([Chl *a*]) in the summer stratified season, as compared to the adjacent shelf and oceanic surface waters. At the shelf break, both in the Celtic Sea and others topographically similar, it is thought that turbulent dissipation of tidal energy into the region of the thermocline, driven by the breaking internal tide and associated internal waves, is instrumental in both cooling the surface layer, and supplying nutrients to support the high surface and subsurface chlorophyll *a* concentrations (Sandstrom & Elliott 1984, Pingree et al. 1986, New & Pingree 1990, Sharples et al. 2001a). Previously however, vertical nitrate flux estimates for the Celtic Sea shelf break have not been made.

A hypothesis is investigated here, whereby increased internal mixing over the shelf break, generated by the action of the barotropic tide over the steep topographic depth change of the shelf break, supports new primary production both within the thermocline and the surface layer by increasing upwards vertical nitrate fluxes from the nitrate rich bottom layer. We also investigate the possibility of spring-neap variation in vertical nitrate fluxes. A combination of

station data (CS2), CTD cast transects and moorings (Fig 5.1) were used to investigate this hypothesis.

This chapter will use the transect data to gain a snapshot of the spatial variation in temperature and chlorophyll *a* across the shelf break, and the station data to obtain an estimate of temporal variation in both water column structure and vertical nitrate fluxes into the SCM.

5.2 Basic observations from transects across the shelf break

Two transects of nine CTD casts and a section of a SeaSoar transect (Fig 5.1) were carried out in order to develop two dimensional spatial representations of the water column across the shelf break in the region of CS2. Recent satellite images were used to determine the position of the transects, ensuring the transects crossed out of the shelf edge patch into open ocean and shelf conditions at each end. The two CTD transect lines were each orientated differently with respect to the general direction of the shelf break. CTD transect line N, carried out 7th – 8th August 2003, was situated within a canyon feature and CTD transect line T, carried out 21st –2nd July 2005, over a spur. The SeaSoar section (8th August 2003) followed the course of line N.

All transects' data exhibited similar structure, with surface and bottom waters separated by a thermocline both over the shelf and the deeper oceanic waters (Figs 5.2 – 5.4). A subsurface chlorophyll maximum (SCM) occurred

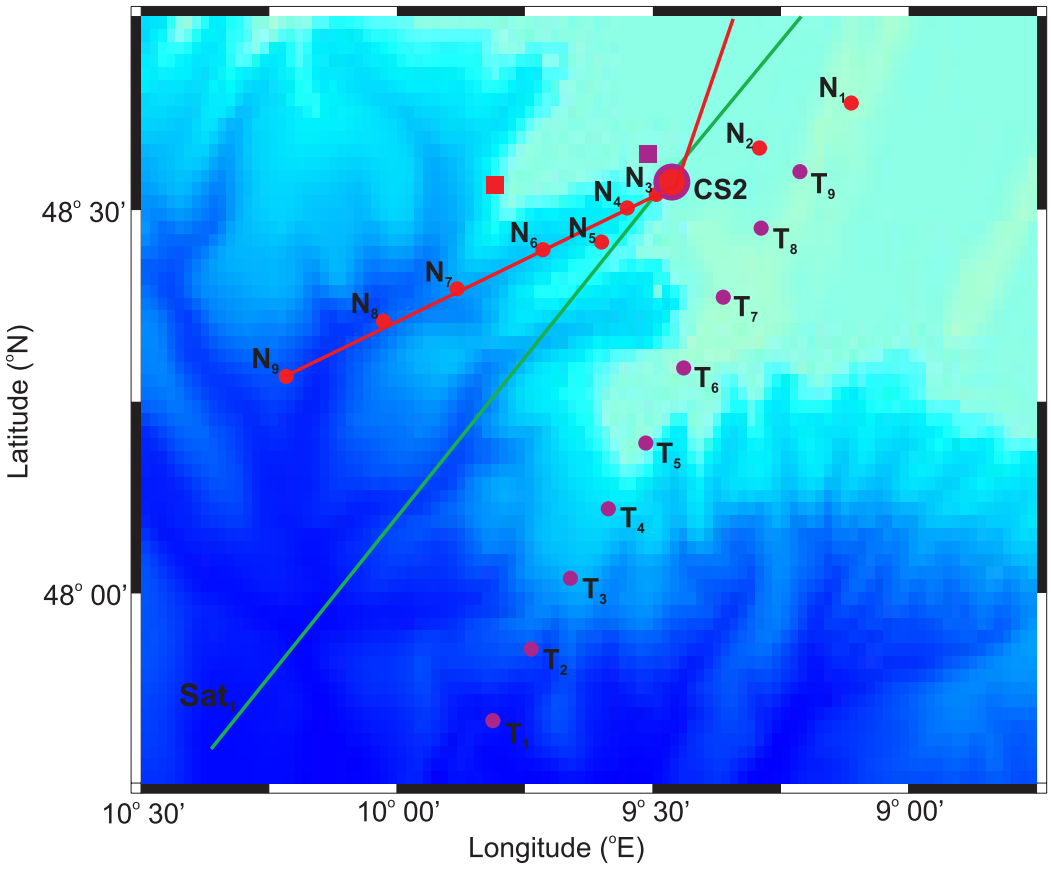

Figure 5.1.

Celtic Sea shelf break, in the region of station position CS2. The large circles show positions used for CTD and FLY stations, smaller circles are CTD casts, squares are the mooring positions, and solid lines are the SeaSoar transects, carried out during JR98 (2003, red) and CD173 (2005, purple). The green solid line is remotely sensed transect Sat_1 (Chapter 6). See chapter 2 for detailed positions and methods. The bathymetry scale runs from 100–1000 m (white–blue), below 1000 m masked in dark blue. Bathymetry data from IOC et al. (2003).

within the thermocline, and a nitracline was associated with the base of the SCM. The transects represent only a snapshot of a region where the position of the thermocline and SCM may move vertically due to internal wave activity, and therefore not always be as observed here. There was some indication of lowered isothermals over the shelf break, particularly during the SeaSoar transect (Fig 5.4).

The thickness and vertical position of the thermocline, SCM and nitracline varied along the transect lines, becoming more diffuse over the region of the shelf break (nominally the 200 m depth contour), with significantly cooler temperatures (F>115, F_{crit}=4, p<0.05) and elevated chlorophyll *a* concentrations (F>243, F_{crit}=4, p<0.05) outcropping at the surface (0–10 m depth) over the shelf break in all transects. The ships underway data (section 2.1.6) highlighted the cooler, higher [Chl *a*] band of surface water situated over the shelf break both during sampling of line N (Fig 5.5) and line T (data not shown). Line T, the only transect where surface nitrate concentrations could be analysed for variance, had significantly higher [Nitrate] (F=4.7, F_{crit}=3, p=0.01) in the surface waters over, compared to away from, the shelf break.

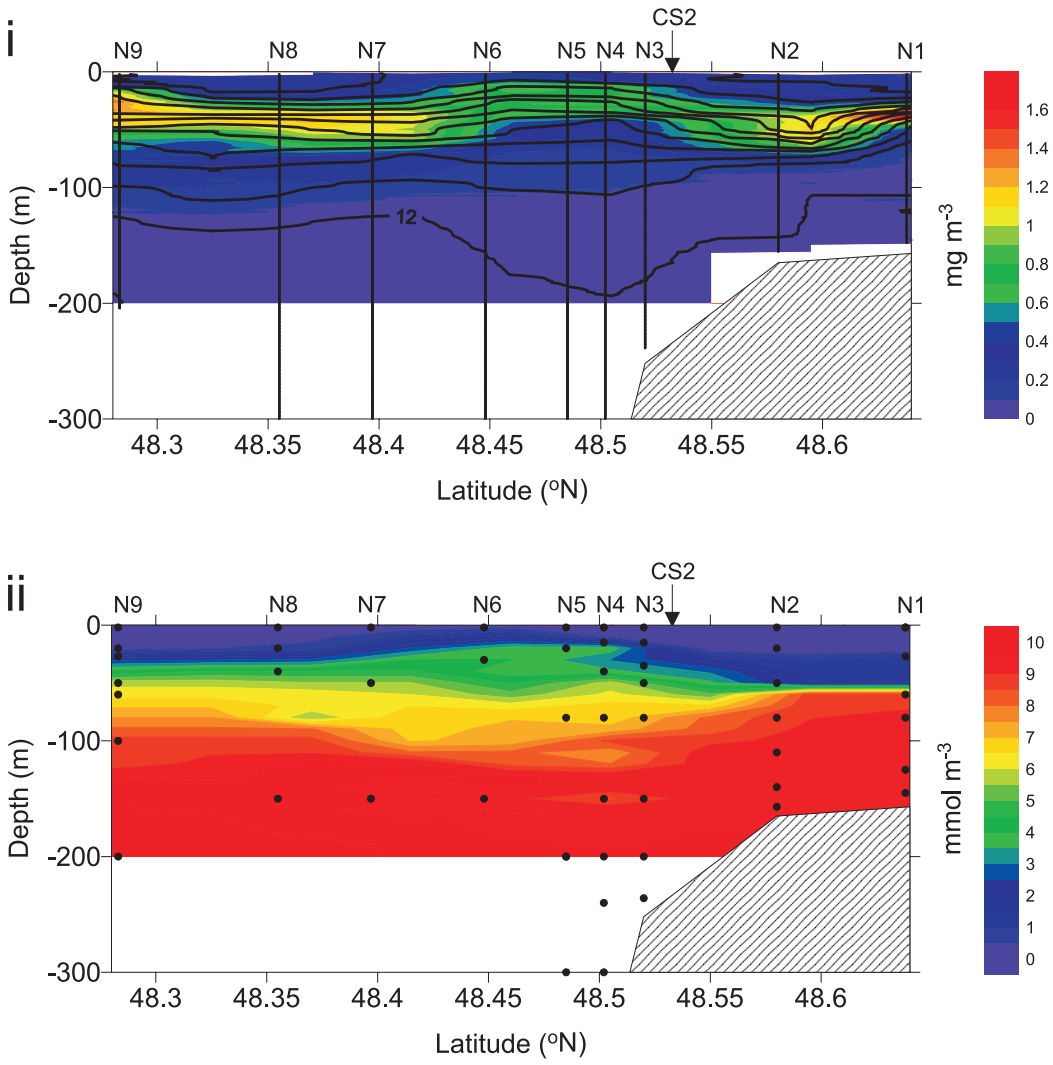

Figure 5.2

Line N CTD transect over the shelf break, 13:54 7th – 11:03 8th August 2003. CTD i) chlorophyll *a* concentrations (coloured contours) and temperature (black lines, every 0.5 °C) and ii) water sample nitrate concentrations. Data points are indicated, as is topography.

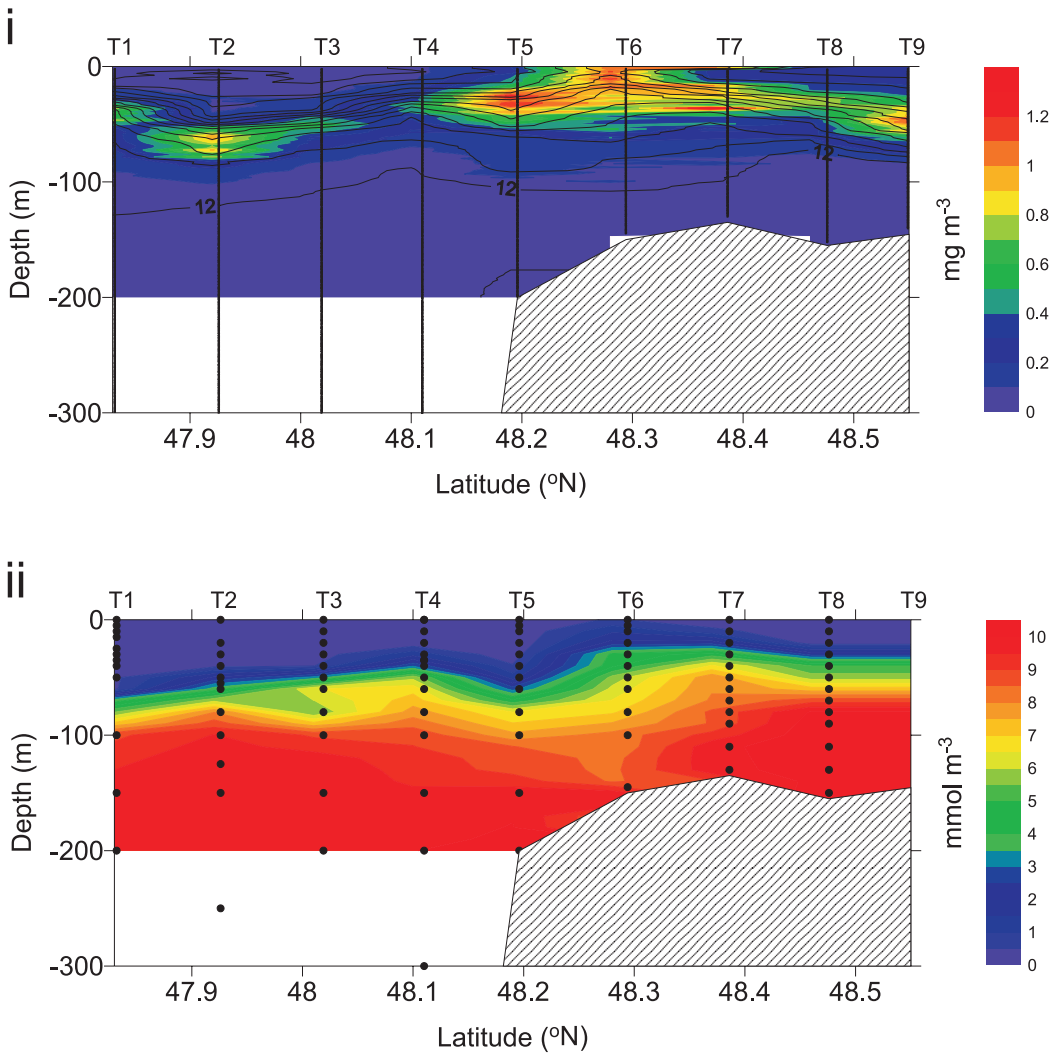

Figure 5.3

Line T CTD transect over the shelf break, 20:25 21st – 20:02 2nd July 2005. As Figure 5.2.

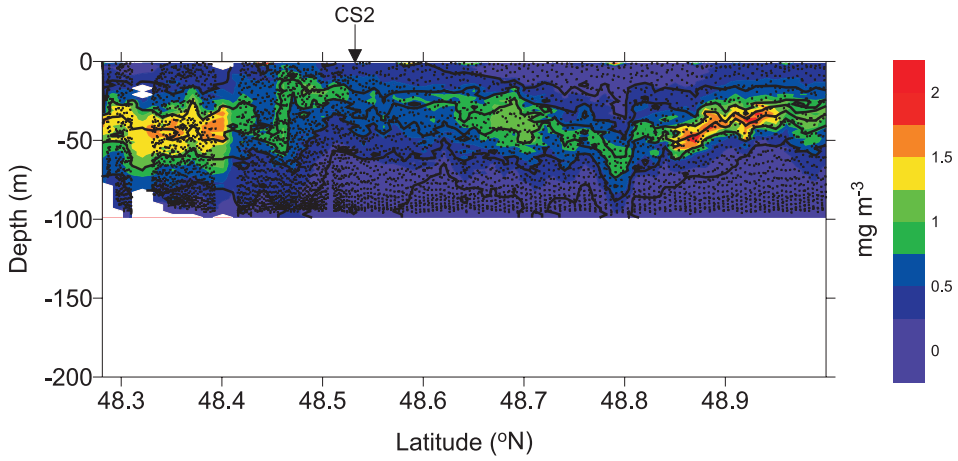

Figure 5.4

SeaSoar data over the shelf break (48.28–48.99 °N, 14:30–23:43, 8th August 2003) during the cross shelf transect in 2003. SeaSoar chlorophyll *a* concentrations (coloured contours) and temperature (black lines, every °C). Every 5th data point is indicated.

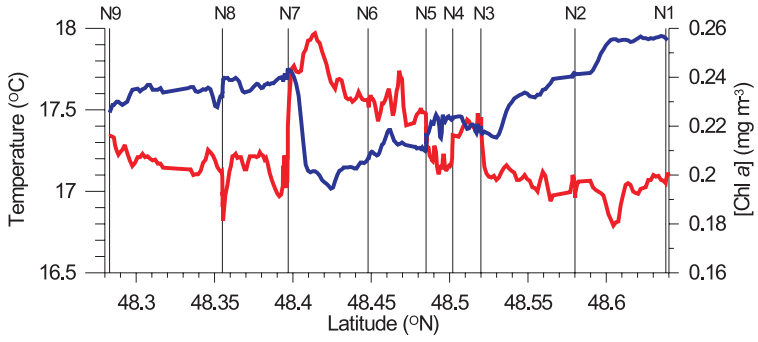

Figure 5.5

Ship's underway temperature (blue) and chlorophyll *a* concentrations (red) over CTD transect N, (48.28–48.64 °N, 13:54 7th–11:03 8th August 2003). Positions of CTD casts indicated.

5.3 Results from fixed stations and moorings

Position CS2, sited over the Celtic Sea shelf break (Fig 5.1), was occupied on a total of three occasions, once during cruise JR98 (CS2a, 29th – 30th July 2003, spring tide) and twice during cruise CD173 (CS2b, 17th – 18th July 2005, neap tide, and CS2c, 22nd –23rd July 2005, spring tide). Temperature logging and ADCP moorings were deployed in both years, data collection spanning the times of the 25 hour sampling stations (see section 2.1 for station and mooring methods).

At CS2 during CD173 all instrumentation was deployed from the RRS *Charles Darwin*. It was found to be problematical to try and carry out a full FLY ensemble, reposition, and deploy the CTD without loosing continuity in either microstructure or CTD data. From the 2003 CS2a, and initial CS2b, casts there was found to be temperature to [Nitrate] relationships which could be applied to FLY temperature in order to estimate nutrient fluxes. Thus, the decision was made to concentrate efforts on FLY deployment. The CTDs which were carried out involved intensive nutrient sampling to allow confidence in the temperature to [Nitrate] relationships calculated.

5.3.1 Hydrographic characteristics of the thermocline, chlorophyll *a* concentrations and the nitracline

CS2 was situated in ~200 m water depth. The water column generally displayed a mixed surface layer of around 20–30 m depth, a weakly stratified bottom layer, and a diffuse thermocline between the two (Fig 5.6). Density was controlled primarily by temperature (r^2 >0.999). Significantly cooler (F=19, F_{crit}=4, p<0.05) sea surface (0– -10 m) temperatures were seen during CS2c (spring tide) compared to CS2b (neap tide) in 2005.

A chlorophyll *a* concentration maximum was found within the thermocline, the base of the SCM corresponding to the base of the thermocline, with high [Chl *a*] often extending upwards and reaching the surface (Fig 5.7). There was no significant difference (F=0.3, F_{crit}=4, p>0.05) in surface (0– -10 m) [Chl *a*] between the 2005 stations CS2b and CS2c.

Throughout all three occupations of CS2 the [Chl *a*] distribution against temperature was diffuse (Fig 5.8), however all the stations had dissimilarities in the shape of the distribution. During CS2a the SCM was distributed asymmetrically against temperature (Fig 5.8 a). Conversely to the shelf stations (Figs 3.5, 3.17 and 4.9) the asymmetry was towards higher temperatures. This was partly due to the weak stratification in the bottom layer causing a long "tail" of low [Chl *a*] at lower temperatures but mostly due to high, almost equivalent to peak SCM, chlorophyll *a* concentrations extending to the surface (Fig 5.7 a).

During CS2c [Chl *a*] distribution was also slightly asymmetrical, with the peak biased towards higher temperatures (Fig 5.8 c), again due to high [Chl *a*] extending to the surface (Fig 5.7 c). CS2b demonstrated the most symmetrical

distribution of [Chl *a*] to temperature (Fig 5.8 b), and had the lowest surface [Chl *a*] in comparison to peak SCM values of all CS2 stations (Fig 5.7 b).

[Nitrate] was usually undetectable at the surface (Fig 5.6) though there were periods during CS2a and CS2c when surface [Nitrate] was above detection limits. Nitrate concentrations through the nitracline were strongly related to temperature rather than [Chl *a*] at all stations (Fig 5.8 and section 2.3).

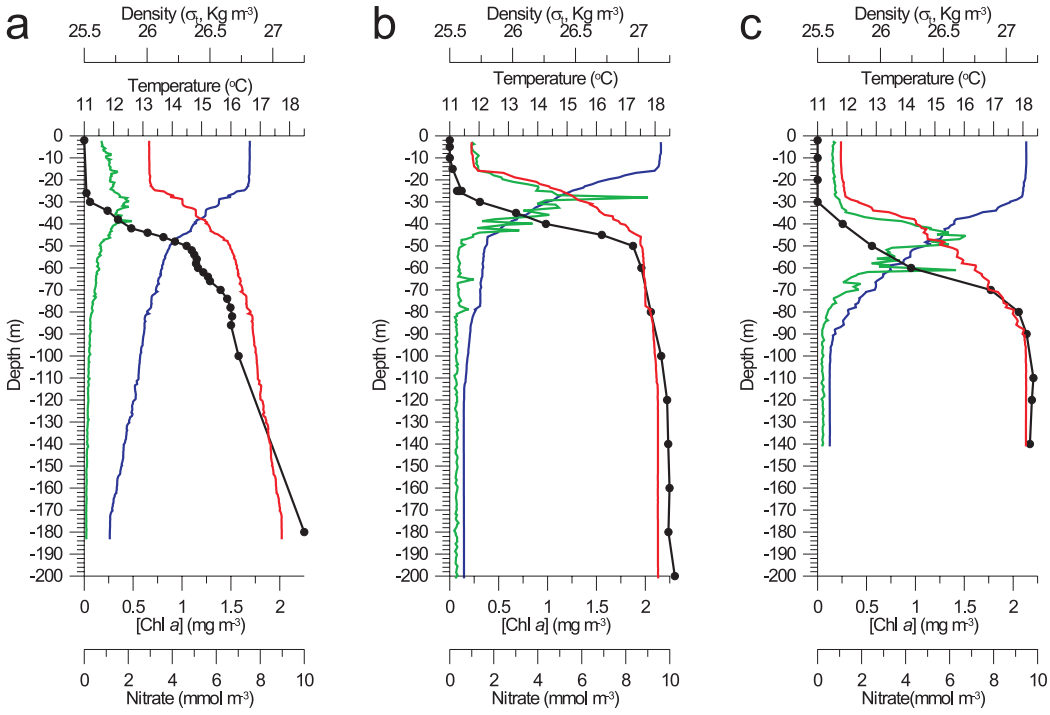

Figure 5.6

Examples of CTD and water sample nutrient profiles for a) CS2a (09:20, 29th July 2003, b) CS2b (07:20, 18th July 2005) and c) CS2c (21:30, 22nd July 2005). Blue represents CTD temperature, red CTD density, green CTD chlorophyll *a* concentrations and black water sample nitrate concentrations.

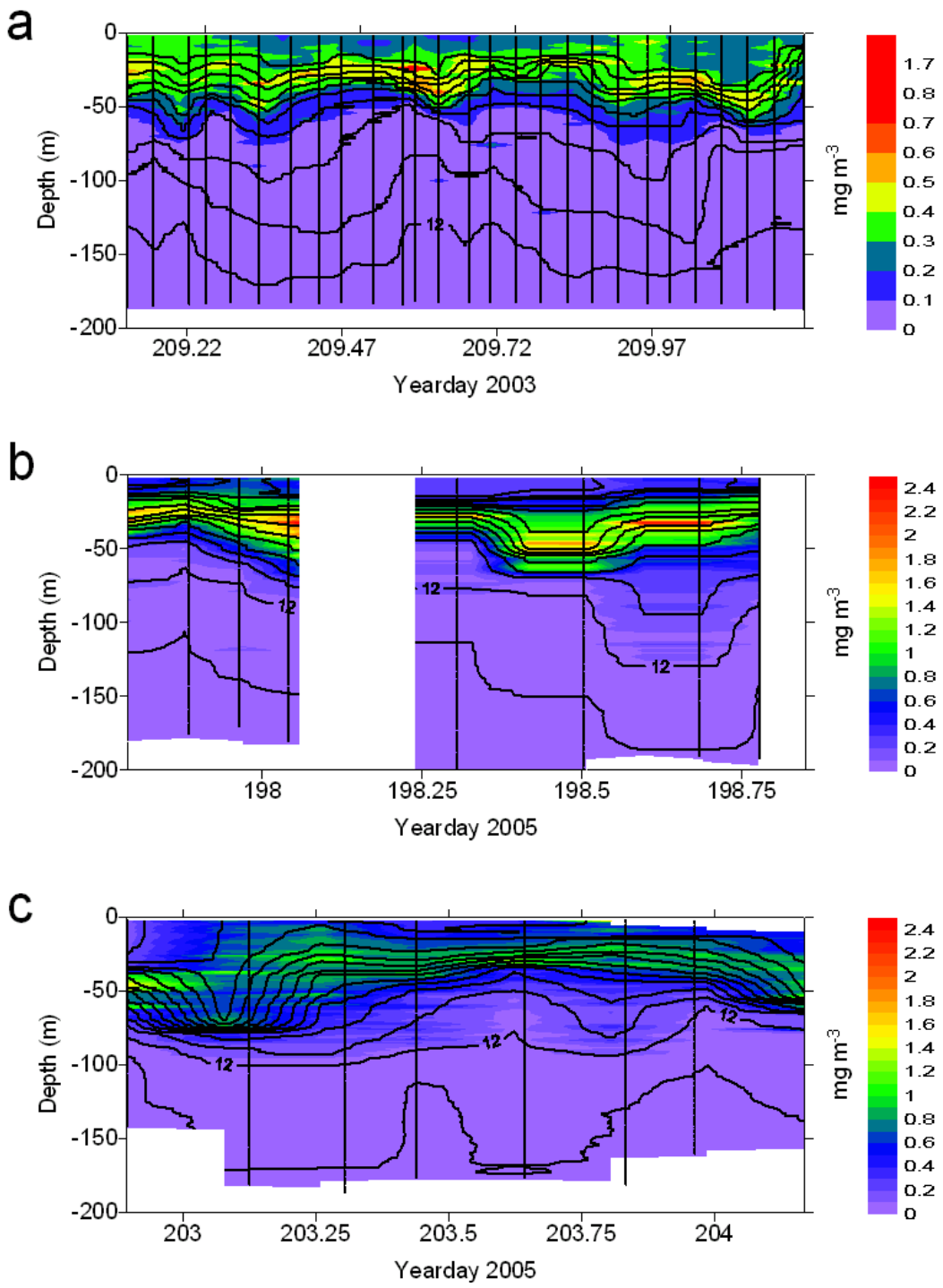

Figure 5.7

Time series of CTD chlorophyll *a* concentrations (coloured contours) and temperature (black lines, every 0.5 ^{o}C) against depth during a) CS2a, b) CS2b and c) CS2c. Data points indicated. Note differing scales.

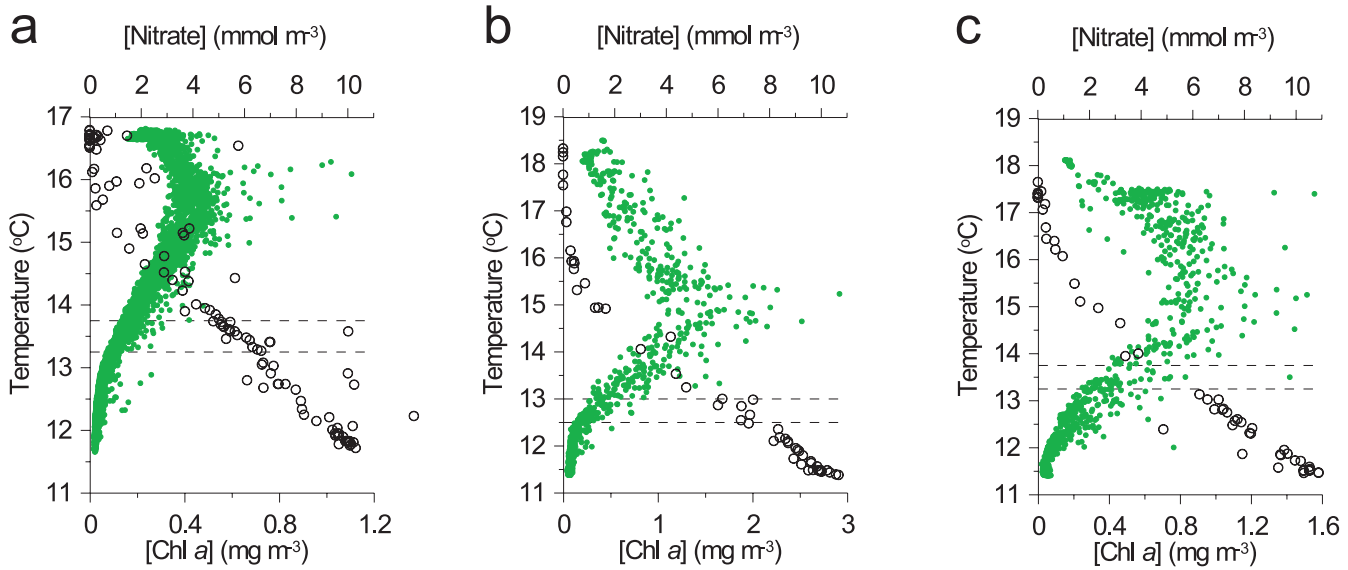

Figure 5.8

Stations a) CS2a, b) CS2b and c) CS2c CTD chlorophyll *a* concentrations (green dots) and water sample nitrate concentrations (black circles) against temperature. Note differing scales. The black dashed lines mark the boundaries of the temperature ranges over which the vertical nitrate flux into the SCM was calculated for each profile. CS2a 13.25–13.75 ^{o}C, CS2b 12.5–13.0 ^{o}C, CS2c 13.25–13.75 ^{o}C.

A semi-diurnal signal was present in CTD isothermal depths at all three CS2 visits (Fig 5.7), whereby the isothermals periodically moved deeper into the water column, seen particularly clearly at lower temperatures. The SCM moved with the thermocline. The temporal spacing of the CTD casts, of one hour or more, meant that any signals of shorter than several hours period would be missed.

Temperature profiles measured by FLY (Fig 5.9), which had a temporally denser sampling strategy than the CTD, showed both the semi-diurnal signal seen in the CTD data and higher frequency vertical internal motions of the isothermals. Individual profiles from a single FLY ensemble, which would last around 40 minutes, could display vertical isothermal displacements of over 20 m, for example between 203.19 – 203.22 (Fig 5.10) which corresponded to maximum off shelf flow.

Mooring data from both cruises (Fig 5.11), provided a more complete temporal context of internal tide behaviour. A clear semi-diurnal signal was present throughout the water column, with isothermals moving downwards associated with off-shelf tidal currents, reaching maximum depth at maximum flow. Superimposed on the semi-diurnal signal, there was considerable short time scale activity (20–30 minute period vertical isotherm oscillations). There appeared to be variability over the spring-neap tidal cycle, with more high frequency internal motions at spring tide (Yearday 203) than neap tide (Yearday 197, Fig 5.11 b). The high frequency waves occurred most strongly at spring tides, as the thermocline reached its shallowest. Sea surface temperatures were also generally cooler around spring tide. This corresponded well with the differences between CS2b and CS2c.

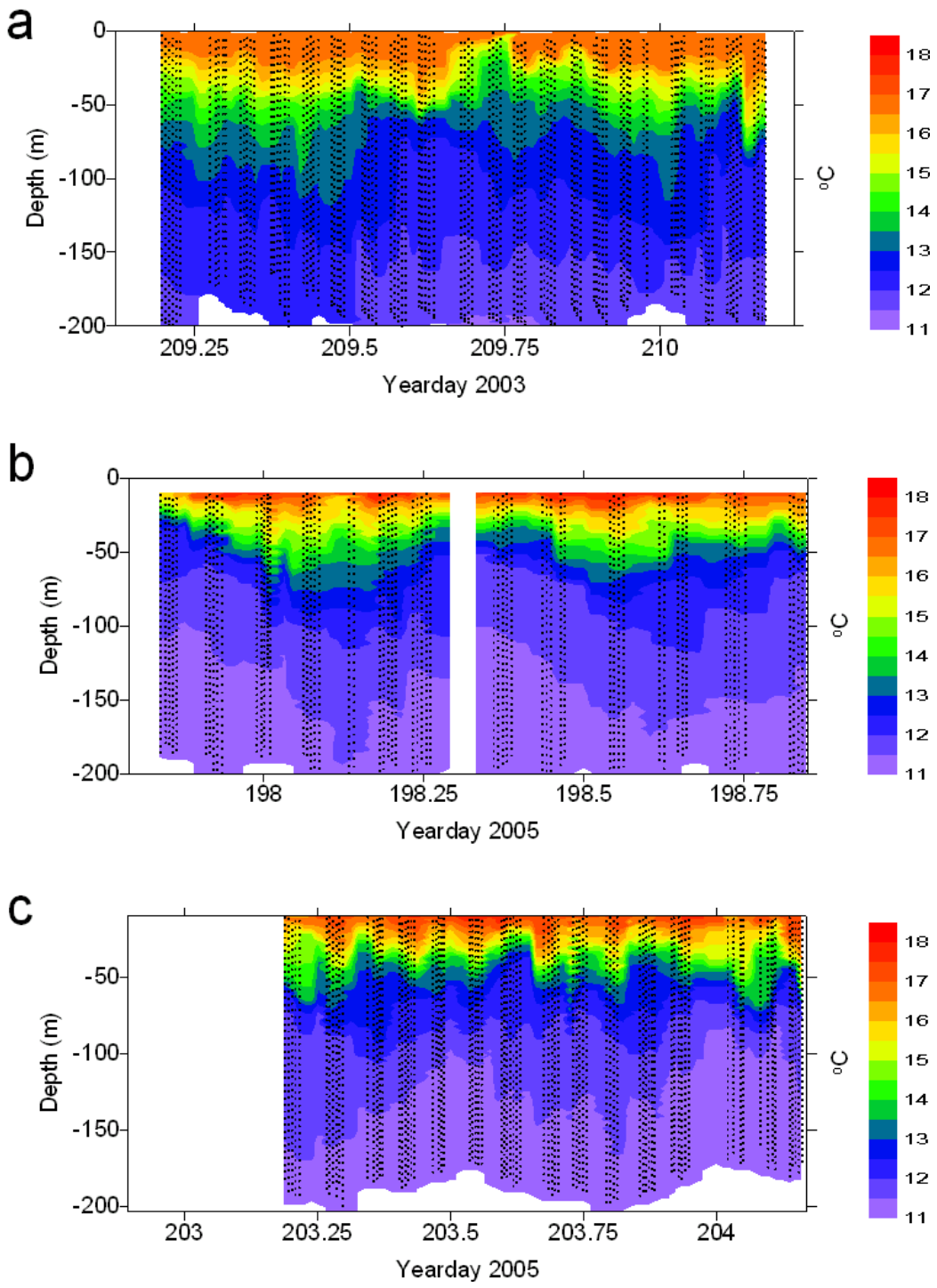

Figure 5.9

Time series of FLY temperature against depth for a) CS2a, b) CS2b and c) CS2c. Every 5th data point indicated. Large data gap in c) due to FLY cable being replaced.

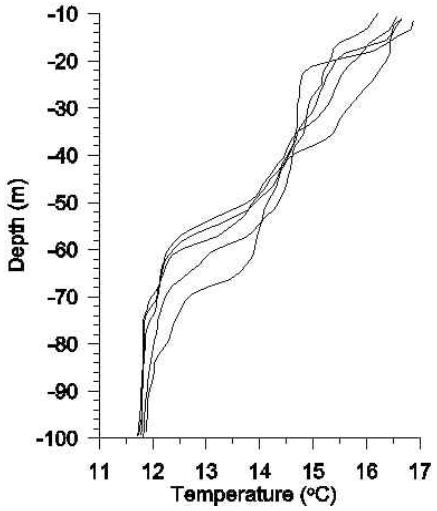

Figure 5.10

Individual FLY temperature profiles at CS2c between Yearday 203.19 – 203.22, 2005.

Profiles of $\Delta N/\Delta z$ were calculated for all FLY profiles using the methods described in section 2.3, *ΔN/Δz derived from a Temperature to [Nitrate] relationship*. Mean values of $\Delta N/\Delta z$ at the base of the SCM for each profile fluctuated throughout the stations (Fig 5.12). There was no significant relationship between $\Delta N/\Delta z$ and Δ*[Chl a]*$/\Delta z$ at CS2 ($r^2<0.15$, $p>0.05$), contrary to what was found over the shelf (Sections 3.3.1, 3.4.1 and 4.3.1). It appears that, up to a certain temperature (about equivalent to the base of the surface mixed layer), the effect of uptake of nitrate by phytoplankton was overcome by nitrate redistribution through mixing. Therefore, $\Delta N/\Delta z$ was related to the temperature gradient at CS2 and greatest $\Delta N/\Delta z$ occurred when the base of the thermocline was tightest, and smallest values of $\Delta N/\Delta z$ when the base of the thermocline was most diffuse.

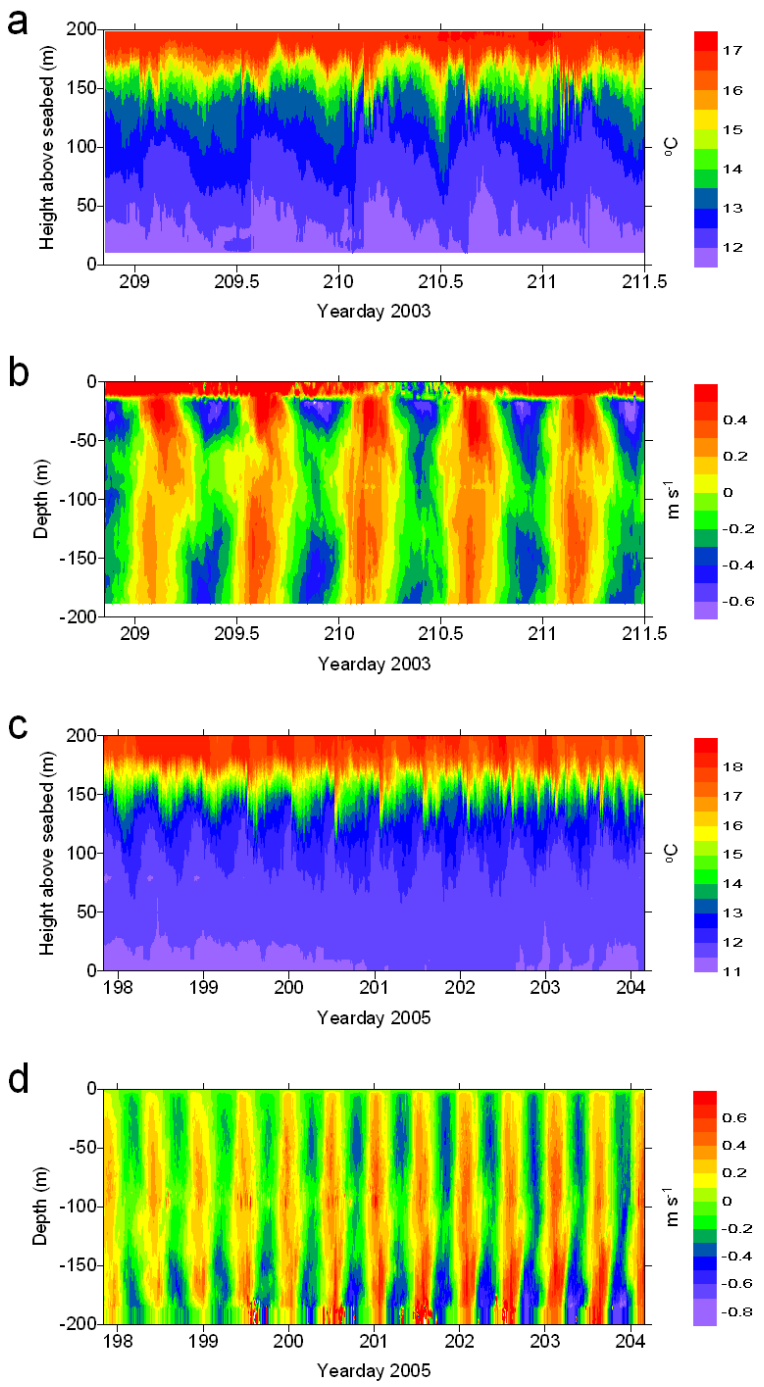

Figure 5.11

Temperature and northwards current velocity from the moorings deployed at CS2 in 2003 (a and b, data every 2 minutes) and 2005 (c and d, data every 1 minute). In 2005 neap tide occurred at Yearday 197 and spring tide Yearday 203. Note differing scales.

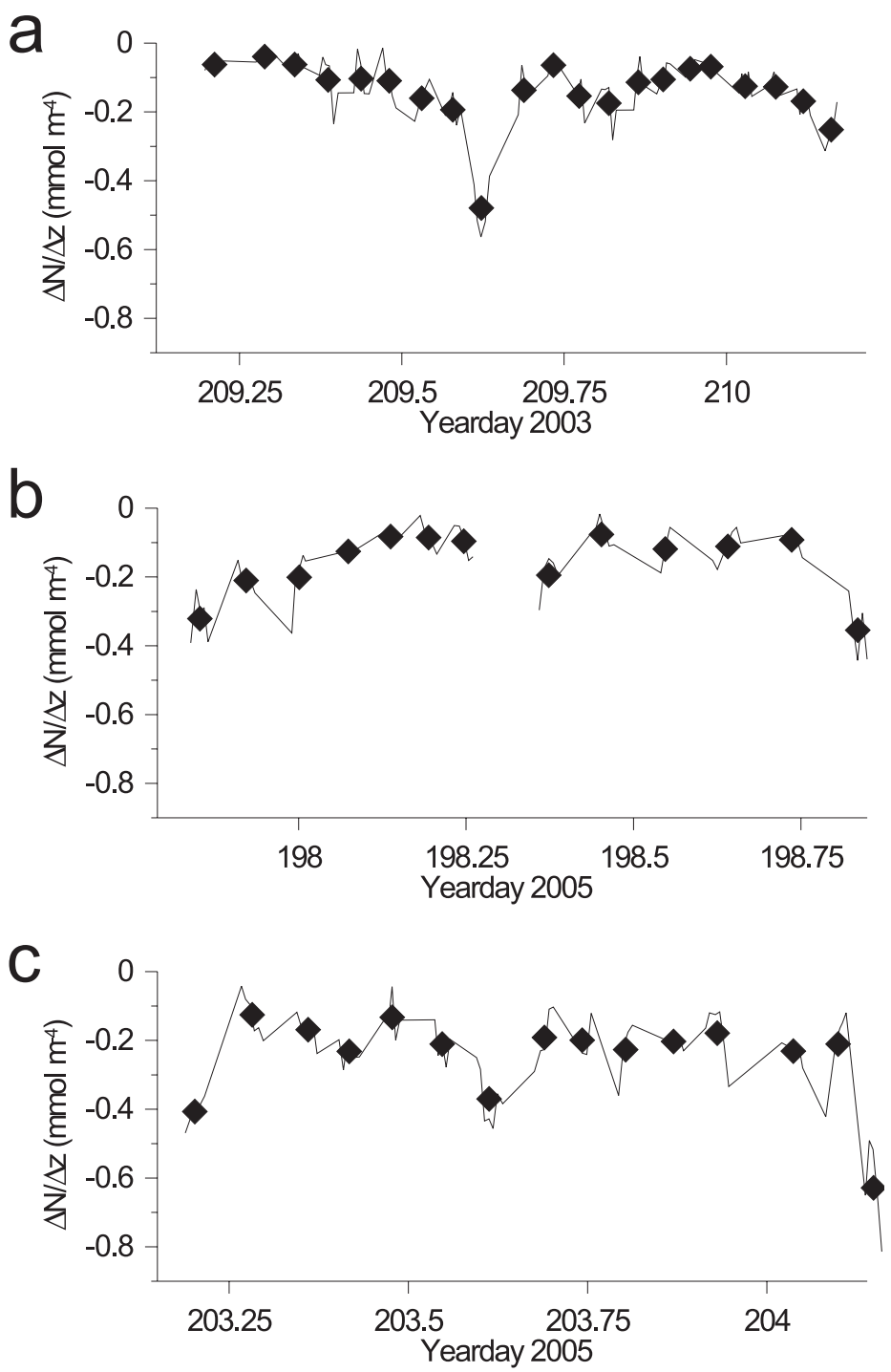

Figure 5.12

Mean nitrate gradient, over the temperature ranges used to calculate the vertical nitrate flux for each profile during a) CS2a, b) CS2 and c) CS2c. The black diamonds mark the average value for each FLY ensemble.

A semi-diurnal signal, related to the signal in isotherm depths, was weakly present in $\Delta N/\Delta z$, seen strongest in the large increases of $\Delta N/\Delta z$ when the thermocline was tightest (Fig 5.12). However, within single FLY ensembles (which lasted around 40 minutes) $\Delta N/\Delta z$ could vary by more than 0.2 mmol m^{-4}. This was possibly related to the passage of internal waves affecting the structure of the thermocline on shorter periods than the semi-diurnal signal. Variations in $\Delta N/\Delta z$ were larger during CS2c, sampled at spring tide, than CS2b, samples at neap tide. CS2c also displayed larger, more frequent vertical isotherm displacements than CS2b.

5.3.2 Currents, turbulence and mixing

CS2 displayed semi-diurnal oscillations in tidal velocities (Figs 5.13 – 5.15, a) during all visits. The mooring data exhibited maximum near bed velocities of -0.4 m s^{-1} at CS2a, -0.6 m s^{-1} at CS2b and -0.8 m s^{-1} at CS2c. The difference in current velocities between CS2b and CS2c was due to the spring-neap tidal cycle, which was clearly present in the full mooring data set (Fig 5.11 d). Although CS2a was also sampled at spring tide, its current velocities were the lowest of the three stations.

The shelf break stations had consistently high turbulent dissipation rates, ε, close to the surface (Figs 5.13 – 5.15, b) due to wind and wave effects. Quarter-diurnal increases in ε near the seafloor, which appeared to move vertically up through the water column with time due to vertical movement of the region of greatest shear (Simpson et al. 2000), were associated with maximum

near bed currents, both off and on shelf. Periods of intensification of ε occurred within the water column at all CS2 stations. These were associated with periods of large vertical isotherm movements and not with bed generated shear, for example during CS2c, at ~Yearday 203.8, ε increased dramatically (around 2.5 orders of magnitude above background thermocline levels, Fig 5.13 b) and considerable vertical isotherm displacements were seen in both the FLY (Fig 5.9 c) and mooring (Fig 5.11 c) temperature data.

As with ε, the largest values in K_z were at the bed (Figs 5.13 – 5.15, c). Within the water column large K_z values were associated with the base of the thermocline, particularly at CS2b and CS2c where the thermocline was more defined than at CS2a. These seemed to be particularly large when current velocities were off shelf.

During all CS2 sampling periods high K_z within the thermocline were coincident with large vertical isotherm displacements, and generally occurred as the lowered isotherms were rising again, as currents flowing off shelf began to weaken and turn back on shelf. In 2005, during CS2b, sampled at neap tide, there were less instances of increased K_z within the thermocline compared to CS2c, sampled at spring tide, however periods of higher K_z in the thermocline did occur when isotherms were displaced vertically.

Mean K_z at the base of the SCM (Fig 5.16), varied by up to 3 orders of magnitude during all three CS2 station visits. The higher values of mean K_z were all associated with vertical displacements of isotherms.

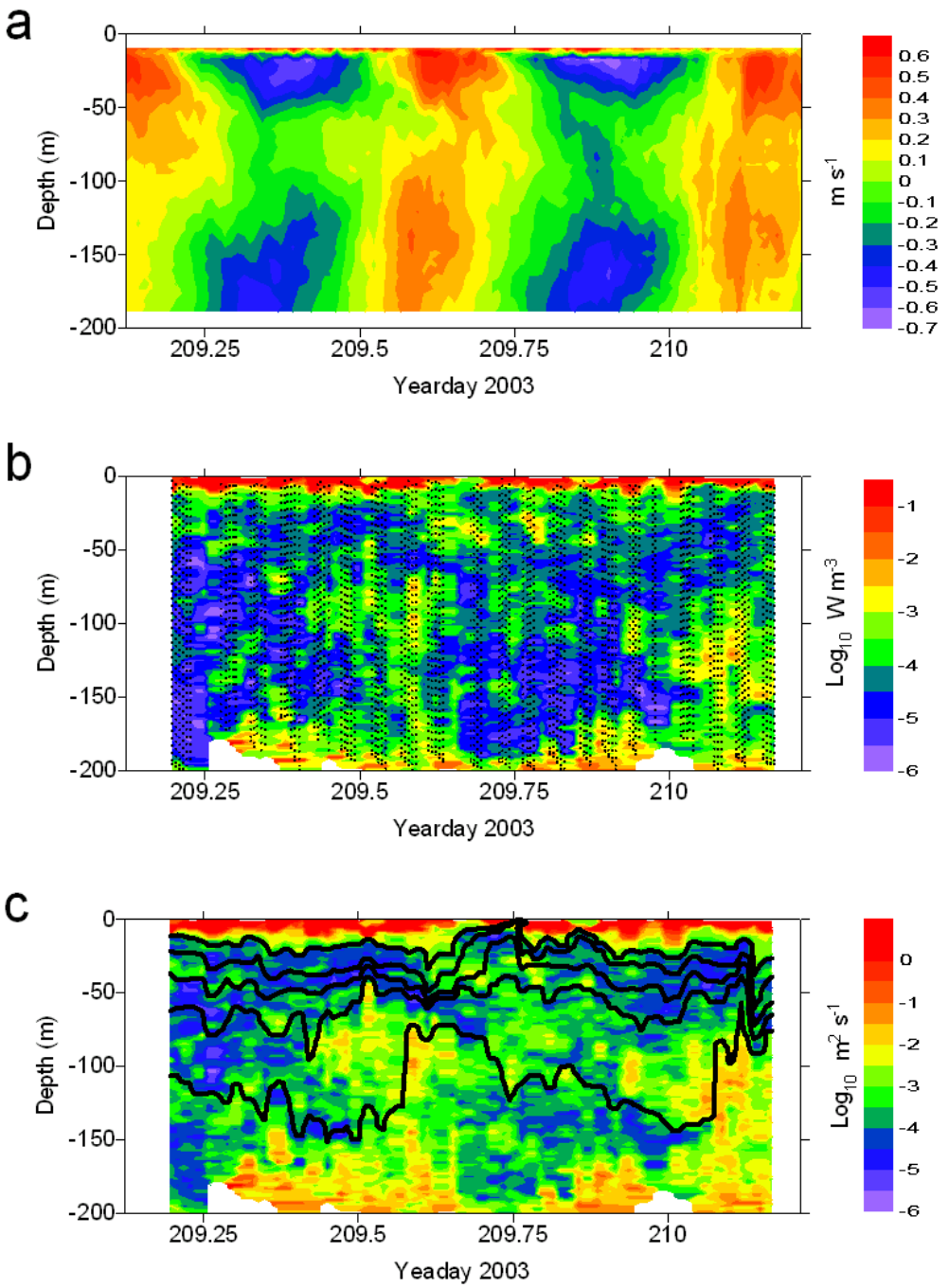

Figure 5.13

CS2a i) ADCP mooring northwards current velocity, ii) FLY turbulent dissipation rate (every 5th FLY data point marked) and iii) FLY vertical diffusivity (coloured contours) and FLY temperature (black lines, every 1 ^{o}C)

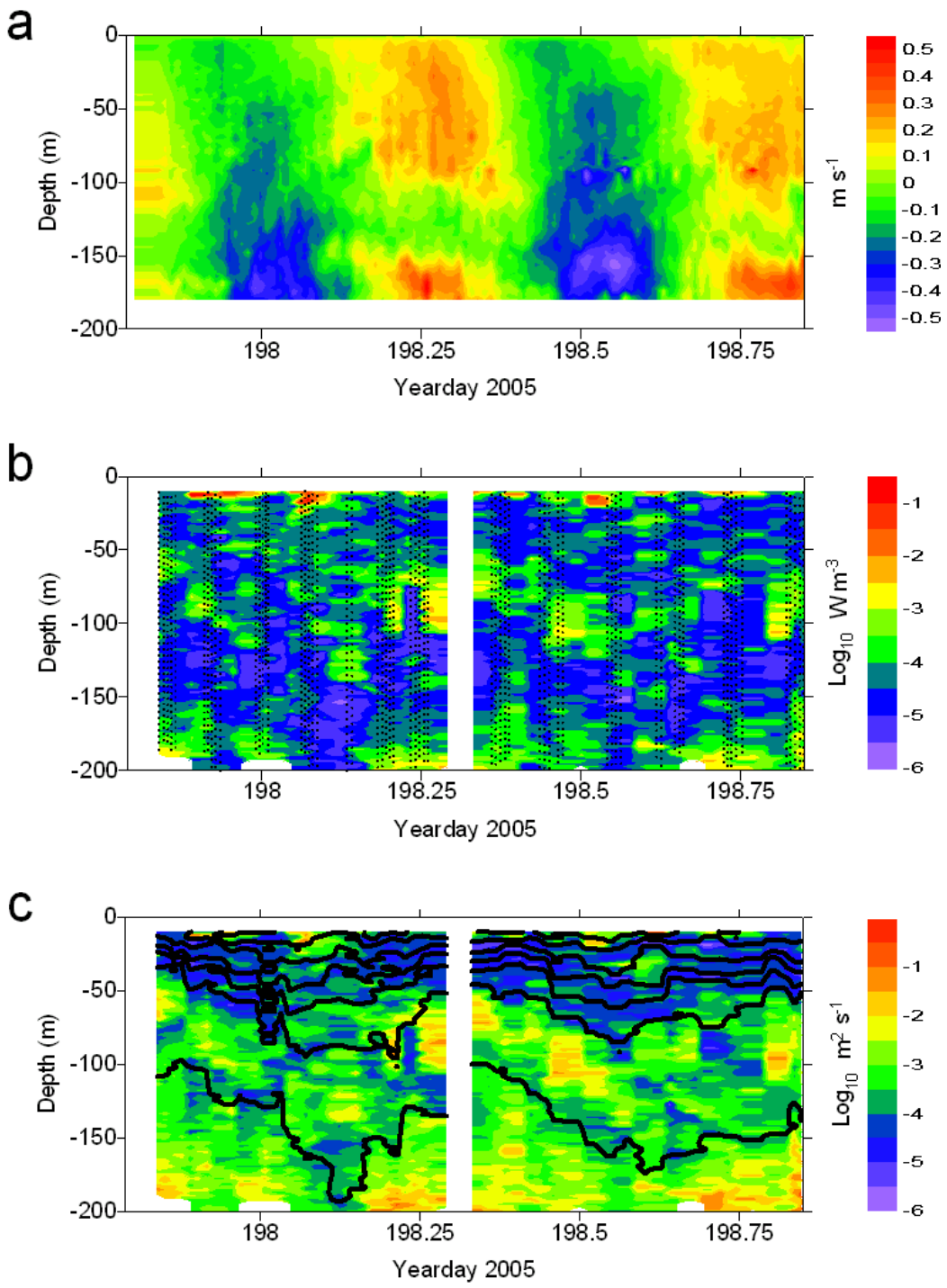

Figure 5.14

CS2b. As Fig 5.15

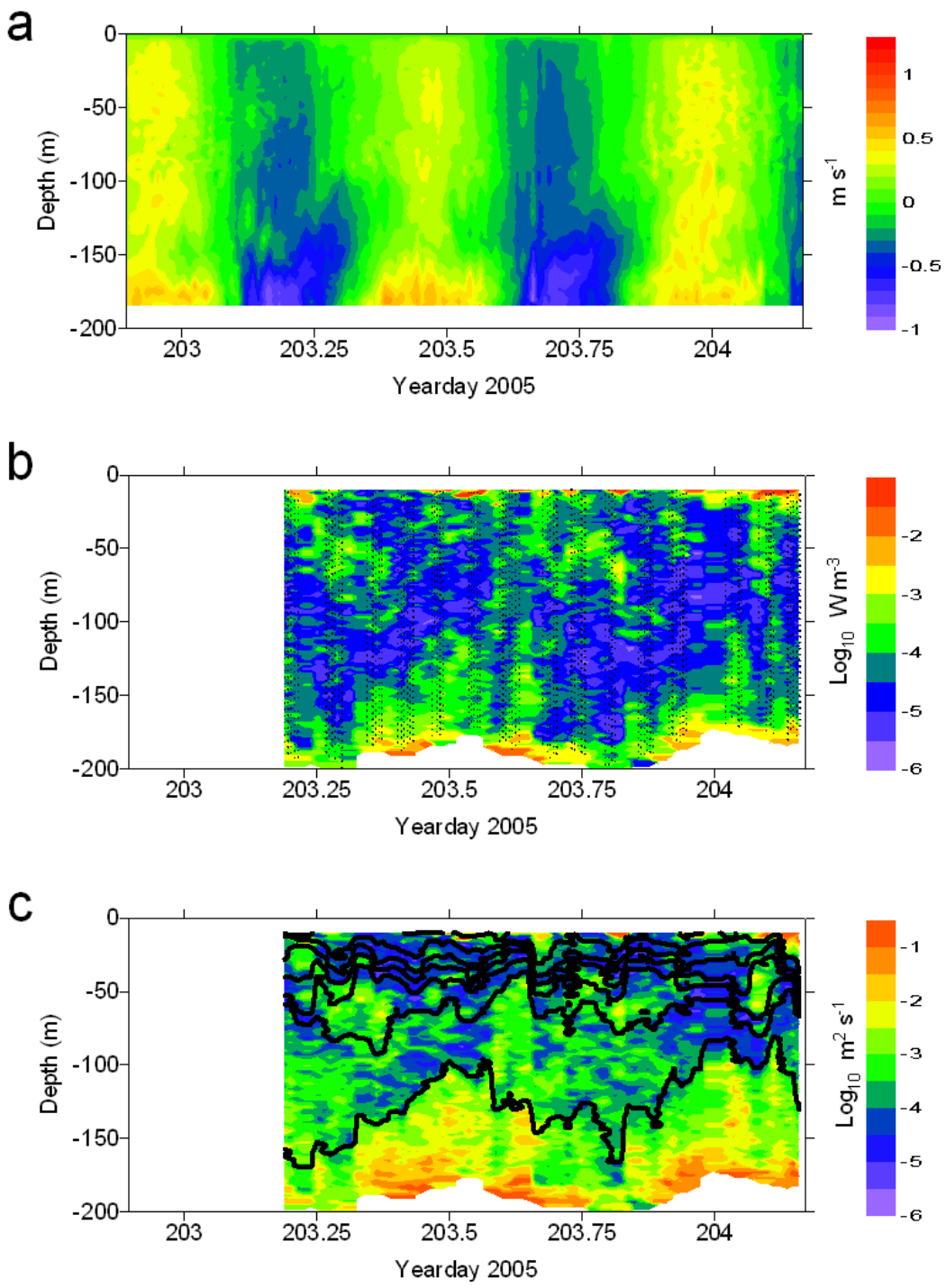

Figure 5.15

CS2c. As Fig 5.15

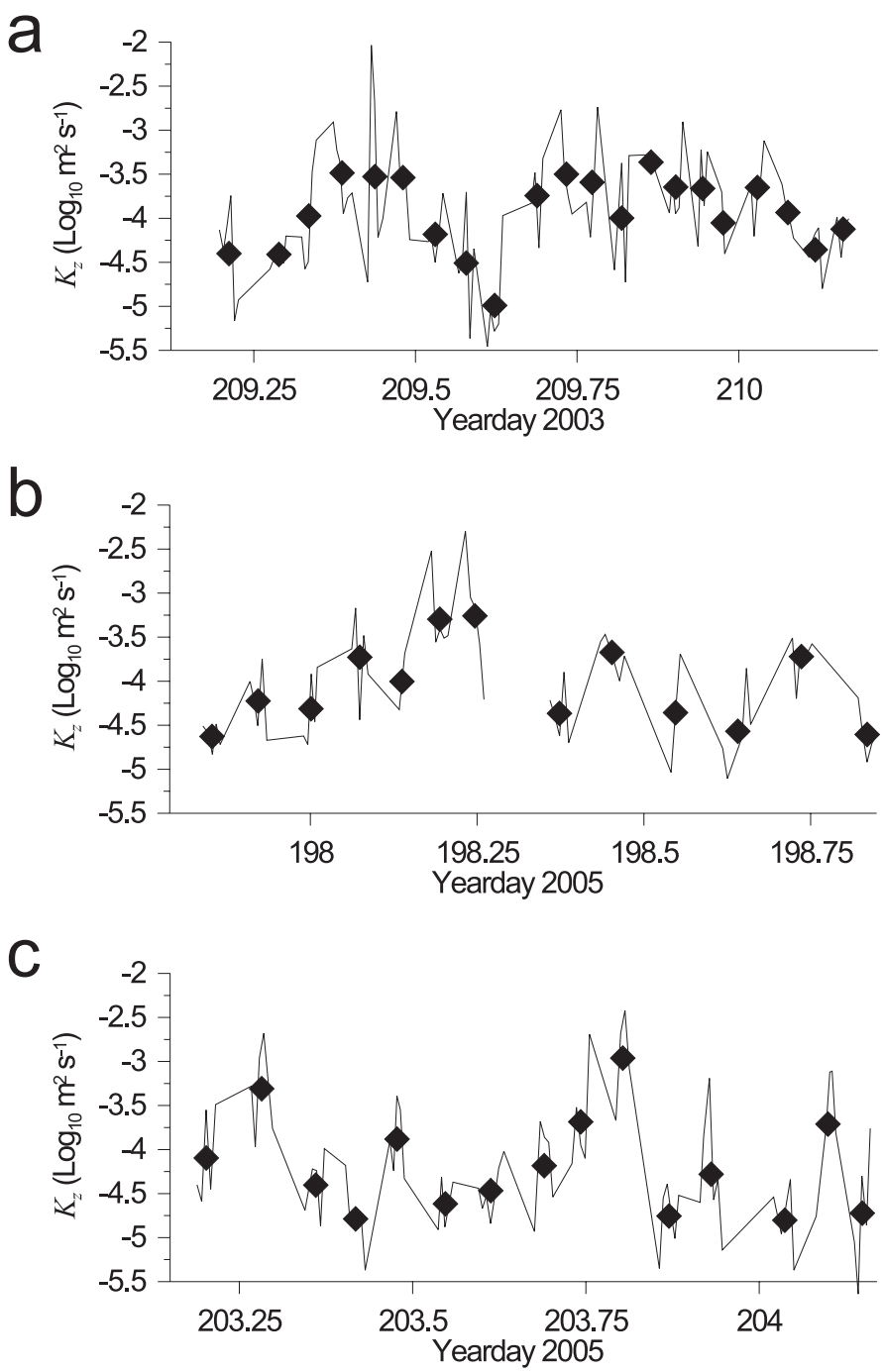

Figure 5.16

Mean vertical diffusivity, over the temperature ranges used to calculate J_N, for each profile during a) CS2a (spring tide), b) CS2b (neap tide) and c) CS2c (spring tide). The black diamonds mark the average value for each FLY ensemble.

5.3.3 Nitrate fluxes

Vertical nitrate flux into the SCM from the nitrate rich bottom water was estimated for each FLY profile during all three stations (Fig 5.17, see section 2.3 for methods). Regression of J_N against both $\Delta N/\Delta z$ and K_z demonstrated that, like the stations over the shelf, variation in J_N at the shelf break was controlled to a greater extent by K_z ($r^2>0.74$, $p<0.05$ for all CS2 stations) than $\Delta N/\Delta z$ ($r^2<0.003$, $p>0.05$ for all CS2 stations). Accordingly, high vertical nitrate fluxes into the SCM occurred when K_z was high at the base of the SCM.

Table 5.1

Daily mean vertical nitrate flux into the SCM from the bottom layer, J_N, and associated mean nitrate gradients, $\Delta N/\Delta z$, turbulent dissipation ε, and vertical diffusivity K_z, for stations CS2a, CS2b and CS2c, positioned over the shelf break.

Station	$\Delta N/\Delta z$ (mmol m^{-4})	ε (W m^{-3})	K_z (m^2 s^{-2})	J_N (mmol m^{-2} day^{-1})
CS2a	-0.1 ± 0.03 (-0.2 – -0.1)	9.6 ± 4.8 x10^{-5} (6.1–14.2 x10^{-5})	3.5 ± 1.8 x10^{-4} (1.7–6.7 x10^{-4})	2.0 ± 1.2 (1.3 – 3.0)
CS2b	-0.2 ± 0.01 (-0.2 – -0.1)	8.4 ± 4.2 x10^{-5} (5.0–12.8 x10^{-5})	2.8 ± 1.4 x10^{-4} (1.1–5.8 x10^{-4})	1.8 ± 0.9 (1.0 – 3.0)
CS2c	-0.3 ± 0.03 (-0.3 – -0.2)	21.9 ± 11.0 x10^{-5} (12.7–32.7 x10^{-5})	3.2 ± 1.6 x10^{-4} (1.7–5.4 x10^{-4})	3.9 ± 2.0 (2.5 – 5.7)

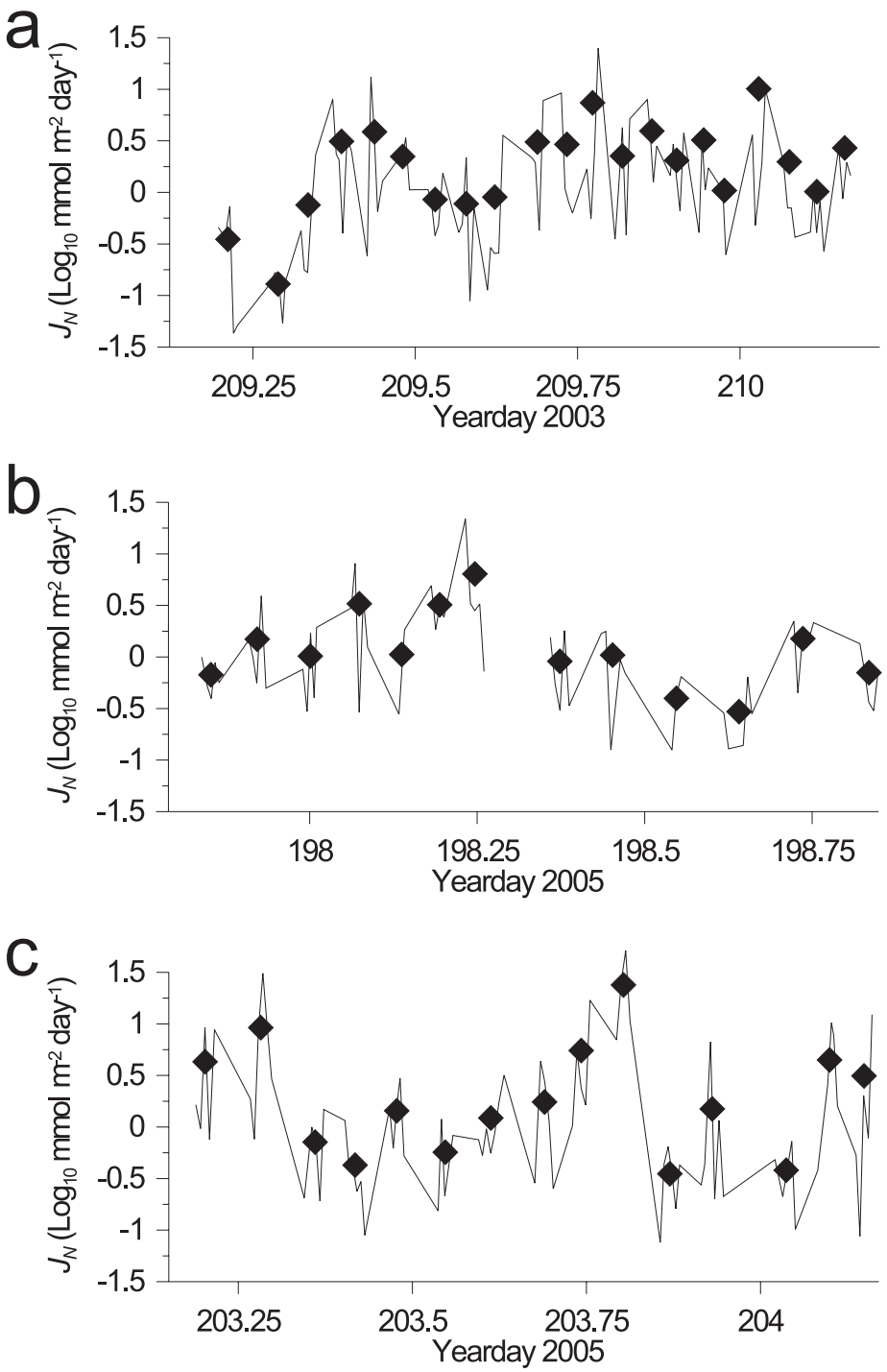

Figure 5.17

Vertical nitrate fluxes, J_N, into the subsurface chlorophyll maximum from below the thermocline during a) CS2a, b) CS2b and c) CS2c. The black diamonds mark the average value for each FLY ensemble.

5.4 Discussion

The data collected at the shelf break during cruises JR98 and CD173 are used here to evaluate the effect of internal tides and shorter frequency internal waves on vertical nutrient fluxes in the region. The possibility of spring-neap tidal cycle variations is explored, and the effect of internal mixing and associated nitrate fluxes on primary production is also investigated.

Temperature data collected using CTD, FLY and temperature logging moorings displayed waves of semi-diurnal period in the thermocline (Figs 5.7, 5.9 and 5.11), consistent with the oscillation of the internal tidal wave (section 1.1.3 *Internal wave driven mixing*). The greater temporal sampling of FLY and particularly of the temperature logging moorings revealed higher frequency internal waves which were particularly apparent around spring tides. The physical structure and movements of the thermocline were similar to earlier surveys of shelf breaks (see section 1.1.3, Pingree & Mardell 1985, Pingree 1988, Inall et al. 2000), and the daily mean K_z values at the base of the SCM (Table 5.1) were comparable to other shelf break estimates within the thermocline (Sandstrom & Oakey 1995, Inall et al. 2000, Sharples et al. 2001a, Rippeth & Inall 2002).

The thermocline diffuseness displayed during the CS2 station occupations and mooring deployments, and over the shelf break during all transects is confirmation of the regular occurrence of internal mixing at the Celtic Sea shelf break. At all stations the diffuseness of the SCM (Fig 5.8 and Section 5.3.1), and lack of skew towards lower temperatures, confirmed internal mixing had occurred, smearing out the chlorophyll *a* signal by preventing phytoplankton

accumulation at the base of the thermocline.

As in previous studies over the shelf break (Sandstrom & Oakey 1995, Inall et al. 2000) increased turbulence in the thermocline region was associated with internal waves. While the range of K_z values (Fig 5.16 and Table 5.1) did not vary greatly between CS2 stations, episodes of higher vertical diffusivities at the base of the SCM occurred more frequently at spring tides (CS2a and CS2c) than at neap tides (CS2b) due to the increasing number of high frequency internal waves (Fig 5.11 c), and dissipation occurring higher in the water column, around spring tides (Figs 5.13–5.15 c).

J_N values were greatly influenced by variations in vertical diffusivities at the base of the thermocline (section 5.3.3). Although the daily mean K_z was not particularly different between station visits, enhanced J_N associated with internal wave induced intensified K_z events biased the daily nitrate flux estimates, providing much of the daily nitrate supply. As such CS2c displayed higher vertical nitrate fluxes (3.9 mmol m^{-2} day^{-1}) into the SCM than CS2b (1.8 mmol m^{-2} day^{-1}).

The vertical diffusivities did not vary smoothly over the tidal cycle but were punctuated by short timescale high K_z events. Therefore, the sampling strategy, which involved breaks in order to recharge FLY batteries and carry out CTD casts, may have missed some high K_z events and caused under-estimation of J_N.

As seen in the mooring data, the high turbulence events are associated with specific points in the tidal cycle, and are much more prevalent around spring tides. Assuming the FLY measurements were spread equally over the tidal cycle, at CS2c the FLY, which sampled approximately 38% of the time (a total of 10.25

hours out of the 25 hour occupation), would have sampled 38% of the high K_z events. As these events bias the mean daily nitrate flux into the SCM taking into account the 62% of events which were missed would raise the estimated daily flux to ~15 mmol nitrate m^{-2} day^{-1}. The same reasoning applied to CS2b raised the daily estimates to ~4 mmol nitrate m^{-2} day^{-1}, increasing the difference in vertical nitrate fluxes between spring and neap tides. At CS2a the vertical nitrate flux rose to ~6 mmol nitrate m^{-2} day^{-1}.

Variations in $\Delta N/\Delta z$ did not have a significant influence on variations in J_N during each sampling period. However, overall changes in $\Delta N/\Delta z$ between occupations did affect J_N. Although daily mean vertical diffusivities were highest during CS2a, lower $\Delta N/\Delta z$ values (~1/3 of CS2c) resulted in lower J_N than CS2c. The lower $\Delta N/\Delta z$ values were partly the result of a more diffuse temperature gradient, and partly due to a smaller regression value of *m* against temperature (Table 2.5, section 2.3 *ΔN/Δz derived from a Temperature to [Nitrate] relationship*), which was possibly driven by lower phytoplankton standing stock in 2003.

The carbon fixation rates supported by the vertical nitrate fluxes were calculated assuming phytoplankton growth followed the Redfield ratio (106C:16N), and were compared to the observed primary production rates supplied by A. Hickman (Table 5.2, see section 2.1.7 for methods). The observed primary production rates were lower at spring tide and higher at neap tide, a difference more clearly visible under sunny conditions. This difference was caused by lower standing stock and changes in phytoplankton physiology (personal communication A. Hickman). The physiology was possibly affected by the greater number of internal waves and higher turbulence levels within the

thermocline around spring tides causing rapid vertical movements within the vertically changing light field, leaving the phytoplankton unable to acclimate to the ambient light.

Table 5.2

Calculated primary production rates (personal communication A Hickman) and new production supported by calculated vertical nitrate fluxes into the SCM from the bottom layer (i from directly flux, ii from estimated flux taking into account under-sampling of turbulent events).

Station	Integrated Primary Production (mg C m^{-2} day^{-1})		New primary production supported (mg C m^{-2} day^{-1})	
	Cloudy	Sunny	I	ii
CS2a	364 (± 109.2)	623 (± 186.9)	186 (± 110)	557 (± 329)
CS2b	396 (± 118.8)	940 (± 282)	167 (± 84)	371 (± 186)
CS2c	300 (± 90)	645 (± 194)	362 (± 185)	1410 (± 719)

At neap tide (CS2b) the observed production rates were greater than the vertical nitrate flux could support, resulting in a *f*-ratio which ranged from 0.18 in sunny conditions to 0.42 if cloudy. At spring tides (CS2c) observed production was lower and J_N was higher, resulting in *f*-ratios of 0.6 under sunny conditions and 1.2 under cloudy. If under-estimation of J_N is accounted for, the *f*-ratios rise to 0.4–0.9 at neap tide and 2.2–4.7 at spring tide. Thus, it appears nitrate supply is in excess of demand at spring tide. This is supported by non-zero surface

[Nitrate] sampled during both CS2a and CS2c (spring tide), whereas surface [Nitrate] was below detection limits at CS2b (neap tides). As neap tide surface [Nitrate] is below detection the excess nitrate supplied at spring tides must be utilised in the following few days. The chlorophyll appears to lag the nitrate supply by ~3.5 days (Sharples et al. In Press).

Chapter 6: Remote Sensing of the Celtic Sea shelf break.

6.1 Introduction

During times of seasonal stratification a band of cool, chlorophyll rich water is reliably observed over the Celtic Sea shelf break in AVHRR sea surface temperature (SST) and SeaWiFS and MODIS sea surface chlorophyll *a* concentration ([Chl *a*]) images (Fig 6.1). This band is a result of the large baroclinic tides generated over the upper continental slope, and of subsequent solitary internal wave activity as the internal tide evolves both on and off the continental shelf (Pingree et al. 1986 and see section 1.1.3 *Impacts of internal mixing*).

Observations of the vertical processes that drive the properties of the band, such as changes in surface water temperature and nutrient fluxes from deeper waters to the subsurface chlorophyll maximum (SCM) and surface, have been presented in the previous chapter, and indicate a spring-neap tidal cycle influence. Possible modifications in the structure of the shelf break band potentially revealed by a more synoptic temporal and spatial view are unfeasible by ship, but may be identified using remote sensing by satellite, if cloudiness allows. This chapter addresses the potential for remote sensing to provide a longer-term view of variability at the shelf edge.

Three transects (Sat_1, Sat_2 & Sat_3) were selected across the Celtic Sea southern shelf break (Fig 6.2), and data extracted from under the transects for AVHRR (SST, 2000-2005), SeaWiFS ([Chl *a*] and normalised water-leaving radiance at 555nm, nLw_{555}, 2000-2004) and MODIS ([Chl *a*] and nLw_{551}, 2005) satellite images. These remotely sensed data were processed and analysed as detailed in section 2.4 in order to elucidate any changes in the band, both over time and in space.

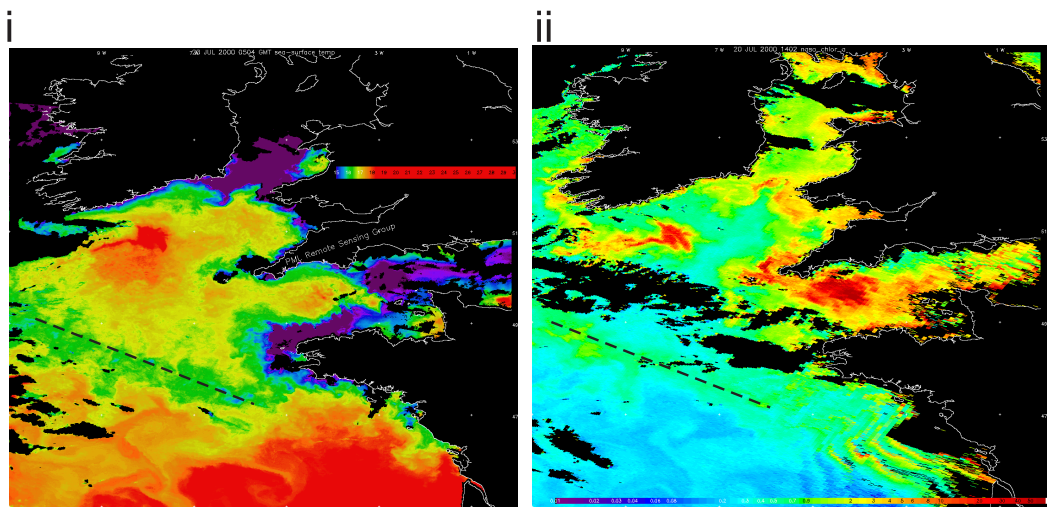

Figure 6.1

Celtic Sea i) AVHRR image of sea surface temperature (^{O}C, blue =15 ^{o}C, red>18 ^{o}C, 20th July 2000 at 0504) and ii) SeaWiFS image of sea surface chlorophyll *a* concentration (mg m^{-3}, purple<0.1 mg m^{-3}, red>10 mg m^{-3}, 20th July 2000 at 1402). For both images black represents land and cloud. The cooler waters associated with the Celtic Sea shelf break (indicated by black dashed line) are clearly seen, with associated increased [Chl *a*] values. *Images courtesy of RSDAS.*

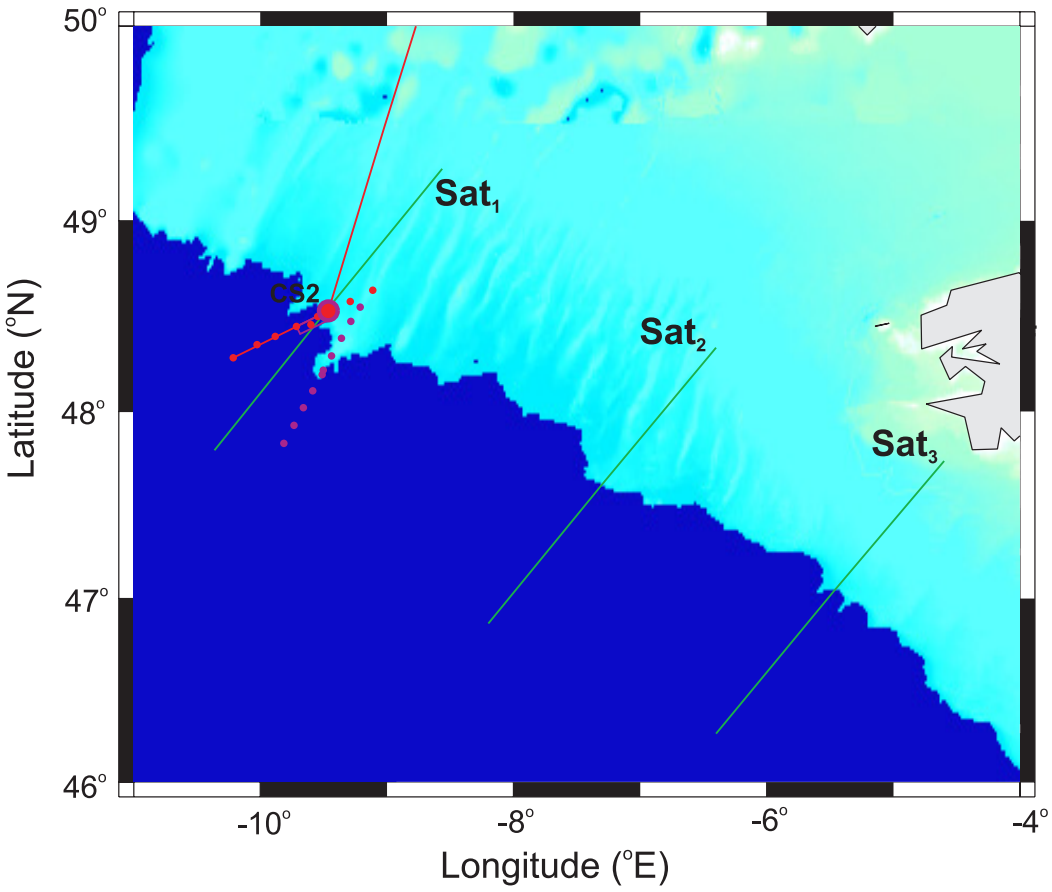

Figure 6.2

Remotely sensed transects over the shelf break region of the Celtic Sea. Green solid lines show the positions of the data transects taken from satellite images. The large circles show the positions used for CTD and FLY stations, smaller circles are CTD casts, and red solid lines are the SeaSoar transects, carried out during JR98 (2003, red) and CD173 (2005, purple). See chapter 2 for detailed positions and methods. Bathymetry data from IOC et al. (2003).

6.2 Basic observations from transects across the shelf break

Data extracted from the images showed a consistently cooler band situated over the region of the shelf break, and coincident increases in chlorophyll *a* concentrations, for example as seen in both the raw SST and [Chl *a*], and normalised $SST_{\%}$ and $[Chl\ a]_{\%}$ (see section 2.4.2 for method of normalisation), from Sat_1 in 2000 (Fig 6.3). Every year from 2000–2005 a relatively cooler band, varying in strength, but having up to a 10% temperature difference with the mean SST, was present over the shelf break region, and corresponded to the position of a band of enhanced [Chl *a*], which also varied in strength but exhibited increases of over 100% relative to the mean.

There was a tendency over all transects and years for [Chl *a*] to increase with decreasing SST (Fig 6.4). The data showed a similar exponential correlation between SST and [Chl *a*] under Sat_1 ($\ln([Chl\ a]) = -0.34 \times SST + 5.05$, $r^2=0.45$, $p<0.05$) and Sat_2 ($\ln([Chl\ a]) = -0.33 \times SST + 5.05$, $r^2=0.46$, $p<0.05$). This relationship appeared to be less robust under Sat_3, which also displayed an exponential relationship, though with a weaker relationship between [Chl *a*] and SST ($\ln([Chl\ a]) = -0.20 \times SST + 2.79$, $r^2=0.28$, $p<0.05$).

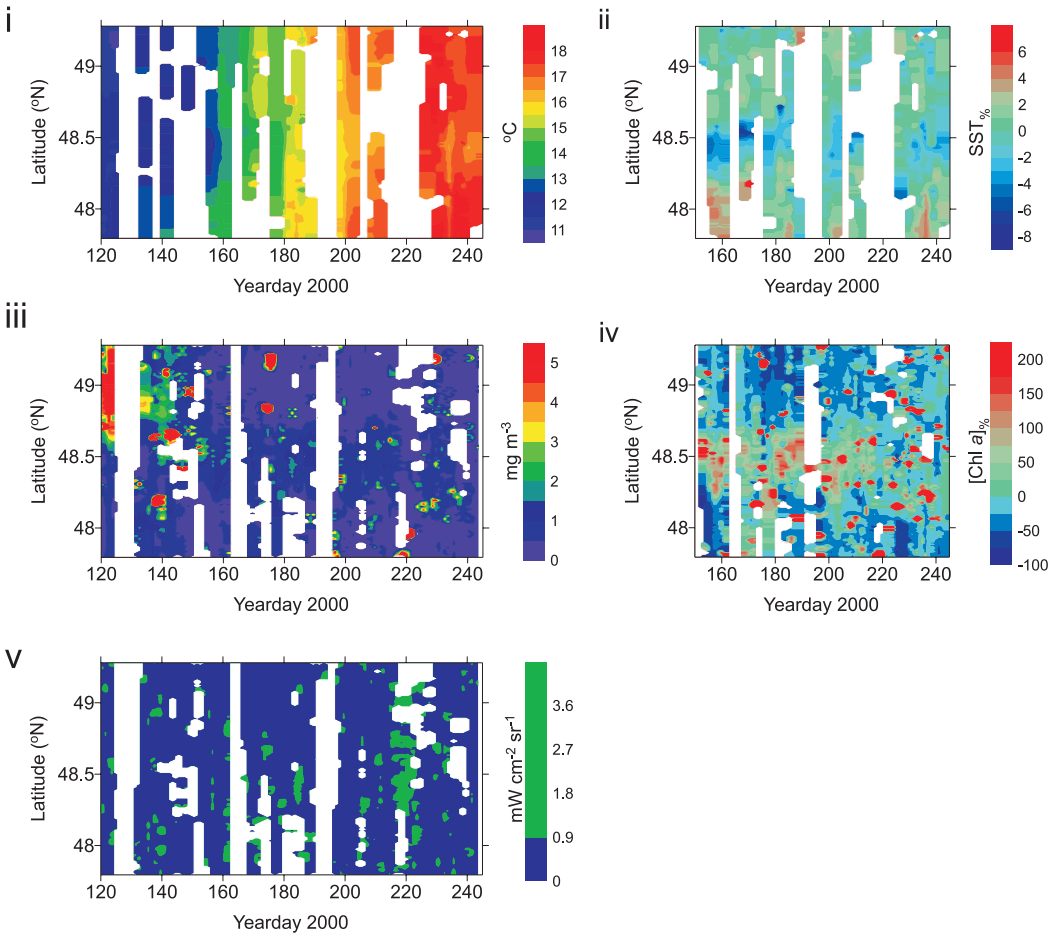

Figure 6.3

Sat_1 transect data for year 2000. i) AVHRR sea surface temperature, ii) normalised sea surface temperature, iii) SeaWiFS surface chlorophyll *a* concentration, iv) normalised surface chlorophyll *a* concentrations and v) SeaWiFS normalised water-leaving radiance at 555nm. In v) blue represents non-coccolithophore bloom conditions, and green represents potential coccolithophore bloom conditions (Cokacar et al. 2004). White contoured intervals represent data missing due to cloud cover. Shelf break lies at latitude 48.53 °N.

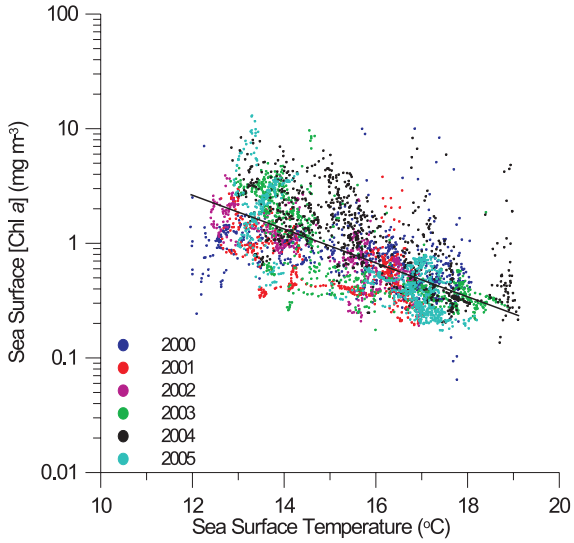

Figure 6.4

Relationship under Sat_1 between sea surface temperature and surface chlorophyll *a* concentration (ln([Chl *a*]) = -0.34xSST + 5.05, r^2=0.45, p<0.05).

6.3 Inter-annual variations in sea surface temperature and chlorophyll *a* over the shelf break

Mean $SST_{\%}$ and [Chl a]$_{\%}$ for the stratified season were calculated at every sample point along transect Sat_1, in order to elucidate inter-annual variations in the position, width and intensity of the shelf break band (Fig 6.5). The feature was present in all years and appeared to be consistent between years.

Bootstrapping was used to calculate the 95% confidence intervals on each transect's data at all sampled latitudes, and Gaussian curves were fitted to the yearly mean transects (see Fig 6.6 for Sat_1 2000 example), as a consistent method

of quantifying band width, position and intensity. For each of Sat_1, Sat_2 and Sat_3, there was no significant difference in the fitted Gaussian curves between years ($F<1.9$, $F_{crit}>2.3$, $p>0.05$).

As the difference between years was found to be insignificant, an overall mean band, covering 2000–2005, for the summer stratified period was obtained by calculating the average $SST_{\%}$ and [Chl a]$_{\%}$ for all years at each latitude along the transect (Fig 6.7), and Gaussian curves were fitted. As a check on the applicability of using a Gaussian curve, the Gaussian descriptors of the fitted bands were compared to the mean band values under all remotely sensed transects (Table 6.1 for Sat_1 example). They were found not to be appreciably different. Therefore, the mean Gaussian curve of all years' data was a good estimate of the band's general position, width and intensity, under all transects.

The findings of inter-annual consistency in the band provide evidence that the feature was produced in a manner which is consistent between years. However averaging of data into yearly examples would have removed smaller scale, intra-annual variability, for example over a spring-neap tidal cycle. This will be investigated further in section 6.5.

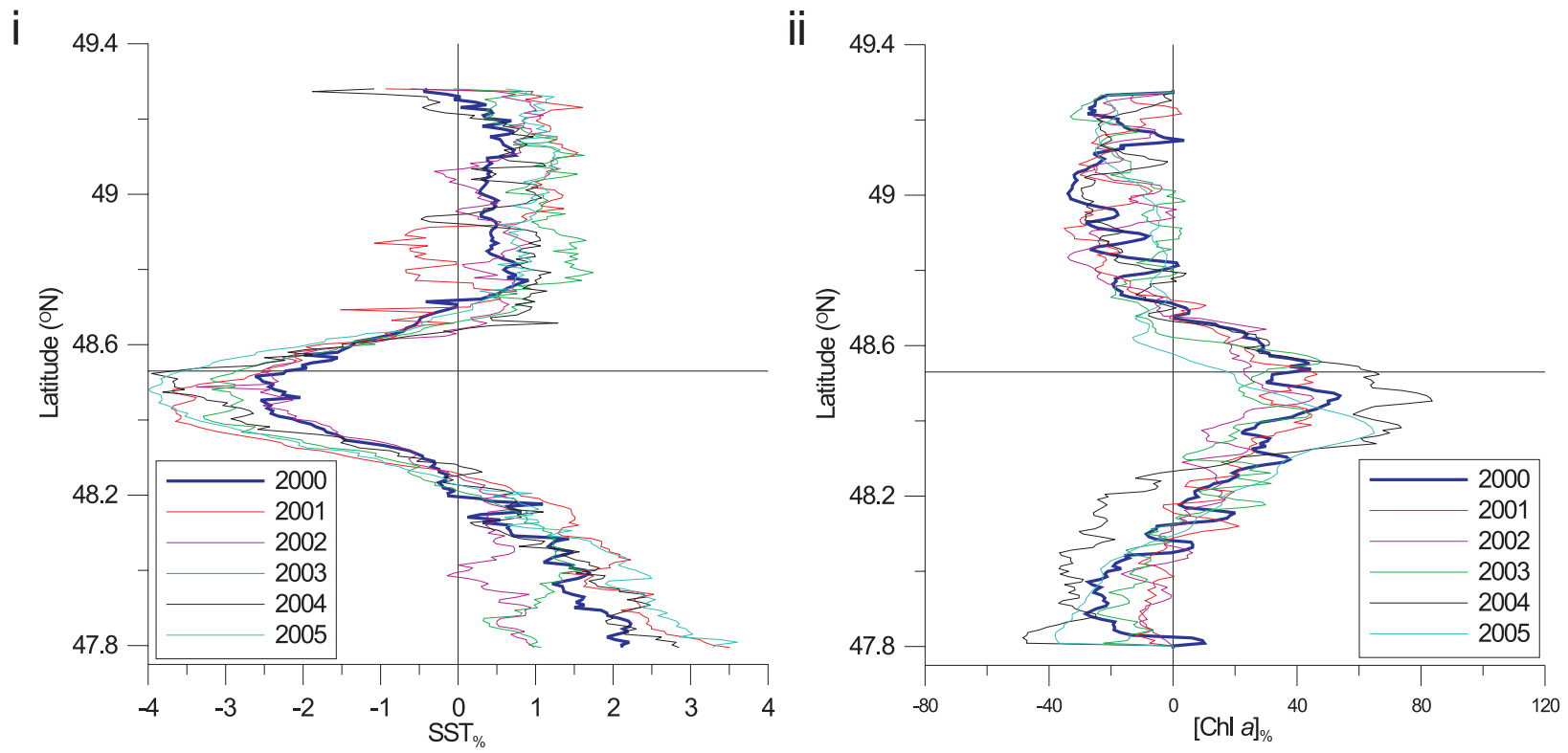

Figure 6.5

Sat_1 i) mean $SST_{\%}$ and ii) mean $[Chl\ a]_{\%}$ for each year for 2000 through 2005, during the stratified summer period (Yearday 150-242).

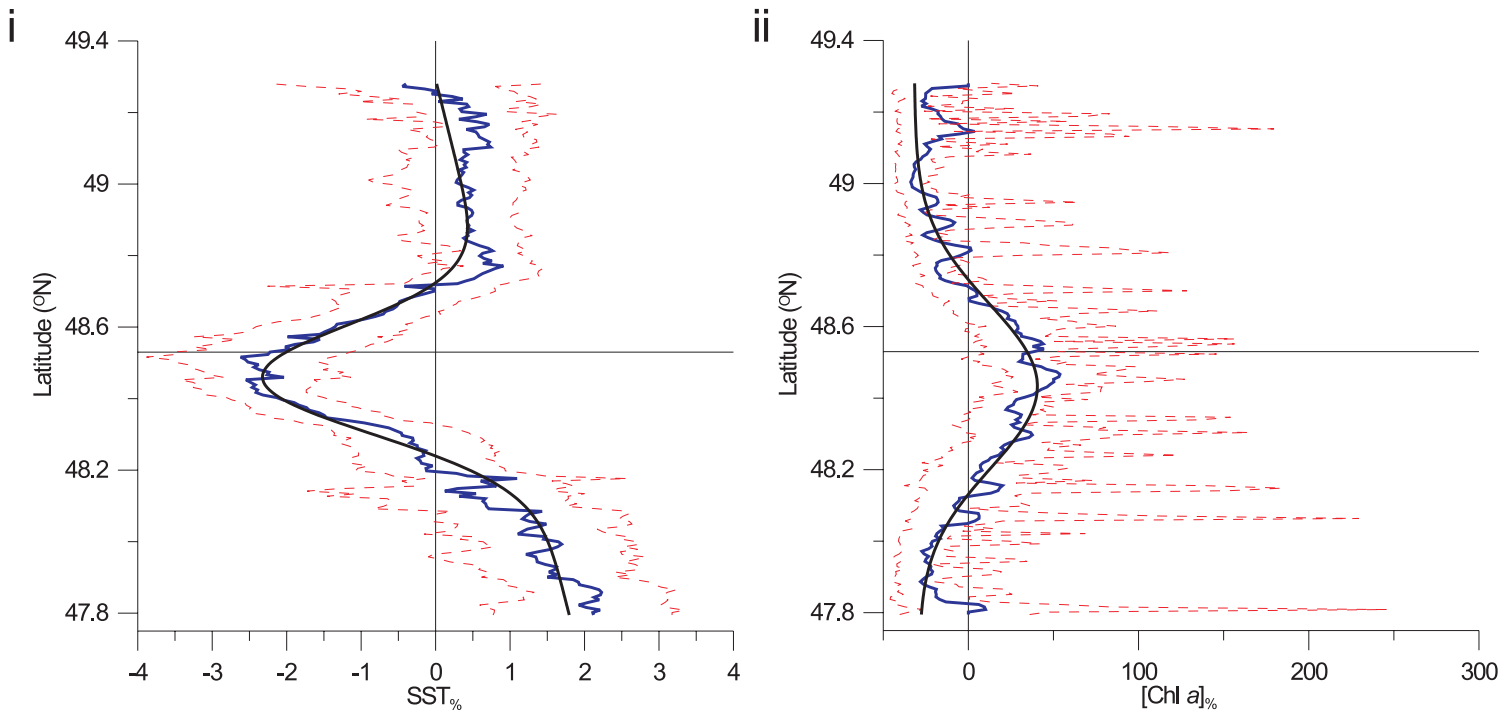

Figure 6.6

Sat_1 i) Mean $SST_{\%}$ and ii) $[Chl\ a]_{\%}$ for 2000, during the stratified summer period (Yearday 150-242). The blue solid line is the mean transect data, the red dashed lines the 95% confidence intervals calculated using bootstrapping and the black solid line the fitted Gaussian curve.

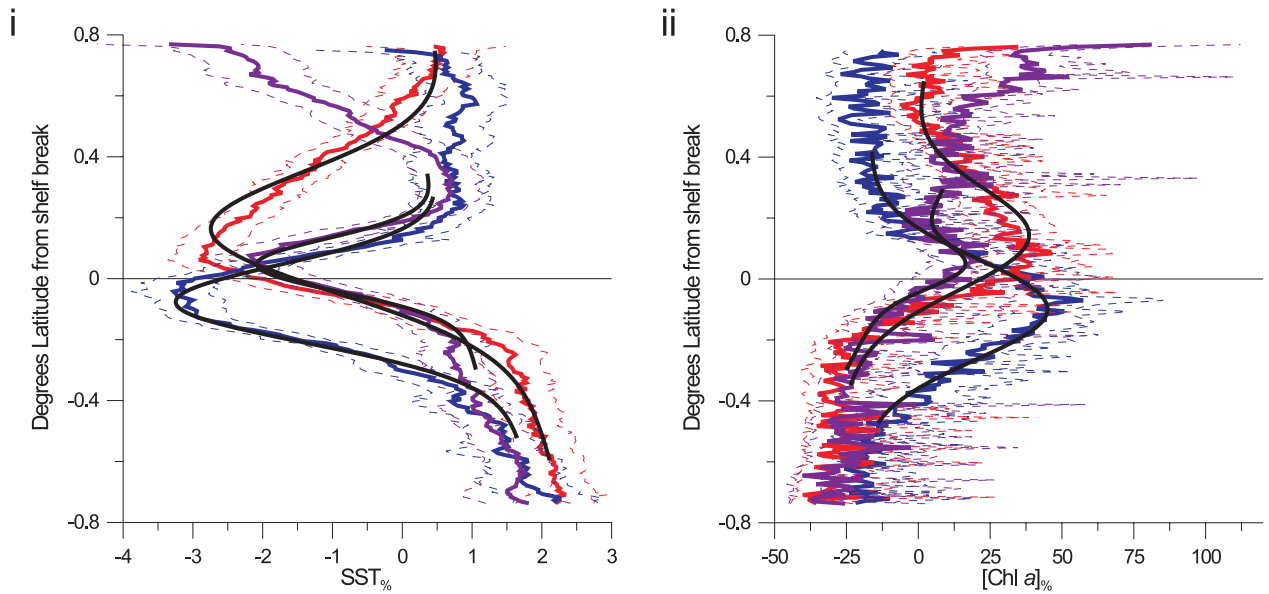

Figure 6.7

i) Mean $SST_{\%}$ and ii) mean $[Chl\ a]_{\%}$ over all years under Sat_1 (blue), Sat_2 (red) and Sat_3 (purple) during the stratified summer period (Yearday 150-242). The coloured solid lines represent mean values and dashed lines the 95% confidence intervals, calculated using the bootstrapping technique, and black solid lines the Gaussian curves fitted to the mean data. The latitude scale has been adjusted so all data is plotted relative to the shelf break (0 = 200m contour).

Table 6.1

$SST_{\%}$ and [Chl *a*]$_{\%}$ band position, width and intensity for transect Sat_1.

	$SST_{\%}$		[Chl *a*]$_{\%}$	
	Fitted	Mean	Fitted	Mean
Position (^{o}N ± km)	48.45	48.46 ± 1.4	48.43	48.42 ± 5.1
Width (km)	40.44	39.29 ± 6.4	52.22	60.18 ± 13.5
Intensity (% of transect mean)	-4.28	-4.22 ± 0.8	62.99	67.48 ± 19.5

6.4 Spatial variations in sea surface temperature and chlorophyll *a* over the shelf break

The apparent consistency of the band between years allows the mean transects of all years (over stratified season, 2000–2005) to be used to evaluate differences between the three spatially separate Sat transects (Fig 6.7). The average positions, widths and intensities of the $SST_{\%}$ and [Chl *a*]$_{\%}$ bands (Table 6.2) were calculated using Gaussian curve fitting.

Sat_1 and Sat_3 displayed symmetrical bands (Fig 6.7), which enabled a good fit of the Gaussian curve. Sat_2, however, was asymmetric, with a steeper gradient of change, in both temperature and chlorophyll *a* concentration, on the oceanic side of the band compared to the shelf side. The Sat_2 fitted Gaussian curves described width and intensity effectively, but, due to the asymmetry, placed position too far onto the shelf. Assessed by eye, the position of the Sat_2 peak was similar, relative to the shelf break, to Sat_3. Unlike Sat_1, where the

maximum band intensity was ocean-wards of the shelf break, Sat_2 and Sat_3 displayed maximum intensity in both $SST_{\%}$ and $[Chl\ a]_{\%}$ shelf-wards of the shelf break (Table 6.2).

All transects displayed increased chlorophyll *a* concentrations overlying the relatively cooler band, with no significant differences between the SST and [Chl *a*] band positions or widths at each site (Table 6.2). Comparing between the three Sat transects, maximum intensity of the Sat_1 and Sat_2 bands were not found to be significantly different, however the intensity of both cooling and enhanced chlorophyll *a* concentration under Sat_3 appeared to be less than under the other two transects. The width of the band also appeared to be less under Sat_3.

Table 6.2

Descriptors of mean $SST_{\%}$ and $[Chl\ a]_{\%}$ bands for each transect, taken from fitted Gaussian curves. Values stated with 95% confidence interval.

		Position (km from shelf break)	Width (km)	Intensity (% of transect mean)
Sat_1	$SST_{\%}$	-9.11 ± 2.8	40.44 ± 24.7	-4.28 ± 0.8
	$[Chl\ a]_{\%}$	-11.11 ± 10.0	52.22 ± 22.5	62.99 ± 35.9
Sat_2	$SST_{\%}$	16.89 ± 12.3	62.44 ± 38.1	-3.96 ± 0.9
	$[Chl\ a]_{\%}$	14.44 ± 15.0	52.22 ± 35.0	50.27 ± 34.7
Sat_3	$SST_{\%}$	4.89 ± 5.3	27.56 ± 17.4	-2.77 ± 5.6
	$[Chl\ a]_{\%}$	4.33 ± 6.9	21.78 ± 20.5	22.02 ± 16.3

6.5 Intra-annual variations in sea surface temperature and chlorophyll *a* over the shelf break at CS2.

Investigations were concentrated on transect Sat_1 as this overlay station CS2, which was the focus of Chapter 5.

6.5.1 Annual trends

In section 6.3 $SST_{\%}$ and [Chl *a*]$_{\%}$ were used in an effort to de-trend the remotely sensed data. Although inter-annual variation was not significant (section 6.3), the normalisation of the data may have removed significant intra-annual variability and trends through the year. In particular the potential for spring-neap variability, as displayed in Chapter 5.

As expected, the sea surface warmed through the year as solar radiation continued to heat the surface waters throughout the summer (Fig 6.8 i). [Chl *a*] showed no annual trends in the oceanic (latitudes<47.9 ^{o}N) or shelf (latitudes>49 ^{o}N) sections of the transect, but did display a generally decreasing band maxima (Fig 6.8 ii). The same patterns were present in both sea surface [Chl *a*] and SST for years 2000–2005.

In addition to the regional data, trends within the fitted Gaussian curve descriptors were examined. SST descriptors exhibited no trend across the year (Fig 6.9 i). [Chl *a*] intensity decreased through the year (Fig 6.9 ii), due to the decrease in the band's maximum [Chl *a*] (Fig 6.8 ii).

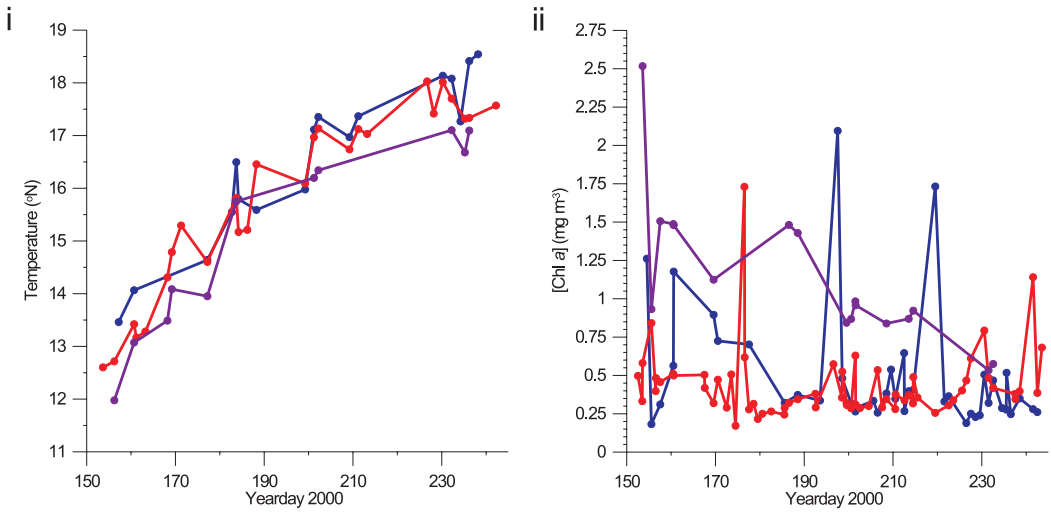

Figure 6.8

Sat_1 oceanic (blue, latitudes<47.9 °N), shelf (red, latitudes>49 °N) and band peak (purple) i) sea surface temperature and ii) chlorophyll *a* concentrations over the stratified summer period (Yearday 150-242) for 2000.

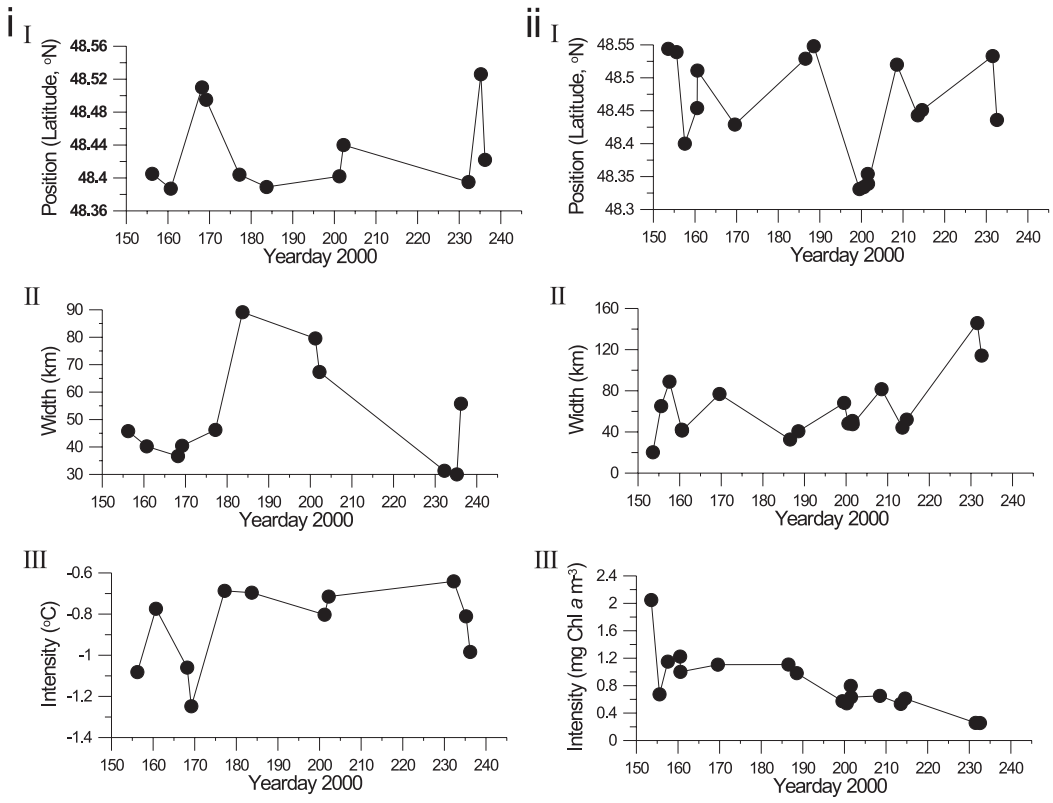

Figure 6.9

Descriptors of the shelf break surface feature under Sat_1, taken from fitted Gaussian curves for individual image's transect data in 2000. i) Sea surface temperature and ii) sea surface [Chl *a*] I) position, II) width ½ way down curve, and III) intensity of band.

6.5.2 Intra-annual cycles

At each sampled latitude along Sat_1 the normalised data was fitted to a spring-neap function, in order to estimate the variability of the data with the spring-neap cycle across the shelf break (see section 2.4.2). χ^2 for the spring-

neap cycle regressions acted as a relative indicator of the strength of the fit to the function along the transect (Fig 6.10). A lower χ^2 was indicative of a good fit, and hence a stronger spring-neap signal in the data, compared to a high χ^2 indicating a poor fit and weak spring-neap signal.

The centre of the $SST_{\%}$ band exhibited the weakest fit and the oceanic edge of band the strongest, all years showing the same pattern. [Chl *a*]$_{\%}$ had very high χ^2 values at all latitudes, demonstrating no regions with a strong fit to a spring-neap cycle. When $SST_{\%}$ data at the latitude with the strongest fit (lowest χ^2, latitude 48.26 ^{o}N) was compared to the calculated spring-neap regression line (Fig 6.11) it was found 29% of variability in the $SST_{\%}$ data was explained (r^2=0.29, p<0.05). $SST_{\%}$ was lowest ~2–3 days after spring tides and highest 10–12 days after spring tide (i.e. 2–4 days after neap tides).

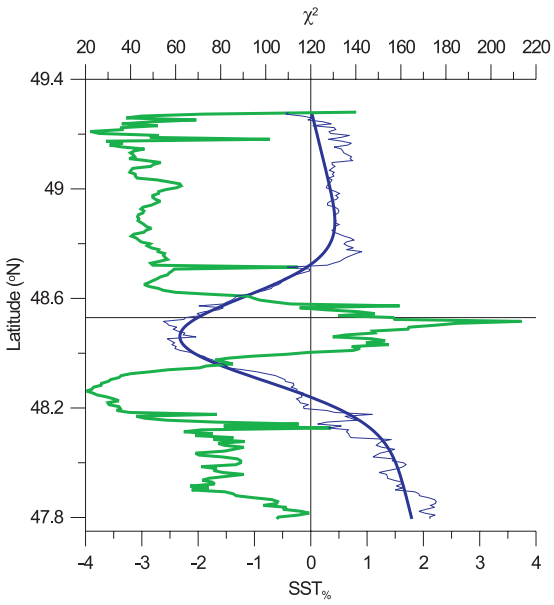

Figure 6.10

χ^2 of spring-neap function fitted to $SST_{\%}$ 2000 data across Sat_1. Thin blue line represents the mean 2000 $SST_{\%}$ transect, the thick blue line the fitted Gaussian curve and the thick green line the χ^2 values f a spring-neap function fitted to all 2000 spring-neap $SST_{\%}$ data.

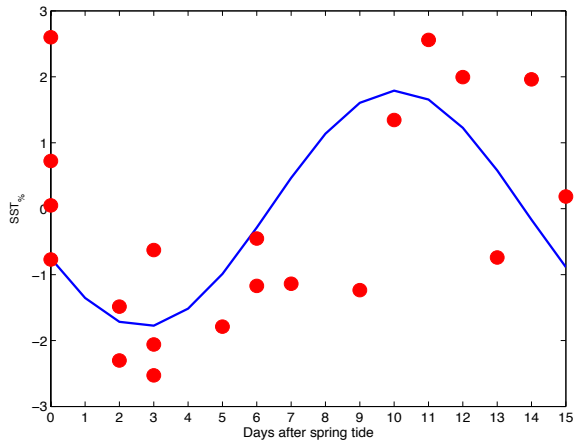

Figure 6.11

2000 $SST_{\%}$ data (red circles) and fitted spring-neap cycle (blue solid line) for latitude (48.262 ^{o}N) of lowest χ^2 under Sat_1 (Fig 6.10).

6.6 Discussion

Remotely sensed images have been used here to reveal a fuller representation of temporal variability in the cool, enhanced [Chl *a*] band over the shelf break, than was gained in Chapter 5. The images also allow investigation into spatial variability along shelf break. Using Gaussian curves to describe the shape and intensity of the band, a calculation of the production over the shelf break can be made, and the required nitrate supply estimated. However, the abundance of cloud cover over the Celtic Sea shelf break and surrounding area during the summer resulted in less complete temporal cover than was hoped for. The least cloudy year was 2000, giving 20 clear SST transects out of a total of 95 AVHRR images. SeaWiFS and MODIS, which generally passed over the Celtic Sea later in the day (when it was cloudier), supplied even fewer clear images each year. This made it difficult to fit a meaningful spring-neap tidal function to SST or [Chl *a*] data.

The relatively high surface [Chl *a*] at the shelf break, compared to over the shelf, could be caused either by internal mixing of SCM phytoplankton into the surface layer or by phytoplankton growth in response to the presence of nitrate, or by a combination of the two. Residence times in the surface mixed layer ($RT = L^2/K_z$, RT is residence time, L is depth of layer), calculated for neutrally buoyant phytoplankton at CS2, were ~8–14 days. Non-zero concentrations of nitrate were also sampled in surface waters, suggesting phytoplankton were able to grow within the surface mixed layer.

6.6.1 Temporal variations in sea surface temperature and sea surface chlorophyll *a* concentrations at the Celtic Sea shelf break

Two types of intra-annual variations were displayed in the remotely sensed data, annual trends and shorter-scale variability. [Chl *a*] within the band showed a gradual decrease in intensity throughout the stratified period (Fig 6.9 ii III). The decrease is unlikely to be due to less mixing (leading to a smaller nutrient flux into the base of the thermocline) as the year progresses, as SST band intensity showed no such trend (Fig 6.9 i III). Daily irradiance peaks ~Yearday 190, and less light after then could lead to lower primary production rates and phytoplankton growth, however surface [Chl *a*] decreases from the start of the stratified period, before Yearday 190. As stratification develops, the flux of nitrate into the thermocline and surface waters, driven by the internal mixing, may be greater than the capability of the deep water system to replace nitrate directly below the thermocline. Thus, as the stratified season continues, nitrate supply into the thermocline may become rate limited by deep water mixing rates replenishing the nitrate below the thermocline. Also, phytoplankton lower in the water column may become more dominant later in the season, allowing less nutrients through to the surface and reducing the sea surface [Chl *a*] signal seen by the satellites. This may also have masked any periodic increases in [Chl *a*] due to the spring-neap tidal cycle, as the increase would have occurred below the surface, out of range of the satellites' sensors.

Non-zero surface [Nitrate] was sampled at the shelf edge station (CS2) during both CS2a and CS2c (spring tide), whereas surface [Nitrate] was below detection limits at CS2b (neap tides). This implies there was at least a periodic

(fortnightly) supply of nitrate into the surface layer around spring tides, which would enhance surface phytoplankton growth at the shelf break. However the intra-annual trend of decreasing intensity would complicate fitting a spring-neap tidal cycle function to [Chl *a*] data, and may hide any signal that did exist.

Trends in sea surface temperature were as expected, with temperature increasing as the year progressed. While the minimum SST within the band (SST_{band}) did increase throughout the stratified period, the difference between SST_{band}, and SST_{shelf} and SST_{ocean}, i.e. the intensity of the band, varied. Although there was some indication of spring-neap tidal variability of SST at the edge of the band (Fig 6.10), there was little indication of a strong spring-neap tidal effect on cooling intensity at the centre of the band. The majority of internal wave energy moved either along the shelf break to the west or out to sea (personal communication, M. Green) which may be why the oceanic band edge had a stronger spring-neap signal in all years than the shelf band edge. The higher internal wave activity and stronger mixing at spring tides (Chapter 5) could be causing the band feature to expand (producing lower temperatures at the band edge) and contracting around neap tides (resulting in higher temperatures at the band edge) when there is less internal wave activity. In situ data from CS2, situated at the shelf side edge of the cool band (Fig 5.1), suggested that there is variation in SST, with significantly cooler waters found at the surface at spring tide, in comparison to neap tide, although the gradations between are not known.

Inter-annual variability was small, although only 6 years of data was used, which would not show longer scale tidal cycles, such as the 18.9 year lunar influenced cycle. The small variability allowed comparison of the overall mean band shape between positions along the shelf break.

6.6.2 Spatial variations in sea surface temperature and sea surface chlorophyll *a* concentrations at the Celtic Sea shelf break

The cool, enhanced [Chl *a*] band feature was centred in the region of the shelf break, but at different relative positions along the shelf edge (Fig 6.7). The band appeared to move either onto the shelf (Sat_2 and Sat_3) or oceanwards (Sat_1). However, the shelf break was nominally considered to be at the 200 m depth contour, which did not necessarily represent the position of the start of the steep continental slope, where the internal tidal waves were most likely being generated (Baines 1973, Baines 1974). Under Sat_2 and Sat_3 the start of the slope was shallower than 200 m (Fig 6.12 b and c), and so would generate the internal tide shelfwards of the 200 m contour. Under Sat_1 the bathymetry was more complex (Fig 6.12 a), but the shelf slope began steeply sloping deeper than 200 m, and so greatest internal wave generation would occur oceanward of the 200 m contour.

Unlike the symmetrical bands under Sat_1 and Sat_3, the asymmetric band under Sat_2 extended further onto the shelf, returning to shelf background levels of SST and [Chl *a*] more gradually (Fig 6.7). This could be caused by a variety of mechanisms. Stronger advection over the shelf under Sat_2 could spread the signal seen by satellites, or stronger horizontal diffusion. The stratification parameters (Eq 1.3, section 1.1.1) of both Sat_1 and Sat_3 shelf regions were greater than 2, indicating strongly stratified waters, whereas the stratification parameter over the shelf under Sat_2 was ~1.5 indicating transitional waters, i.e. less strongly stratified. The weaker stratification may result in a lower buoyancy frequency and lead to lower values of R_i (Eq 1.5), which, in turn, would allow greater

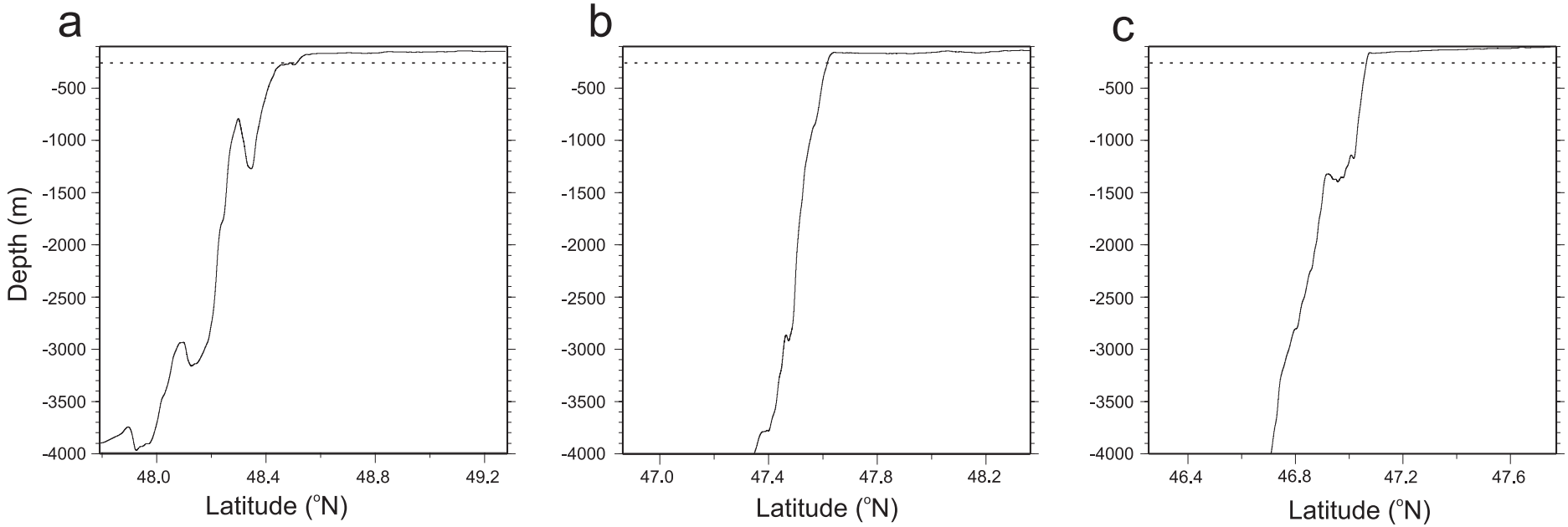

Figure 6.12

Bathymetry under transects a) Sat_1, b) Sat_2 and c) Sat_3. The dashed line marks 200m depth, the arbitrary shelf break proxy. Bathymetry data is from IOC et al. (2003).

turbulent mixing to be generated by the internal tide. The lower R_i would allow the effect of the mixing to been seen at the surface further on shelf than when stratification was stronger, as the lower energy contained in the internal tide further on shelf would still be able to drive greater mixing where the stratification is weaker.

The intensity of the band under Sat_3 was much lower than the other two transects, particularly in sea surface [Chl *a*]. This, though, may partly have been due to cool, productive, coastal waters near France (Kelly-Gerreyn et al. 2006), which intruded into the northern third of transect Sat_3, biasing the transect mean used to calculate normalised SST and [Chl *a*] (Eq 2.23 and 2.24) and hence lowering the relative intensity of the band. The spatial extent of the band over the shelf is difficult to ascertain as the coastal waters may intrude into the region affected by the internal tide. As such Sat_3 was considered to cover a different hydrological regime than the other Sat transects.

A regime change between Sat_3 and $Sats_{1\&2}$ is further supported by the SST to [Chl *a*] relationship calculated within the region of the bands. Sat_1 and Sat_2 had a very similar relationship (section 6.2), whereas, although Sat_3 also had an exponential relationship, it displayed a smaller increase in [Chl *a*] per decrease in SST. Again, this may be due to the coastal waters encroaching into Sat_3.

6.6.3 Nitrate requirements of the shelf break enhanced chlorophyll feature

Under Sat_1 the fitted Gaussian curve described highest chlorophyll *a* concentrations situated in a band of 52 km width over the shelf break. If the average concentration of Chl *a* away from the shelf break was assumed to be ~0.5 mg m^{-3} then an intensity increase of 63% (Table 6.2) equated to an increase of 0.32 mg Chl *a* m^{-3}. This was equivalent to an average 0.16 mg Chl *a* m^{-3} increase across the whole band at the surface, i.e. an average [Chl *a*] within the band of 0.66 mg m^{-3}.

Assuming the chlorophyll layer depth extends to 50 m (as suggested by the CTD and SeaSoar transects across the shelf break, Figs 5.2–5.4), this suggests a total Chl *a* per water column of 33 mg Chl *a* m^{-2}. This is equivalent to 16.5 mg Chl *a* m^{-2} day^{-1}, using an estimated turnover time of 2 days. Flow cytometry gave a Mass:Pigment of ~10 for CS2, so C:Chl was assumed to be 10. Therefore, 16.5 mg Chl *a* m^{-2} day^{-1} equals 165 mg C m^{-2} day^{-1}. This would require an average of ~ 2.2 mmol nitrate m^{-2} day^{-1}, assuming Redfield ratio between carbon and nitrogen.

This nitrate flux of 2.2 mmol m^{-2} day^{-1} is similar to those estimated for shelf break station CS2 (Table 5.1), however it does represent an average over the stratified period, smoothing out annual trends in intensity and shorter term variations.

There was no significant difference between the width and intensity of the bands under Sat_1 and Sat_2, and the temperature to chlorophyll *a* relationships are similar, despite the variation in stratification parameters, implying nutrient fluxes along the shelf break are comparable.

Chapter 7: Discussion and conclusions

Three hydrographic regimes were investigated in the course of the two cruises JR98 and CD173; over flat shelf topography, over banks on the shelf, and over the shelf break (Chapters 3 and 4, and Chapters 5 and 6 respectively). The rates of supply of new nitrate into the subsurface chlorophyll maximum were the focus of this thesis, and how these rates varied both spatially and temporally. The questions originally posed were:

1) What are the rates of supply of nitrate to the thermocline, and hence the subsurface chlorophyll maximum, across the Celtic Sea?
2) How do these rates of supply change temporally and spatially?
3) What levels of production are supported by the estimated nitrate fluxes across the shelf?

7.1 Supply of new nitrate to the subsurface chlorophyll maximum across the Celtic Sea

The vertical nitrate flux (J_N, Eq 2.4) was a complex balance of K_z at the base of the thermocline, determined by both the vertical K_z profile through the water column and the position of the base of the SCM within the K_z profile, and

$\Delta N/\Delta z$ at the base of the SCM, which was itself affected by mixing in the region of the SCM and nitrate uptake.

Large (orders of magnitude) changes in K_z often overwhelmed any variations in J_N due to variations in $\Delta N/\Delta z$. During individual station occupations, greater than 74% of temporal variability in vertical nitrate fluxes into the SCM was driven by temporal variations in K_z at the base of the SCM. Stations with similar $\Delta N/\Delta z$ could have very different daily average J_N, resulting from spatial differences in the K_z experienced, e.g. CS3a and B2a where mean $\Delta N/\Delta z$ = 0.6 mmol m^{-4}, but mean daily $K_z = 1.3 \times 10^{-4}$ and 5.3×10^{-4} m^2 s^{-1} respectively, and hence daily mean J_N = 3.8 and 15.7 mmol m^{-2} day^{-1} respectively. Thus, a key result of this work is that mechanisms influencing the K_z experienced at the base of the SCM at each station were the dominant influences on variations in J_N.

Changes in primary production rates, and hence SCM [Chl *a*], due to changes in irradiance would be temporally and not spatially patchy in the Celtic Sea, as the light falling on the sea surface can be considered constant over the Celtic Sea area at any one time. A combination of variations in K_z and $\Delta N/\Delta z$ experienced at the base of the thermocline appear to be capable of explaining some of the patchiness seen in SCM [Chl *a*] in the 2003 cross shelf SeaSoar transect (Fig 3.1), through influencing vertical supply of nitrate to the SCM.

Over flat topography

Over flat shelf regions K_z at the base of the SCM seemed to be driven by two major mechanisms- shear generated at the seabed by the barotropic tide and inertial oscillations.

Periodic pulses of mixing occur at the base of the thermocline, driven by vertical shear of the barotropic tidal currents. The spring-neap tidal cycle was an important component of this, directly affecting the levels of K_z at the base of the SCM through changing tidal current velocities and consequently the shear generated. This was hypothesised in Sharples et al. (2001b), and confirmed here at CS3 (Chapter 3). The spring-neap cycle also caused variation in the position of the SCM within the vertical K_z profile, as demonstrated at CS3. Nitrate gradients were also steeper approaching and around spring tides (e.g. Table 3.1), due to the action of the increasing bed generated shear sharpening the base of the SCM. Vertical nitrate fluxes due to barotropic tidally generated turbulence were greater approaching spring tides than approaching neap tides (e.g. CS3b J_N = 2.8 mmol N m^{-2} day^{-1} and CS3a J_N = 1.3 mmol N m^{-2} day^{-1}, respectively). Quarter diurnal increases in J_N were observed approaching and around spring tide (CS3b and CS1), linked to quarter diurnal increases in K_z driven by maximum tidal current velocities, but were not seen approaching or at neap tide (CS3a, OB, B2a, B2b).

The effect of inertial oscillations on J_N is hard to evaluate. Due to hydrographic and sampling considerations the occurrence of these motions could only be confirmed at station CS3, and were observed in particular during CS3a (personal communication M. Palmer). However, changes in J_N between CS3a and CS3b were also due to differing positions within the spring-neap tidal cycle, and a single enhanced K_z event during CS3a (the exact cause of which is unknown). Therefore it is impossible to quantify how much of an affect inertial oscillations have on J_N across the Celtic Sea. However, where the thermocline is not particularly stable (Richardson numbers of ~1, e.g. at CS3) small shear

instabilities can increase K_z, enhancing J_N, and inertial oscillations would provide a source of shear.

Over topographic features

Mean daily vertical nutrient fluxes over topographic features such as banks (CS1, B2, mean J_N = 15.7 mmol N m^{-2} day^{-1}) were increased by up to an order of magnitude compared to over a flat seabed (CS3, OB, mean J_N = 2.6 mmol N m^{-2} day^{-1}). The shallower water column over banks places the thermocline in closer proximity to the seabed, allowing increased (barotropic) tidal shear to reach the base of the thermocline. As over a flat seafloor K_z generated this way is stronger approaching and at spring tides.

An additional process acts over the bank slopes to enhance mixing between the bottom layer and thermocline, mixing both phytoplankton out of, and nitrate into, the SCM. A bank slope signature of increased SCM [Chl *a*] and bottom water [Chl *a*] appears to be caused by lee wave formation (e.g. Maxworthy 1979). This process increases internal mixing, causing the thermocline and SCM to become more diffuse. The extremely high ($\sim 1 \times 10^{-2}$) vertical diffusivities measured at CS1 at spring tide, and the positioning and timing of the event, supported the formation of a lee wave, such as seen over a bank on the Oregon shelf (Moum & Nash 2000, Nash & Moum 2001). Unfortunately, over Jones Bank in 2005 the temperature logging mooring at B1, situated where a lee wave was thought to form, was lost. However the temperature logging moorings at B2 and B3, and the CTD data at B2, show evidence of internal wave structures passing through first B2 then B3, as the tide slowed and turned, as would be expected (Maxworthy 1979). The ADCP

mooring and FLY data at B2 show these wave structures were associated with increased shear and vertical turbulent diffusivities within the region of the thermocline. Associated shorter period waves were more common around spring tide, further enhancing J_N.

At the shelf break, as over the banks, observations were consistent with the breakdown of a generated lee wave (the internal tide), increasing K_z relative to a shelf site over flat bathymetry throughout the spring-neap tidal cycle. The greater number of shorter-period waves generated at spring tides further increased mixing at the base of the SCM, as internal waves and their associated shear drove higher K_z and enhanced J_N. However the higher internal mixing acted to decrease $\Delta N/\Delta z$, lowering the vertical nitrate fluxes at neap tide towards similar levels as over a flat shelf. Therefore, although short temporal variations caused by $\Delta N/\Delta z$ were masked by the larger variations in K_z, overall $\Delta N/\Delta z$ was an important factor in J_N evaluation. In comparison to the shelf break, internal mixing generated by lee waves over banks acting to decrease $\Delta N/\Delta z$ was counteracted by barotropic bed generated mixing sharpening $\Delta N/\Delta z$. Thus, in addition to increased K_z $\Delta N/\Delta z$ was also increased over the shelf banks, ensuring high vertical nitrate fluxes.

Spring-neap tidal variability is an important factor in the rates of supply of nitrate but also in the rates of removal of [Chl *a*] from the SCM. The higher (nitrate) fluxes into the SCM at spring tides are matched by higher ([Chl *a*]) fluxes out of the SCM. However, a period of relative stability occurs approaching, and during, neap tides, which may provide favourable conditions for the phytoplankton to respond to the enhanced nitrate fluxes which occurred at spring tides. Sharples et al. (In Press) found potential for excess nitrate supplied

over the shelf break at CS2 during springs to be utilised over the following few days, maximum [Chl *a*] occurring ~3.5 days after maximum nitrate flux. There is the potential for an analogous effect to also occur over banks, allowing the phytoplankton to utilise the supplied nitrate in the days following large nitrate fluxes, without the need for sudden large increases in primary production rates.

7.2 Biological influences of the vertical nitrate flux across the Celtic Sea

Primary production

The phytoplankton, particularly those living within the SCM, are light limited on cloudy days (personal communication A. Hickman), and the majority of overall production occurs on sunny days. Extended periods of cloudy weather could possibly result in less nitrate uptake, though this would in turn potentially reduce $\Delta N/\Delta z$ and the vertical nitrate flux. The following calculated rates of new production will be those supportable in the SCM if all nitrate supply is utilised. The undetectable surface nitrate concentrations over the flat shelf, and banks and shelf break at neap tides, suggests all nitrate is taken up by phytoplankton in the SCM and so supports this assumption. Although detectable concentrations of surface nitrate were observed at spring tides over the shelf break and banks, this nitrate disappears within a few days, probably taken up by the phytoplankton present. This suggests all nitrate supplied into the SCM is

utilised, even if not immediately, and new production estimates based on the flux calculations are valid.

The estimated average flux of new nitrate into the SCM over flat topography in the Celtic Sea (~2.6 mmol N m^{-2} day^{-1}) was similar to the previous values of ~2 mmol N m^{-2} day^{-1} obtained for shelf seas around the UK (Sharples et al. 2001b, Rippeth et al. In Press), and would support a rate of carbon fixation of 207 mg C m^{-2} day^{-1} (assuming Redfield ratio). The undetectable surface nitrate concentrations seen at CS3 and OB suggest all nitrate supplied from the below the SCM is taken up by phytoplankton within the SCM over a flat shelf. Assuming a growing season of 120 days this would result in ~24.8 g C m^{-2} new production in the SCM (and overlying waters) through the summer. The spring bloom would contribute ~19 g C m^{-2} new production, assuming a surface mixed layer depth of 30 m and a surface winter nitrate concentration equivalent to deep water values (~8 mmol N m^{-3}) being reduced to zero during the bloom. Thus over the Celtic Sea shelf the SCM could contribute over 56% of yearly new production to the system, in comparison to estimates of between 37% and 66% for the North Sea (Weston et al. 2005 and Richardson et al. 2000 respectively). The total area of the Celtic Sea shelf was estimated to be ~167,300 km^2. This would give a possible total new production of 4.15×10^{12} g C (4.15×10^6 Tonnes C) over the summer over the entire Celtic Sea.

This above calculation of Celtic Sea carbon fixation does not take into account the enhanced nitrate fluxes into the SCM occurring over banks, which would serve to raise potential new production rates even higher. It is difficult to calculate the full contribution of banks to new production, as a) the occurrence of lee waves and associated shorter period internal waves has not been fully

elucidated throughout the spring-neap tidal cycle and so the true mean vertical nitrate flux is unknown, b) the total area affected by a lee wave produced over one bank is unknown and c) the number of banks producing lee waves is unknown. However, assuming the J_N values estimated over B2 and CS1 are representative, a mean J_N of 15.7 mmol N m^{-2} day^{-1} over the spring-neap tidal cycle would lead to 1.2 g C m^{-2} day^{-1}, or 144 g C m^{-2} each summer. There was a distance of ~ 7.2 km between moorings B2 and B3, both of which showed the effects of lee waves over one slope of Jones Bank. The wave seems to occur over both opposing slopes running perpendicular to the major tidal current axis, as suggested by the high SCM [Chl *a*] and bottom water [Chl *a*] over both slopes (Fig 4.3). Even if the waves travel in a narrow path this could result in a substantial amount of new production, and there are many banks in the Celtic Sea (Figs 2.1 and 3.2). The SeaSoar transect data over Jones bank showed the increased SCM and bottom water [Chl *a*] patches to be ~7 km in length. The width of the bank was estimated as 8 km, producing a possible affected area of 56 km^2 over each of the two opposing slopes. Over Jones Bank this would result in 8×10^9 g C yr^{-1} new production each stratified season. Estimating about 20 banks in the Celtic Sea results in 1.6×10^{11} g (1.6×10^5 Tonnes) C new production over banks in the summer. This increases new production over the shelf by ~4%.

Over the shelf break, *in situ* data displayed vertical fluxes of 2.6 mmol N m^{-2} day^{-1}, or an estimated 4–15 mmol N m^{-2} day^{-1} allowing for missed K_z events. The latter estimates are similar to those over the shelf break off the Malin shelf (Rippeth et al. In Press) and NE New Zealand (Sharples et al. 2001a).

Remote sensing was used to estimate vertical nitrate fluxes into the surface layer over the shelf break, through the amount of nitrate required to

support the [Chl *a*] measured. This suggested mean nitrate fluxes of 2.2 into the surface layer overlying the Celtic Sea shelf break. The satellite derived estimate is an average across the whole shelf break surface feature and makes no allowance for the presence of a subsurface chlorophyll maximum. The gradual decline of [Chl *a*] surface band intensity throughout the stratified season, with no simultaneous decrease in SST band intensity, suggested the possibility that there was formation of an SCM over the shelf break to some extent. The *in situ* data was collected at the base of the thermocline at the edge of the band, where there was an SCM present. This could be why the satellite estimates are lower than the *in situ* estimates which allow for missed K_z events, as increased [Chl *a*] (increased production) within an SCM would not be included in the remotely sensed flux calculation.

A J_N value of 2.6 mmol N m^{-2} day^{-1} at the shelf break would support 207 mg C m^{-2} day^{-1} or ~25 g C m^{-2} yr^{-1}. The J_N estimates allowing for missed K_z events (4–15 mmol N m^{-2} day^{-1}) would support on average ~660 mg C m^{-2} day^{-1} or 79 g C m^{-2} over the stratified period. An average value of ~52 g C m^{-2} seems a reasonable mean estimate given the values of J_N found by Rippeth et al. (In Press), Sharples et al. (2001a) and Joint et al. (2001), obtaining estimates of new production ranging from 46–57 g C m^{-2} over the stratified period.

Analysis of the satellite images showed the shelf break band of enhanced surface [Chl *a*] had a mean width of 52 km under Sat_1 and Sat_2. The length of the Celtic Sea shelf break is roughly 700 km, giving an affected area of approximately 36,400 km^2. This equates to a total of 1.9×10^{12} g C day^{-1}, or ~ 1.9×10^{6} metric Tonnes C yr^{-1}.

Total new production of 6.21×10^6 Tonnes C is therefore supported over the Celtic Sea shelf and shelf break through the stratified season, with the greatest contribution spread over the shelf in the subsurface chlorophyll maximum (~66.8%). The shelf break contributes almost a third (~30.6%) of new production in the Celtic Sea area, and internal mixing over banks on the shelf supports ~2.6% of the total.

Biological effects beyond primary production

Further evidence of the possible biological importance of the large production rates fuelled over banks comes from fisheries vessel data supplied by the Department of Enviroment, Food and Rural Affairs (DEFRA). Plots of fishing effort by all EU boats in UK waters over years 2001–2005 demonstrate the fishing interest in the area around Jones Bank (Fig 7.1). Fishing effort is high over the banks during the summer (Fig 7.1 c and d), when the SCM is active. Individual boat tracks show how the vessels often head straight to the banks region (personal communication J. Sharples). As mentioned previously Jones Bank was selected for investigation partly because it was named, implying a long-term interest of fishermen. Anecdotal evidence of high fishing activity over the banks was seen by the large number of vessels actively fishing observed from the survey ships whilst in the region of the banks (several moorings were lost through being trawled). This is corroborated by the DEFRA data. The DEFRA fishing vessel data also showed high fishing activity concentrated at the shelf break (Fig 7.1 a–e) suggesting the enhanced primary production rates possibly also supported enhanced production at higher trophic levels. High fishing activity by fishermen is presumably because of high fish catches in the area, though

whether this is due to high primary productivity supporting increased production through all trophic levels, or through some other cause such as the topography and hydrography making predator prey interactions more successful for the predator (fish) is unknown.

The new production fuelled within the SCM and enhanced over the banks would account for the differences between previously estimated production over the Celtic Sea shelf (100 g C m^{-2} yr^{-1}, Joint et al. 1986) and the energy demands of the higher trophic levels of the Celtic Sea (estimated at ~200 g C m^{-2} yr^{-1}).

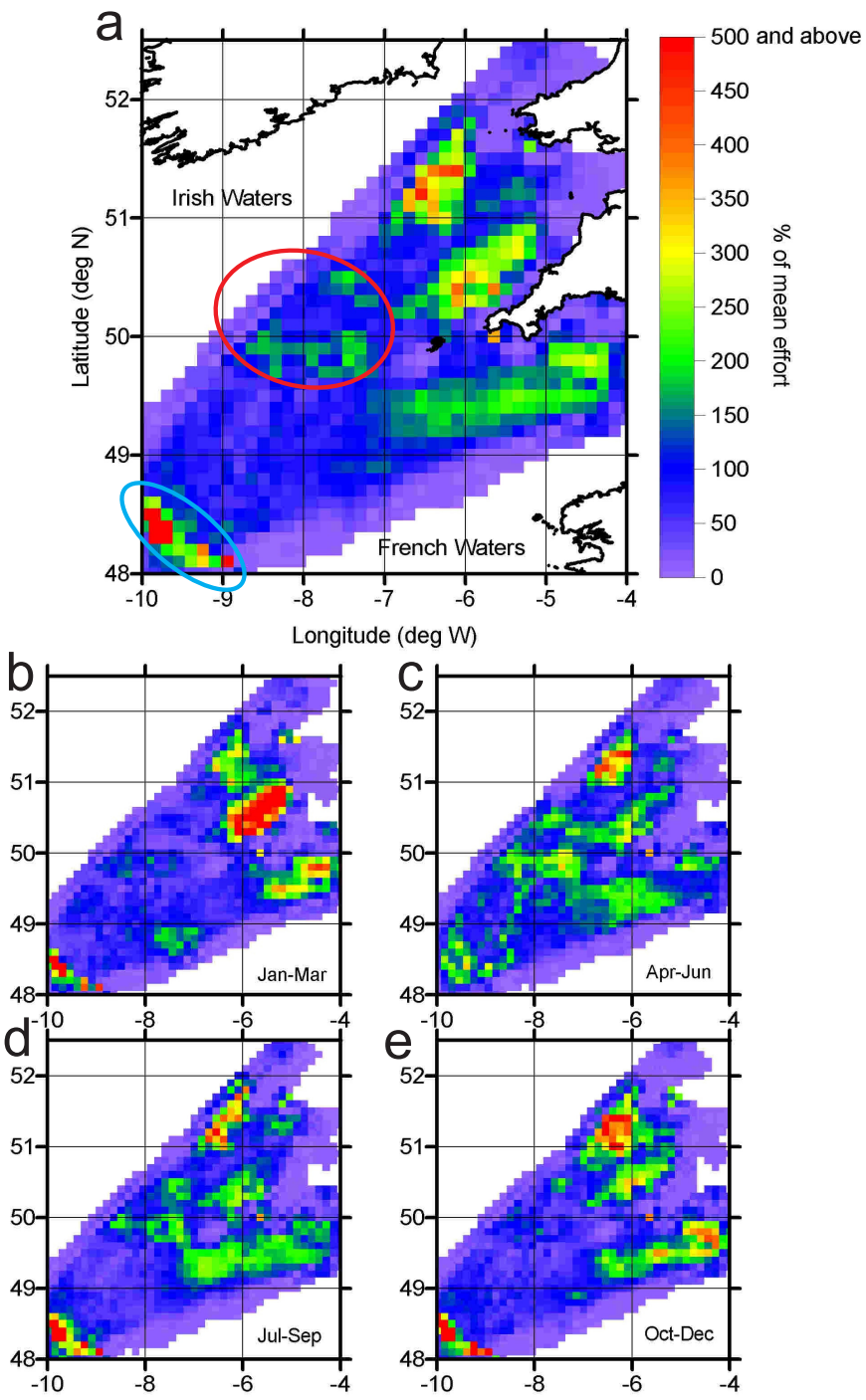

Figure 7.1

Plot of the percentage of mean fishing effort of all EU fishing vessels in UK waters 2000–2005 for a) the whole year (banks marked by a red ellipse and the shelf break by a blue ellipse), b) January to March, c) April to June, d) July to September and e) October to December. Figure courtesy of J. Sharples.

Appendix 1:
Acknowledgments of data used by the author collected and initially processed by other personnel.

Data	Personnel in charge of data collection and analysis
CTD calibrations	J. Sharples[1] J. Tweddle[2] S. Bates[3] (Chl *a* CD173)
SeaSoar calibrations	J. Sharples
On board chlorophyll *a* concentrations	P. Holligan[2]
On board nutrients	D. Hydes[2] (JR98) Y.N. Kim[2], M. Qurban[2] (CD173)
SUV6 Nitrate Sensor	J. Tweddle
^{14}C primary production estimates	A. Hickman[2]
FLY processing and calibrations	M. Palmer[4] (JR98 & CD173), M. Green[4] (CD173)
Temperature and ADCP moorings	M. Palmer UKORS
Shipboard ADCP	M. Palmer (RV *Prince Madog*) J. Sharples (RRS *James Clark Ross* and RRS *Charles Darwin*)
HPLC	Y.N. Kim
Analytical flow cytometry	Y.N. Kim (JR98) C.M. Moore[2] (CD173)
Microscope identification and counts of phytoplankton	Y.N. Kim
In situ Fast Repetition Rate Fluorometry	J. Tweddle C.M. Moore
SURFMET underway system	UKORS
In situ optics data, using SATLANTIC profiler	G. Tilstone[5] (JR98) V. Krivtsov[4] (CD173)
PAR	J. Tweddle

[1] Proudman Oceanographic Laboratory, Liverpool
[2] National Oceanography Centre Southampton, affiliated with the University of Southampton
[3] Work experience student from West Kirby Grammar School
[4] University of Wales, Bangor
[5] Plymouth Marine Laboratory

Allen, JI, Siddorn, JR, Blackford, JC & Gilbert, FJ (2004). Turbulence as a control on the microbial loop in a temperate seasonally stratified marine systems model. *Journal of Sea Research* **52** 1-20

Anderson, TR & Williams, PJL (1998). Modeling the seasonal cycle of dissolved organic carbon at station E-1 in the English Channel. *Estuarine Coastal and Shelf Science* **46** 1: 93-109

Armi, L & Farmer, D (2002). Stratified flow over topography: bifurcation fronts and transition to the uncontrolled state. *Proceedings of the Royal Society of London Series a- Mathematical Physical and Engineering Sciences* **458** 2019: 513-538

Baines, PG (1973). The generation of internal tides by flat-bump topography. *Deep-Sea Research* **20** 179-205

Baines, PG (1974). Generation of internal tides over steep continental slopes. *Philosophical Transactions of the Royal Society of London Series a-Mathematical Physical and Engineering Sciences* **277** 1263: 27-58

Baines, PG (1982). On internal tide generation models. *Deep-Sea Research Part a-Oceanographic Research Papers* **29** 3: 307-338

Barlow, RG, Mantoura, R, Gough, MA & Fileman, TW (1993). Pigment signatures of the phytoplankton composition in the Northeastern Atlantic during the 1990 spring bloom. *Deep-Sea Research II* **40** 459-477

Baumert, HZ, Simpson, JH & Sundermann, J (2005). Marine Turbulence: theories, observations and models. Cambridge University Press, Cambridge. 630.

Behrenfeld, MJ, O'Malley, RT, Siegel, DA, McClain, CR, Sarmiento, JL, Feldman, GC, Milligan, AJ, Falkowski, PG, Letelier, RM & Boss, ES (2006). Climate driven trends in contemperary ocean productivity. *Nature* **444** 7120: 752-755

Bell, PR (1992). Green plants: Their origin and diversity. Cambridge University Press, Cambridge.

Bevington, PR & Robinson, DK (1991). Data reduction and error analysis for the physical sciences. 2nd. McGraw-Hill, Boston. 328.

Borges, AV, Delille, B & Frankignoulle, M (2005). Budgeting sinks and sources of CO_2 in the coastal ocean: Diversity of ecosystem counts. *Geophysical Research Letters* **32** L14601: doi:10.1029/2005GL023053

Cai, W-J, Dai, M & Wang, Y (2006). Air-sea exchange of carbon dioxide in ocean margins: A province-based synthesis. *Geophysical Research Letters* **33** L12603: doi:10.1029/2006GL-26219

Campbell, NA (1996). Biology. 4th. The Benjamin/ Cummings Publishing Company, Inc, Menlo Park, Ca, USA. 1206.

Cokacar, T, Oguz, T & Kubilay, N (2004). Satellite-detected early summer coccolithophore blooms and their interannual variability in the Black Sea. *Deep-Sea Research Part I-Oceanographic Research Papers* **51** 8: 1017-1031

Cummins, PF, Vagle, S, Armi, L & Farmer, DM (2003). Stratified flow over topography: upstream influence and generation of nonlinear internal waves. *Proceedings of the Royal Society of London Series a-Mathematical Physical and Engineering Sciences* **459** 1467-1487

da Silva, JCB, New, AL, Srokosz, MA & Smyth, TJ (2002). On the observability of internal tidal waves in remotely-sensed ocean colour data. *Geophysical Research Letters* **29** 12: art. no.-1569

Denman, KL & Gargett, AE (1983). Time and space scales of vertical mixing and advection of phytoplankton in the upper ocean. *Limnology and Oceanography* **28** 5: 801-815

Dewey, RK, Crawford, WR, Gargett, AE & Oakey, NS (1987). A microstructure instrument for profiling oceanic turbulence in coastal bottom boundary layers. *Journal of Atmospheric and Oceanic Technology* **4** 288-297

Dickson, RR, Gurbutt, PA & Pillai, VN (1980). Satellite evidence of enhanced upwelling along the European continental slope. *Journal of Physical Oceanography* **10** 5: 813-819

DuRand, MD, Olson, RI & Chisholm, SW (2001). Phytoplankton population dynamics at the Bermuda Atlantic Time-series station in the Sargasso Sea. *Deep-Sea Research II* **48** 1983-2003

Edwards, KA, MacCready, P, Moum, JN, Pawlak, G, Klymak, JM & Perlin, A (2004). Form drag and mixing due to tidal flow past a sharp point. *Journal of Physical Oceanography* **34** 6: 1297-1312

Efron, B & Gong, G (1983). A leisurely look at the bootstrap, the jacknife, and cross-validation. *The American Statistician* **37** 1: 36-48

Ewing, GC (1950). Relationship between band slicks at the surface and internal waves in the sea. *Science* **111** 2874: 91-94

Falkowski, PG & Raven, JA (1997). Aquatic Photosynthesis. Blackwell Science, Oxford. 375.

Farmer, D & Armi, L (1999a). The generation and trapping of solitary waves over topography. *Science* **283** 188-190

Farmer, DM & Armi, L (1999b). Stratified flow over topography: the role of small-scale entrainment and mixing in flow establishment. *Philosophical Transactions of the Royal Society of London Series a-Mathematical Physical and Engineering Sciences* **455** 3221-3258

Farmer, DM & Armi, L (2001). Stratified flow over topography: models versus observations. *Proceedings of the Royal Society of London Series a-Mathematical Physical and Engineering Sciences* **457** 2827-2830

Fasham, MRJ, Holligan, PM & Pugh, PR (1983). The spatial and temporal development of the spring phytoplankton bloom in the Celtic Sea, April 1979. *Progress in Oceanography* **12** 87-145

Figueiras, FG & Pazos, Y (1991). Microplankton assemblages in three Rías Baixas (Vigo, Arosa and Muros, Spain) with a subsurface chlorophyll maximum: their relationships to hydrology. *Marine Ecology- Progress Series* **76** 219-233

Finch, MS, Hydes, DJ, Clayson, CH, Weigl, B, Dakin, J & Gwilliam, P (1998). A low power ultra violet spectrophotometer for measurement of nitrate in seawater: introduction, calibration and initial sea trials. *Analytica Chimica Acta* **377** 167-177

Frankignoulle, M & Borges, AV (2001). European continental shelf as a significant sink for atmospheric carbon dioxide. *Global Biogeochemical Cycles* **15** 569-579

Gerkema, T (1996). A unified model for the generation and fission of internal tides in a rotating ocean. *Journal of Marine Research* **54** 3: 421-450

Godin, G (1988). Tides. CICESE, Ensenada BC, Mexico. 290.

Gowan & Bloomfield (1996). Chlorophyll standing crop and phytoplankton production in the western Irish Sea during 1992 and 1993. *Journal of Plankton Research* **18** 1735-1751

Grasshoff, K, Ehrhardt, M & Kremling, K (1983). Methods of seawater analysis. 2nd. Verlag Chemie, Weinheim. 419.
Guizien, K, Barthélemy, E & Inall, ME (1999). Internal tide generation at a shelf break by an oblique barotropic tide: Observations and analytical modeling. *Journal of Geophysical Research* **104** C7: 15655-15668
Hale, WG, Margham, JP & Saunders, VA (1995). Collins Dictionary of Biology. 2nd. HarperCollins Publishers, Glasgow.
Hearn, CJ (1985). On the value of the mixing efficiency in the Simpson-Hunter h/u^3 criterion. *Deutsch. Hydrogr. Z.* **58** 133-145
Heathershaw, AD (1985). Some observations of internal wave current fluctuations at the shelf edge and their implications for sediment transport. *Continental Shelf Research* **4** 485-493
Helland-Hansen, B & Nansen, F (1909). The Norwegian Sea. *Norw. Fish. Mar. Invest. Rep.* **2** 87-132
Hickman, AE (In prep). Faculty of Engineering, Science and Mathematics, School of Ocean and Earth Sciences, University of Southampton, Southampton.
Holligan, PM & Harbour, S (1977). The vertical distribution and succession of phytoplankton in the Western English Channel in 1975 and 1976. *Journal of the Marine Biological Association of the UK* **57** 1075-1093
Holligan, PM, Balch, WM & Yentsch, CM (1984a). The significance of subsurface chlorophyll, nitrite and ammonium maxima in relation to nitrogen for phytoplankton growth in stratified waters of the Gulf of Maine. *Journal of Marine Research* **42** 1051-1073
Holligan, PM, Williams, PJleB, Purdie, D & Harris, RP (1984b). Photosynthesis, respiration and nitrogen supply of phytoplankton populations in stratified, frontal and tidally mixed shelf waters. *Marine Ecology- Progress Series* **17** 201-213
Holligan, PM, Pingree, RD & Mardell, GT (1985). Oceanic solitons, nutrient pulses and phytoplankton growth. *Nature* **314** 6009: 348-350
Holligan, PM & Groom, SB (1986). Phytoplankton distributions along the shelf break. *Proceedings of the Royal Society of Edinburgh* **88B** 239-263
Holloway, PE (1987). Internal hydraulic jumps and solitons at the shelf break region on the Australian north west shelf. *Journal of Geophysical Research* **92** C5: 5405-5416
Holloway, PE (1994). Observations of internal tide propagation on the Australian north-west shelf. *Journal of Physical Oceanography* **24** 8: 1706-1716
Holloway, PE (1996). A numerical model of internal tides with application to the Australian North West Shelf. *Journal of Physical Oceanography* **26** 1: 21-37
Horne, EPW, Loder, JW, Namie, CE & Oakey, NS (1996). Turbulent dissipation rates and nitrate supply in the upper water column on Georges Bank. *Deep-Sea Research II* **43** 1683-1712
Huisman, J & Sommeijer, B (2002). Population dynamics of sinking phytoplankton in light-limited environments: simulation techniques and critical parameters. *Journal of Sea Research* **48** 2: 83-96
Huthnance, JM (1995). Circulation, exchange and water masses at the ocean margin: the role of physical processes at the shelf edge. *Progress in Oceanography* **35** 353-431

Inall, ME, Rippeth, TP & Sherwin, TJ (2000). Impact of nonlinear waves on the dissipation of internal tidal energy at a shelf break. *journal of Geophysical Research* **105** C4: 8687-8705

Inall, ME, Cottier, F, Griffiths, C & Rippeth, T (2004). Sill dynamics and energy transformation in a jet fjord. *Ocean Dynamics* **54** 3-4: 307-314

Inall, ME, Rippeth, T, Griffiths, C & Wiles, P (2005). Evolution and distribution of TKE production and dissipation within stratified flow over topography. *Geophysical Research Letters* **32** 8:

Jeans, DRG & Sherwin, TJ (2001). The evolution and energetics of large amplitude nonlinear internal waves on the Portuguese shelf. *Journal of Marine Research* **59** 3: 327-353

Joint, I & Pomroy, AJ (1986). Photosynthetic characteristics of nanoplankton and picoplankton from the surface mixed layer. *Marine Biology* **92** 465-474

Joint, I & Groom, SB (2000). Estimation of phytoplankton production from space: current status and future potential of satellite remote sensing. *Journal of Experimental Marine Biology and Ecology* **250** 1-2: 233-255

Joint, I, Wollast, R, Chou, L, Batten, S, Elskens, M, Edwards, E, Hirst, A, Burkill, P, Groom, S, Gibb, S, Miller, A, Hydes, D, Dehairs, F, Antia, A, Barlow, R, Rees, A, Pomroy, A, Brockmann, U, Cummings, D, Lampitt, R, Loijens, M, Mantoura, F, Miller, P, Raabe, T, Alvarez-Salgado, X, Stelfox, C & Woolfenden, J (2001). Pelagic production at the Celtic Sea shelf break. *Deep-Sea Research Part Ii-Topical Studies in Oceanography* **48** 14-15: 3049-3081

Joint, IR, Owens, NJP & Pomroy, AJ (1986). Seasonal production of photosynthetic picoplankton and nanoplankton in the Celtic Sea. *Marine Ecology- Progress Series* **28** 251-258

Kelly-Gerreyn, BA, Hydes, DJ, Jegou, AM, Lazure, P, Fernand, LJ & Puillat, I (2006). Low salinity intrusions in the western English Channel. *Continental Shelf Research* **26** 11: 1241-1257

Kirk, JTO (1994). Light and photosynthesis in aquatic ecosystems. 2nd. Cambridge University Press, Cambridge.

Klymak, JM & Gregg, MC (2001). Three-dimensional nature of flow near a sill. *Journal of Geophysical Research* **106** C10: 22295-22311

Klymak, JM & Gregg, MC (2003). The role of upstream waves and a downstream density pool in the growth of lee waves: stratified flow over the Knight Inlet sill. *Journal of Physical Oceanography* **33** 1446-1461

Klymak, JM & Gregg, MC (2004). Tidally generated turbulence over the Knight Inlet sill. *Journal of Physical Oceanography* **34** 1135-1151

Kolber, ZS, Práʃil, O & Falkowski, PG (1998). Measurements of variable chlorophyll fluorescence using fast repetition rate techniques: defining methodology and experimental protocols. *Biochimica et Biophysica Acta* **1367** 88-106

Laney, S (2000). v4. http://picasso.oce.orst.edu/ORSOO/FRRF/

Lewis, MR, Harrison, WG, Oakey, NS, Hebert, D & Platt, T (1986). Vertical nitrate fluxes in the oligotrophic ocean. *Science* **234** 4778: 870-873

Lizon, F, Lagadeuc, Y, Brunet, C, Aelbrecht, D & Bentley, D (1995). Primary production and photoadaptation of phytoplankton in relation with tidal mixing in coastal waters. *Journal of Plankton Research* **17** 5: 1039-1055

Lizon, F, Seuront, L & Lagadeuc, Y (1998). Photoadaptation and primary production study in tidally mixed coastal waters using a Lagrangian model. *Marine Ecology-Progress Series* **169** 43-54

Longhurst, AR & Harrison, WG (1989). The biological pump: Profiles of plankton production and consumption in the upper ocean. *Prog. Oceanog.* **22** 47-123

Lorenzo, LM, Figueiras, FG, Tilstone, GH, Arbones, B & Mirón, I (2004). Photosynthesis and light regime in the Azores Front region during summer: are light-saturated computations of primary production sufficient? *Deep-Sea Research I* **51** 1229-1244

Lueck, RG & Mudge, TD (1997). Topographically induced mixing around a shallow seamount. *Science* **276** 5320: 1831-1833

Maas, LRM & van Haren, JJM (1987). Observations on the vertical structure of tidal and inertial currents in the central North Sea. *Journal of Marine Research* **45** 293-318:

MacKinnon, JA & Gregg, MC (2003). Mixing on the late-summer New England Shelf- solibores, shear, and stratification. *Journal of Physical Oceanography* **33** 1476-1492

Maxworthy, T (1979). A note on the internal solitary waves produced by tidal flow over a 3-dimensional ridge. *Journal of Geophysical Research-Oceans and Atmospheres* **84** NC1: 338-346

Mazé, R (1987). Generation and propagation of non-linear internal waves induced by the tide over a continental slope. *Continental Shelf Research* **7** 9: 1079-1104

Millott, C & Crépon, M (1981). Inertial oscillations on the continental shelf of the Gulf of Lions- observation and theory. *Journal of Physical Oceanography* **11** 639-657

Moore, CM (2002). Small scale physical processes and phytoplankton growth in shelf seas. School of Ocean and Earth Science, University of Southampton, Southampton.

Moore, CM, Suggett, DJ, Hickman, AE, Kim, YN, Tweddle, JF, Sharples, J, Geider, RJ & Holligan, PM (2006). Phytoplankton photoacclimation and photoadaptation in response to environmental gradients in a shelf sea. *Limnology and Oceanography* **51** 2: 936-949

Moore, DS & McCabe, GP (1998). Introduction to the practice of statistics. 3rd. W.H. Freeman and Company, U.S.A.

Morel, A, Antoine, D, Babin, M & Dandonneau, Y (1996). Measured and modeled primary production in the northeast Atlantic (EUMELI JGOFS program): The impact of natural variations in photosynthetic parameters on model predictive skill. *Deep-Sea Research I* **43** 8: 1273-1304

Moum, JN (1996). Efficiency of mixing in the main thermocline. *Journal of Geophysical Research-Oceans* **101** C5: 12057-12069

Moum, JN & Nash, JD (2000). Topographically induced drag and mixing at a small bank on the continental shelf. *Journal of Physical Oceanography* **30** 2049-2054

Moum, JN, Farmer, DM, Smyth, WD, Armi, L & Vagle, S (2003). Structure and generation of turbulence at interfaces strained by internal solitary waves propagating shoreward over the continental shelf. *Journal of Physical Oceanography* **33** 10: 2093-2112

Muller-Karger, FE, Varela, ZR, Thunell, R, Luerssen, R, Hu, C & Walsh, JJ (2005). The importance of continental margins in the global carbon cycle. *Geophysical Research Letters* **32** L01602

Munk, W (1997). Once again: once again- tidal friction. *Prog. Oceanog.* **40** 7-35

Napp, JM, Incze, LS, Ortner, PB, Siefert, DLW & Britt, L (1996). The plankton of Shelikof Strait, Alaska: Standing stock, production, mesoscale variability and their relevance to larval fish survival. *Fisheries Oceanography* **5** 1: 19-38

Nash, JD & Moum, JN (2001). Internal hydraulic flows on the continental shelf: High drag states over a small bank. *Journal of Geophysical Research-Oceans* **106** C3: 4593-4611

New, AL & Pingree, RD (1990). Evidence for internal tidal mixing near the shelf break in the Bay of Biscay. *Deep-Sea Research* **37** 12: 1783-1803

New, AL & Pingree, RD (2000). An intercomparison of internal solitary waves in the Bay of Biscay and resulting from Korteweg-de Vries-Type theory. *Progress in Oceanography* **45** 1: 1-38

New, AL & Da Silva, JCB (2002). Remote-sensing evidence for the local generation of internal soliton packets in the central Bay of Biscay. *Deep-Sea Research Part I-Oceanographic Research Papers* **49** 5: 915-934

Nielsen, TG, Løkkegaard, B, Richardson, K, Pedersen, FB & Hansen, L (1993). Structure of plankton communities in the Dogger Bank area (North Sea) during a stratified situation. *Marine Ecology- Progress Series* **95** 115-131

Nincevic, Marasovic, I & Kuʃpilic, G (2002). Deep chlorophyll-a maximum at one station in the middle Adriatic Sea. *Journal of the Marine Biological Association of the UK* **82** 1: 9-19

Osborn, TR (1974). Vertical profiling of velocity microstructure. *Journal of Physical Oceanography* **4** 109-115

Osborn, TR (1980). Estimates of the local rate of vertical diffusion from dissipation measurements. *Journal of Physical Oceanography* **10** 83-89

Pingree, RD & Pennycuick, L (1975). Transfer of heat, fresh water and nutrients through the seasonal thermocline. *Journal of the Marine Biological Association of the United Kingdom* **55** 261-274

Pingree, RD, Holligan, PM, Mardell, GT & Head, RN (1976). The influence of physical stability on spring, summer and autumn phytoplankton blooms in the Celtic Sea. *Journal of the Marine Biological Association of the UK* **56** 845-873

Pingree, RD, Maddock, L & Butler, EI (1977). The influence of biological activity and physical stability in determining the chemical distributions of inorganic phosphate, silicate and nitrate. *Journal of the Marine Biological Association of the UK* **57** 1065-1073

Pingree, RD, Holligan, PM & Mardell, GT (1978). The effects of vertical stability on phytoplankton distributions in the summer on the northwest European Shelf. *Deep-Sea Research* **25** 1011-1028

Pingree, RD & Mardell, GT (1981). Slope turbulence, internal waves and phytoplankton growth at the Celtic Sea shelf-break. *Philosophical Transactions of the Royal Society of London. A* **302** 663-682:

Pingree, RD, Mardell, GT, Holligan, PM, Griffiths, DK & Smithers, J (1982). Celtic Sea and Armorican current structure and the vertical distributions of temperature and chlorophyll. *Continental Shelf Sea Research* **1** 1: 99-116

Pingree, RD & Mardell, GT (1985). Solitary internal waves in the Celtic Sea. *Progress in Oceanography* **14** 431-441
Pingree, RD, Mardell, GT & New, AL (1986). Propagation of internal tides from the upper slopes of the Bay of Biscay. *Nature* **321** 154-158
Pollard, RT (1980). Properties of near-surface inertial oscillations. *Journal of Physical Oceanography* **10** 385-397
Pond, S & Pickard, GL (1995). Introductory Dynamical Oceanography. 2nd. Butterworth-Heinemann,
Probyn, TA, Mitchell-Innes, BA & Searson, S (1995). Primary production and nitrogen uptake in the subsurface chlorophyll maximum on the Eastern Agulhas Bank. *Continental Shelf Research* **15** 15: 1903-1920
Richardson, K & Chistoffersen, A (1991). Seasonal distribution and production of phytoplankton in the southern Kattegat. *Marine Ecology- Progress Series* **78** 217-227
Richardson, K, Nielsen, TG, Pederson, FB, Heilmann, JP, Løkkegaard, B & Kass, H (1998). Spatial heterogeneity in the structure of the planktonic food web in the North Sea. *Marine Ecology- Progress Series* **168** 197-211
Richardson, K, Visser, AW & Pedersen, FB (2000). Subsurface phytoplankton blooms fuel pelagic production in the North Sea. *Journal of Plankton Research* **22** 9: 1663-1671
Rippeth, TP & Inall, ME (2002). Observations of the internal tide and associated mixing across the Malin Shelf. *Journal of Geophysical Research-Oceans* **107** C4: art. no.-3028
Rippeth, TP, Simpson, JH, Player, RJ & Garcia, M (2002). Current oscillations in the diurnal-inertial band on the Catalonian shelf in spring. *Continental Shelf Research* **22** 247-265
Rippeth, TP, Palmer, MR, Simpson, JH, Fisher, NR & Sharples, J (2005). Thermocline mixing in summer stratified continental shelf seas. *Geophysical Research Letters* **32** L05602: doi:10.1029/2004GL022104
Rippeth, TP, Palmer, MR, Tweddle, JF, Sharples, J, Inall, M, Fisher, N, Hickman, AE, Holligan, P, Kim, YN, Moore, CM & Simpson, JH (In Press). Diapycnal nutrient fluxes in seasonally stratified shelf seas. *Limnology & Oceanography*
RSDAS, RSDAS (2006). RSDAS Satellite Image Archive Guide. http://www.npm.ac.uk/rsdas/data/guide
Salat, J, Tintoré, S, Font, J, Wang, D-P & Vieira, M (1992). Near-inertial motion on the shelf-slope front off northeast Spain. *Journal of Geophysical Research* **97** C5: 7277-7281
Sandstrom, H & Elliott, JA (1984). Internal tide and solitons on the Scotian Shelf: A nutrient pump at work. *Journal of Geophysical Research* **89** C4: 6415-6426
Sandstrom, H, Elliott, JA & Cochrane, NA (1989). Observing groups of solitary internal waves and turbulence with Batfish and echo-sounder. *Journal of Physical Oceanography* **19** 7: 987-997
Sandstrom, H & Oakey, NS (1995). Dissipation in internal tides and solitary waves. *Journal of Physical Oceanography* **25** 4: 604-614
Sharples, J & Simpson, JH (1995). Semi-diurnal and longer period stability cycles in the Liverpool Bay region of freshwater influence. *Continental Shelf Research* **15** 2/3: 295-313

Sharples, J (1999). Investigating the seasonal vertical structure of phytoplankton in shelf seas. *Marine Models Online* **1** 3-38

Sharples, J, Moore, CM & Abraham, ER (2001a). Internal tide dissipation, mixing, and vertical nitrate flux at the shelf edge of NE New Zealand. *Journal of Geophysical Research* **106** C7: 14,069-14,081

Sharples, J, Moore, CM, Rippeth, TP, Holligan, PM, Hydes, DJ, Fisher, NR & Simpson, JH (2001b). Phytoplankton distribution and survival in the thermocline. *Limnology and Oceanology* **46** 3: 486-496

Sharples, J, Tweddle, JF, Green, JAM, Palmer, MR, Kim, YN, Hickman, AE, Holligan, PM, Moore, CM, Rippeth, TP, Simpson, JH & Krivtsov, V (In Press). Spring-neap modulation of internal tide mixing and vertical nitrate fluxes at a shelf edge in summer. *Limnology & Oceanography*

Sherwin, TJ (1988). Analysis of an internal tide observed on the Malin Shelf, north of Ireland. *Journal of Physical Oceanography* **18** 7: 1035-1050

Simpson, JH & Hunter, JR (1974). Fronts in the Irish Sea. *Nature* **250** (5465): 404-406

Simpson, JH, Crawford, WR, Rippeth, TP, Campbell, AR & Cheok, JVS (1996). The vertical structure of turbulent dissipation in shelf seas. *Journal of Physical Oceanography* **26** 1579-1590

Steemann-Nielsen, E (1952). The use of radiocarbon (14C) for measuring organic production in the sea. *J. Cons. int. Explore. Mer.* **18** 117-140

Thomas, H, Bozac, Y, Elkalay, K & Baar, HJW (2004). Enhanced open ocean storage of CO_2 from shelf sea pumping. *Science* **304** 1005-1008

Tilstone, GH, Figueiras, FG, Lorenzo, LM & Ardones, B (2003). Phytoplankton composition, photosynthesis and primary production during different hydrographic conditions at the Northwest Iberian upwelling system. *Marine Ecology- Progress Series* **252** 89-104

Tsunogai, S, Watanabe, S & Sato, T (1999). Is there a "continental shelf pump" for the absorption of atmospheric CO_2? *Tellus* **51B** 701-712

van Haren, H, Mills, DK & Wetsteyn, L (1998). Detailed observations of the phytoplankton spring bloom in the stratifying central North Sea. *Journal of Marine Research* **56** 3: 655-680

van Haren, H, Maas, L, Zimmerman, JTF, Ridderinkhof, H & Malschaert, H (1999). Strong inertial currents and marginal internal wave stability in the central North Sea. *Geophysical Research Letters* **26** 19: 2993-2996

Welschmeyer, NA (1994). Fluorometric analysis of chlorophyll a in the presence of chlorophyll b and pheopigments. *Limnology & Oceanography* **39** 8: 1985-1992

Weston, K, Fernand, L, Mills, DK, Delahunty, R & Brown, J (2005). Primary production in the deep chlorophyll maximum of the central North Sea. *Journal of Plankton Research* **27** 909-922

Yool, A & Fasham, MJR (2001). An examination of the 'continental shelf pump' in an open ocean circulation model. *Global Biogeochemical Cycles* **15** 831-844

Young, JW, Bradford, R, Lamb, TD, Clementson, LA, Kloser, R & Galea, H (2001). Yellowfin tuna (*Thunnus albacares*) aggregations along the shelf break off southeastern Australia: links between inshore and offshore processes. *Marine and Freshwater Research* **52** 463-474

Zeilon, N (1912). On tidal boundary-waves and related hydrodynamical problems. *Handl. K. svenska Vetens. Akad* **47** 4: 1-46

Zubkov, MV, Sleigh, MA, Tarran, GA, Burkill, PH & Leakey, RJG (1998). Picoplanktonic community structure on an Atlantic transect from 50 degrees North to 50 degrees South. *Deep-Sea Research I* **45** 1339-1355